AGE AND ORIGIN OF THE BRUCEJACK EPITHERMAL AU-AG DEPOSIT, NORTHWESTERN BRITISH COLUMBIA

by

Sean Patrick Tombe

A thesis submitted in partial fulfillment of the requirements for the degree of

Master of Science

Department of Earth and Atmospheric Sciences

University of Alberta

ABSTRACT

Brucejack is an epithermal Au-Ag deposit located in northwestern British Columbia. The deposit is one of many world-class economic deposits that formed in association with extensive volcanic arc-related magmatism in Late Triassic–Early Jurassic time in the Canadian Cordillera. Brucejack mineralization is hosted by island arc-related Early Jurassic porphyritic latite flows, volcanic ash–block-sized fragmental rocks, and volcanic sandstones, siltstones and conglomerates. The variably altered and mineralized volcanic host rocks yield U-Pb zircon dates ranging between 196.4 ± 0.7 Ma and approximately 184 Ma. Molybednite Re-Os age estimates for mineralization at Brucejack range between 191.7 ± 0.8 Ma (Bridge Zone) and 188.9 ± 0.8 Ma (West Zone). Individual mineralizing events spanning ~3 m.y. are unlikely, and multiple pulses of ore formation are more probable, whereby earlier intermediate-sulfidation-style epithermal Au-Ag mineralization (Bridge Zone and Valley of the Kings), which was perhaps distally related to porphyry-type hydrothermal activity, was followed by a younger low-sulfidation epithermal Ag-Au event (West Zone).

Brucejack is crosscut by late stage andesite–basaltic andesite amygdaloidal dykes, which truncate all mineralized veins, and which are crosscut by late stage (post-mineralization) quartz-calcite veins. A U-Pb zircon age of 182.7 ± 1.0 Ma has been determined for one of these dykes, providing a minimum age for mineralization. With the exception of West Zone, the deposit shows features typical of intermediate-sulfidation epithermal deposits, characterized by the presence of crustiform and cockade vein textures, minor open space filling, the presence of various sulfosalt minerals, including tetrahedrite-tennantite, chalcopyrite, and FeS-poor sphalerite, scarce arsenopyrite,

absence of pyrrhotite, and the vertical extent of mineralization is >1000 m. Wallrocks at Brucejack are moderately phyllic-altered, with variable amounts of pervasive and texturally destructive sericite, pyrite, quartz, and carbonate. Early sericitization and pyritization is recognized, as well as hydrothermal sericitization contemporaneous with gold mineralization.

Five vein stages have been recognized at the Valley of the Kings: (I) highly deformed and discontinuous pyrite stringer veins containing carbonate and quartz commonly with chlorite and sericite-altered vein margins, containing no electrum; (II) weakly deformed quartz-carbonate stockwork veins, breccias veins, and subvertical stringer quartz vein networks, also hosting electrum; (III) Zn-Pb-(Cu) sulfide veins containing Ag-sulfosalts and electrum; (IV) highly deformed carbonate ± quartz veins containing abundant orange-coloured, manganoan calcite and electrum; (V) late stage quartz-carbonate shear veins with asymmetrical sericite, chlorite, and pyrite vein banding, often with associated subhorizontal tension gash veins.

Fluid inclusions from vein generations II, III, and IV have relatively low homogenization temperatures (means of 166 ± 11˚C, n = 25; 154 ± 18˚C, n = 89; 156 ± 9˚C, n = 34, respectively) and a narrow range in salinity (0.5 to 7.4 wt % NaCl equiv.; n = 54), with the exception of stage III veins which have a range of 0.5 to 15.5 wt % NaCl equiv. (n = 89). Evidence for boiling is recognized in stages II and IV, and therefore homogenization temperatures can be taken as approximating the actual trapping temperature. Boiling is thought to be responsible for the deposition of high-grade gold mineralization for these vein stages in the VOK, where gold precipitated from condensed magmatic liquids during near-surface depressurization. Stage III fluid inclusion

assemblages indicate fluid mixing between cooler, more saline meteoric fluids and warmer, dilute magmatic fluids resulting in Pb-Zn-Ag-Au deposition.

Oxygen isotopic compositions of vein quartz and calcite (calculated $\delta^{18}O_{fluid}$ values ranging from -9.8 to -1.5‰ and -5.8 to +1.4‰ respectively) indicate a progressive dilution from modified magmatic fluids mixing with metal-depleted meteoric surface waters. Carbon and sulfur isotopic compositions also suggest a magmatic source for these components in electrum-bearing veins; hydrothermal calcites have mean $\delta^{13}C_{CO2}$ value of -6.4 ± 1.3 ‰ (n = 25), and sulfur isotopic compositions of pyrite, sphalerite, and galena average -0.7 ± 0.3 ‰ (n = 16). With consideration to fluid inclusion and stable isotope analysis, a magmatic fluid is the most likely source for bonanza gold mineralization in the Valley of the Kings at Brucejack.

ACKNOWLEDGEMENTS

My sincerest thanks and gratitude is extended to Dr. Jeremy Richards for his patient mentorship throughout the last three years. Jeremy, you have shown me the value of concise scientific writing and have encouraged me to think more critically academically and personally.

I am also indebted to Dr. Warwick Board and Charles Greig for their ongoing support, geological insight and knowledge. Certainly their endless debates helped influence the current understanding at Brucejack. Charles provided a large amount of raw data for the lithogeochemistry for this project, of which I am deeply grateful for. Much of the U/Pb zircon dating has also been gathered from painstaking hours in the field from these two, and is certainly an asset to the property. Early renditions of the vein paragenesis were constructed by Warwick and Charles, and have since stood the test of time. Further thanks are extended to the entire geology team at Brucejack, for their support, and geological contributions.

Dr. Karlis Muehlenbachs and Olga Levner are thanked for their assistance in becoming familiar with the stable isotope lab, and the methodology of stable isotope analysis. Their insight into isotopic systems, combined with that of Dr. Tom Chacko, was greatly helpful and appreciated.

Dr. Robert Creaser is thanked for his contributions to the project, where his isotope lab yielded several Re-Os molybdenite ages, providing dates for mineralized veins on the system. Terry Spell is thanked for several Ar/Ar dates, which helped in the understanding of the property.

Thanks to Dr. Peter Larson and all involved in prompt work done on all oxygen isotope analyses at the Washington State University GeoAnalytical Lab. Further thanks are extended to the Isotope Sceince Lab at the University of Calgary for analyses run for sulfide isotopes.

Funding for this work was provided in part by NSERC grants to Dr. Richards and also industry contributions from Pretium Resources Inc.

TABLE OF CONTENTS

LIST OF TABLES

LIST OF FIGURES

SOURCES OF DATA

S. Tombe collected ten samples for whole-rock lithogeochemistry, where analyses were done at Actlabs (Ancaster, Ontario). Re-Os (molybdenite) samples were collected and submitted to R. Creaser at the University of Alberta for analysis. Two U-Pb (zircon) samples were collected, where A. DuFrane ran analyses at the University of Alberta. Four phyllosilicate samples were collected for $^{40}Ar/^{39}Ar$ geochronology and sent to T. Spell at the University of Nevada for analysis. Several thin sections were examined for fluid inclusions, where nine thin sections were chosen and analyzed by S. Tombe at the University of Alberta. S. Tombe also collected thirty-one calcite vein samples, where he isolated carbon and oxygen isotopes; purified samples were submitted to O. Levner for ICP-MS analysis at the University of Alberta. S. Tombe collected fifteen quartz vein samples, where they were sent to P. Larson for analysis at Washington State University GeoAnalytical Lab. Thirteen sulfide samples were also collected by S. Tombe and sent to the Isotope Science Laboratory at the University of Calgary for analysis. S. Tombe contributed to the vein paragenesis with a detailed petrographic analysis.

C. Greig constructed geologic maps used by Ireland et al., 2013 and are presented herein. Seventy-two samples for whole-rock lithogeochemistry were collected by C. Greig, and sent to ALS (Vancouver, British Columbia) for analysis. Twelve samples were also collected for U-Pb (zircon) dating and sent to the Pacific Center for Isotopic and Geochemical Research (PCIGR) facility at the University of British Columbia, where analyses were done by R. Friedman. C. Greig, together with W. Board, established early renditions of the vein paragenesis.

1.0 Introduction

The Sulphurets mineral district of northwest British Columbia lies within a remote mountainous region of the Canadian Cordillera in the western part of the Stikinia (or Stikine) tectonic terrane (Fig. 1). Over 20 mineralized zones and showings occur in the mineral district (Roach and MacDonald, 1992), and the area has been heavily explored and prospected for over a century. Several world-class deposits have been found in the area in addition to the Brucejack deposit including: Eskay Creek, Snip, Johnny Mountain, Kerr, Sulphurets, Mitchell, Granduc, Scottie Gold, Silbak-Premier, and Big Missouri (Fig. 2). The Kerr-Sulphurets-Mitchell (KSM) deposits, located approximately 5 km to the west of the Brucejack deposit, collectively comprise the Sulphurets Mining Camp.

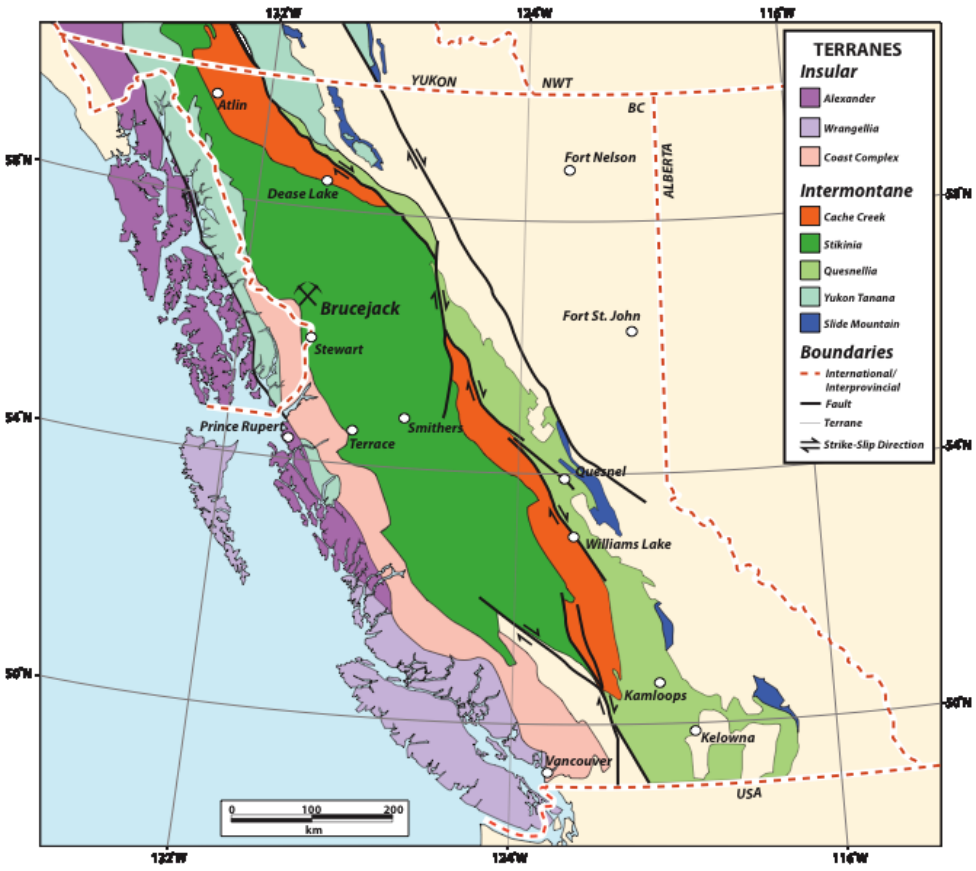

Figure 1: Map of British Columbia showing relevant accreted terranes within the Intermontane and Insular Belts. Modified from Nelson and Colpron (2011)

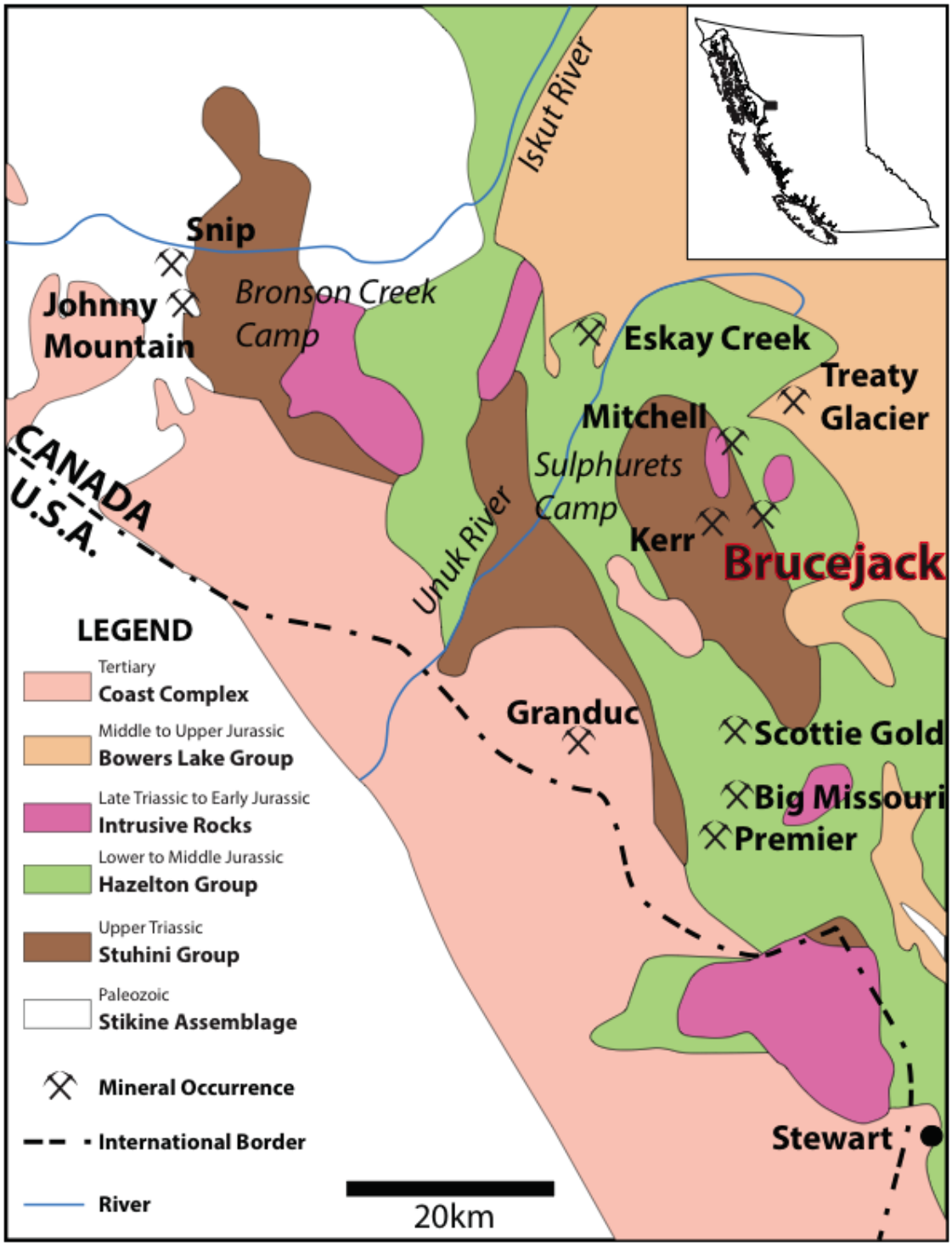

Figure 2: Regional geological map of the Iskut River region showing major mineral occurrences (modified from Ghaffari et al., 2010). Inset map shows location within British Columbia.

The region was first prospected in the 1880s, with continued interest recently by several exploration companies. Pretium Resources Inc. and Seabridge Gold Inc. staked large claims throughout the Sulphurets mineral district in the last decade. Pretium is currently focusing exploration on the Valley of the Kings (VOK) section of the Brucejack deposit, which is composed of high-grade Au-Ag quartz-carbonate stockwork vein system. Mineralization at Brucejack contains proven and probable reserves of 16.5 Mt grading 14.1 g/t Au (7.5 Moz Au) and 58 g/t Ag (30.7 Moz Ag) (VOK and West Zone collectively; Ireland et al., 2014).

At surface, throughout the Sulphurets mining camp, large pyritic gossans are present and are cospatial with mineralized stockworks and breccia veins. Mineralization is hosted in quartz and calcite veins and concentrated throughout Lower to Middle Jurassic Hazelton Group volcanic and sedimentary rocks, and occurs as sphalerite, galena, chalcopyrite, rutile, Ag-sulfosalts, electrum, minor arsenopyrite and acanthite, and rare molybdenite. Mineral showings throughout the area range from porphyry deposits (Cu-Au, Cu, and possibly Au-only) to mesothermal and epithermal vein deposits (MacDonald, 1993). At Brucejack, stockwork veining and breccia-veins, and minor vuggy quartz along with adularia, acanthite, and bladed calcite suggest that ore-forming conditions were near surface, and likely involved boiling. However, the absence of open-space fillings and higher molybdenite contents at the Bridge and West Zone prospects suggest deeper levels of deposition for these parts of the deposit, perhaps reflecting a mesothermal or porphyry-style system.

Several previous studies have described the geology and mineralization of the West Zone prospect (Roach and MacDonald, 1992; MacDonald, 1993; Davies et al.,

1994; Kirkham and Margolis, 1995; MacDonald, 1996). However, data are limited to this part of the deposit, and a comprehensive paragenetic and deposit model for the larger Brucejack system is not well developed. In this study we attempt to address this shortcoming by constraining the absolute timing of volcanism and hydrothermal mineralization, establishing the tectonomagmatic affiliation from whole rock lithogeochemistry, establishing a vein paragenesis, and identifying the compositions, temperatures, and sources of ore-forming fluids from fluid inclusion and stable isotope studies.

2.0 Mesozoic–Present Cordilleran Tectonics and Geologic History

The Canadian Cordillera is host to a considerable number of economic deposits that were formed as a consequence of arc-related magmatism throughout the Late Triassic–Early Jurassic. The northwestern Cordillera is subdivided into five tectonic belts that were accreted to the ancient Laurentian craton beginning in the Late Proterozoic, some 750 million years ago (Monger and Price, 2002). From east to west these tectonostratigraphic belts include the Foreland, Omineca, Intermontane, Coast, and Insular belts. The Brucejack deposit is located on the western margin of the Intermontane Belt.

These large tectonic provinces can be divided into several terranes, each having fault-bounded margins and dissociated or "suspect" relationships to adjacent terranes as well as the continent (Fig. 1; Nelson and Colpron, 2007). The Intermontane belt contains several comparable terranes that formed along the North American margin in the Paleozoic to Early Mesozoic, and which have been identified as an affiliated set of

volcanic arcs, marginal seas, and continental fragments (Colpron, 2007). The major parautochthonous, marginal pericratonic terranes belonging to the Intermontane belt include the Yukon-Tanana, Quesnellia, and Stikine terranes (Nelson and Colpron, 2007), collectively comprising the peri-Laurentian realm. The Brucejack deposit is found on the western margin of the Stikine terrane, adjacent to the Coast Complex and the later accreted Alexander and Wrangellia terranes (Fig. 1).

The peri-Laurentian realm abuts a distinctive sequence of Devonian to Permian pillow basalt, gabbro, ultramafic, chert, argillite, and minor carbonaceous rocks of the Slide Mountain terrane (Coney, 1989), which is positioned more inboard and to the east. The Mississippian to Upper Triassic Cache Creek oceanic accretionary complex also bounds this belt of parautochthonous terranes on its eastern margin, and consists of chert, argillite, carbonate, mafic volcanic rock, and alpine-type ultramafic rocks (Monger, 1977; Monger et al., 1978). Paleontological studies indicate that the amalgamated belt of terranes was 2000–3000 km longitudinally offset from the western perimeter of the North American craton by the Early Permian (Belasky et al., 2002). By the Late Permian, subduction of the Slide Mountain Ocean brought the peri-Laurentian realm, or remnants of the Intermontane terranes, closer to North American margin (Colpron et al., 2007).

The current positions of the Intermontane terranes present an enigma, because Stikinia has accreted to the western margin of the Cache Creek terrane, whereas in the late Paleozoic Stikinia is thought to have been located to the east of the Cache Creek terrane. Two competing mechanisms have been suggested to explain this relationship: (1) northward strike-slip fault movement and juxtaposition of Stikinia to the western reaches of the Cache Creek terrane (Wernicke and Klepacki, 1998); or (2) anti-clockwise

oroclinal rotation of the Stikine terrane with no latitudinal variation (Mihalynuk et al., 1994). By comparing stratigraphic, paleomagnetic, and faunal characteristics of the Stikine terrane with other terranes in the Cordilleran collage, Wernicke and Klepacki (1998) suggested that Stikinia tectonically escaped northward via strike-slip faulting beginning in Middle Jurassic time with the collision and penetration of Wrangellia into North America. This tectonic escape led to juxtaposition of Stikinia with the western margin of the Cache Creek terrane (Fig. 1). Although palaeobiogeographic evidence allows for northward advance of Stikinia since Sinemurian and Pliensbachian times, conflicting paleomagnetic results show minimal latitudinal displacements (Mihalynuk et al., 1994; Aberhan, 1999) and can not be explained by this model.

A more popular model, first proposed by Mihalynuk et al. (1994), circumvents the problem of latitudinal displacement and is in concordance with palaeobiological, palaeomagnetic, and stratigraphic data. This model suggests a counter-clockwise oroclinal rotation of Stikinia, pivoting at the Yukon-Tanana terrane (Fig. 3). The enclosure of the Cache Creek Ocean, separating Quesnellia from the more outboard Stikine terrane, occurred by the early Mesozoic. Oroclinal rotation was caused by either: (1) oblique-sinistral convergence of the ancient Pacific oceanic plate with the Stikinia-Quesnellia arc; or (2) trench rollback, resulting in arc migration toward the subduction zone (Mihalyuk et al., 1994; Norkleberg et al., 2000). Distribution patterns of ammonites and bivalves suggest that rotation occurred prior to the Pliensbachian (Aberhan, 1999).

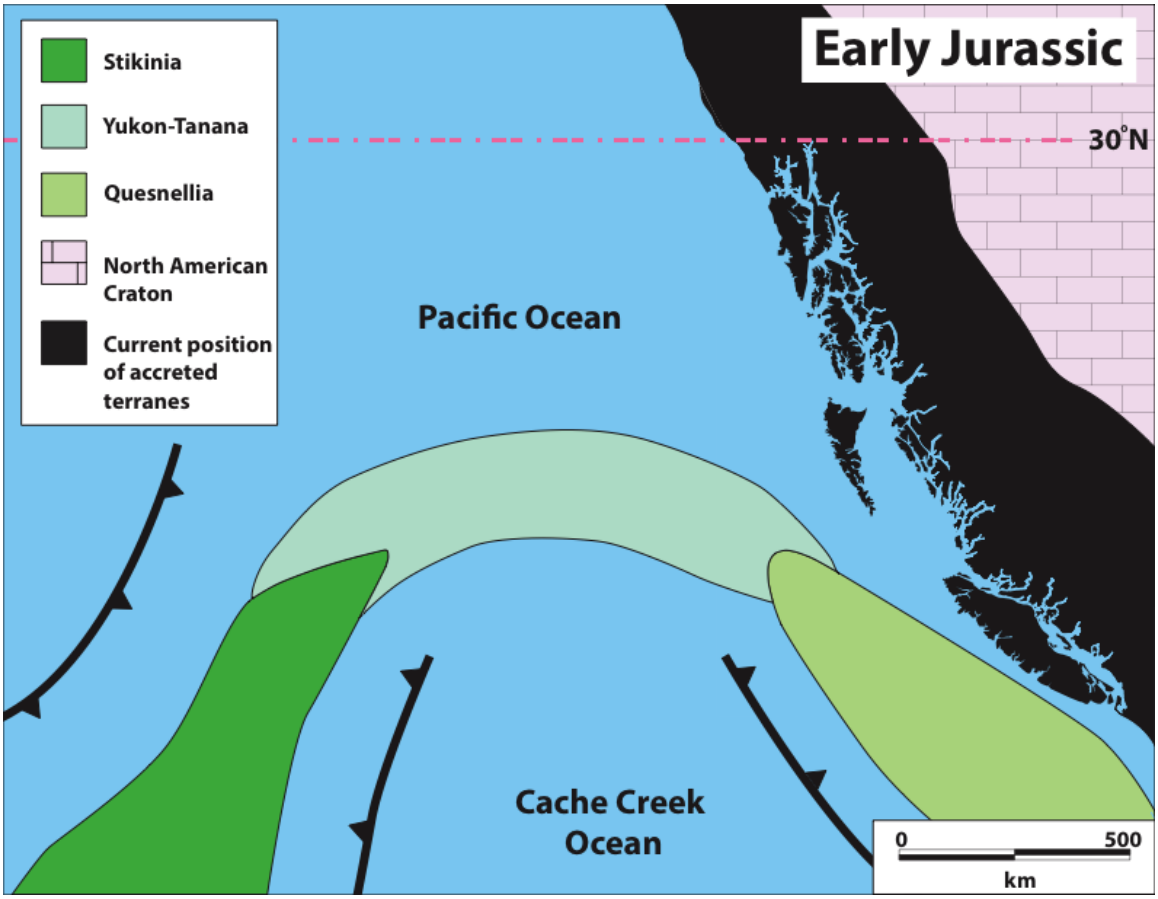

Figure 3: Paleogeographic map of western margin of Canadian Pacific in the Early Jurassic (modified from Nelson and Colpron, 2007; Colpron and Nelson, 2011).

In the final stages of Stikinia rotation, prior to enclosure and collision with the Cache Creek terrane, Stikinia was not part of the Intermontane Superterrane as suggested by Monger et al. (1982). Instead it consisted of an oceanic micro plate with subduction occurring on opposing margins: the Pacific oceanic lithosphere was subducting from the west and the Cache Creek ocean basin from the east (Fig. 4; Marsden and Thorkelson, 1992). This tectonic disposition, analogous to the modern Philippine archipelago (Marsden and Thorkelson, 1992; Thorkelson et al., 1995; Nelson and Colpron, 2007; Gagnon et al., 2012), provided ideal conditions for large-scale volcanism. This arc

magmatism is associated with scores of Late Triassic to Early Jurassic porphyry Cu-Au and Cu-Mo, and porphyry-affiliated deposits throughout Stikinia, making it one of the most significant groups of deposits in British Columbia (Nelson and Colpron, 2007). The duration and complexity of tectonics along the passive western margin of the North American craton at this time is attributed to rich mineral deposits such as the Brucjeack deposit in northwestern British Columbia.

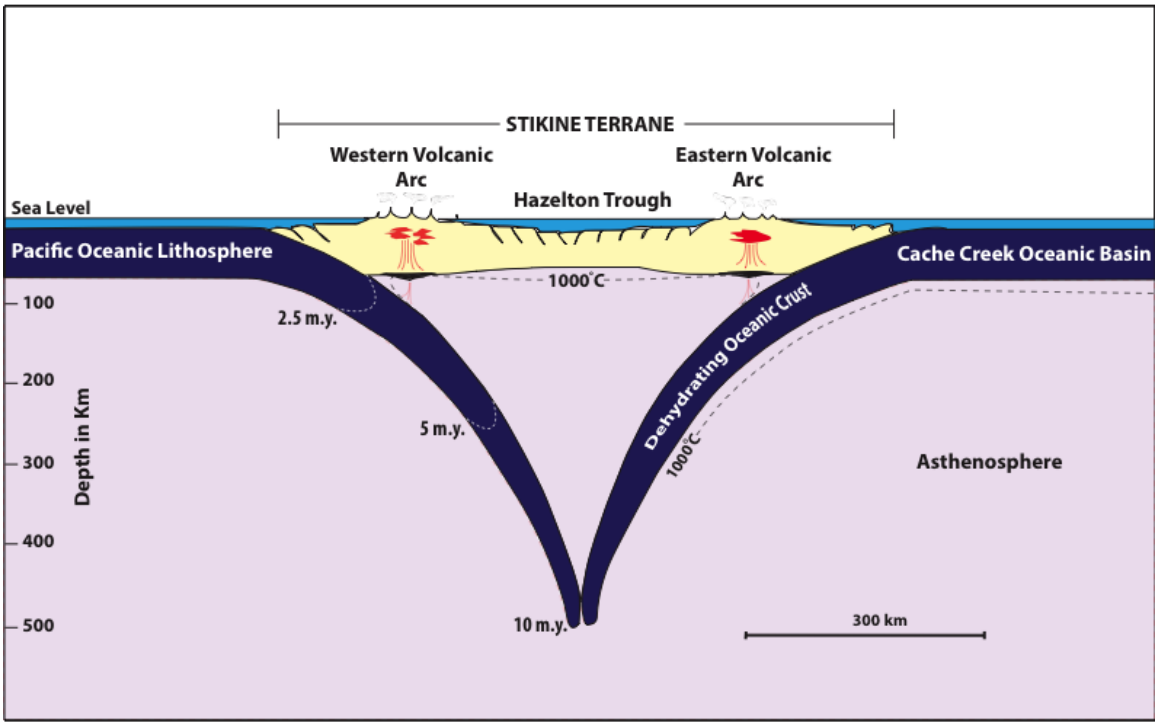

Figure 4: Proposed tectonic setting of the Hazelton volcanic belt in the Early Jurassic. Subduction occurs symmetrically beneath the Stikine micro plate beginning in early Hettangian. Based on subduction rates of 7 cm/yr, positions of the descending oceanic plates are shown for 1.5, 5, and 10 m.y. of subduction (modified from Marsden and Thorkelson, 1992).

The Jurassic period in the Canadian Cordillera saw the Laurentian cratonic margin evolve from a series of island arcs, marginal basins, and offshore crustal blocks and fragments to an accretionary orogen (Gagnon et al., 2012). Monger et al. (1972) suggested that the Stikinia and Cache Creek terranes had accreted by Late Triassic time based on evidence that radiolarian chert of the Cache Creek terrane is intercalated with greywacke coeval with Upper Triassic volcaniclastic rocks of Stikinia. However, Cordey et al. (1987) showed that deposition of radiolarian cherts continued to at least Pliensbachian to Bajocian time, suggesting an Early–Middle Jurassic age of accretion. Furthermore, Cache Creek deformation is estimated to have occurred at around 152 ± 5 Ma (K-Ar on hornblende; Mortimer, 1987) for southern British Columbia latitudes, indicating a Middle Jurassic age of regional deformation and accretion. Thus, accretion of the Stikinia and the Cache Creek accretionary complex to North America is considered to have occurred by the Middle Jurassic (Mortimer, 1987; Cordey et al., 1987; Samson et al., 1989; Norkleberg et al., 2000; Mihalynuk et al., 2004).

As the Stikine terrane impinged and eventually collided with the already accreted Quesnel terrane, Hazelton Group volcanism, which hosts the Brucejack deposit, waned and ultimately stopped, as did volcanism in Quesnellia. With Stikinia-Quesnellia arc accretion beginning at about 185 Ma (Norkleberg et al., 2000), the Cache Creek accretionary complex and remaining ocean floor became trapped between the two arcs (Nelson and Colpron, 2007) and signaled the start of mountain building in the North American Cordillera. Multiple southward-oriented thrust faults and affiliated folds involving Triassic and Jurassic strata in northern Stikinia were formed from the convergence of the Cache Creek terrane, likely producing the King Salmon Fault

(Gabrielse, 1991). By the Early Jurassic the Stikine terrane underthrust the Cache Creek terrane along the SW-verging Nahlin and King Salmon faults (Monger and Price, 2002). Sedimentary detritus from the overthrust Cache Creek terrane deposited in the Bower Basin, a large, deep, subsiding sedimentary basin (Gagnon et al., 2012). Deep-water siliclastic sedimentary rocks consisting of siltstones, shale, sandstone, and conglomerate were deposited and collectively contribute to 4000 m of Bowser Basin Group stratigraphy (Evenchick, 1991, and references therein).

The amalgamation and eventual accretion of the Intermontane and Insular superterranes to the continent coincided roughly with the separation of North America from Africa (~180 Ma; Coney, 1972), leading to the opening of the Atlantic Ocean. The North American plate began to move rapidly westward causing outboard terranes to collide (Nelson et al., 2013), and culminating with accretion and collision of the Insular Belt terranes. Accretion of the Alexander and Wrangellia terranes to the western margin of Stikinia caused crustal thickening by tectonic stacking of crustal slabs (Crawford et al., 1987); estimated pressures exceeding 7 kbar through prograde metamorphism in high-grade metasedimentary rocks suggest depths of burial >25 km (Monger et al., 1982). Subsequent thrusting tectonically exhumed the supracrustal rocks, which form part of the Coast Plutonic metamorphic sequence. Late Cretaceous east-directed thrusting is recognized up to 700 km along the eastern margin of the Coast Plutonic Complex (Rushmore and Woodsworth, 1991), which is composed of mainly of metamorphic and plutonic rocks ranging in age from Jurassic to Eocene (Coney and Evenchick, 1994).

Through the Early Jurassic into the late Paleocene (185–58 Ma) the arc region was mainly under compression coupled with sinistral and dextral transpression (Monger

and Price, 2002), leading to considerable strike-slip movements throughout the Canadian Cordillera. This transcurrent motion, mainly established on consolidated terrane boundaries, likely occurred in response to oblique subduction (Monger et al., 1972). This Early Cretaceous deformation affected much of the eastern margin of the Coast Plutonic Complex (Rusmore and Woodsworth, 1991), including Brucejack rocks and the surrounding area. The deformation was accompanied by metamorphism throughout much of Stikinia. Metamorphic grade throughout the region is lower greenschist facies, with maximum temperatures and pressures of ~290°C and 4.5 kbar respectively (Alldrick, 1993). From field relationships, Alldrick (1993) suggested that metamorphism and deformation was restricted to between the deposition of 175 Ma sedimentary rocks in the Stewart mining camp and the intrusion of the unaltered 55 Ma Hyder Plutonic Suite.

The largest exposure of contractionally deformed rocks east of the Coast Belt is the Skeena Fold Belt (Crawford et al., 1987; Evenchick, 2001). The Skeena Fold Belt is a regional fold and thrust belt occurring mainly in the sedimentary detritus of the Bowser Basin, and stretches nearly the entire width of the northern Intermontane Belt (Evenchick, 1991a, b, 2001). Crustal thickening in the Coast Plutonic Complex, with dextral strike-slip faulting east of the Skeena Fold Belt, and shortening and compression in the Rocky Mountain Fold and Thrust Belt resulted in as much as 160 km of northeastward shortening in the Skeena Fold Belt (Evenchick, 1991a). The McTagg anticlinorium and the southeasterly directed Sulphurets thrust fault (two other structurally significant features in northwestern Stikinia; Fig. 5), are consistent with Late Jurassic to Early Tertiary structural features in the Skeena Fold Belt, located 150 km to the northwest (Bridge, 1993). Additionally, throughout the Late Cretaceous and extending into the

Tertiary, 860 km of northward translation of the Intermontane terranes occurred along dextral transcurrent strike-slip faults (Denali and Tintina Faults; Gabrielse et al., 2006; Colpron et al., 2007): this is not to be confused with northward strike-slip faulting occurring in the Middle Jurassic suggested by Wernicke and Klepacki (1998).

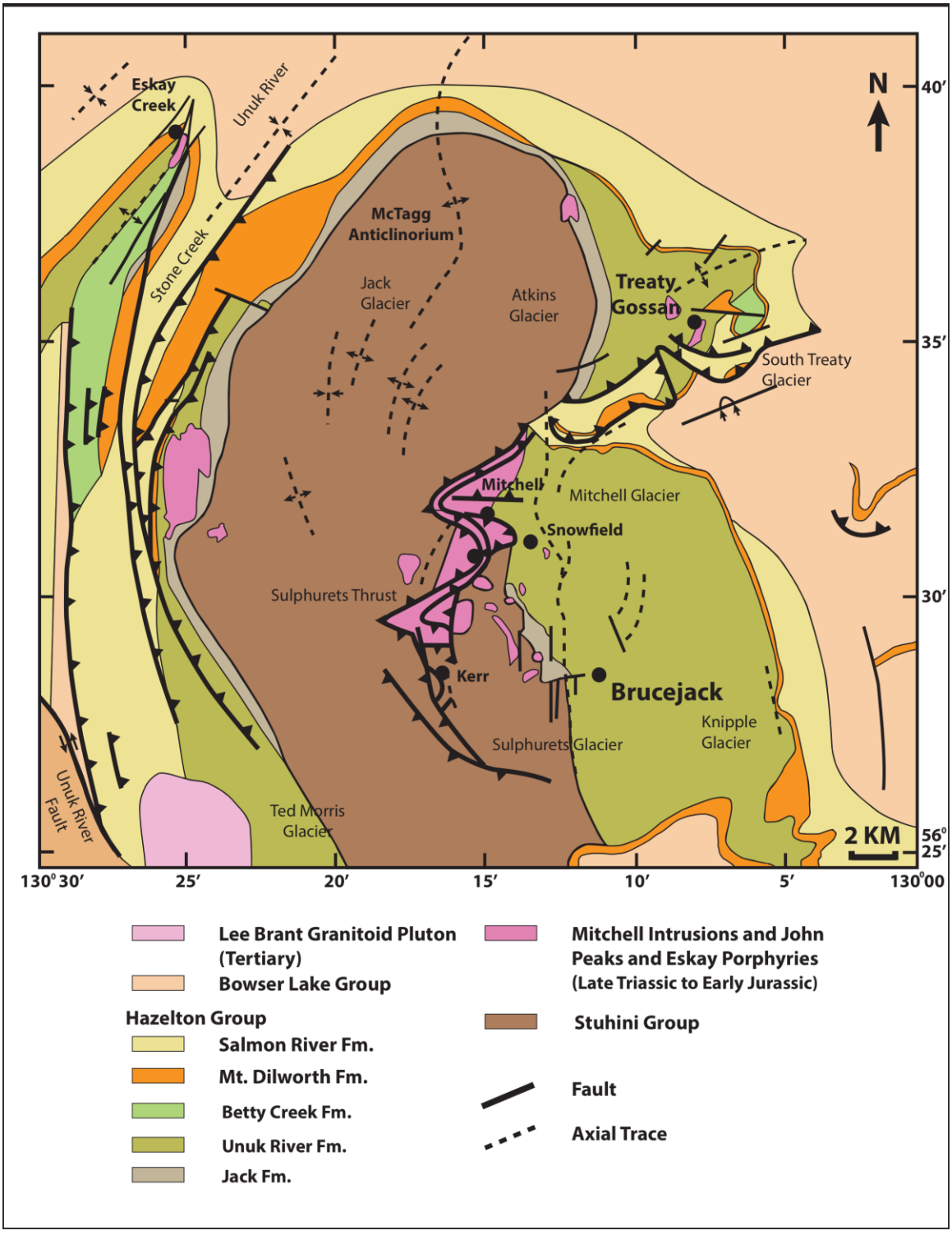

Figure 5: Regional geologic map showing relevant structural features and proximal deposits (modified from Kirkham and Margolis, 1995).

By the Middle Eocene (~45 Ma) Cordilleran magmatism had waned and volcanism had shifted to the Aleutian arc and Cascades of southern British Columbia and western United States (Norkleberg, 2005; Nelson and Colpron, 2007). Shortly thereafter, by ~40 Ma, formation of the Coast Plutonic Complex suddenly ended, perhaps in response to interrupted subduction off the west coast of Canada (Nelson and Colpron, 2007). At this time in the late Cenozoic the Pacific margin may have experienced decreased compressive stress due to slowed subduction of the easterly subducting Juan de Fuca plate and northerly subducting Pacific plate (Coney, 1987), possibly shifting volcanism to the current tectonic regime.

3.0 Regional Geological Setting of the Brucejack Deposit

The Sulphurets mineral district is located in western Stikinia and is approximately 25 km east of the Coast Plutonic Complex, which is dominated by Tertiary igneous intrusions and high-grade metamorphic rocks (Kirkham and Margolis, 1995). Regionally, the mineral district is underlain by the Early Devonian to late Paleozoic Stikine assemblage (Monger, 1977), Late Triassic volcanic and sedimentary rocks of the Stuhini and Talka Groups (Monger and Church, 1977; Brown and Greig, 1989), Early to Middle Jurassic rocks (mainly volcanic) of the Hazelton Group (Marsden and Thorkelson, 1992), which host the Brucejack deposit, and Middle Jurassic to Middle Cretaceous sedimentary rocks belonging to the Bowser Lake Group (Ricketts et al., 1992).

The Stikine assemblage, as described by Monger (1977), consists of upper Paleozoic rocks exposed around the perimeter of the Bowser Basin and west and southwest of the Cache Creek Group accretionary complex. The Stikine assemblage is

present as northwest to northeast-trending belts of Early to Middle Devonian, Carboniferous, and Permian rocks in the Iskut River area (Brown et al., 1991), and is the stratigraphic basement of Stikinia. This unit consists of Lower to Middle Devonian deformed and metamorphosed dacitic to rhyolitic lithic tuffs with lesser intermediate to mafic flows with thinly interbedded laminated sandstones, carbonate, shale, minor chert and aphanitic dacitic tuffs (Gunning, 1990; Monger, 1977).

Uplift and erosion within the Permo-Triassic (Tahltanian) period led to unconformable deposition of Late Triassic Stuhini Group volcaniclastic rocks onto Early Permian limestone of the Stikine assemblage (Logan and Koyanagi, 1994). Stuhini Group stratigraphy consists of dark grey turbiditic siltstone interbedded with minor micritic limestone (Kirkham and Margolis, 1995), subaqueous mafic crystal-lithic lapilli tuff, lapilli tuff-breccia, and ash tuff (Brown and Greig, 1990), and pyroxene-phyric breccia flows interlayered with massive andesites and coarse-bladed feldspar porphyry flows (Logan and Koyanagi, 1994). Stuhini Group dark turbiditic sandstones are found to the immediate west of the Brucejack deposit. The Talka Group stratigraphically overlies the Stuhini Group succession, and consists of subaerial and submarine intermediate lava flows and breccias with interbedded sedimentary conglomerate and shale (Monger and Church, 1977).

The Early to Middle Jurassic Hazelton Group unconformably overlies the Late Triassic Stuhini and Talka Groups and is composed of diverse volcanic rocks including: subaerial to subaqueous heterogeneous mafic to felsic volcanic rocks (tholeiitic to calc-alkaline compositions), polymictic conglomerate, sandstone, and other coarse-grained interbedded sedimentary rocks (Tipper and Richards, 1976). Calc-alkaline and tholeiitic

rocks are geochemically constrained by depletions of Nb and Ti, and enrichments in large ion lithophile elements relative to high-field-strength elements (Marsden and Thorkelson, 1992), indicating a subduction-related genesis. Marsden and Thorkelson (1992) suggested that Hazelton Group magmatism persisted for about 35 m.y. from the Hettangian or lower Sinemurian to the Bajocian.

Brucejack mineralization is hosted by Hazelton Group rocks, and in the Iskut River area they have been subdivided into five formations: the Jack, Unuk River, Betty Creek, Mount Dilworth, and Salmon River Formations (Fig. 6; Grove, 1989; Anderson and Thorkelson, 1990; Gagnon et al., 2012). The Brucejack deposit is contained within the Unuk River and Betty Creek Formations. Lower Hazelton Group volcanic rocks are calc-alkaline to tholeiitic and have typical arc geochemical signatures (Anderson and Thorkelson, 1990; Logan et al., 2000). Deposition was likely in oxidizing subaerial environments, probably building stratovolcanoes within an evolving arc system (Alldrick et al., 1989; Gagnon, 2012).

The basal unit of the Hazelton Group, the Jack Formation, is exposed along the edge of the northern and northwestern limbs of the McTagg anticlinorium to the northwest of the Brucejack deposit (Fig. 5; Jakobs and Palfy, 1994). The Jack Formation is comprised of granitoid-clast conglomerate and limy fossiliferous sandstone and siltstone horizons (Kirkham and Margolis, 1995). Ammonoid and bivalve assemblages found locally within calcareous mudstone provide a Hettangian–Sinemurian age constraint (MacDonald et al., 1996). The Jack Formation is succeeded by thick accumulations of hornblende-plagioclase-phyric andesitic to dacitic flows and subordinate volcanic breccias and fragmental rocks with local interbedded lapilli–block

tuff, and minor volcaniclastic wacke of the Unuk River Formation (MacDonald et al., 1996). These rocks are overlain by the Betty Creek Formation, a distinct succession of andesitic and dacitic pyroclastic and epiclastic rocks, interbedded by mafic flows and dark carbonaceous mudstone (Kirkham and Margolis, 1995), which have a variable vertical thickness of up to 1200 m (Alldrick, 1993). Maroon-coloured clastic sedimentary rocks of the Betty Creek Formation are disconformably overlain by massive, aphanitic green to maroon ash tuffs of the Mount Dilworth Formation (Alldrick, 1993). The Mount Dilworth Formation contains felsic pyroclastic rocks and flows, and also includes thin interbedded welded and non-welded tuffaceous rocks (Roach and MacDonald, 1992). The resistive nature of the felsic pyroclastic and flow horizons coupled with their large lateral extent make the Mount Dilworth Formation an important stratigraphic marker unit.

Pliensbachian fossils in the underlying Betty Creek Formation and Toarcian fossils found in the overlying Salmon River Formation (belemnites and *Weyla*; Anderson and Thorkelson, 1990) constrain the age of the Mount Dilworth Formation to the Early Jurassic (Marsden and Thorkelson, 1992). The complexly folded Salmon River Formation is composed of siltstones and wackes with locally interbedded homogeneous conglomerates, limestones, tuffaceous siltstones (Alldrick, 1993), and voluminous basaltic sequences, which occur as pillowed to massive flows in the eastern Iskut River area (MacDonald et al., 1992). These mafic volcanic rocks host the Eskay Creek precious metal-rich volcanogenic massive sulfide deposit.

It should be recognized that both Anderson and Thorkelson (1990) and Alldrick (1993) suggested that the Salmon River Formation belongs to the upper Hazelton Group, although Britton (1991) and Henderson et al. (1992) suggested that it belongs to the lower

Bowser Lake Group. Hazelton Group rocks are conformably overlain by the Middle Jurassic to Middle Cretaceous Bowser Lake Group and are composed of clastic sedimentary rocks consisting of fine-grained subaqueous sandstone, siltstone, and shale with turbidite successions and chert pebble conglomerate (Evenchick et al., 1992).

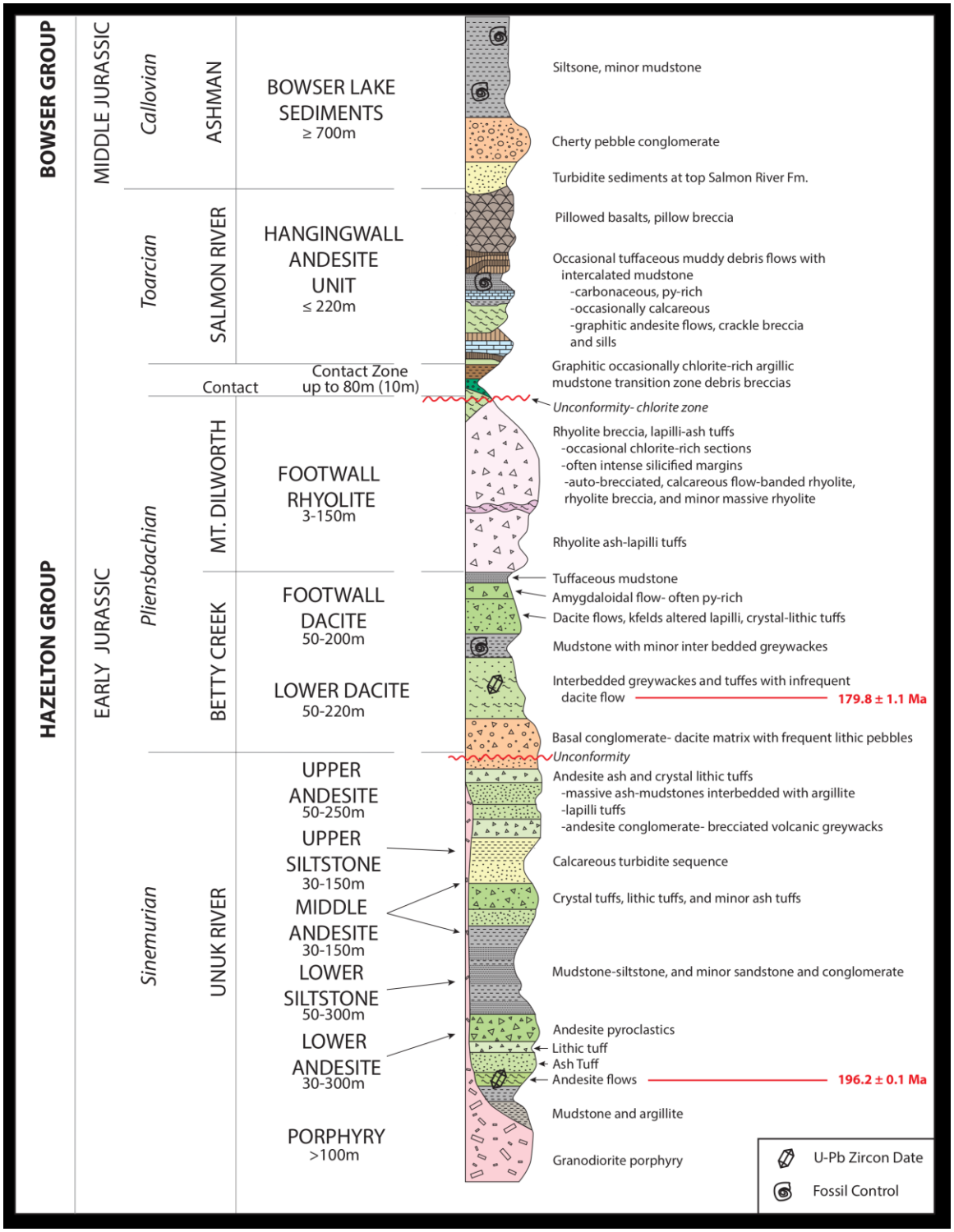

Figure 6: Regional stratigraphic column (modified from McCrea, 2007; Konkin, 2007)

4.0 Brucejack Deposit Geology

Several authors have published lithostratigraphic observations at, or near, Brucejack Lake (Davies et al., 1994; Henderson et al., 1992; Kirkham and Margolis, 1995; MacDonald, 1993; Roach and MacDonald, 1992), and many authors have published geologic maps of the immediate area (e.g. Kirkham, 1963,1992; Alldrick and Britton, 1988; Britton and Alldrick, 1988; Febbo et al., 2015). Brucejack mineralization occurs within thick sequences of interbedded volcaniclastic sedimentary rocks, and intermediate composition porphyritic lava flows, and crystal–block fragmented tuffaceous rocks of the Early Jurassic Hazelton Group, which overlies the Late Triassic Stuhini Group. Lithological contacts between these differentiated units are mostly sharp, but are commonly gradational between Hazelton Group sedimentary and volcanic rock units. Stuhini Group rocks are found generally to the west of the Brucjeack Fault, where unconformable, younger Hazelton Group rocks occur to the east, suggesting tilted stratigraphy and an eastward younging progression. Stratigraphy at Brucejack is complex due to the severity of folds and faults (Davies et al., 1994), which are suggested to have formed in the Early Jurassic and later in the Cretaceous. The Brucejack deposit appears to have been formed after the main stage of folding, which likely occurred in response to arc collision events on the continental margin, although the exact timing of deformation is unknown due to later Cretaceous deformation. However, strong hydrothermal phyllic alteration and post-mineralization faulting and folding, have also affected Brucejack (see below).

Large pyritic gossans containing intensely sericitized (phyllic) altered rocks occur at surface throughout the Sulphurets mining camp. Mineralization at Brucejack occurs

mainly beneath an approximate north–south trending band of heavily phyllic-altered (quartz-sericite-pyrite) Early Hazelton Group rocks running parallel the Brucejack Fault (a major north–south-trending structure to the immediate west of the deposit). Gold at Brucejack is present as gold-rich electrum and is found in all lower Hazelton Group lithologies.

The deposit is subdivided into nine zones based on mineralization style, alteration, and stratigraphic features. From north to south, these are: Golden Marmot, Bonanza Zone, Gossan Hill, Shore Zone, West Zone, Galena Hill, Valley of the Kings (VOK), Waterloo, and Bridge Zone (Fig. 7). Current exploration is focused on bonanza grade gold mineralization found in the VOK, West Zone, and Bridge Zone prospects, which are the focus of this study (Fig. 8).

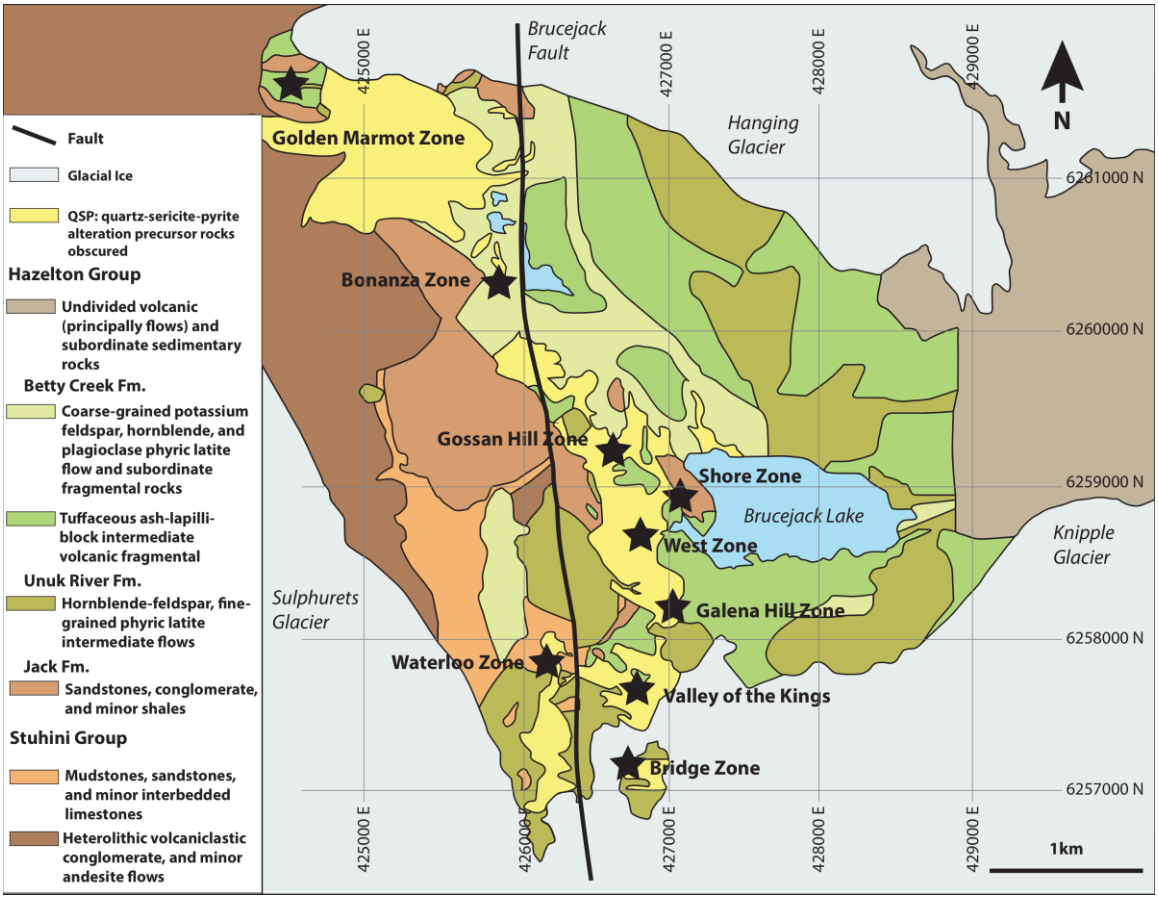

Figure 7: Geology of the Brucejack deposit and locations of main mineralized zones (modified from Ghaffari et al., 2010). UTM zone: NAD83-9V.

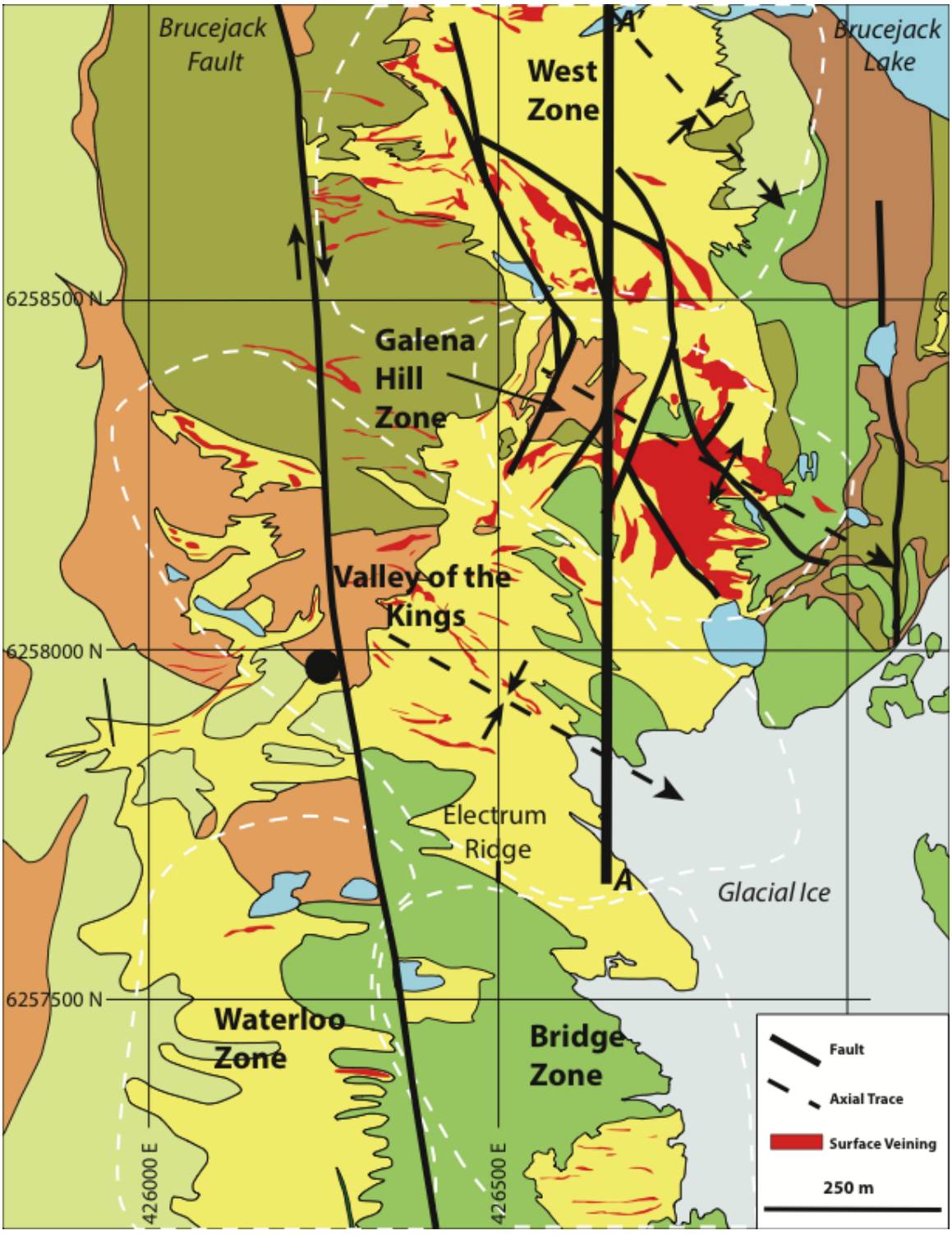

Figure 8: Detailed map of West Zone to Bridge Zone. Refer to legend in Figure 7 for lithologies. Ore zone boundaries are shown with white dashed line. Black dot indicates location of photo in Figure 9. Cross-section in Figure 10 is defined by solid line with limits A–A'. UTM zone: NAD83-9V (modified from Ireland et al., 2013)

4.1 Ore Zones

4.1.1. Valley of the Kings

The Valley of the Kings (VOK) zone is defined over a 1000 m southeast–northwest extent, 600 m northeast–southwest, and 650 m in vertical extent from surface (Ireland et al., 2014) and at surface is blanketed by abundant oxidized pyritic gossans (Fig. 9). The mineralization in this zone follows the alignment of Electrum Ridge (Figs. 8 and 9; trending west-northwest to east-southeast), a topographic high where Bridge Zone lies above, to the south. The north–south trending Brucejack fault crosscuts western VOK stratigraphy, where rocks are displaced tens of meters (see below for detailed description). The Valley of the Kings forms a syncline containing moderately sericitized pyroclastic and volcaniclastic sedimentary rocks plunging moderately to the east-southeast (Figs. 8 and 10).

Pyroclastic rocks overlie a polymictic conglomerate sequence with abundant pervasive silicification near the basal contact with volcanic sandstone, siltstones, and monomictic conglomerates. Fine-grained plagioclase feldspar ± potassium feldspar ± hornblende porphyritic volcanic latite flows occur below these volcanic sedimentary rocks (~830 m below surface; not shown in Fig. 10) and extend to unknown depths. Siliceous horizons of strongly and pervasively altered conglomerate occur on both limbs of the syncline and are generally cospatial with intervals of intense stockwork veining and lithological contacts. Adjacent to silica alteration, conglomerates are commonly completely metasomatized to monomineralic green sericite for several meters. Mineralization in this zone occurs mainly in deformed quartz stockwork veins and

breccias, deformed carbonate-quartz stringer veins, and highly deformed pinch and swell carbonate veins. Sparse cockade and crustiform banded veins occur proximal to large stockwork systems in the VOK. Gold is hosted by all lithological units, and Au:Ag ratios in the VOK are typically 2:1 or higher (Ireland et al., 2014). Exploration drilling in this zone commonly intersects high-grade gold, with values as high as 41582 g/t Au over 0.5m.

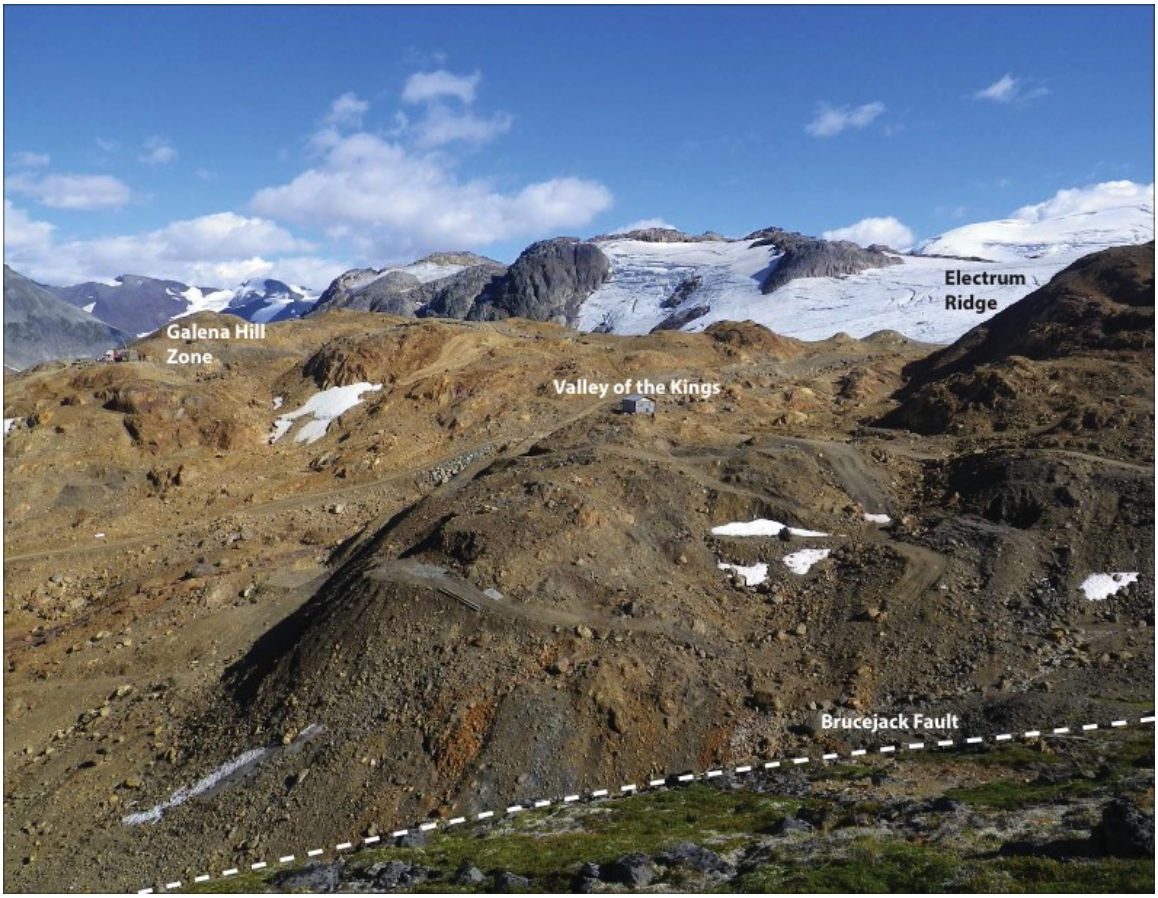

Figure 9: Photograph looking east over the Valley of the Kings (VOK) prospect showing surface gossans and intense phyllic alteration. Bridge Zone is located to the immediate south of Electrum Ridge.

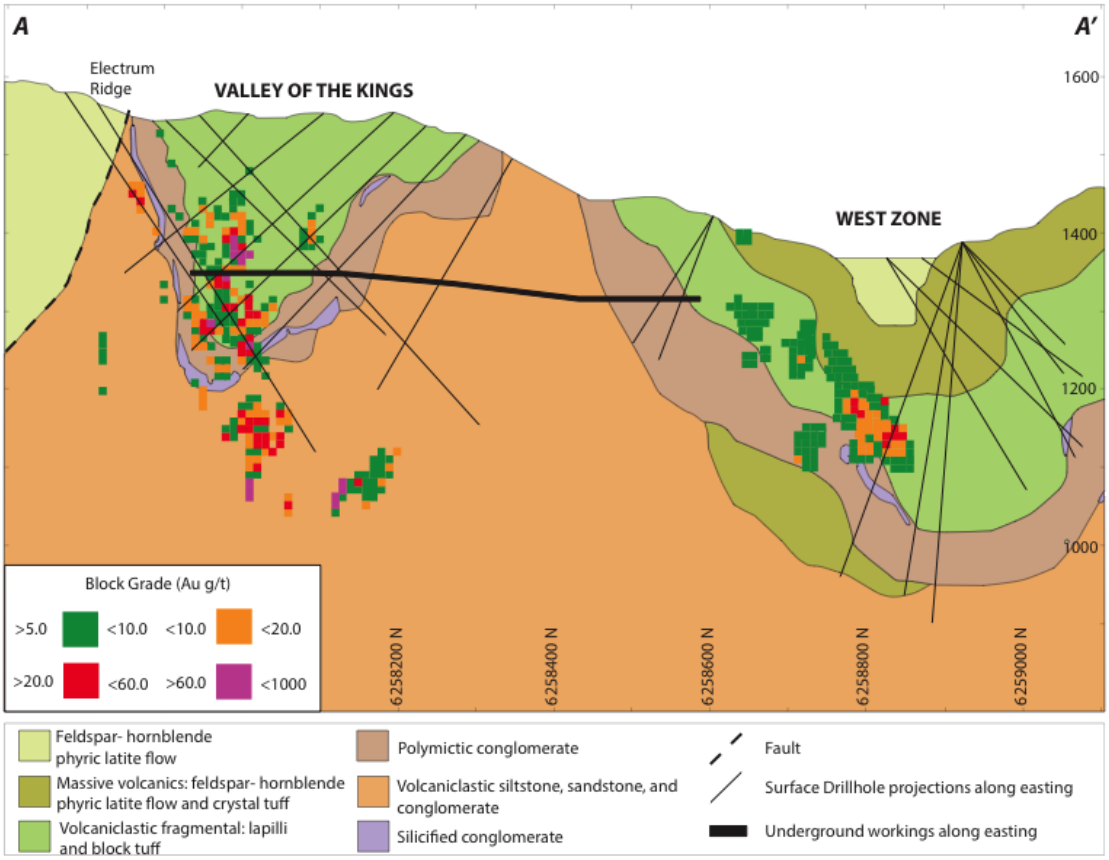

Figure 10: VOK to West Zone geological section along 426600E (looking west; modified Jones, 2013). High-grade gold blocks are 10x10 m, using measured and indicated resource categories.

4.1.2. West Zone and Shore Zone

West Zone and Shore Zone rocks are believed to correlate with northwesterly trending volcanic and sedimentary rocks of the Lower Hazelton Group, Unuk River Formation (Alldrick and Britton, 1988; Britton and Alldrick, 1988; Roach and MacDonald, 1992). Intermediate composition tuffs and derived sedimentary rocks are present and are highly silicified proximal to deformed quartz stockwork and vein offshoots. Volcanic and sedimentary rocks in this area also form a syncline plunging to the southeast, similar to the VOK (Fig. 10). The West Zone and Shore Zone contain gold

and silver grades exceeding several grams per ton, and have anomalously high Ag/Au ratios with respect to the rest of the property. Pre-mineralized sericite ± quartz ± carbonate alteration of wallrocks is present throughout the host lithologies and is texturally destructive and consistent with other prospective ore zones on the property. This alteration is continuous in a north–south trend, although is mainly restricted to 500 m east–west. Similar to other prospects at Brucejack, pervasive phyllic alteration is also penecontemporaneous with mineralized veins. MacDonald et al. (1996) recognized that low-sulfidation epithermal features are present peripheral to West Zone, including cockade and crustiform textures, cryptocrystalline quartz, and replacement of bladed calcite by quartz (indicating boiling conditions).

4.1.3. Bridge Zone

Bridge Zone is located on a topographic high to the south of Valley of the Kings and to the immediate north and west of the Sulphurets glacier. The Bridge Zone is hosted by fine-grained feldspar-amphibole-porphyritic latite flows, which are cut by quartz veinlets and stockworks. Pervasive sericite, chlorite, and minor carbonate-altered wallrock is common throughout Bridge Zone volcanic host rocks.

4.2 Host Rocks

4.2.1. Volcanic Host Rocks

Volcanic host rocks at Brucejack are plagioclase feldspar ± potassium feldspar ± hornblende-phyric latite flows (Fig. 11a), and are described in the field on the basis of

their phenocryst mineralogy and grain-size. Fine-grained porphyritic rocks have smaller (<3 mm) phenocrysts, whereas their coarse-grained counterparts have larger crystals. Phenocrysts in these porphyritic rocks are mainly plagioclase feldspar, with small amounts of hornblende, and potassium feldspar. Throughout the north–south band of phyllic alteration (Figs. 7 and 8), these rocks are strongly sericite-, chlorite-, and carbonate-altered. Phenocrysts in these rocks are commonly replaced by sericite and calcite (Fig. 11b, c); pyrite (up to 10%) commonly accompanied by rutile occurs as replacements along cleavage planes of relict mafic phenocrysts (Fig. 11d). Porphyritic flows have been dated in the Valley of the Kings and in the far eastern limits of Brucejack, yielding U/Pb zircon dates of 196.2 ± 0.2 Ma (SU-277) and 179.8 ± 1.1 Ma (ST2015-002) respectively (Appendix I; pers. comm. W. Board, June 2015). These dates support the interpretation of tilted stratigraphy with a general younging progression to the east.

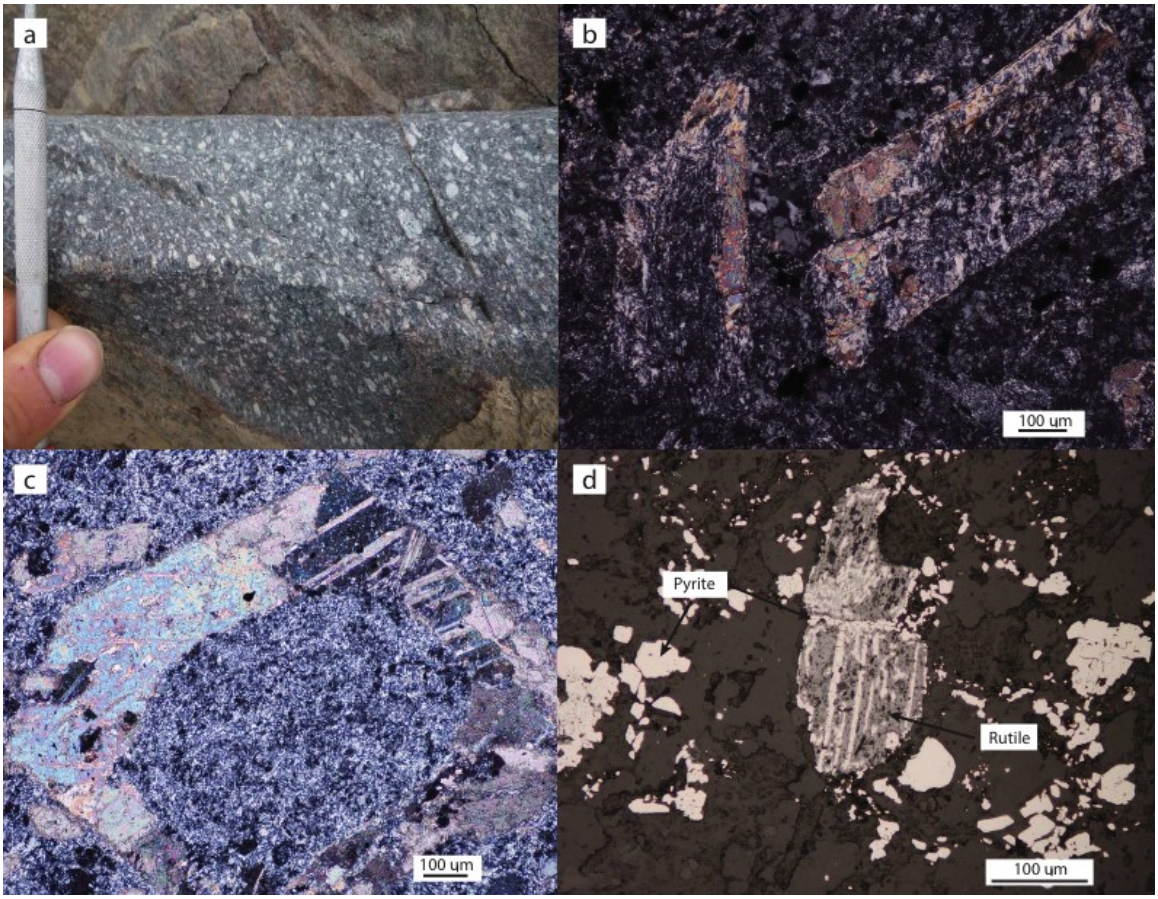

Figure 11: Photographs and microphotographs of altered Brucejack lithologies and mineralogical features: (a) Megacrystic feldspar-hornblende latite porphyritic flow with sericite-replaced phenocrysts (426910E, 6258686N, 1389 m); (b) cross-polarized microphotograph of relict feldspar phenocrysts replaced by sericite and calcite (sample A2); (c) cross-polarized microphotograph of megacrystic feldspar-hornblende latite porphyritic flow with sericite and calcite replacing hornblende phenocryst (sample A11); (d) reflected light microphotograph of rutile replacing relict hornblende or pyroxene phenocrysts and pyrite growing along cleavage planes (sample A2).

4.2.2. Volcaniclastic and Sedimentary Rocks

Volcaniclastic fragmental rocks are variably derived from pophyritic flows and welded crystal tuffs. Lapilli to block-sized fragments are typically angular to sub-angular and are poorly sorted (Fig. 12a), and fragments are typically much darker green than their

groundmass hosts. The groundmass is composed of fine-grained quartz, plagioclase feldspar, and sericite, carbonate, and chlorite alteration products. Rutile and euhedral pyrite are also disseminated throughout the groundmass, where pyrite mineralization may locally exceed 15% (Fig. 12b). Alteration is locally intense, perhaps reflecting higher water/rock ratios within more permeable horizons.

Volcanic sedimentary rocks show evidence of deposition under both subaerial and subaqueous dynamic conditions. Volcanic conglomerates, sandstones, and siltstones are generally massive, although sandstone and siltstone horizons commonly have relict bedding where pyrite replaces bedding. Sedimentary rocks have variable grain sizes, and are typically strongly altered to sericite, carbonate, and chlorite. Pebble to boulder polymictic conglomerates typically are well to moderately sorted, with sub-rounded clasts containing variable amounts of sandstone, siltstone, rare porphyritic latite, dark argillite siltstone, and silicified clasts (Fig. 12c). Alteration is locally heterogeneous, and individual clasts may be either sericitized, chloritized, or silicified. Complete monomineralic metasomatism of sedimentary rocks (most commonly polymictic conglomerate rocks) to apple green sericite (Fig. 12d) locally exists for several meters at the basal and upper contacts with strongly silicified polylithic clastic sedimentary rocks in the VOK and to a lesser extent in West Zone. Strongly silicified wall rocks contain hydraulic fracture veinlets, which may be evidence for local overpressure conditions (Fournier, 1999). Volcaniclastic siltstones (Fig. 12e) are generally subaqueous and have abundant, variably sized calcite-chlorite-pyrite-replaced concretions; black argillaceous mudstones contain abundant pyrite mineralization forming along relict bedding planes (Fig. 12f). Volcaniclastic sandstones are also common throughout the sedimentary

package, and are commonly found interbedded with volcaniclastic siltstone and monomictic conglomerate. These volcanic-sedimentary sequences yielded U/Pb zircon ages between 196 and 188 Ma (pers. comm. W. Board, June 2015).

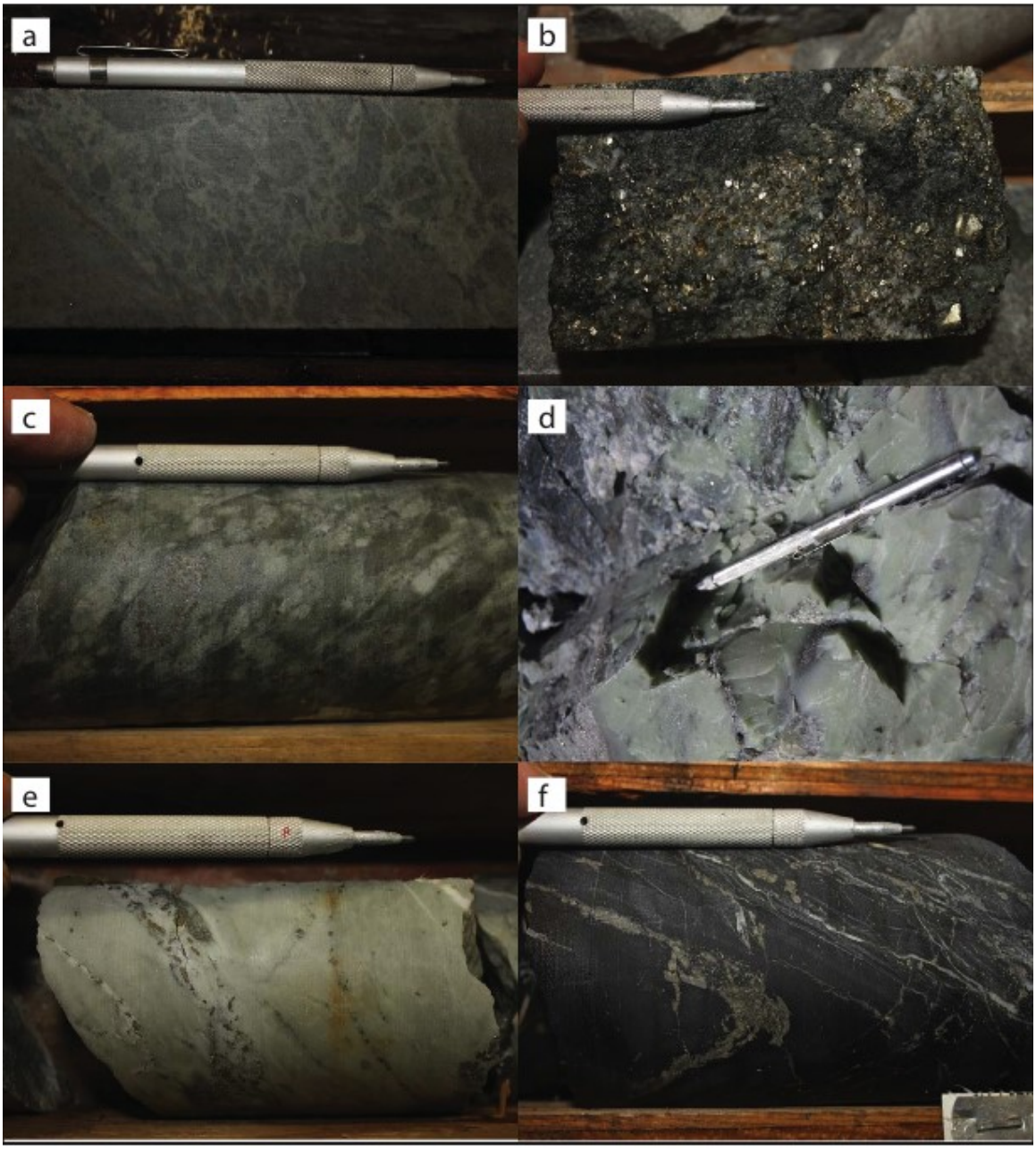

Figure 12: Photographs and microphotographs of Brucejack lithologies and mineralogical features containing: (a) Lapilli tuff showing abundant sericitized groundmass (light-coloured) and chloritized subangular fragments (dark-coloured; SU-125 at 55m: 426435E, 625739N, 1488 m); (b) Intense pyritic mineralization with 2-5 mm euhedral pyrite crystals (SU-289 at 410m: 426648E, 6257959N, 1160 m); (c)

Clast supported polylithic conglomerate with variably altered subrounded, moderately sorted clasts (sample A17); (d) volcaniclastic sandstone altered to pure sericite (426565E, 6258113N, 1325 m); (e) Coarse-grained volcaniclastic siltstone with minor discontinuous pyrite stringers (SU-632 at 584m: 426534E, 6257984N, 995 m); (f) Siliceous black argillaceous siltstone with abundant pyrite stringers, mainly following bedding (SU-460 at 149m: 426370E, 6258137N, 1403 m)

4.2.3. Post-mineralization Mafic Dykes

Post-mineralization trachybasaltic dykes are the most common dykes found at Brucejack. They are subvertical and generally <1.5 m wide (Fig. 13), with northwest–southeast and north–south trends. The dykes cross-cut all lithologies and ore zones, but commonly follow fluid pathways in the ore zones, and are cross-cut by late-stage, barren tectonic veins. These dykes have been weakly deformed by a late-stage east–west compressive deformation event, although they cross-cut penetrative fabric and folding within sedimentary horizons. They are commonly a dark olive green colour and contain small (<4 mm) calcite-filled amygdules. The fine to medium-grained groundmass is pervasively altered to sericite and carbonate, while minor chlorite, euhedral pyrite, and anhedral rutile are also variably present. Igneous mineralogy and relict textures are heavily masked by the pervasive alteration, making identification difficult. One of these dykes has been dated at 182.7 ± 1.0 Ma (U/Pb zircon; sample SU-562; Appendix I; pers. comm. C. Greig, June 2015) suggesting emplacement immediately after mineralization, but before hydrothermal activity had ceased.

Figure 13 Trachybasaltic dyke showing subvertical nature (205/85W; underground location at 426664E, 6258158N, 1293m)

4.2.4. Cenozoic Basaltic Trachyandesite Dykes

Cenozoic basaltic trachyandesite dykes (up to several meters wide) also occur at Brucejack, most commonly intruding strata to the east of the Brucejack fault, and are not typically found intruding ore zones. These dykes are undeformed, and cross-cut all fabric, folding, veins, alteration zones, and earlier intruded trachybasaltic dykes, and are interpreted to be Cenozoic in age (and unrelated to the Mesozoic sequence and Brucejack mineralization). The dykes are aphyric and relatively unaltered, although small (<2 mm) calcite-filled amygdules occur throughout, and minor chlorite and pyrite occur in the groundmass, which consists of fine-grained plagioclase feldspar, quartz, hornblende, actinolite, biotite and magnetite.

4.3 Structure and Metamorphism

The Brucejack fault is a significant structure occurring to the immediate west of West Zone. The fault is a steeply dipping (>60˚E), dextral, north-striking, oblique dextral and reverse dip-slip fault that cross-cuts all stratigraphic successions, dykes, vein networks, and alteration zones (Davies et al., 1994). As fault movements have occurred at different times, the structure may have been reactivated at unspecified times before and after mineralization. Structural fabrics and offset contacts near the Mitchell Glacier provide evidence for east side down, reverse dip-slip displacement exceeding 500 m (Kirkham, 1963; Kirkham and Margolis, 1995). Preserved slickenside and cast elongation lineations northwest of Brucejack Lake also indicate a sense of reverse vertical movement (Davies et al., 1994). At Brucejack, contacts are only offset dextrally tens of

meters, with an unknown vertical component (Britton and Alldrick, 1988; Davies et al., 1994; Kirkham and Margolis, 1995). Although exploration drilling has encountered gold mineralization at intersections with the Brucejack fault, this mineralization appears to have been remobilized from previously mineralized wallrock and adjacent veining; fault movement is therefore interpreted to have been largely post-mineralization. It is suggested that the Brucejack fault formed in response to late brittle deformation, which reactivated a pre-existing syn-depositional fault on the margins of a volcanic sub-basin that was formed during deposition of lower Hazelton Group rocks (Ireland et al., 2014).

Other faults in the immediate area trend NNW–SSE and less commonly ENE–WSW. They show sinistral to dextral strike-slip motions with either a normal or reverse component. Commonly fault surfaces preserve slickensides with multiple orientations, indicating variable fault movements, likely under different stress regimes.

Two stages of penetrative fabric are observed throughout the deposit and typically trend north–south and east–west (see below); the fabric is particularly well developed in heavily sericitized zones. Hazelton Group rocks on the property have been folded into synclines and anticlines with wavelengths >100 m (north–south deformation; Figs. 8 and 10), and locally into small-scale parasitic folds. The Brucejack deposit appears to have been formed after the main-stage of folding, because veins are commonly observed cutting stratigraphy and penetrative fabric with minimal subsequent deformation. Mesozoic trachybasaltic dykes show moderate compressive (east–west) deformation, which is believed to be the major post-emplacement deformation event. Field observations of this east–west post-emplacement fabric are observed throughout the Sulphurets region, and this deformation event is suggested to have occurred in the Late

Jurassic–Early Cretaceous (Margolis, 1993; Febbo et al., 2015) contemporaneous with accretion of the Insular terrane and the subsequent formation of the Skeena Fold Belt (Evenchick, 1991b).

Kirkham and Margolis (1995) suggested that the whole Sulphurets district has been exposed to lower-greenschist facies regional metamorphism indicated by the presence of greenschist mineral assemblages (quartz ± sericite ± calcite ± chlorite ± epidote) and the absence of biotite, hornblende, or actinolite in bulk compositions within host volcanic rocks outside the hydrothermal alteration envelope. At Brucejack, wallrocks within hydrothermal alteration zones have been exposed to high water:rock ratios and are moderately to strongly phyllic altered, where volcanic and sedimentary rocks have abundant sericite ± muscovite ± quartz ± calcite ± chlorite alteration products. Adjacent to ore zones wallrocks are not strongly altered and volcanic rocks contain abundant plagioclase and potassium feldspar phenocrysts throughout their groundmass. If subsequent metamorphism had reached lower-greenschist facies, it would be expected that these minerals would include muscovite ± chlorite ± albite ± quartz alteration products. Their absence suggests that alteration at Brucejack is mainly hydrothermal in origin and that there is little evidence for post-emplacement lower-greenschist facies regional metamorphism.

Pyrite crystals occurring within strained rocks commonly contain well-developed quartz-sericite pressure shadows indicating that pyrite grains are pre or syn-kinematic. This may suggest that mineralizing conditions occurred in a tectonically dynamic environment, which is expected for the Stikine terrane prior to accretion with North America. Margolis (1993) sampled sericite from these pressure shadows in a sample from

the West Zone and obtained a K-Ar date of 110.4 ± 2.6 Ma. Similarly Kirkham (1989) dated pure metasomatic sericite that yielded ages of 110.2 ± 2.3 Ma ($^{40}Ar/^{39}Ar$). In addition to these dates, in this study we also provide age estimates from hydrothermally altered volcanic sedimentary rocks and quartz-calcite stockwork veining ($^{40}Ar/^{39}Ar$ sericite and muscovite respectively), where plateau ages are similar to the studies above (105 to 112 Ma; see details below). These dates provide a minimum age for sericite and muscovite and likely reflect thermal resetting during the formation of the Skeena Fold Belt (Evenchick, 1991b).

4.4 Alteration and Mineralization

Large oxidized, pyritic gossans occur at surface above quartz-sericite-pyrite hydrothermally altered rocks at Brucejack, and form a concave-northwest arcuate belt on either side of the Brucejack Fault (Fig. 7). This sericitic (phyllic) alteration envelope extends through mineralized zones from Golden Marmot Zone to Bridge Zone (4.5 km) and is typically <700 m wide; it occurs as a pervasive overprint to all extrusive volcanic and sedimentary host rocks. Intense phyllic wallrock alteration is cospatial and cogenetic to large zones of mineralized quartz-carbonate stockwork veins and lithological contacts, and appear to have formed in response to the mineralizing hydrothermal fluids.

Hydrothermal alteration is locally intense proximal to ore zones and lithological contacts. Sedimentary rocks are commonly completely metasomatized to sericite, which are proximal to texturally destructive silicified conglomerates near geologic contacts. Sericite, quartz, pyrite, chlorite, and calcite alteration is found disseminated in wallrocks and preferentially replacing clasts in conglomerates. Pyrite alteration occurs as subhedral

clots, blotches, blebs, and discontinuous stringers throughout the host rocks. Pyritic masses also are observed replacing volcanic fragments, sedimentary clasts, submarine siltstone concretions, and bedding in sedimentary horizons.

Host rocks at Brucejack also show evidence for a sulfidization event occurring prior to mineral deposition. Wallrocks outside (but proximal to) the phyllic alteration envelope at Brucejack contain sericite and abundant disseminated pyrite (locally exceeding 10%), and are suggested to have been generated from hydrothermal fluids prior to Au-deposition. Sericite, epidote, quartz, and carbonate minerals pseudomorph replace K-feldspar crystals; phenocrysts are euhedral suggesting primary K-feldspar. Pre-sulfidized rocks at Brucejack are present across the property, but proximal to the northwest trending band of phyllic alteration.

There is no host rock control on gold mineralization, although the key stratigraphy for Au-deposition is commonly found throughout the volcaniclastic units (sandstones, siltstones, conglomerates, and tuffaceous rocks). Mineralization at Brucejack is generally cospatial with the northwest-trending band of intense phyllic alteration and is identified within stockwork veining, and coeval vein-breccias and stringer veins composed of quartz, calcite, and commonly sericite.

Bladed calcite and vuggy quartz have been observed in West Zone and the VOK, and adularia and barite are restricted to mainly West Zone and Shore Zone. Cockade and crustiform vein textures occur infrequently (Fig. 14), and are cospatial with stockwork and breccia veins. Stockwork veins and breccia veins are mostly several meters in thickness, and extend for tens of meters, whereas cospatial sheeted vein networks are subvertical, and sub-centimeter to several centimeters in thickness. All veins hosting

mineralization are weakly strained by post-mineralization deformation, where disjointed and truncated vein networks are present. Ptygmatic vein textures are also observed in stringer veinlets (Fig. 15), suggesting that veins propagated through unconsolidated sediment, or partially lithified or ductile host rocks. Veins in the VOK dominantly trend northwest–southeast, whereas a dominant vein orientation is not yet recognized for West Zone or other prospects.

Figure 14: Crustiform banding within silica-flooded quartz stockwork-breccia vein (underground: 426647E, 6258039N, 1345 m)

Figure 15: Ptygmatic vein within lapilli tuff (SU-158 at 47m: 426483E, 6257441N, 1498m)

Mineralized veins contain variable amounts of pyrite, rutile, sphalerite, galena, tetrahedrite, chalcopyrite, arsenopyrite, electrum, freibergite, pyrargyrite, pearceite, molybdenite, and acanthite. Arsenopyrite occurs in all vein generations that host gold, whereas other minerals occur inconsistently with gold mineralization, and pyrite and sericite occur in all veins. Gold occurs in the form of electrum, as coarse-grained blebs, clots, stringers, and lace-like dendritic networks within the quartz-calcite veins (Fig. 16). Microscopic electrum is mostly found as free grains (Fig. 17a), but also as microscopic blebs or filling fractures within pyrite grains, where it is found intergrown with acanthite (Fig. 17b) and less commonly chalcopyrite. Silver sulfosalts (commonly tetrahedrite and pyrargyrite) occur in isolation (Fig. 17c), intergrown with other sulfides (Fig. 17d), and

less commonly electrum. Gold-silver ratios in electrum are generally 2:1 throughout the VOK (Ireland et al., 2014), although West Zone and Shore Zone have anomalously higher silver content (Au:Ag = 1:28; Ireland et al., 2014).

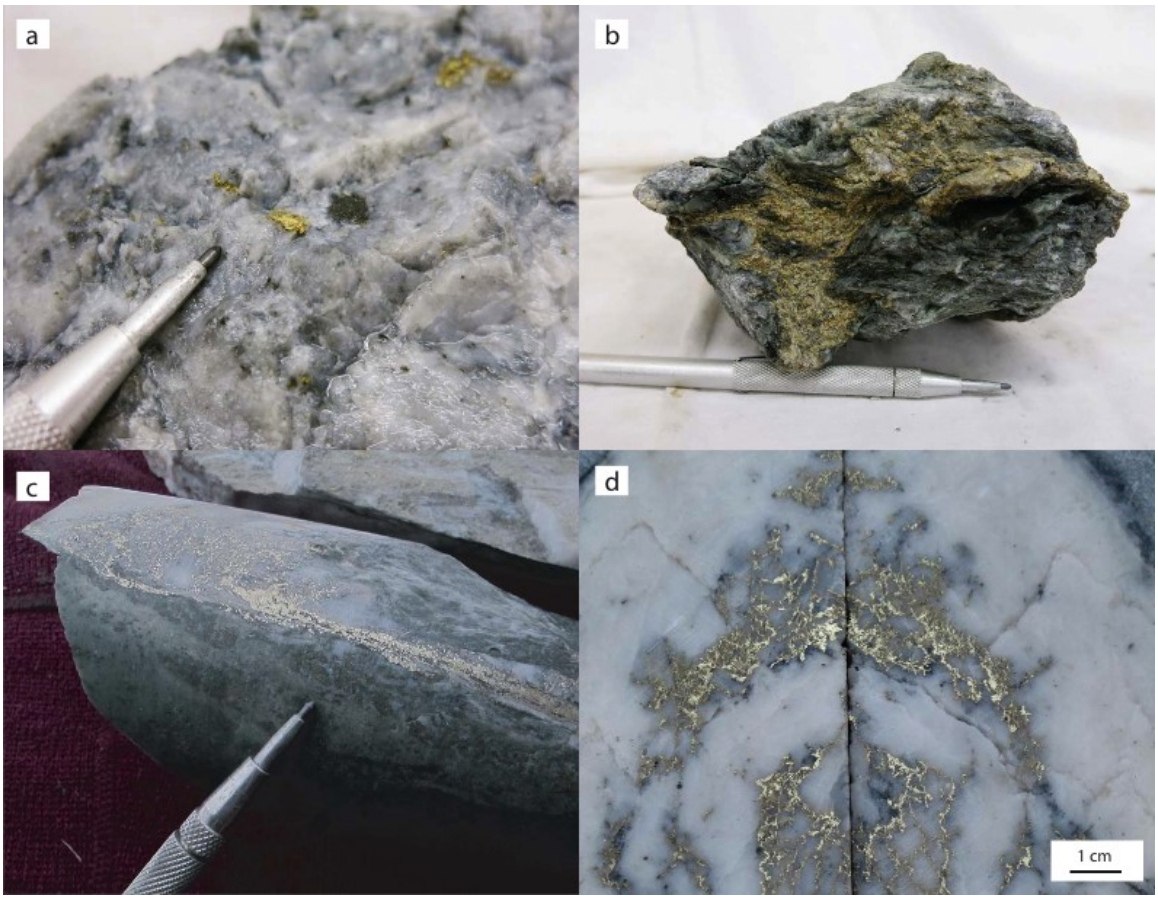

Figure 16: Various textures of electrum found at Brucejack: (a) small <1cm blebs of Au-rich electrum within quartz-calcite stockwork vein (426659E, 6258033N, 1350 m); (b) >1000 g/t Au hand sample of electrum clots within tuff (426614E, 6257970N, 1350 m); (c) Stringers of electrum throughout calcite-rich veining (sample >41,000 g/t Au over 0.5 m; SU-542 at 203m: 426619E, 6257987N, 1376 m); and (d) dendritic lattice-like electrum intergrown with Ag-sulfosalts within quartz vein (SU-115: 426548E, 6257973N, 1484 m)

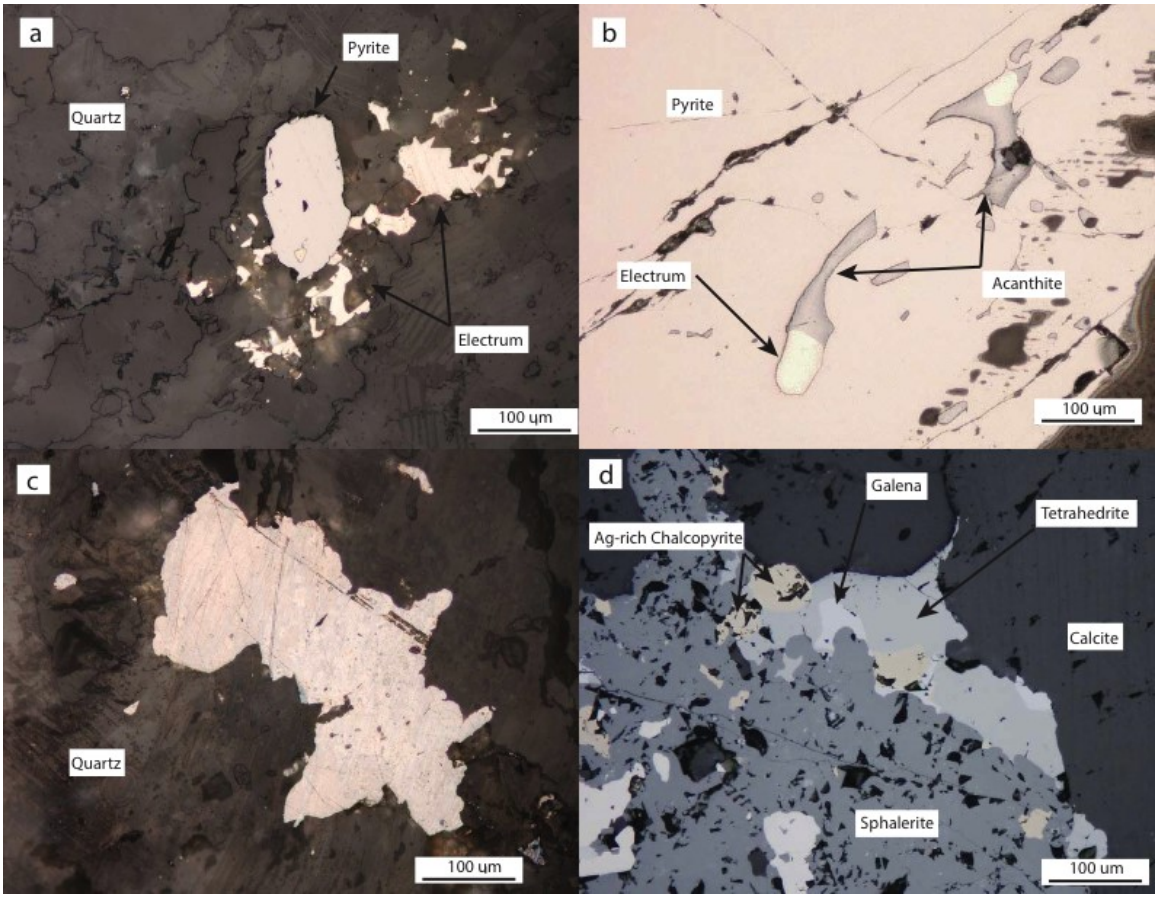

Figure 17: Reflected light photographs of electrum and Ag-sulfosalts: (a) disseminated electrum cospatial with pyrite, and occurring within pyrite as a single bleb; hosted by vein quartz (HG-05); (b) intergrown acanthite and electrum within pyrite fractures; hosted by quartz vein (HG-02); (c) pyrargyrite (ruby silver) occurring separate from other mineral phases; hosted by quartz vein (HG-02); and (d) intergrown sphalerite, galena, Ag-rich chalcopyrite, and tetrahedrite; hosted by quartz and calcite vein (VP-054)

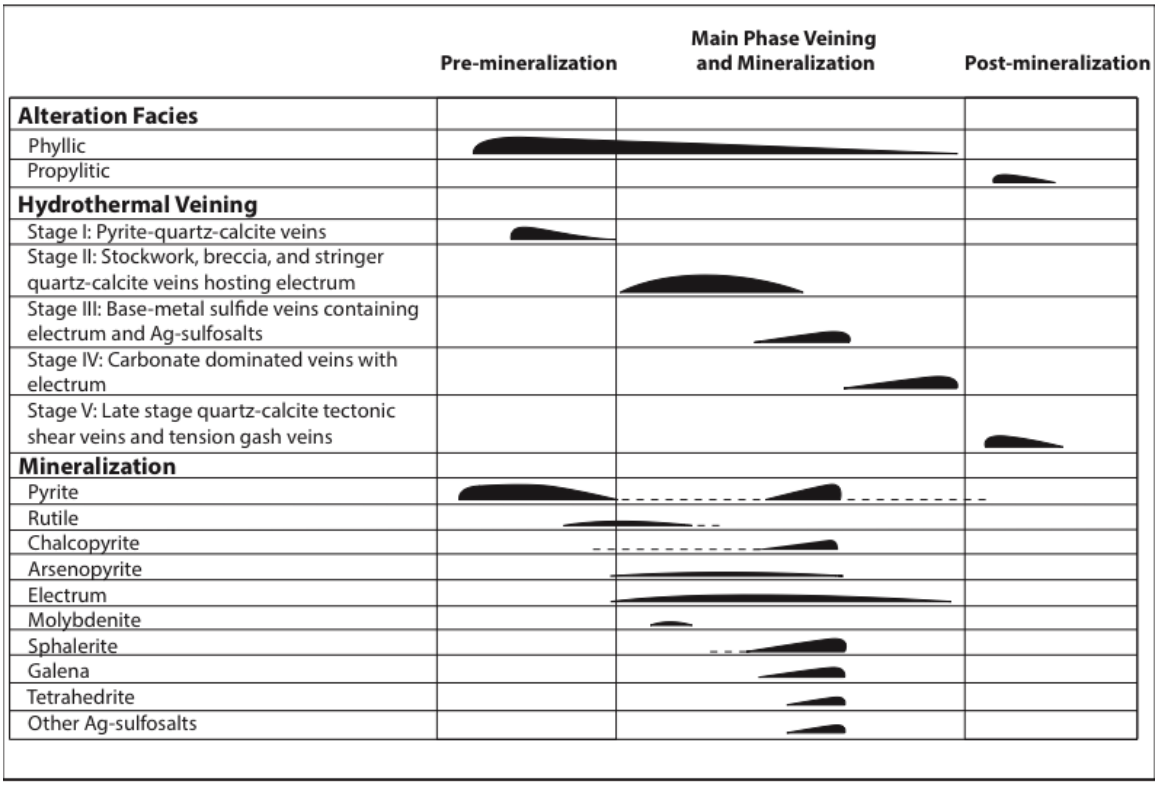

Figure 18: Paragenetic sequence of alteration, vein assemblages, and mineralization for the Valley of the Kings. Insufficient work has been done on other prospects to delineate a paragenetic sequence

4.5 Vein Paragenesis for the Valley of the Kings

Five vein stages have been recognized at in the VOK: (1) highly deformed and discontinuous, barren, pyrite stringer veins containing calcite and quartz with common sericite ± chlorite wallrock alteration; (2) electrum-bearing deformed quartz-calcite ± dolomite stockwork veins and breccias, which are spatially associated with sub-vertical stringer quartz veinlets also hosting Au-mineralization; (3) Zn-Pb-(Cu) sulfide veins containing quartz, minor calcite, and common Ag-sulfosalts and electrum; (4) highly deformed carbonate veins containing abundant orange-coloured, Mn-bearing calcite, also

containing electrum; (5) late stage quartz-calcite shear veins with asymmetrical sericite, chlorite, and pyrite vein banding, and cogenetic, subhorizontal bull-quartz tension gash veins with abundant vein chlorite.

4.5.1 Vein Stage I

Stage I veins contain pyrite, calcite, quartz, and minor vein sericite and commonly have sericite ± chlorite alteration along vein margins. Electrum is very uncommon, where it is found within pyrite as microscopic blebs. It is apparent that there are multiple subdivisions of stage I veins based on pyrite grain sizes and crystal habit, abundance of sericite and chlorite in alteration halos around the vein margins, and proportion of quartz and calcite to pyrite (Fig. 19). For the purposes of this study, different stage I sub-stages are not distinguished.

Euhedral–subhedral pyrite crystals are typically large (1–7 mm in diameter) and have common microscopic (1–10 μm) anhedral inclusions of sphalerite, chalcopyrite, and minor tetrahedrite and galena. Rutile and chalcopyrite are sparsely found disseminated throughout the veins. Sericite occurs frequently on the boundaries of veins, and less commonly within the veins. Chlorite is less abundant than sericite, but occurs in 2–3 mm-wide alteration halos at vein margins and as disseminated patches and blebs within the veins. Most calcite and quartz crystals show penetrative deformation, and syn-kinematic quartz-filled pressure shadows occur on the flanks of euhedral pyrite crystals. These deformed pyrite stringer veins are discontinuous and do not appear to have a general trend or orientation; they are crosscut by all other vein generations (Fig. 19d).

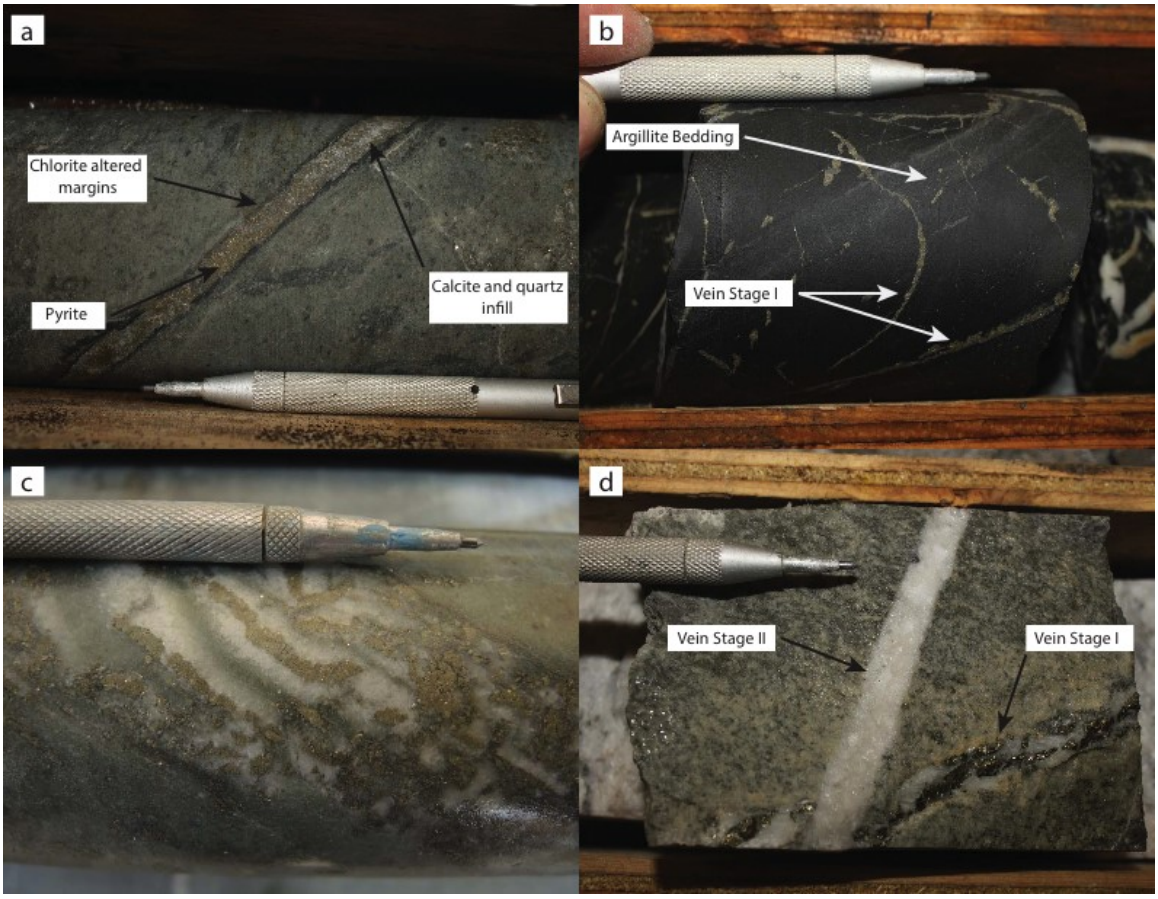

Figure 19: Stage I pre-mineralization pyrite ± quartz-calcite veins: (a) 1 cm wide pyrite-dominated vein with chlorite-altered margins and quartz-calcite vein infill (SU-125 at 87m: 426436E, 6257414N, 1464 m); (b) thin (<2 mm), discontinuous pyrite stringer veinlets within black siliceous argillite siltstone (426370E, 6258137N, 1403 m); (c) 4 cm-wide early-stage pyrite vein with abundant quartz and minor calcite vein infill; minor sericite alteration on vein margins (VU-418: 426648E, 6257980N, 1222 m); (d) stage I pyrite vein cross-cut by stage II quartz-calcite vein (SU-289 at 70.1 m: 426647E, 6258045N, 1488 m)

4.5.2 Vein Stage II

Deformed quartz-calcite ± dolomite stockwork veins and breccias, with cospatial subvertical stringer quartz veinlets, represent the earliest stage of Au-mineralization. Stockwork, breccia, and stringer veins are likely cogenetic and episodic, because they are

cospatial and frequently found crosscutting one another throughout the deposit. These vein sets generally trend east–west in the Valley of the Kings, are steeply dipping, and are weakly to moderately deformed. Stockwork veins are macroscopically observed as deformed silica-flooded, quartz-calcite ± dolomite veins, and are typically several meters in width. Stockwork veins commonly show good vertical continuity and along strike, with one of the veins traceable over a strike length of more than 100 m in a combination of underground workings and diamond drill hole intersections (Fig. 20a). Quartz-carbonate breccia veins are commonly proximal to stockwork veins, where veins regularly overprint one another. Silica-flooded breccia veining isolates and suspends poorly sorted, angular wall rock clasts, which are commonly highly silicified (Fig. 20b). Narrow stringer quartz veinlets (Fig. 20c) are also found cospatial to cogenetic stockwork and breccia veins.

Although individual Stage II veins show textural variability, they have consistent mineralogical features and modal abundances. Quartz is the dominant vein mineral (>80%), and occurs as coarse-grained (typically 1–2 mm), equigranular, mosaic style crystal masses. Calcite (with minor dolomite) generally fills fractures between large quartz crystals, and fine-grained calcite is associated with vein sericite and microcrystalline quartz. Anhedral pyrite is generally 0.25–1 mm in size and disseminated with other base metal sulfides, which occur infrequently and are commonly associated with sericitized zones. Sericite within veining is common and mainly occurs as discontinuous stringers, and narrow lenses. Small amounts of rutile, sphalerite, galena, and chalcopyrite ± arsenopyrite are disseminated throughout the veins, and Ag-sulfosalts are rare. Molybdenite is present in stockwork veins in Bridge Zone (dated at ~192 Ma;

see below), although is recognized in the VOK only as trace amounts. Electrum is common in this vein generation, where it is intergrown with vein quartz and sericite.

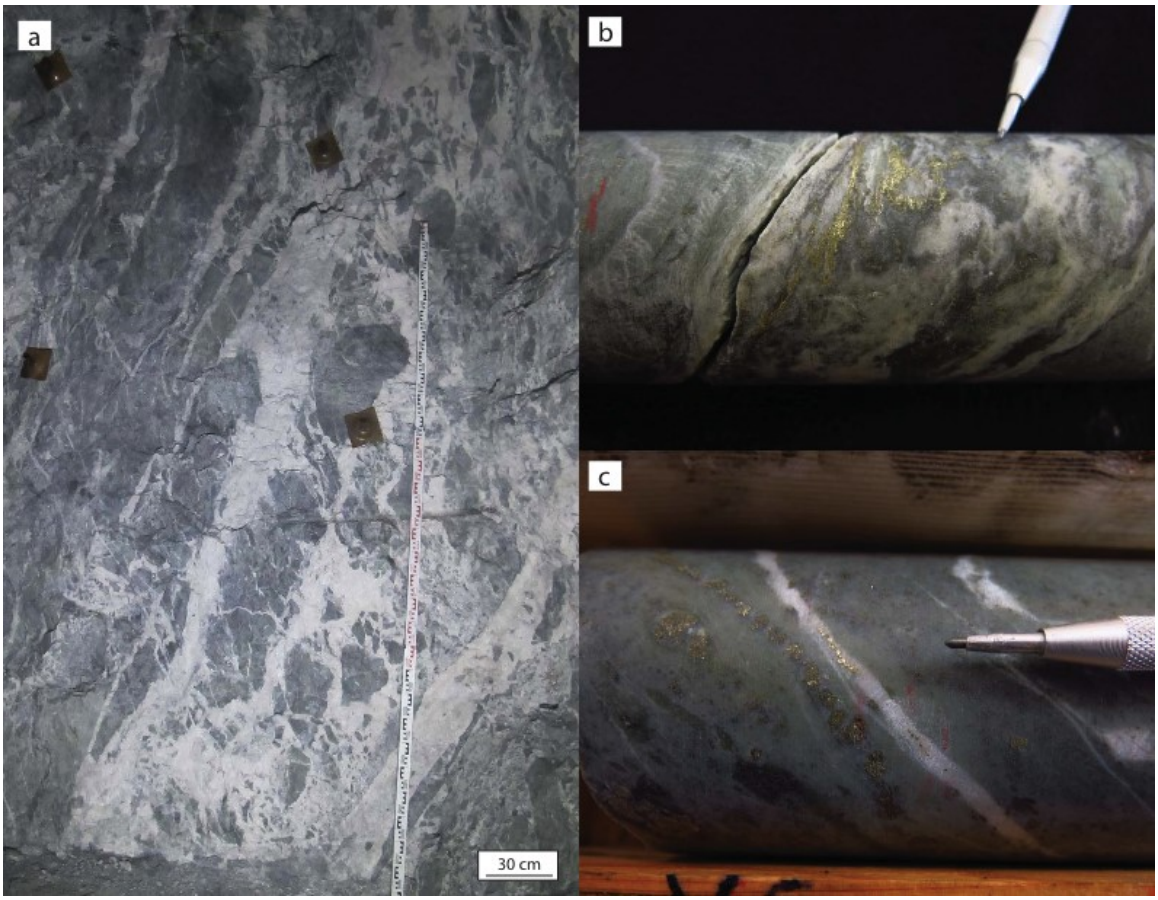

Figure 20: Stage II stockwork, breccia, and stringer veins: (a) Intense stockwork and breccia veining within crystal lithic tuff (underground: 426643E, 6258039N, 1345 m); (b) silica-flooded breccia vein with coarse-grained electrum throughout (VU-032); (c) electrum-bearing quartz-calcite stringer veinlet adjacent to pyrite stringer vein cutting lapilli tuff (left; VU-049)

4.5.3 Vein Stage III

Base metal sulfide-bearing veins contain copious amounts of pyrite, sphalerite, galena, tetrahedrite, chalcopyrite, and lesser amounts of electrum, arsenopyrite ±

acanthite, and trace Ag-sulfosalts (freibergite, pyrargyrite, and pearceite) intergrown with quartz and calcite and rare sericite. The distinguishing characteristic of this vein stage is the much higher proportion of base metal sulfides compared to stage I or other vein generations; in some cases, base metal sulfides account for >25% of the vein mineralogy. The veins are typically 1–10 cm wide, but extend to >30 cm in some localities. Macroscopically, the veins are typically banded with sulfides, where asymmetric banding consists of sphalerite, galena, and pyrite. Electrum is found as blebs, stringers, clots and dendritic masses throughout base metal sulfide veins and is cospatial and commonly intergrown and rimmed by Ag-sulfosalts (Fig. 21a,b).

The veins are mildly deformed, which is observable in microscopic features involving strained and elongated quartz, and microscopically deformed calcite twin planes. Veins containing significant amounts of base metal sulfides commonly have sharp contacts with the wall rock. Quartz and calcite crystals throughout the vein matrix are commonly overprinted by semi-continuous stringers of sericite, which are accompanied by microcrystalline quartz, and fine-grained calcite. Sulfide mineralization is commonly found proximal to bands of sericitization.

Sulfide ore-paragenesis in this vein stage is: (1) early pyrite and sphalerite; (2) galena texturally replaces sphalerite on grain margins and replaces pyrite through fracture controlled replacement; (3) chalcopyrite pervasively replaces galena and is found as chalcopyrite-disease in sphalerite; (4) tetrahedrite, freibergite, pyrargyrite, and pearceite accompanied by electrum, replace all earlier ore-minerals; and (5) acanthite commonly rims Ag-sulfosalt aggregate grains. Electrum and Ag-sulfosalts are also found disseminated throughout veins unaccompanied by other metals. Electrum content is

variable, although veins contain similar grades to that of other ore-bearing vein generations. Sphalerite compositions are typically uniform, with honey-brown colours (Fig. 21d) reflecting low Fe contents and lower temperature conditions.

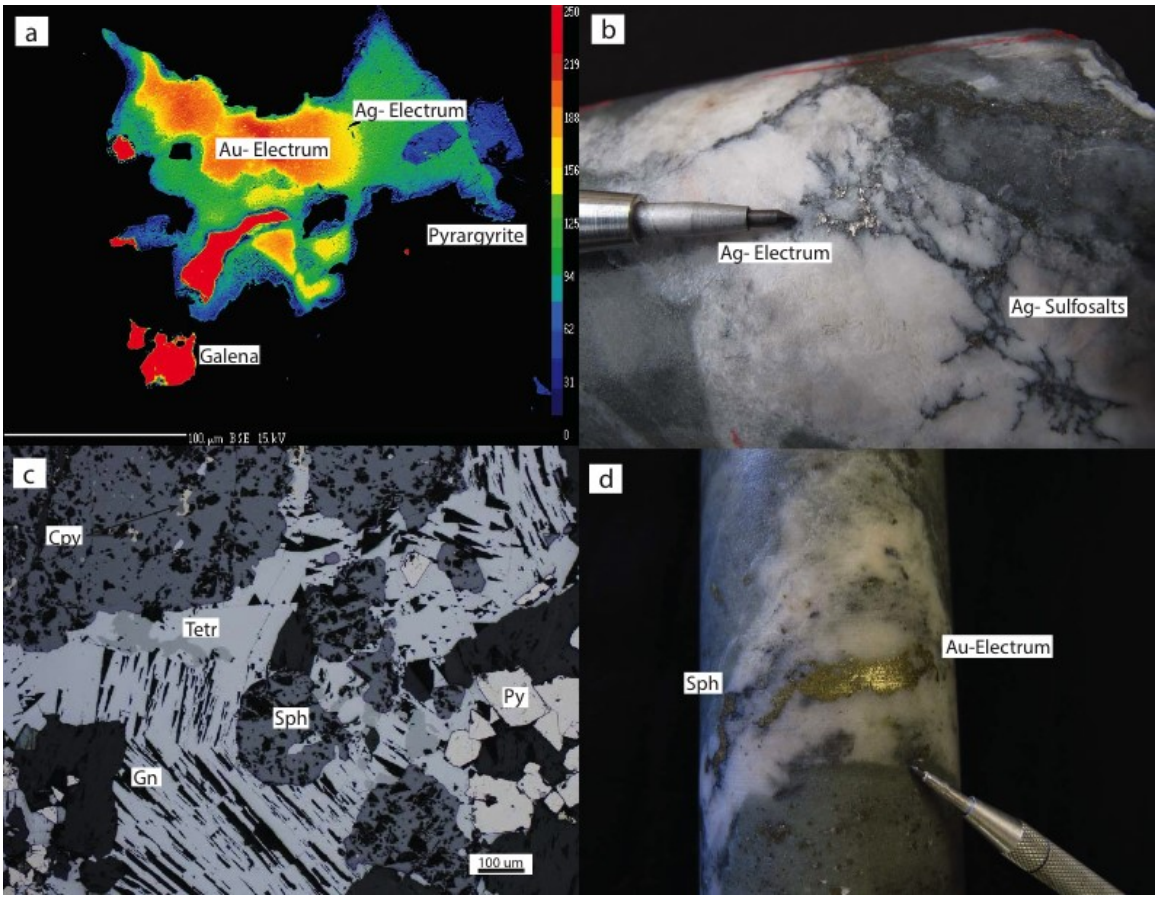

Figure 21: Vein stage III base metal sulfide veins: (a) backscattered electron image of electrum zoning with sulfosalt rims (HG02); (b) base metal sulfide vein with dendritic Ag-rich electrum intergrown with Ag-sulfosalts (SU-123 at 531m: 426596E, 6258569N, 979 m); (c) reflected light microphotograph showing textural relationships between pyrite, sphalerite, galena, tetrahedrite, and chalcopyrite (VP014); (d) drill core with electrum and abundant sphalerite (VU-036). Abbreviations: Gn- galena, Py- pyrite, Sph- sphalerite, Cpy- chalcopyrite, and Tetr- tetrahedrite.

4.5.4 Vein Stage IV

These veins also contain electrum and are dominated by calcite (generally >80%), with subsidiary quartz. A distinguishing feature of this vein generation is the presence of orange-coloured Mn-calcite (Fig. 22a), which forms diffuse crystals in white-coloured calcite, and less commonly in dark grey-coloured calcite. The orange and grey-coloured calcite are restricted to stage IV veins, but pure white calcite is also observed in other vein stages. Grey and white calcite appear to have precipitated from different fluids, as trigonal-hexagonal crystal growth zones with alternating white–grey calcite are common; implying periodic discrete calcite precipitation events. Grey calcite displays a crustiform banded texture in places with white calcite adjacent to vein margins (Fig. 22b) and within the nucleus of the vein (Fig. 22c); all of which can contain electrum. Orange calcite is scarce and coprecipitated with both white and grey-coloured calcite. Pyrite occurs sparsely as fine-grained anhedral crystals disseminated throughout the vein carbonates. No other sulfides are present within this vein generation, although rutile occurs in small amounts. Electrum is present as anhedral, disseminated masses, which mainly occur in clots, clusters, and dendritic forms dispersed throughout the vein. Minor sericite typically occurs as small discontinuous patches on the margins of veins.

These veins are typically multi-centimeter in width, although in Bridge Zone they reach ~1.5 m; vein widths of ≤30 cm are typical for the VOK. Calcite veins are moderately to strongly deformed and commonly show pinch and swell textures. Several of these veins have been sheared post-emplacement, where shearing has caused disaggregation and boudinage of veining. Shearing along one of these stage IV veins has

caused physical remobilization and slickensiding of electrum along sheared margins (Fig. 23*).*

Calcite veins form orthogonal sets and typically strike east–west and less commonly north–south in the VOK, and dip sub-vertically. Carbonate veins and all preceding vein stages are crosscut by trachybasaltic dykes, which are geochemically identical to dykes in the VOK and West Zone that have been dated at 182.7 ± 1.0 Ma (Appendix I; pers. comm. C. Greig, June 2015), providing a minimum age constraint for Au-deposition.

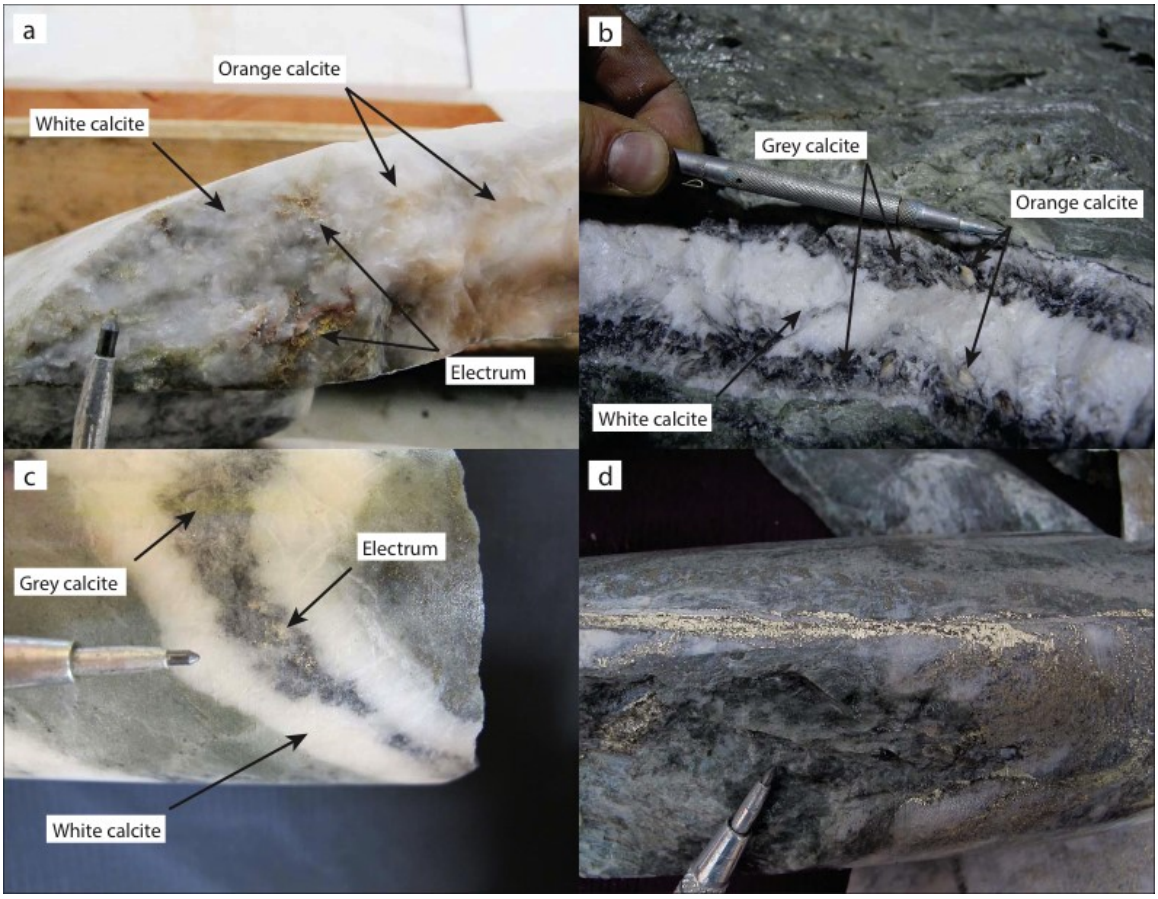

Figure 22: Stage IV carbonate-dominated veins: (a) coprecipitated white and orange calcite with small clots of electrum (SU-452 at 203m: 426619E, 6257987N, 1376 m); (b) crustiform banded carbonate vein with

grey calcite and minor orange calcite on vein margins and medial white calcite (underground: 426596E, 6258191N, 1296 m); (c) white calcite vein containing electrum within medial grey calcite (SU-276 at 338m: 426370E, 6257849N, 1274 m); (d) carbonate vein containing abundant electrum (SU-452 at 203m: 426619E, 6257987N, 1376 m).

Figure 23: Slickensided electrum on footwall of subvertical, sinistral-oblique, reverse dip-slip fault (fault tending 185/81W; photo taken in underground workings: 426614E, 6257970N, 1350 m)

4.5.5 Vein Stage V

Stage V veins do not contain cogenetic electrum and have formed by post-emplacement tectonic deformation. Veins include: (a) late stage quartz-calcite sheared

fault-filled veins with asymmetrical sericite, chlorite, and pyrite banding, and (b) associated subhorizontal bull-quartz and calcite extensional tension gash veins. Shear veins are continuous and typically 10–20 cm wide, whereas tension gash veins that radiate from sheared margins are <15 cm wide and discontinuous. Shear veins have variable orientations, but commonly strike east–west and north–south with shallow dip angles (generally <45° south). Tension gash veins (when present) are typically subhorizontal and often form R and R' reidel shear tension gashes splaying from the dominant sheared margin. Sigmoidal tension gash veins forming en echelon vein arrays are also common (Figs. 24a,b, and 25a) and suggest heterogeneous simple shear under a brittle-ductile regime of deformation.

Fault-filled shear veins contain fine-grained quartz and calcite (<1 mm and 1–4 mm respectively), where quartz and calcite crystals show moderate microscopic deformation (i.e. undulose extinction in quartz, and deformed calcite crystal lattice frameworks), which formed through moderate to strong shearing. Asymmetric banding of fine-grained anhedral pyrite, chlorite, and sericite is common and align parallel to the shear direction (Fig. 24c). Rutile is found disseminated throughout shear veins and generally occurs in close association with pyrite. Very rare electrum and Ag-sulfosalts are present in shear veins, but appear to have been physically remobilized from the wallrock and adjacent veins, and did not coprecipitate with stage V shear veins. Tension gash veins are composed of variable amounts of quartz, calcite, and chlorite, where bull-quartz crystals are 1–3 mm, and large calcite crystals are >3 mm. Chlorite is common and occurs as coarse-grained clots and blebs within veining (Fig. 25b).

Stage V veins are the youngest veins at Brucejack and crosscut vein stage IV veins (Fig. 24d), and all other precursor vein generations. These late-stage tectonic veins also crosscut the Mesozoic trachybasaltic dykes on the property, which in turn crosscuts stage IV veins.

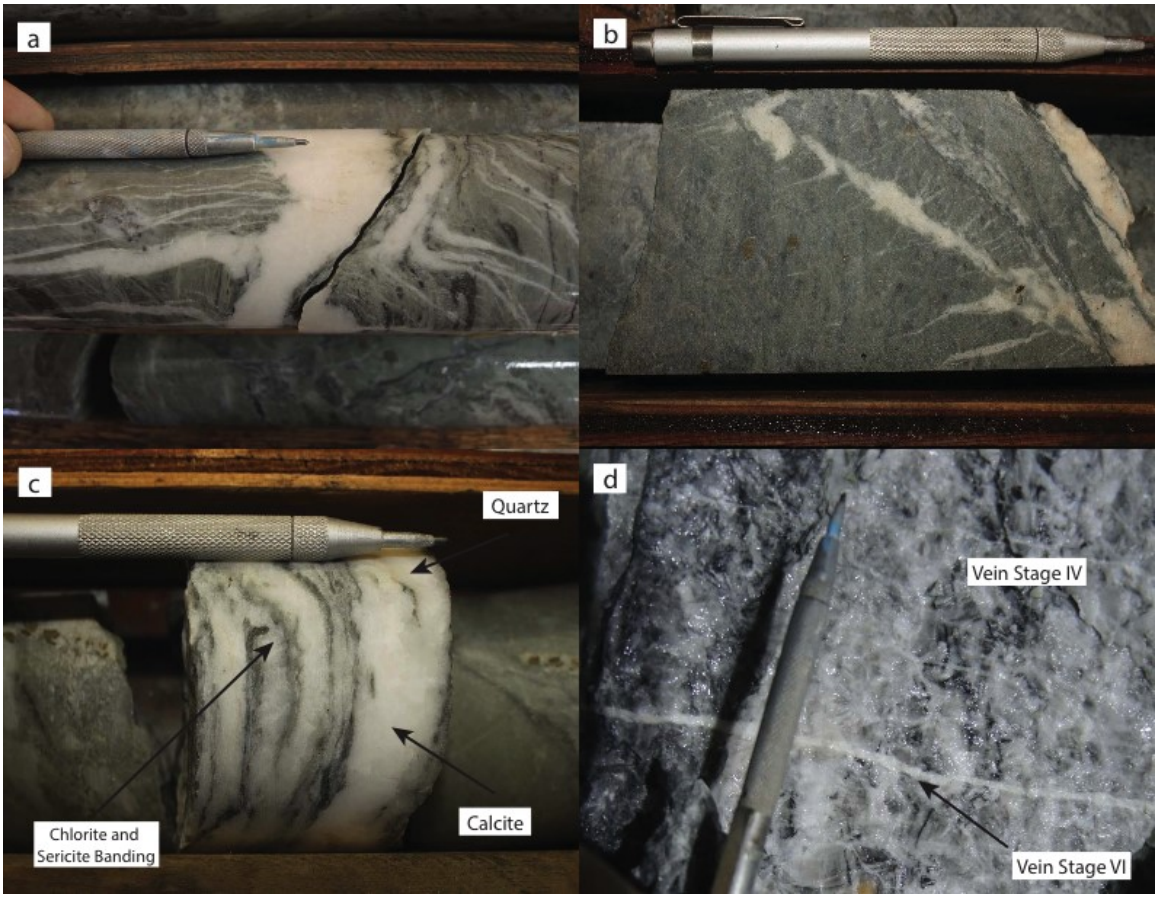

Figure 24: Post-mineralization tectonic stage V veins: (a) sigmoidal tension gash veins radiate from quartz-calcite shear vein (426556E, 6258966N, 1188 m); (b) small tension gash veins radiate from sheared margin (SU-125 at 76m: 426435E, 6257407N, 1472 m); (c) quartz-calcite-chlorite shear banding (SU-289: 426647E, 6258045N, 1488 m); (d) Thin, discontinuous stage V quartz tension gash veins cross-cut through stage IV calcite vein (underground: 426606E, 6258188N, 1295 m)

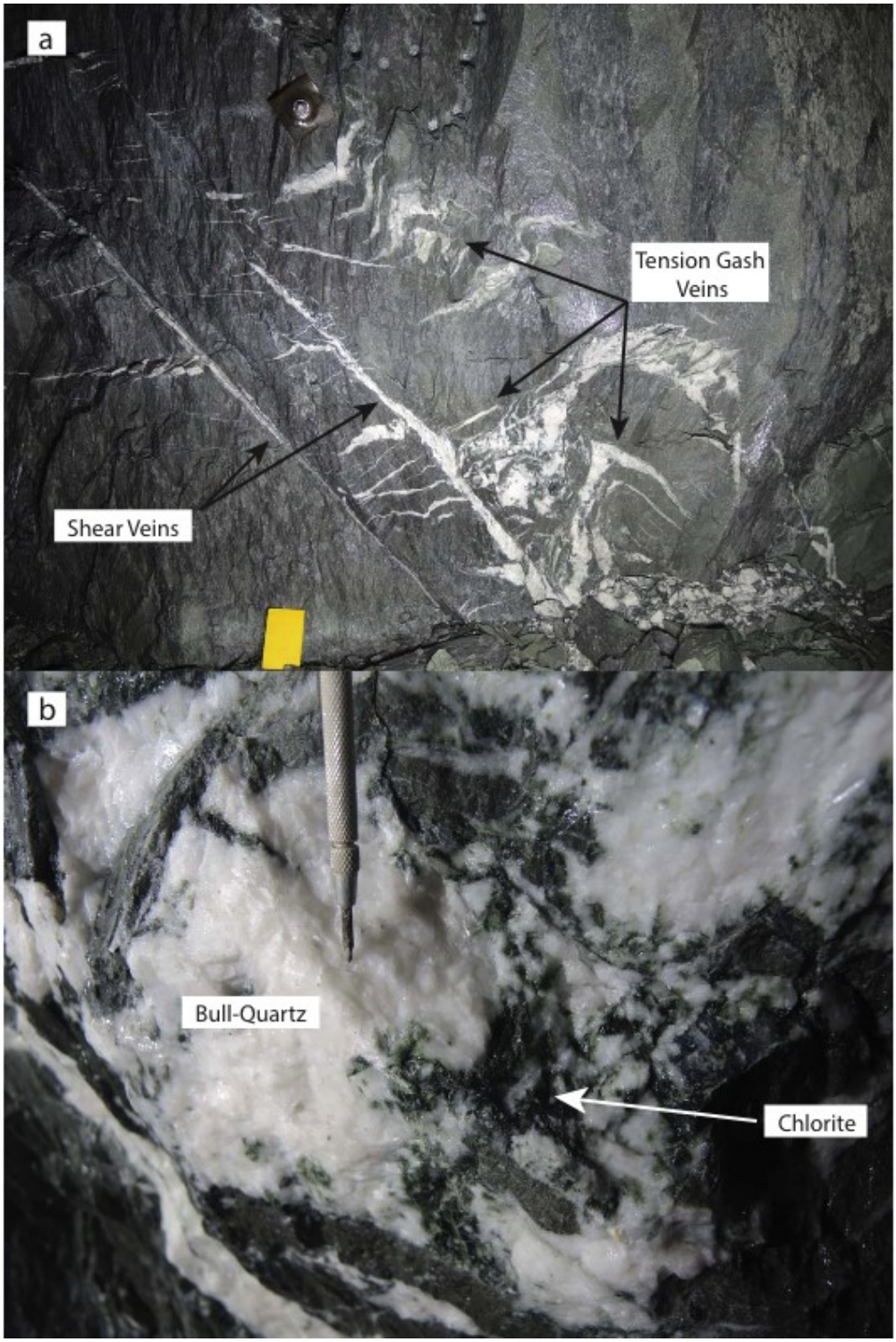

Figure 25: In-situ tectonic veins: (a) quartz-calcite-chlorite-pyrite banded shear veins with bull-quartz veins radiating from sheared margins (underground: 426656E, 6258174N, 1287 m); (b) bull-quartz tectonic veins with chlorite clots (from same vein as above).

5.0 Sampling and Methods

5.1 Samples

Samples for this study were collected from diamond drill core, underground mine exposures, and surface outcrops at the Brucejack deposit. Sample descriptions and locations are provided in Appendices II and III.

5.2 Whole-rock lithogeochemistry

A representative sample suite of least-altered intrusive and volcanic rocks was collected by the author and C. Greig across the Brucejack property for whole-rock lithogeochemistry, consisting of 55 fine-grained plagioclase-feldspar and hornblende porphyry flows, 17 coarse-grained plagioclase-feldspar and hornblende porphyry latite flows, and 13 late-stage dykes.

Five dykes and five porphyritic flows samples were analyzed at Actlabs (Ancaster, Ontario; method 4E-Research) and detection limits for this assay package are listed in Appendix III. Analytical accuracy, determined by reproducibility of lab standards is typically within 5 relative weight percent for major element oxides (except MnO: within 20 relative % at levels <0.2 wt%; and K_2O and P_2O_5, which are within 40 relative % at levels of <0.1 wt%), and to within 10 relative weight percent for minor and trace elements. Lab precision, determined by reproducibility of duplicates, is within 2 relative weight percent for major element oxides and trace elements (except Ge: within 23 relative %). Samples were dried and 1000 g was pulverized so 95% of the sample material passed through a 74 μm screen (200 mesh). Samples were treated by acid

digestion and analyzed by either fusion inductively coupled plasma mass-spectrometry (FUS-ICP/MS), instrumental neutron activation analysis (INAA), or inductively coupled plasma total dissolution (TD-ICP), while multiple analytical methods were used for some elements.

The remaining samples were collected by C. Greig and analyzed by ALS Canada Ltd. (Vancouver). Samples were dried to eliminate moisture and crushed so 70% of the sample passed through a 2 mm mesh screen. The samples were then split using a rifle splitter, and 1000 g was pulverized to >80% of the sample passing through a 75 µm screen. Samples were treated with acid digestion, lithium borate fusion, or aqua regia digestion and analyzed using either ICP-MS (inductively coupled plasma-mass spectrometry) or ICP-AES (inductively coupled plasma-atomic emission spectrometry). Detection limits are in the low ppm and ppb range for trace elements and are reported in Appendix III. Analytical accuracy is generally within 5 relative weight percent for major element oxides and within 10 relative percent for minor and trace elements.

5.3 Re-Os Geochronology

Three molybdenite samples were collected from Brucejack (West Zone and Bridge Zone) for Re-Os geochronology, in order to date the timing of sulfide and Au-mineralization. The West Zone sample was collected from the underground workings (BJ-P003; 426600E, 6258515N, 1327 m), whereas the samples from the Bridge Zone were collected from diamond drill core (SU151A and SU151B; 426707E, 6257287N, 1242 m). All samples were analyzed in the Radiogenic Isotope Facility at the University of Alberta using the methods described by Selby and Creaser (2004). A molybdenite

powder HLP-5 (Markey et al., 1998) was used as the standard, and age uncertainty is expressed at 2 standard deviations, and includes the uncertainty of the ^{187}Re decay constant ($1.666e^{-11}a^{-1}$; Smoliar et al., 1996).

5.4 U/Pb Geochronology

Fourteen porphyritic latite flow samples were collected at surface from across the Brucejack property. Twelve of the samples were collected by C. Greig, and were sent to the Pacific Center for Isotopic and Geochemical Research (PCIGR) facility at the University of British Columbia for analysis. The remaining two samples were collected to the immediate east of the Valley of the Kings by the author and analyzed at the Radiogenic Isotope Facility at the University of Alberta.

At the PCIGR zircon crystals were separated using standard techniques and were analyzed using laser ablation (LA) ICP-MS methods, where the PCIGR facility employed methods as described by Tafti et al. (2009). Zircon crystals were handpicked and mounted in an epoxy puck together with several grains of a Plesovice zircon standard (337.13 ± 0.13 Ma; Sláma et al., 2007). The epoxy pucks were brought to a very high polish and washed with dilute nitric acid. Analyses were run on a New Wave UP-213 laser ablation system and a ThermoFinniganElement2 single collector ICP-MS, where a laser power of 40% was used with 15–30 micrometer spot sizes, depending on the grain size of the zircons. Age uncertainty is reported at 2 standard deviations.

Similar techniques were used for the samples that were analyzed at the University of Alberta, where samples were run on a NuPlasma Multi-Collector ICP-MS equiped with a New Wave Research UP-213 laser ablation system (as described by Simonetti et

al., 2005). The Plesovice zircon standard was used for calibration, and zircons were ablated using a spot size of 40 μm, a fluence rate of 2 J/cm^2, and a repetition-rate of 4 Hz. Age uncertainty is reported at 2 standard deviations.

5.5 $^{40}Ar/^{39}Ar$ Geochronology

Four samples (2 sericite and 2 muscovite) were collected from underground workings and drill core in the VOK and the data are presented in Appendix IV. Sericite (A8 and A20) and muscovite (BJ-P005) were sampled from hydrothermally altered volcanic sedimentary rocks to help constrain the timing of hydrothermal mineralization at Brucejack. One muscovite sample was collected from quartz-calcite stockwork veining (sample BJ-B6), where muscovite was believed to be cogenetic with vein minerals.

Mineral separates were prepared at the University of Alberta by crushing the sample material and individual separates were handpicked under a binocular microscope. Samples and the analytical standard (Fish Canyon Tuff sanidine, 28.02 Ma; Renne et al., 1998) were wrapped in aluminum foil and stacked in sealed fused silica tubes with neutron fluence monitors. The samples were then irradiated at the U.S. Geological Survey TRIGA Reactor, Denver, Colorado for 7 hours in the In-Core Irradiation Tube (ICIT) of the 1 MW TRIGA type reactor. Fission of 4-8 neutron flux monitor positions yielded J factors of <0.5 percent, and isotope correction factors were: $(^{40}Ar/^{39}Ar)_K = 4.80 \pm 0.4828$, $(^{36}Ar/^{37}Ar)_{Ca} = 2.60 \pm 0.000687$, and $(^{39}Ar/^{37}Ar)_{Ca} = 6.77 \pm 0.000505$.

Irradiated samples were analyzed for $^{40}Ar/^{39}Ar$ at the Isotope Geochronology Laboratory, University of Nevada. Samples were step heated using a 20 W CO_2 laser until fused. The gas emitted from each step was analyzed on a MAP 215-50 mass

spectrometer. Over the period of data collection, discrimination, sensitivity, and blanks were constant.

5.6 Fluid Inclusions

Fluid inclusions were studied in order to characterize the hydrothermal fluids contributing to gold mineralization in the VOK. Numerous samples were collected from least-deformed veins genetically related to gold mineralization in the VOK (stages II–IV), but the majority of these samples contained inclusions of inadequate size (<5 μm) or poor preservation. Many inclusions were located along fracture planes (Fig. 26a) and were irregularly shaped or necked (Fig. 26b), these inclusions were classified as secondary in origin (based on the criteria of Roedder, 1984) and were not measured.

Primary fluid inclusions (Roedder, 1984) were preserved mainly in quartz (Fig. 26c) and sphalerite crystals that were enclosed or partially surrounded by calcite and sulfide minerals. Enclosure by these weak minerals shielded the quartz and sphalerite from deformation, and helped preserve primary fluid inclusions. The majority of these inclusions were found in crystal growth zones, in which the inclusions displayed similar sizes (Fig. 26d; 5–10 μm) and vapor/liquid ratios (90:10), and did not appear necked. Such fluid inclusions were grouped into cogenetic fluid inclusion assemblages (FIA) following the criteria of Goldstein and Reynolds (1994).

Nine samples (5 quartz, 4 sphalerite) containing primary fluid inclusions from two stage II quartz veins, four stage III veins (hosted by quartz or light-coloured sphalerite), and three stage IV calcite veins were selected by the above criteria for analysis.

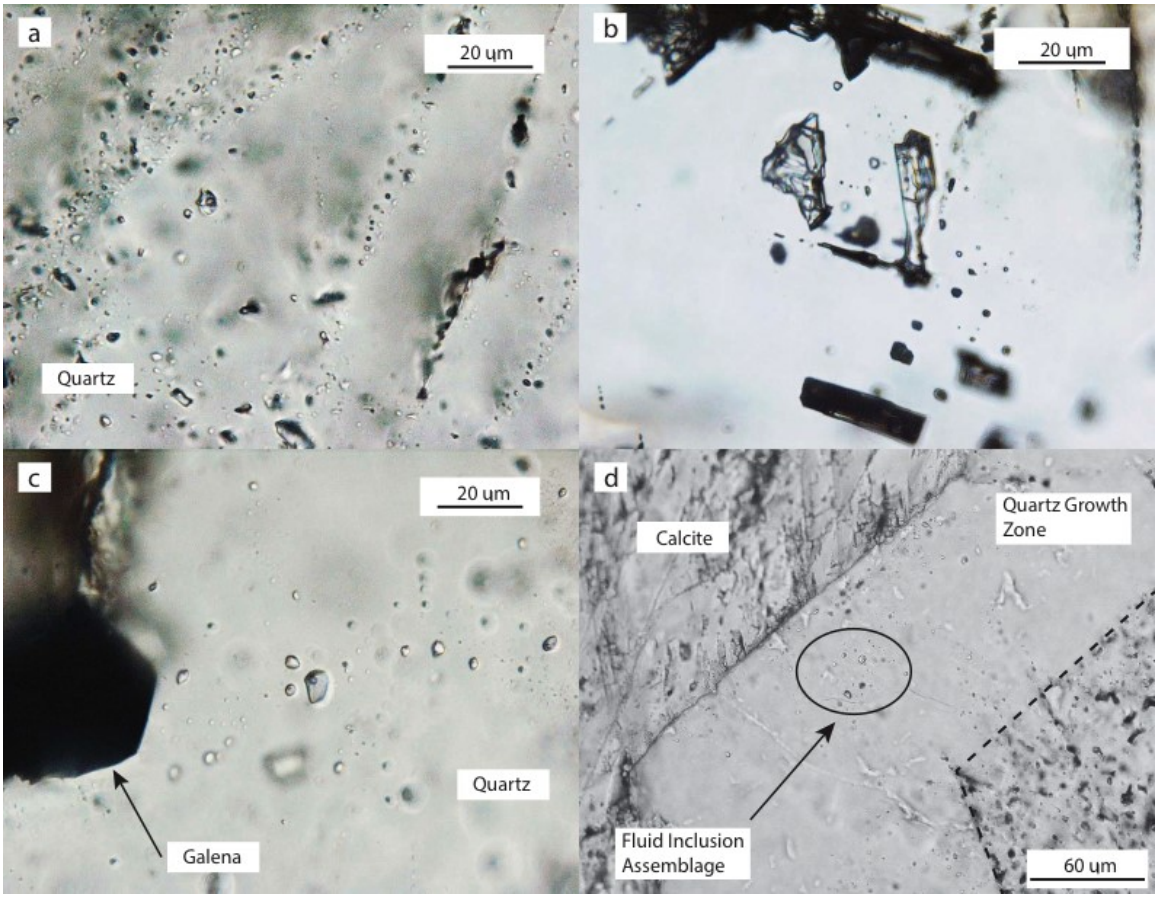

Figure 26: Fluid inclusions microphotographs: (a) secondary fluid inclusions forming along fracture planes in quartz (A4); (b) Necked primary or psuedosecondary fluid inclusions in quartz, occurring in isolation (VP-032); (c) primary fluid inclusion assemblage in quartz, which is partially enclosed by galena (VP-032); (d) euhedral quartz crystal enclosed by calcite, with well-preserved growth zones containing primary fluid inclusion assemblages (VP-017).

Chips containing fluid inclusions from doubly polished thin sections (~100 µm-thick) were microthermometrically analyzed using a Linkam THMSG600 heating/freezing stage. Fluid inclusions were chilled to -100˚C and heated until homogenization, recording phase changes throughout the heating cycle. Standards were run prior to and after data collection (in-house standard AR308: pure H_2O), and the data

(listed in Appendix V) have been corrected for small deviations from the standard values. Analytical accuracy for sub-ambient temperature measurements was ± 0.1˚C, and ± 1˚C for measurements at higher temperatures. Salinity is generally calculated from the depression of ice melting temperature using the equation of Bodnar (1992) for the NaCl-H_2O system. Clathrate, however, was observed in some inclusions from vein stage III. The presence of clathrate causes an increase in salinity (and depression of melting point) of the aqueous liquid phase (Diamond, 1992), such that the equations of Bodnar (1992) do not apply. Salinity for the clathrate-bearing inclusions was therefore calculated using the equation of Diamond (1992) for the 3-phase system NaCl-CO_2-H_2O.

5.7 Stable Isotopes

5.7.1 Calcite

Thirty-one samples of hydrothermal calcite were extracted for C and O isotopic analysis from stage II–V veins collected from drill core and underground exposures in the VOK. Samples were polished using a 2500 grit polishing disc, and then submerged in a dilute HCl solution for 20 seconds to distinguish calcite from intergrown quartz and dolomite. Etched calcite was then subsequently drilled out using a 3 mm coring drill to separate calcite grains from quartz and dolomite crystals. The tops of the calcite cores (the portion that had reacted with acid) were sanded finely to remove any reacted calcite. The samples were powdered and small aliquots were analyzed by X-ray diffraction (XRD) using a Rigaku Powder X-Ray diffractometers at the University of Alberta to confirm purity and correct identification as calcite.

Carbon dioxide was liberated from calcite by reacting the samples with 100% phosphoric acid in vacuum for 4 hours, following the methods of McCrea (1950). The CO_2 was then purified through a series of liquid nitrogen traps, and analyzed on a Finnigan MAT-252 mass spectrometer for oxygen and carbon isotopic compositions. The isotopic results are expressed as per mil deviation of the $^{18}O/^{16}O$ and $^{13}C/^{12}C$ ratios from standard values:

$$\delta\ (‰) = ((R_{SAMPLE}-R_{STANDARD})/R_{STANDARD}) \times 1000 \qquad (1)$$

where R is equivalent to either the $^{18}O/^{16}O$ or the $^{13}C/^{12}C$ ratio of samples and the standard. The oxygen standard used here is VSMOW (Vienna Standard Mean Ocean Seawater), and the carbon standard is VPDB (Vienna Pee Dee Belemnite). A -10‰ correction was applied to the measured $^{18}O/^{16}O$ ratio to account for fractionation during the phosphoric acid dissolution reaction (Clayton and Epstein, 1958; Sharma and Clayton, 1965). Measured $\delta^{18}O$ and $\delta^{13}C$ values have a 2σ error of 0.1‰.

The isotopic values of fluid in equilibrium with the calcite were calculated by correcting for temperature-dependent fractionation using the equations of Chacko et al. (1991) and O'Neil et al. (1969) for C and O respectively. Temperatures used in the equations were derived from measured fluid inclusions, where mean homogenization temperatures of 160˚C are used, assuming boiling conditions.

5.7.2 Quartz

Fifteen samples of quartz were selected for O isotopic analysis from stage II–V veins collected from underground exposures in the VOK zone of the Brucejack deposit.

Quartz samples were microscopically examined for purity and were crushed into 0.5 mg pieces with a mortar and pestle. Ten milligrams of each sample were then sent to the Washington State University GeoAnalytical Lab for analysis.

At the lab pre-fluorinations were first conducted to remove of any moisture on mineral surfaces and within the fluorination system. Each silicate sample (2 mg) was then heated with a 20W CO_2 laser (described by Sharp 1990), and a reaction with BrF_5 was used to liberate oxygen (described by Clayton and Mayeda, 1963; Sharp, 1990). Oxygen was then passed over cold traps and cleaned with KBr, which eliminates the fluorine introduced from the above reaction. The $^{18}O/^{16}O$ isotopic composition of the oxygen gas was then measured on a FinniganTH Delta S Isotope Ratio Mass Spectrometer. Isotopic compositions are reported in parts per mil (‰) and expressed in delta notation (δ) as the relative difference in isotopic composition between the sample and the Vienna Standard Mean Ocean Water (VSMOW). The accuracy of measurements was within 0.1‰ (1σ), based on analysis of standards.

The oxygen isotopic compositions of fluids in equilibrium with the quartz ($\delta^{18}O_{H2O}$) were calculated using the equation of Matsuhisha et al. (1979), at 160ºC (based on fluid inclusion measurements).

5.7.3 Sulfides

Thirteen samples of pyrite, 2 samples of sphalerite, and one sample of galena were extracted from hydrothermal veins from the VOK, and analyzed for their sulfur isotopic composition. Vein samples containing sulfides were crushed and then individual sulfide grains were handpicked in ethanol under a binocular microscope (15–20 mg for

each sample). Reflected light petrographic inspection indicates the presence of small chalcopyrite, sphalerite, and galena inclusions within larger pyrite grains, but this is not expected to significantly affect the $^{34}S/^{32}S$ ratios of pyrite samples, because fractionation between the measured sulfides is very small (Ohmoto, 1972; Rye and Ohmoto, 1974).

Samples were analyzed at the Isotope Science Laboratory (University of Calgary), where sulfur isotope ratios ($^{34}S/^{32}S$) were measured using continuous flow-isotope ratio mass spectrometry (CF-EA-IRMS). Sulfide separates were analyzed following the methods described by Gliesemann et al. (1994), where samples were loaded into tin cups and dropped into a 1050ºC quartz tube combustion reactor (Carlo Erba NA 1500 elemental analyzer). A pulse of O_2 (gas) was injected into the reactor simultaneously with the introduction to a given sample for flash combustion. $\delta^{34}S$ values were analyzed on a Thermo Delta+XL mass spectrometer and calculated by comparing a respective sample to reference peaks and output using ISODAT software. Samples were normalized to VCDT and lab precision at 1σ is ± 0.3‰, based on analysis of standards.

6.0 Results

6.1 Whole Rock Lithogeochemistry Results

All Mesozoic igneous rocks at Brucejack have been affected to varying degrees by hydrothermal alteration, which is observed as sericite, chlorite, quartz, and calcite alteration of groundmass and phenocryst replacement. Samples showing the least degree of alteration (least-altered) were selected for lithogeochemical analysis, but it is recognized that abundances of highly fluid-mobile elements, such as alkalis, have likely

been affected to some extent by this alteration. Major and trace element data are listed in Appendix III.

6.1.1 Major Element Geochemistry

Intrusive rocks and porphyritic latite flows from Brucejack are plotted on a total alkali-silica diagram (Fig. 27), where major element oxide data have been normalized to 100% volatile free. Samples showing higher degrees of alteration are indicated with open symbols, and show wide scatter to high and low alkali contents relative to the least-altered samples. Nevertheless, the least-altered volcanic rocks cluster relatively tightly in the sub-alkaline trachyandesite and trachydacite fields, consistent with their field classification as latites. Least-altered post-mineralization mafic dykes also group tightly in the basalt–trachybasalt fields, suggesting an overall weakly alakine character for igneous rocks in the Brucejack area. Unaltered Cenozoic dykes plot in the basaltic trachyandesite field.

The immobile element petrogenetic classification diagram of Winchester and Floyd (1997) provides a more robust indentification for altered rocks (Fig. 28). The volcanic host-rocks and least-altered post-mineralization Mesozoic dykes mainly cluster in the sub-alkaline andesite and basaltic-andesite fields, but close to the trachyandesite boundary, confirming their weakly alkaline character. In contrast, the unaltered Cenozoic dykes plot in the alkaline basalt field, confirming their mafic, alkaline character.

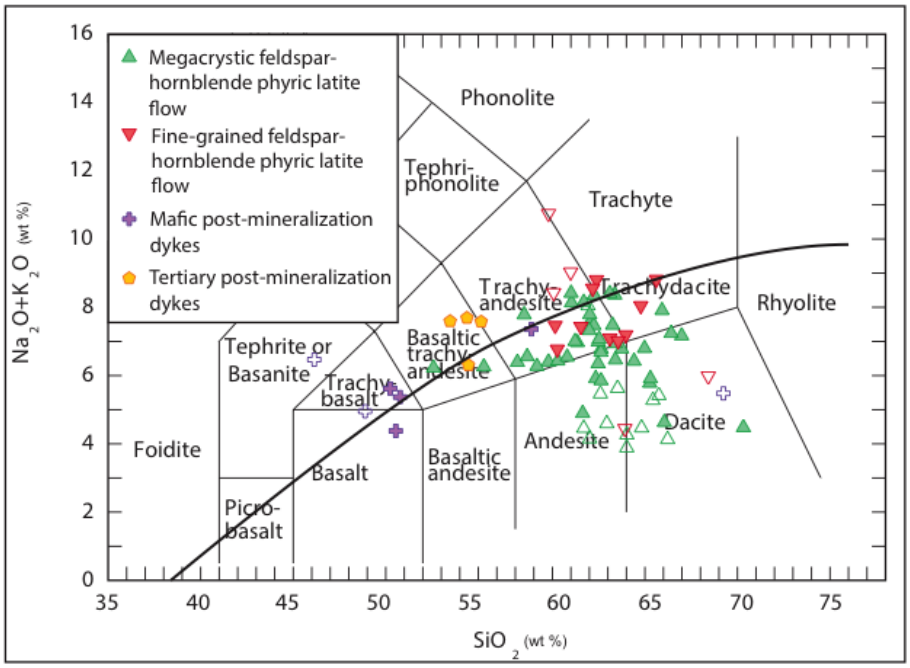

Figure 27: Intrusive and extrusive igneous rock samples from Brucejack plotted on a total alkali-silica diagram (after Le Maitre, 1989). Data are recalculated 100% volatile free. The thick black line represents the alkalic/subalkalic boundary of Irvine and Baragar (1971). Strongly altered samples are shown as open symbols; all other samples except for the Tertiary post-mineralization dykes show some alteration, which may account for the scatter in the data

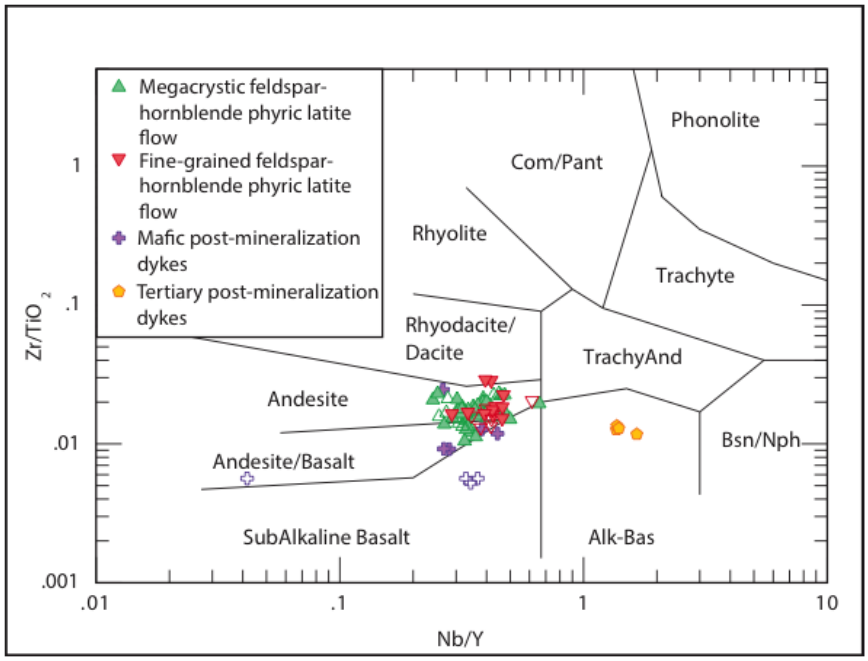

Figure 28: Intrusive and extrusive igneous rock samples from Brucejack plotted on a Zr/TiO_2–Nb/Y discrimination diagram (after Winchester and Floyd 1977). Strongly altered samples are shown as open symbols

On Harker-type diagrams (plotted against SiO_2 as a measure of fractionation; Fig. 29), the alkalis (Na_2O and K_2O) show some scatter (as expected due to variable degrees of hydrothermal alteration). However, other less fluid-mobile elements show more coherent trends, with decreases in Fe_2O_3, MgO, P_2O_5, and TiO_2 with SiO_2 for all suites, reflecting progressive fractionation of ferromagnesian silicate minerals, apatite, and magnetite. Aluminum and CaO show relatively flat trends for the intermediate volcanic rocks, suggesting moderate amounts of plagioclase feldspar fractionation.

There is an insufficient range of SiO_2 compositions in the Cenozoic dyke samples to distinguish fractionation trends, but they plot well above the Mesozoic suite for P_2O_5 and TiO_2, as expected for their more alkaline character.

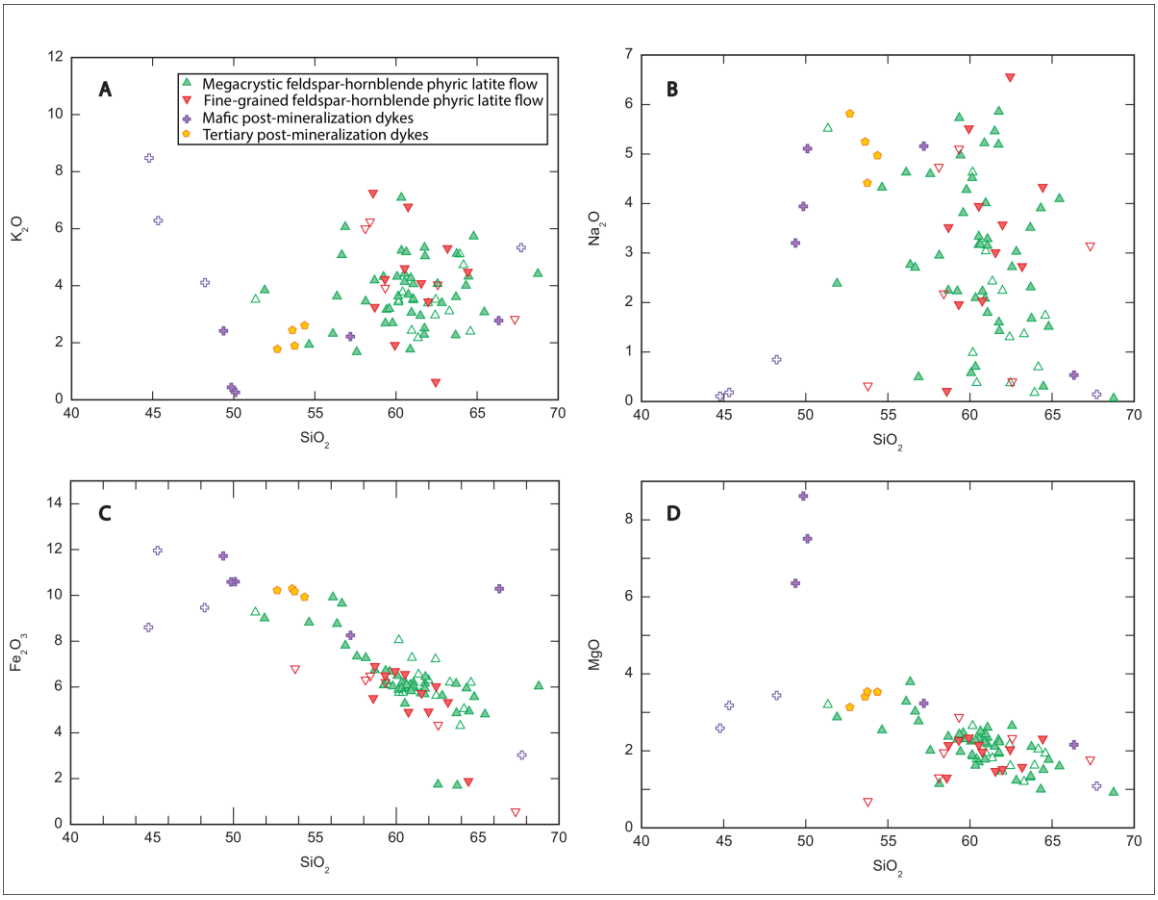

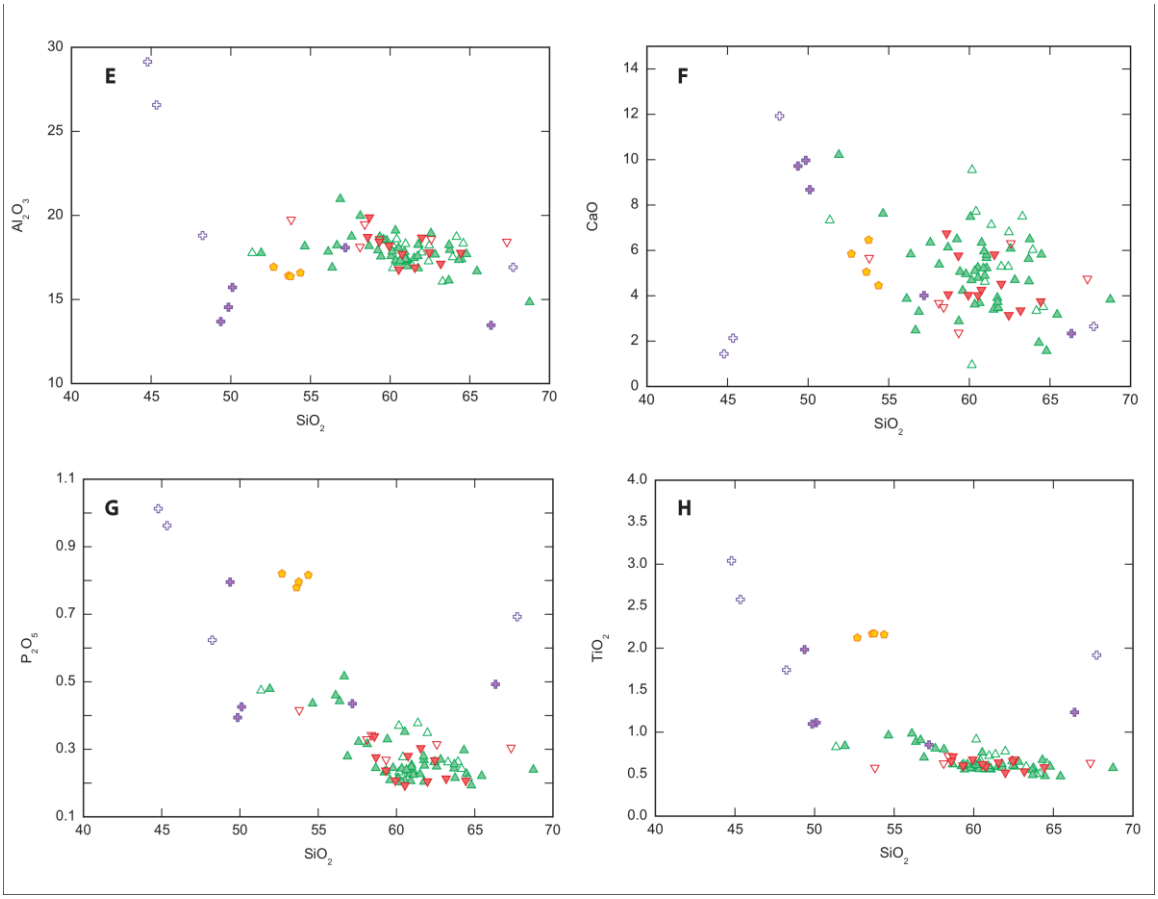

Figure 29: Intrusive and extrusive igneous rock samples from Brucejack plotted on Harker variation diagrams (major element oxide compositions versus SiO_2 in weight percent; recalculated to 100% volatile free): (a) K_2O, (b) Na_2O, (c) Fe_2O_3, (d) MgO, (e) Al_2O_3, (f) CaO, (g) P_2O_5, and (h) TiO_2. Strongly altered samples are shown as open symbols

6.1.2 Trace Element Geochemistry

Chondrite-normalized rare earth element (REE) plots for Brucejack rocks are presented in Figure 30. Porphyritic flow and mafic dyke samples show enrichment in light rare earth elements (LREE) relative to heavy rare earth elements (HREE), with listric-shaped patterns that flatten in the middle rare earth elements (MREE). Weak negative Eu anomalies are common among these samples and reflect minor plagioclase

fractionation (or high magmatic oxidation states), whereas hornblende and titanite fractionation is suggested by the listric trend from MREE to HREEs (Green and Pearson, 1985; Sisson, 1994).

In contrast to the Mesozoic suite, the Cenozoic basaltic trachyandesite dykes are strongly LREE enriched, with uniform trends towards more depleted HREE compositions, and display no Eu anomalies (Fig. 30C). These strongly HREE-depleted patters suggest the presence of garnet as a fractionating or restite phase in the mantle or deep crustal (garnet amphibolitic) source rocks (Green, 1975).

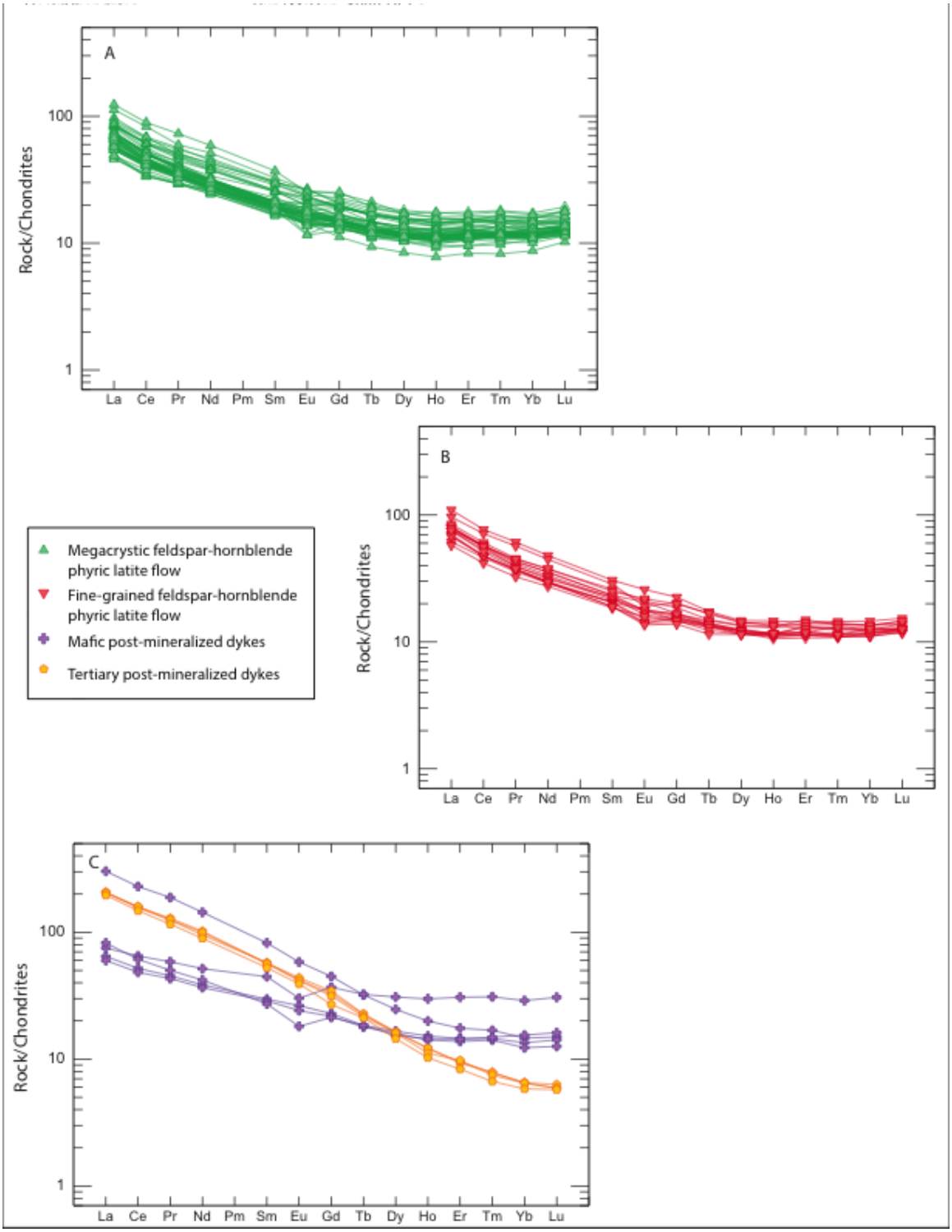

Figure 30: Chondrite-normalized REE plots (normalization values from Sun and McDonough, 1989) for: (a) fine-grained plagioclase-hornblende porphyritic latite flows; (b) coarse-grained plagioclase-hornblende porphyritic latite flows and; (c) trachybasalt and basaltic trachyandesite dykes

Primitive mantle-normalized trace element plots for intrusive and extrusive igneous rocks are shown in Figure 31. Mesozoic porphyritic volcanic rocks and mafic rocks display similar patterns with strong negative Nb, Ta, and Ti anomalies, which are characteristic of arc magmas (Briqueau et al., 1984). Several samples have negative Sr anomalies, and few mafic dyke samples have large negative Rb and Nb anomalies. The Sr anomaly can be explained by the fractionation of plagioclase, and strong negative Rb and Nb anomalies may be a function of alteration.

Cenozoic basaltic trachyandesite dykes show quite distinct patterns to the Mesozoic rocks, with only weak negative Nb-Ta anomalies and no Ti anomaly.

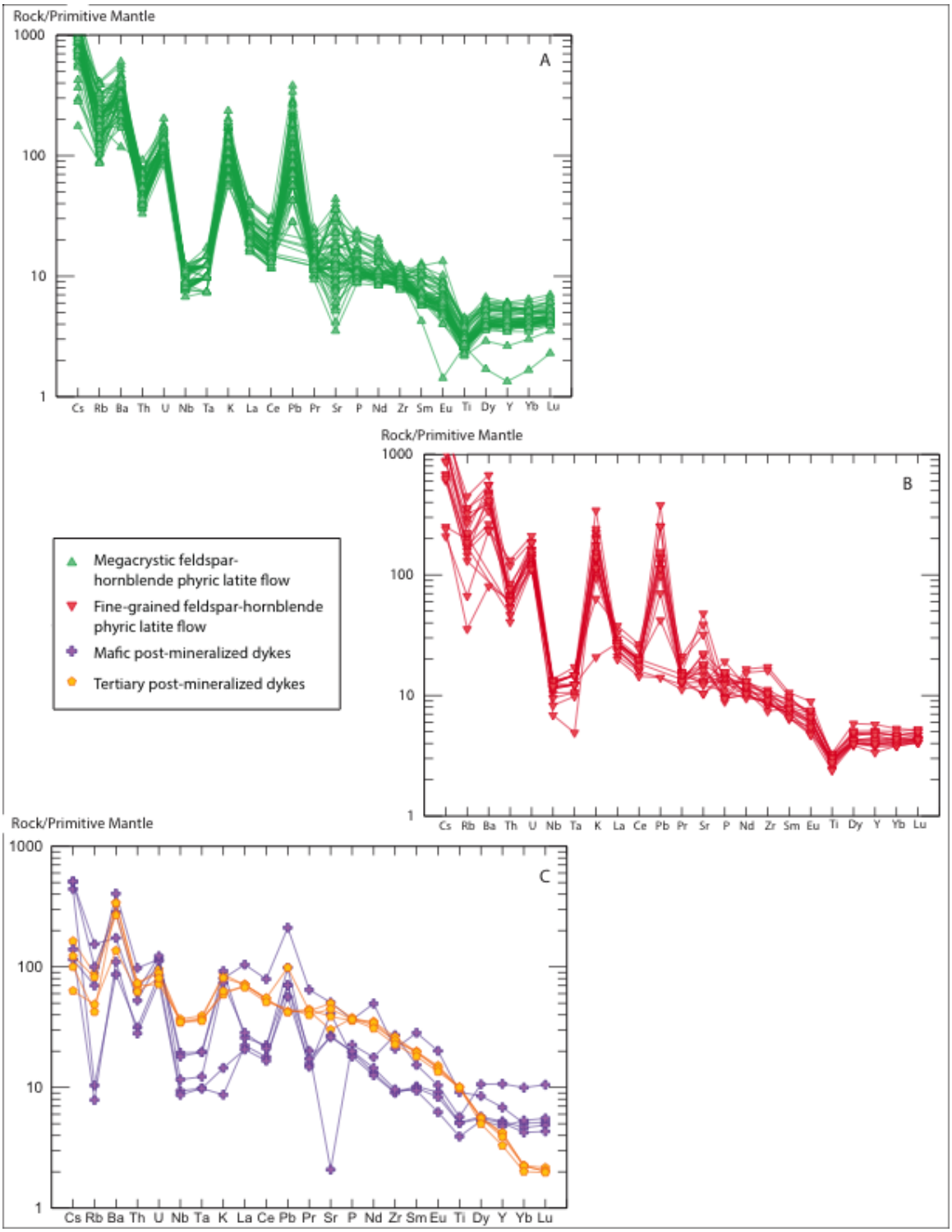

Figure 31: Primitive mantle-normalized trace element plots (normalization values from Sun and McDonough, 1989) for: (a) fine-grained plagioclase feldspar-hornblende porphyritic latite flows; (b)

coarse-grained plagioclase feldspar-hornblende porphyritic latite flows and; (c) trachybasalt (purple crosses) and basaltic trachyandesite (orange hexagons) dyke samples

Tectonic discrimination diagrams using immobile elements are plotted in Figure 32 (after Pearce et al., 1984). The Mesozoic igneous rocks from Brucejack plot mainly within the volcanic arc field, whereas the Cenozoic basaltic trachyandesite dykes are quite distinct, plotting in the syn-collisional field, close to the within-plate field.

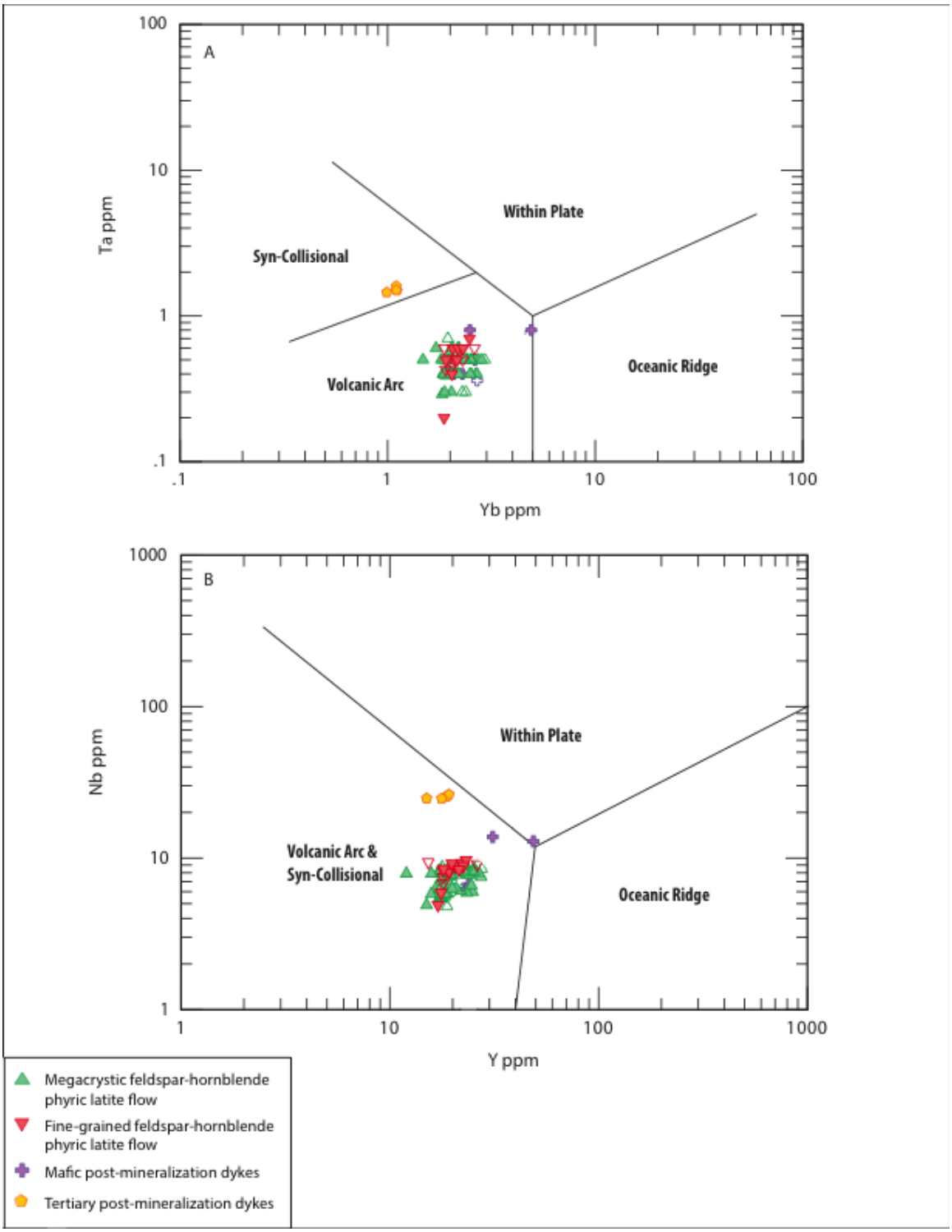

Figure 32: Intrusive and extrusive igneous rock samples from Brucejack plotted on immobile element tectonic discrimination diagrams (after Pearce et al., 1984): (a) Ta–Yb plot showing Mesozoic rocks clustered in the volcanic arc field, and Cenozoic basaltic trachy-andesite dykes plotting in the syn-

collisional field; (b) Nb–Y plot showing Mesozoic rocks clustered in the volcanic arc & syn-collisional field, and Cenozoic dykes plotting close to the within-plate field. Strongly altered samples are shown as open symbols

6.2 Geochronology Results

6.2.1 Re-Os Geochronology Results

Molybdenite found within quartz stockwork veins in the West Zone and Bridge Zone is used to estimate the timing for main-stage Au-mineralization at Brucejack. Results from Re-Os geochronology are reported in Table 1. Ages for Bridge Zone are 191.7 ± 0.8 Ma and 191.5 ± 0.8 Ma, and West Zone is 188.9 ± 0.9 Ma. Both samples from Bridge Zone are within error of one another, but the West Zone sample is significantly younger. Multiple pulses of mineralization in an episodic mineralizing environment can explain this geochronological discrepancy.

Table 1: Re-Os Isotope Data for Molybdenite Samples from quartz veins from the Brucejack deposit

Sample	Area	Host Lithology[1]	Re ppm	± 2σ	^{187}Re (ppm)	± 2σ	^{187}Os (ppb)	± 2σ	Model Age (Ma)[2]	± 2σ with λ (Ma)[3]
SU151A	Bridge Zone	BZP	13563	35	8525	22	27266	20	191.7	0.8
SU151B	Bridge Zone	BZP	11691	30	7348	19	23481	17	191.5	0.8
P-BJ003	West Zone	SST	2068	7	1300	4	4097	3	188.9	0.9

[1] BZP and SST refer to Bridge Zone porphyry and volcanic sandstone (SST) respectively.

[2] Model age calculated from the equation: $t = \ln(^{187}Os/^{187}Re + 1)/\lambda$, where t = model age, and $\lambda = ^{187}$Re decay constant and assuming no initial radiogenic Os

[3] $\lambda = ^{187}$Re decay constant, 1.666×10^{-11} yr^{-1} (Smoliar et al., 2006)

6.2.2 $^{40}Ar/^{39}Ar$ Geochronology Results

$^{40}Ar/^{39}Ar$ data for hydrothermal sericite and muscovite samples are reported at 2 standard deviations and presented in Appendix IV and plotted in Figure 33. All of the samples display disturbed spectra, characterized by late Ar-loss due to thermal overprinting. Nevertheless, plateau ages can be calculated for the sericite samples, which produced dates of 105.4 ± 2.4 Ma and 112.3 ± 2.6 Ma for A8 and A20 respectively. The muscovite samples did not produce plateau ages, although they have apparent plateaus that are approximately the same age as the sericite samples; total gas ages for these samples are 96.9 ± 0.6 Ma and 98.9 ± 0.4 Ma for BJ-B6 and BJ-P005 respectively.

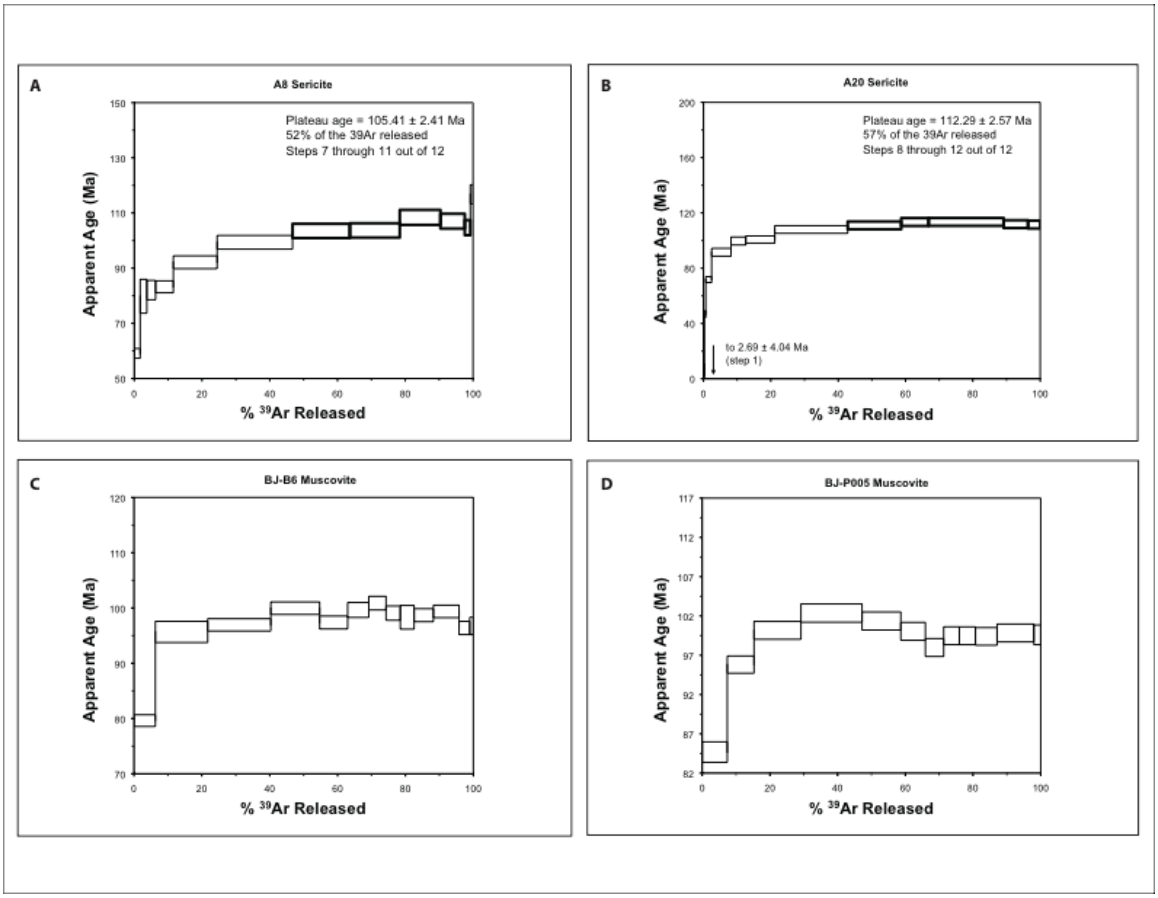

Figure 33: Apparent $^{40}Ar/^{39}Ar$ age spectra for sericite and muscovite from Brucejack: (a) massive monomineralic sericite (A8); (b) hydrothermally sericitized polylithic conglomerate on the margins of strong pervasive silica alteration; (c) hydrothermal muscovite collected from quartz vein stockwork (BJ-B6); (d) fracture-filling muscovite in volcanic sandstone (BJ-P005).

6.3 Fluid Inclusion Results

Measured primary fluid inclusion assemblages (criteria of Roedder, 1984, and Goldstein and Reynolds, 1994) contain two inclusion types: (1) high density, aqueous, liquid-rich inclusions; and (2) low density vapor-rich inclusions. Type 1 and type 2 fluid inclusions occur separately (Fig. 34a,b), or together in all vein stages and suggest that fluids were trapped under two-phase (boiling) conditions. Consequently a pressure correction has not been applied to the measured homogenization temperatures, which are believed to closely approximate original trapping temperatures.

Type 1 fluid inclusions do not contain liquid CO_2 at ambient temperatures, but clathrate melting was observed in some inclusions from vein stage III (Fig. 35d). Hedenquist and Henley (1985) suggested that salinity values may be overestimated by up to ~1.5 wt.% equiv. NaCl where inclusions containing CO_2 clathrate are present, and calculated pressures may also be underestimated.

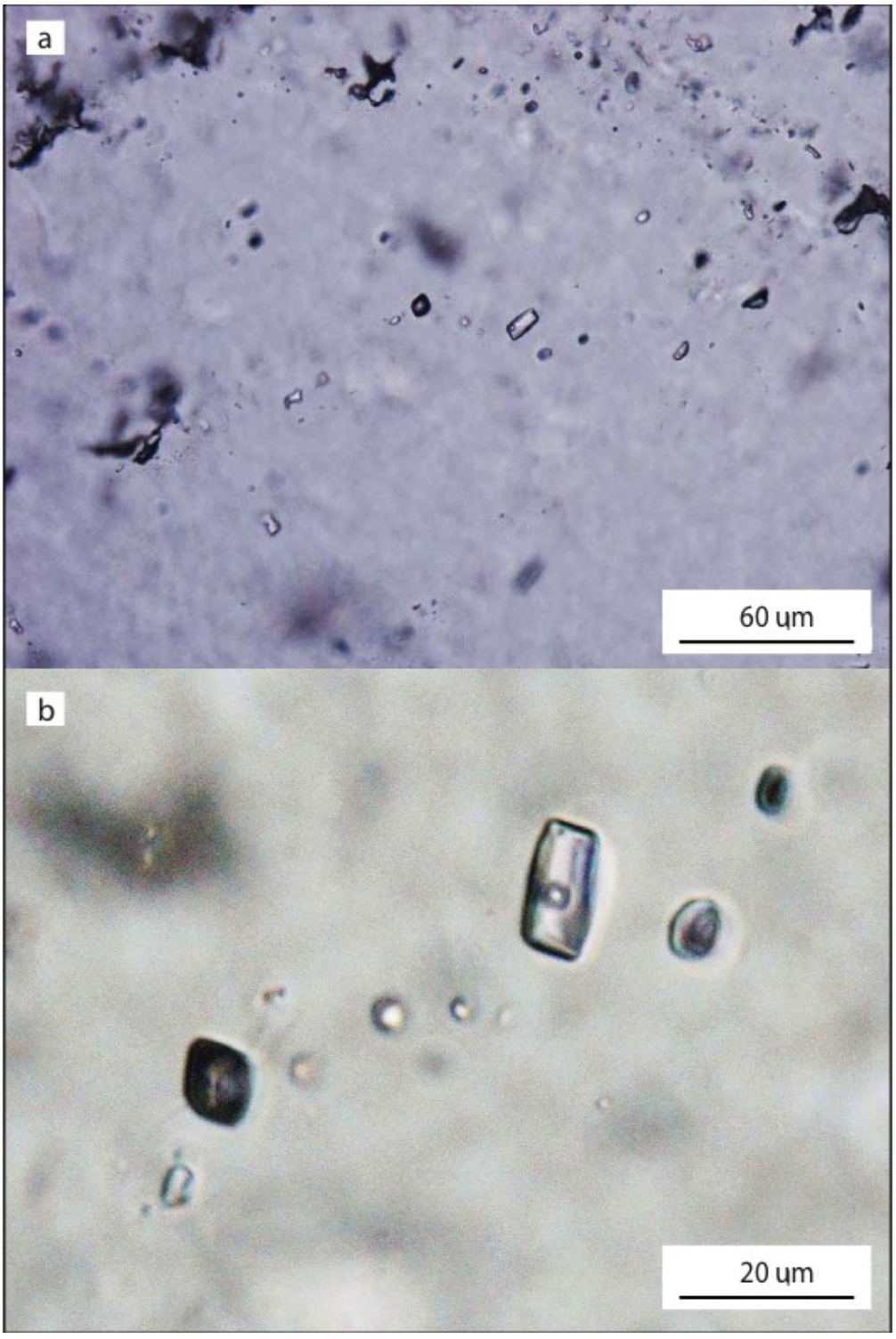
a
60 µm
b
20 µm

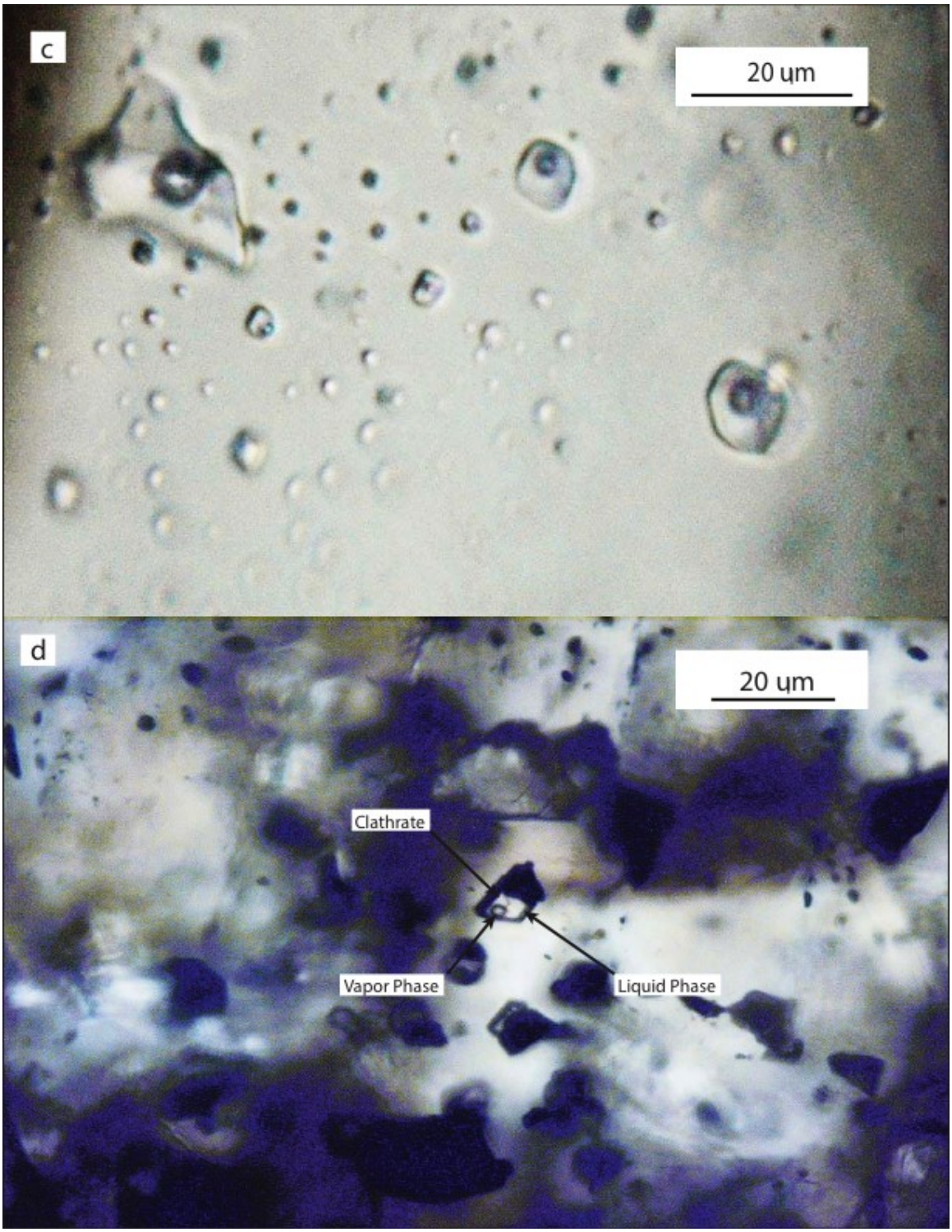

Figure 34: Transmitted light microphotographs of fluid inclusions in veins from the VOK: (a) type 1 primary aqueous fluid inclusion (right) with proximal type 2 primary vapor-rich fluid inclusion (left) suggesting boiling; quartz from stage IV vein. Through adjusting the microscopic stage to variable depths

in the quartz various other neighboring type 1 fluid inclusions are visible, suggesting the inclusions constitute a single fluid inclusion assemblage (VP017-3); (b) close-up of inclusions in (a); (c) type 1 primary fluid inclusions within a 100 μm quartz crystal completely surrounded by galena, stage III vein (VP032-2); (d) fluid inclusion containing clathrate within sphalerite; stage III vein (VP032-15).

6.3.1 Vein Stage II Fluid Inclusion Assemblages

Primary type 1 fluid inclusions from stage II veins homogenized to the liquid-phase between 136°C to 177°C, but with a mode near 170°C. The median homogenization temperature is 170 ± 11°C (*n* = 20; Fig. 35a). Salinity calculated from ice melting temperatures ranges from 3.7 to 13.9 wt. percent NaCl equiv., with a mean value of 5.6 ± 1.1 wt. percent NaCl equiv. (*n* = 20; Fig. 36a). Fluid inclusion assemblages are plotted for stage II veins in Fig. 37 (homogenization temperature against salinity); most of the data cluster around ~160C and ~6 wt.% NaCl equiv., and are generally tightly clustered and show no evidence for fluid mixing.

Type 2 vapor-rich fluid inclusions occur sporadically with type 1 inclusions throughout this vein generation.

6.3.2 Vein Stage III Fluid Inclusion Assemblages

Primary type 1 fluid inclusions from stage III base metal sulfide-rich veins homogenized to the liquid-phase, with homogenization temperatures over a similar range to those of stage II veins from 115 to 196°C. However, stage III data show a weak bimodal distribution with modes at ~150°C and ~180°C, and an overall mean of 154 ± 18 °C (n = 89; Fig. 35b). Salinities of type 1 fluid inclusions have a large range (~1 to ~15

wt. percent NaCl equiv.), with a bimodal distribution and modes at ~5 and ~8 wt. percent NaCl equiv., and an overall mean of 7.6 ± 3.1 wt. percent NaCl equiv. (*n* = 89; Fig. 36b).

Clathrate-bearing fluid inclusions are found exclusively within base metal-sulfide dominated stage III veins and have liquid-phase homogenization temperatures ranging between 115 and 146°C with a median of 125 ± 8°C (*n* = 11; Fig. 35a). Salinities of these inclusions range from 6.5 to 14.4 wt. percent NaCl equiv. and an overall mean of 10.9 ± 2.5 wt. percent NaCl equiv.

Individual fluid inclusion assemblages for stage III veins are plotted in Figure 38, where an unusual correlated trend is observed between higher temperature and lower salinity liquids, and lower temperature, higher salinity liquids. Range in salinity within many fluid inclusion assemblages suggest mixing between these two end-members. The CO_2 clathrate-bearing fluid inclusions appear to belong to the lower temperature higher salinity end-member fluid.

Type 2 fluid inclusions are rarely observed in this vein generation and are not common, suggesting perhaps not all FIA were boiling.

6.3.3 Vein Stage IV Fluid Inclusion Assemblages

Primary type 1 fluid inclusions from stage IV veins show approximately normal distributions of homogenization temperature and salinity, with a means of 158˚ ± 9˚C and 3.6 ± 1.1 wt percent NaCl equiv respectively (*n* = 34; Figs. 35c and 36c). Stage IV veins also contain type 2 vapor-rich fluid inclusions, commonly in the same assemblages as type 1 fluid inclusions, suggesting two-phase (boiling) conditions. Fluid inclusion

assemblages for stage IV veins are plotted in Figure 39, where individual fluid inclusion assemblages are clustered quite tightly and show no evidence for fluid mixing.

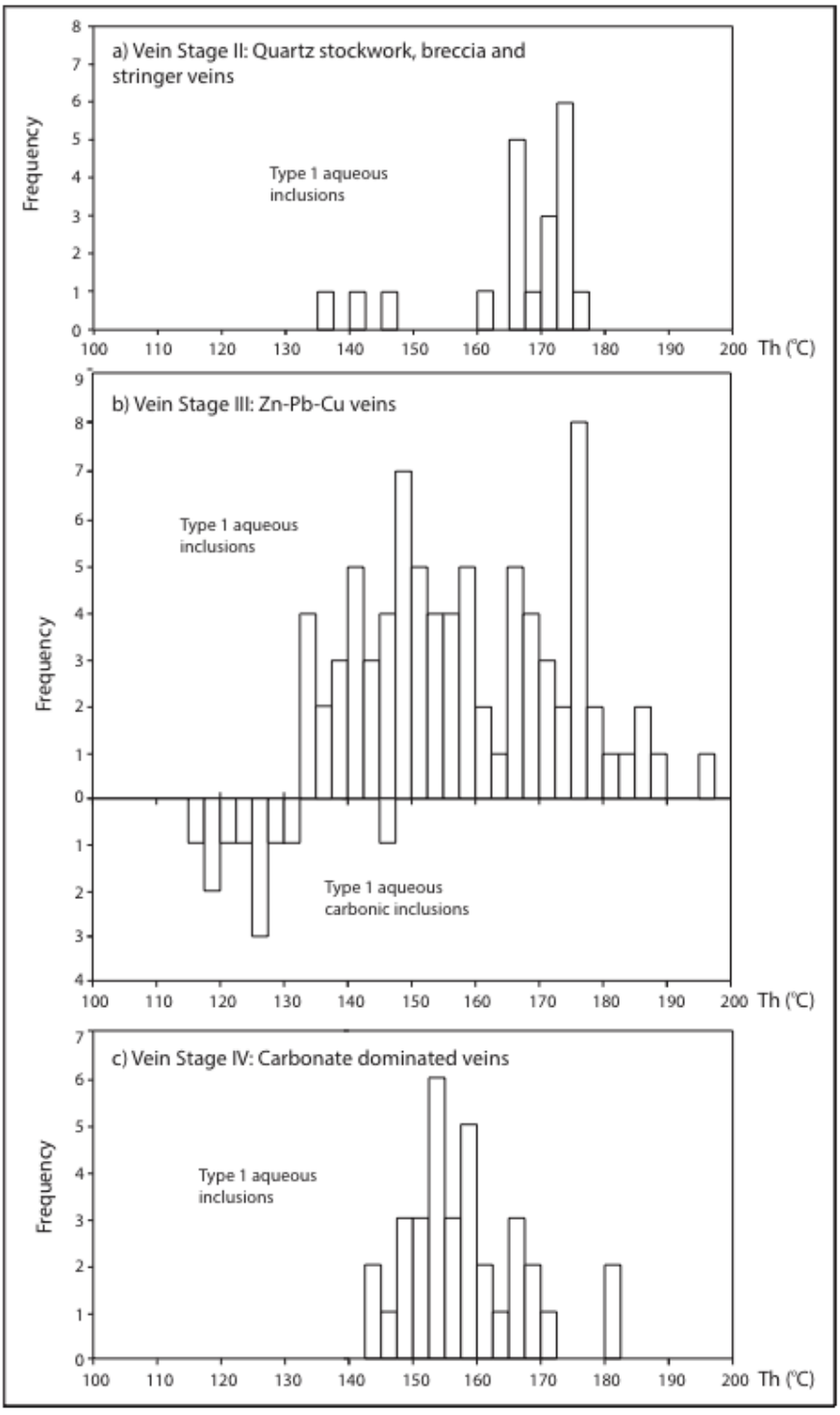

Figure 35: Histogram showing measured homogenization temperatures of type 1 fluid inclusions from: (a) stage II stockwork, breccia, and stringer veins; (b) stage III base metal sulfide-rich veins including CO_2-bearing inclusions; and (c) stage IV calcite-dominated veins

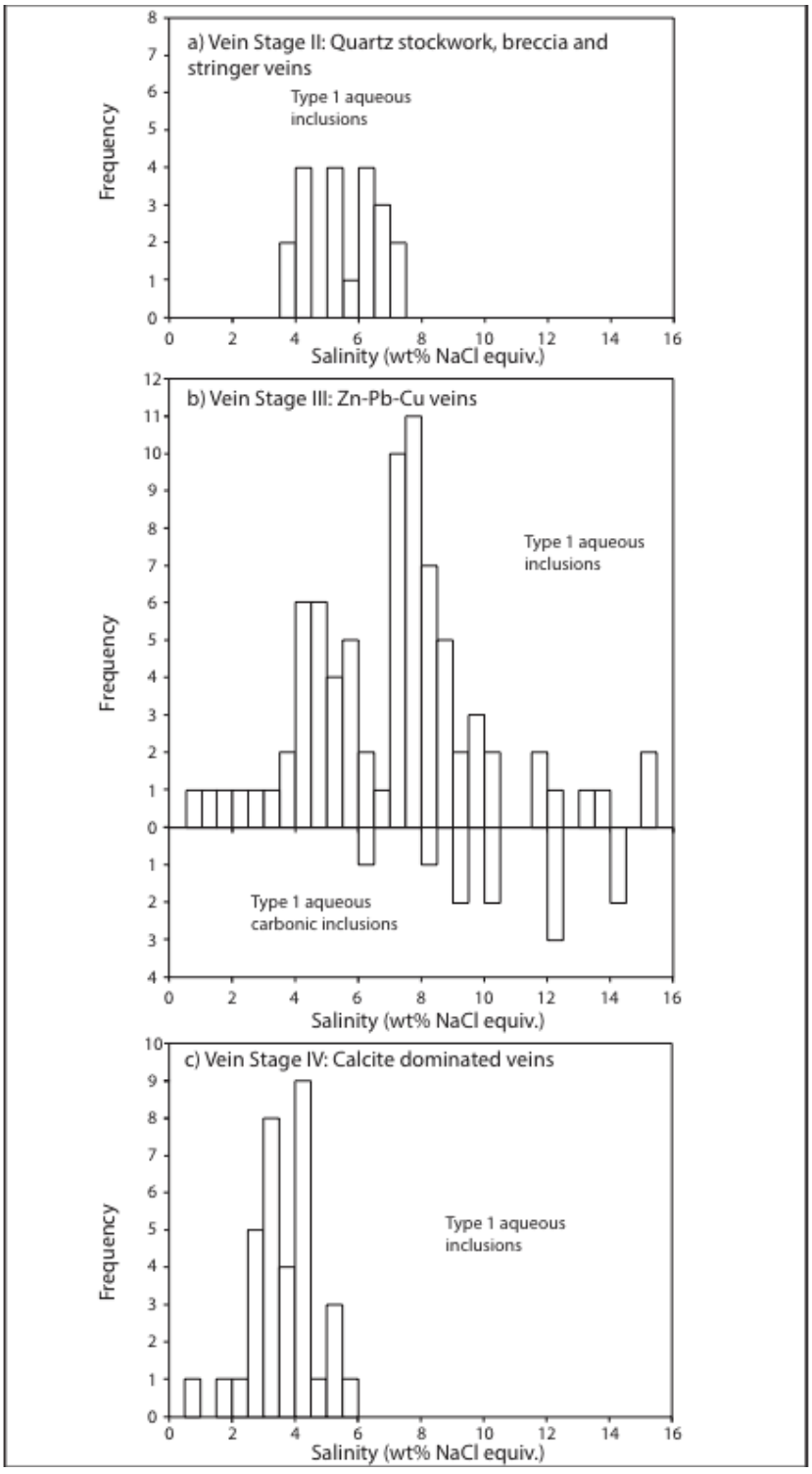
a) Vein Stage II: Quartz stockwork, breccia and stringer veins
Type 1 aqueous inclusions
Frequency
Salinity (wt% NaCl equiv.)
b) Vein Stage III: Zn-Pb-Cu veins
Type 1 aqueous inclusions
Type 1 aqueous carbonic inclusions
Frequency
Salinity (wt% NaCl equiv.)
c) Vein Stage IV: Calcite dominated veins
Type 1 aqueous inclusions
Frequency
Salinity (wt% NaCl equiv.)

Figure 36: Histogram showing calculated salinities of fluid inclusions from: (a) stage II stockwork, breccia, and stringer veins; (b) stage III base metal sulfide-rich veins including CO_2-bearing inclusions; and (c) stage IV carbonate dominated veins.

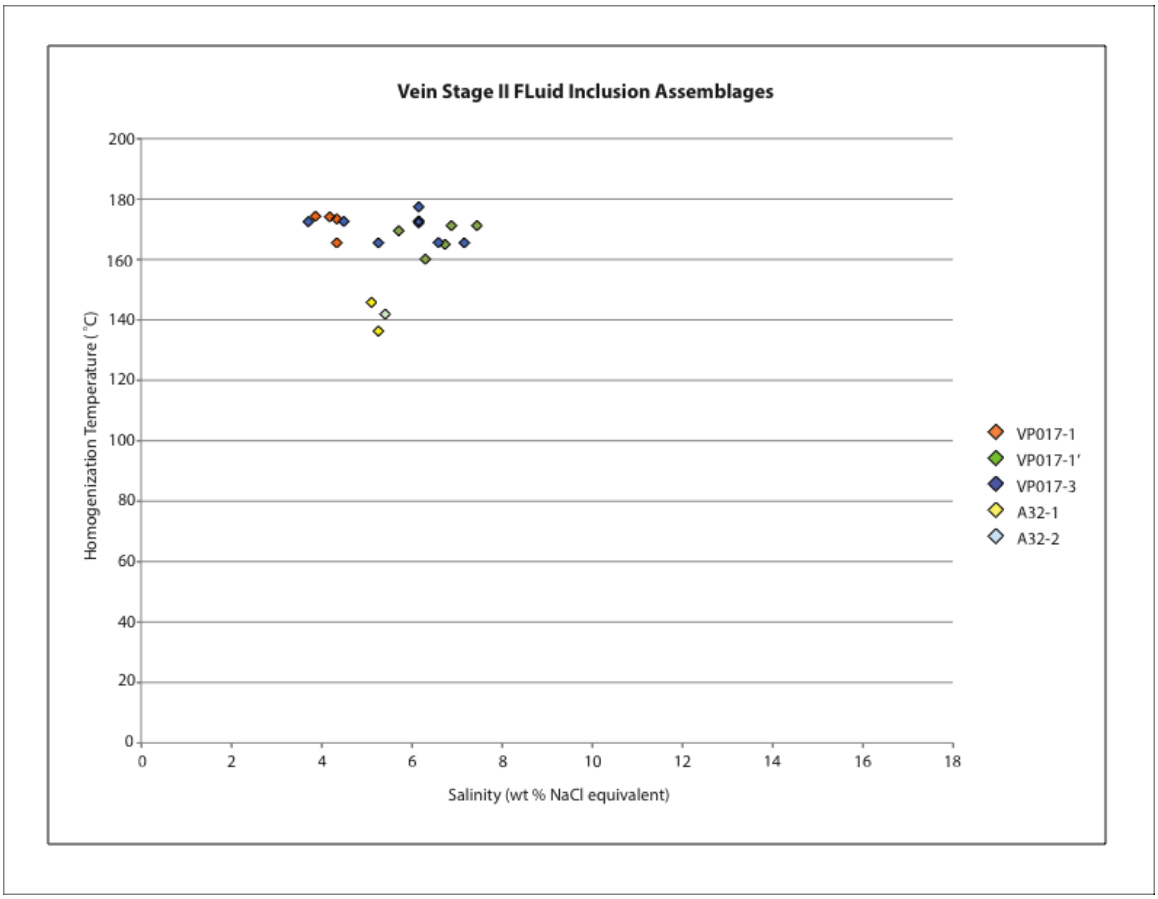

Figure 37: Plot of homogenization temperature against apparent salinity for stage II vein fluid inclusion assemblages.

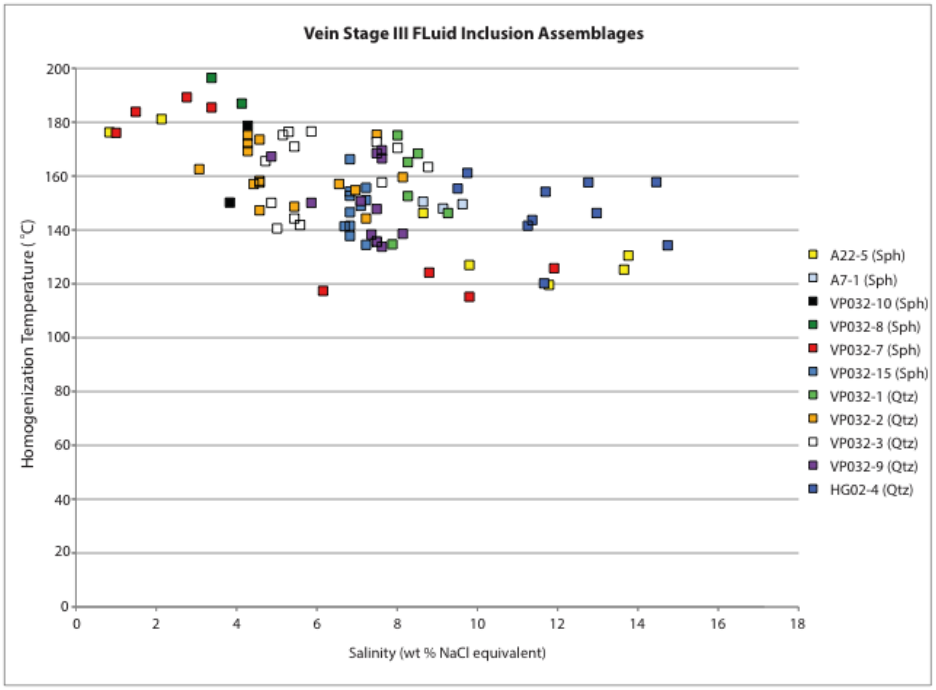

Figure 38: Plot of homogenization temperature against apparent salinity for stage III vein fluid inclusion assemblages. Strong evidence for fluid mixing occurs throughout many individual fluid inclusion assemblages.

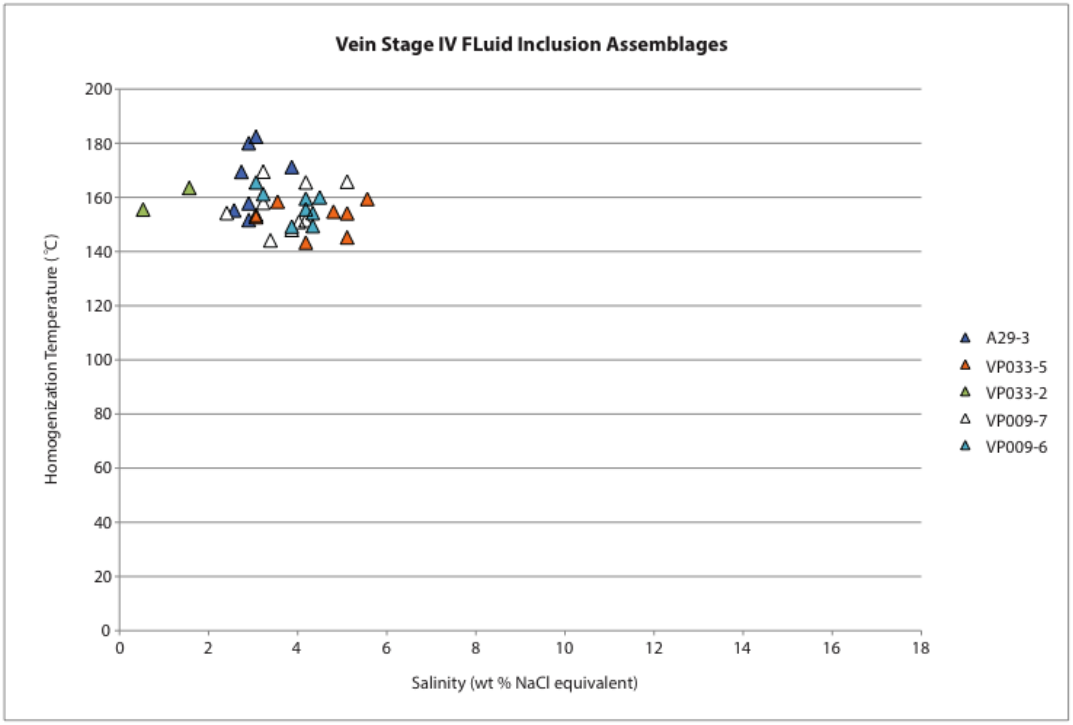

Figure 39: Plot of homogenization temperature against apparent salinity for stage IV vein fluid inclusion assemblages. These fluid inclusion assemblages show no evidence for fluid mixing.

6.3.4 Pressure and Depth Estimates

Vein stages II–IV commonly contain type 1 (liquid-rich) and type 2 (vapor-rich) fluid inclusions in the same fluid inclusion assemblage, suggesting fluids were trapped under two-phase (boiling) conditions (i.e. Th = Tt, and Ph = Pt). Therefore, no correction is needed for fluid pressures under these boiling conditions ($P = P_h = P_f$, where P is the total pressure, P_h is the hydrostatic pressure, and P_f is the fluid pressure; assuming hydrostatic or supra-hydrostatic conditions). Fluid pressures under vapor-saturated (boiling conditions) were calculated for stage II and IV fluids using the data of Haas (1976), and indicate low values of ~6 bar for fluids of 5 wt % NaCl equiv. and ~160˚C. It

is not clear whether stage III fluids were boiling at the time of vein formation, as such a pressure calculation has not been made for these fluids. When using the calculated fluid pressure values and applying them to the formula from Haas (1971):

$$P_h = 0.1897h^{0.8719} \quad (2)$$

where h is the depth below the paleo-surface and measured in meters, a paleo-depth of ~50 m is calculated.

The assumption in these calculations is that the hydrothermal fluids were simple H_2O-NaCl mixtures, and that no gaseous phases were present (i.e. CO_2, CH_4). However, CO_2 clathrate was found in a small number of fluid inclusions, suggesting that at least some CO_2 was present in these fluids. Dissolved CO_2 in hydrothermal liquids has been recognized to increase the vapor pressure of a given liquid (Bodnar et al., 1985; Richards et al., 1997; Wilkinson, 2001), and cause either an increase in the depth of boiling, or decrease the temperature of boiling at a given depth. Hedenquist and Henley (1985) suggested that a typical epithermal fluid may contain up to 0.2 molal dissolved CO_2, which could cause boiling down to depths of 500 m at temperatures below 200˚C (Hedenquist and Henley, 1985).

6.4 Stable Isotope Results

Quartz, calcite, and sulfide (pyrite, sphalerite, and galena) mineral separates from vein specimens across the paragenetic sequence were collected to constrain O, C, and S

isotopic values. The corresponding isotopic compositions of fluids in equilibrium with these minerals were calculated by correcting for temperature-dependent fractionations, using an estimate of 160˚C from fluid inclusions. Vein stage IV calcites are separated into three types based on colour: white (type I), grey (type II), and orange (type III).

6.4.1 Carbon and oxygen isotopic compositions of vein calcite

The carbon and oxygen isotopic ratios of vein calcites are listed in Table 2 and shown in Figure 40.

6.4.1.1 Carbon

Stage II calcites have calculated $\delta^{13}C_{CO2}$ values ranging from -6.7‰ to -3.9‰, with a mean of -5.6 ± 1.1‰ (n = 6). A single sample of stage III calcite sample yielded a $\delta^{13}C_{CO2}$ value of -5.9‰. Type I and II white and grey calcites from vein stage IV have similar ranges of $\delta^{13}C_{CO2}$ from -8.7‰ to -6.4‰ (n = 8) with one outlier at -3.7‰ (sample HG-BJ05). Type III orange calcites range from -9.3‰ to -5.8‰ (n = 7). Taken together, all stage IV calcites yield a mean $\delta^{13}C_{CO2}$ value of -6.8 ± 1.4‰ (n = 15). Stage V calcites have tightly clustered $\delta^{13}C_{CO2}$ values with a mean of -6.4 ± 0.1‰ (n = 3).

6.4.1.2 Oxygen

Stage II calcites have calculated $\delta^{18}O_{fluid}$ values with a small range from -4.3‰ to -1.4‰ and a mean of -2.8 ± 1.3‰ (n = 6). The single stage III calcite sample yielded a $\delta^{18}O_{fluid}$ value of -4.2‰. Stage IV white (type I) and grey (type II) calcites have a narrow

$\delta^{18}O_{fluid}$ range from -5.3‰ to -3.8‰ (n = 8), and orange calcites (type III) have a large range from -5.8‰ to 1.4‰ (n = 7). Collectively, stage IV calcites have a mean $\delta^{18}O_{fluid}$ value of -3.3 ± 2.4‰ (n = 15). Stage V white calcite have a mean $\delta^{18}O_{fluid}$ value of -3.9 ± 0.1‰ (n = 3) and are tightly clustered.

Table 2: Calculated Carbon and Oxygen Isotopic Values for Hydrothermal Vein Calcites

#	Sample	Vein Stage	Comments	$\delta^{18}O$ (VSMOW)	$\delta^{13}C$ (VPDB)	T (°C)	$\delta^{18}O$ Water	$\delta^{13}C$ CO_2
1	HG-BJ-B2	IIa	white calcite	8.4	-6.6	160	-3.6	-5.7
2	HG-BJ-B3	Iia	white calcite	7.9	-7.6	160	-4.1	-6.7
3	HG-BJ-B4	Iia	white calcite	7.6	-7.3	160	-4.3	-6.3
4	BJ-A6-1	Iib	white calcite	10.0	-4.8	160	-1.9	-3.9
5	BJ-A6-2	Iib	white calcite	10.5	-5.8	160	-1.4	-4.9
6	BJ-A9	Iib	white calcite	10.4	-7.1	160	-1.5	-6.2
7	VP004	III	white calcite	7.7	-6.8	160	-4.2	-5.9
8	VP008	IV	white calcite	7.2	-7.3	160	-4.7	-6.4
9	VP010-1	IV	white calcite	6.7	-8.7	160	-5.3	-7.8
10	VP047-2	IV	white calcite	7.6	-7.6	160	-4.4	-6.7
11	VP058-2	IV	white calcite	6.8	-9.6	160	-5.2	-8.7
12	VP010	IV	grey calcite	7.8	-7.9	160	-4.2	-7.0
13	VP047	IV	grey calcite	8.1	-7.7	160	-3.8	-6.8
14	VP058	IV	grey calcite	8.1	-8.9	160	-3.8	-8.0
15	BJ-HG05	IV	grey calcite	8.1	-4.6	160	-3.8	-3.6
16	VP047-1	IV	orange calcite	7.5	-9.0	160	-4.4	-8.1
17	VP058-1	IV	orange calcite	6.6	-10.2	160	-5.3	-9.3
18	BJ-B8	IV	orange calcite	6.1	-8.7	160	-5.8	-7.7
19	A1	IV	orange calcite	13.1	-7.1	160	1.2	-6.2
20	A1-1	IV	orange calcite	13.4	-7.3	160	1.4	-6.4
21	BJ-A29	IV	orange calcite	12.2	-6.7	160	0.2	-5.8
22	BJ-A31	IV	orange calcite	10.1	-7.4	160	-1.9	-6.4
23	VP005	V	white calcite	7.9	-7.4	160	-4.0	-6.5
24	VP040	V	white calcite	8.0	-7.3	160	-3.9	-6.4
25	VP040-1	V	white calcite	8.0	-7.2	160	-3.9	-6.3

**Note: Vein generation Iia and Iib correspond to stringer and breccia veins respectively. Temperature correction for oxygen and carbon isotope values calculated using O'Neil et al. (1969) and Chacko et al. (1991) respectively.*

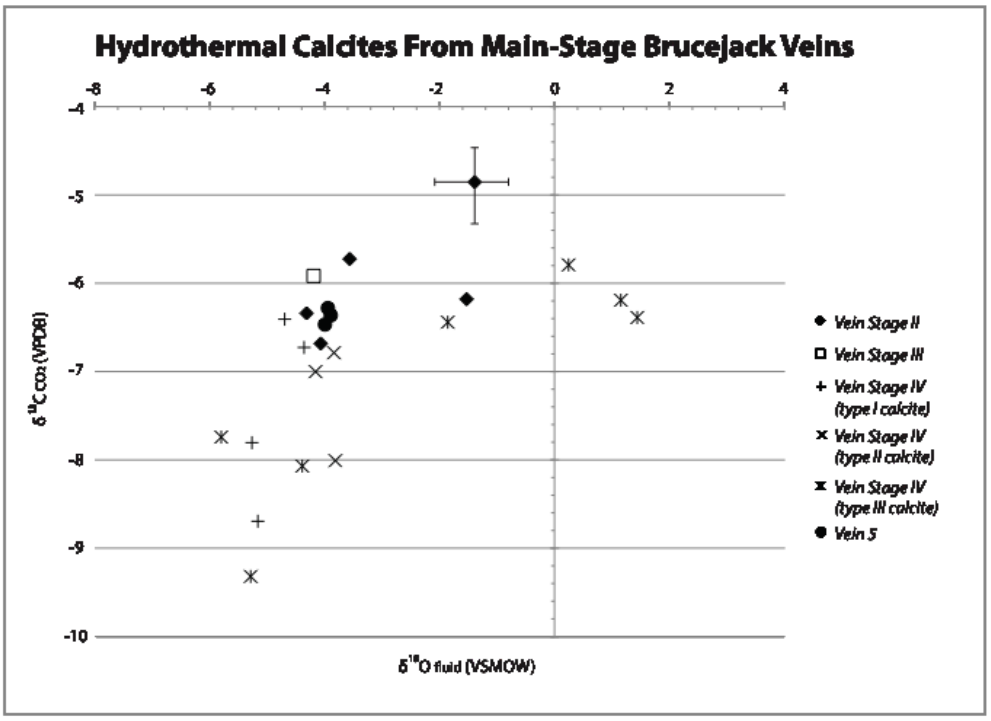

Figure 40: Plot of calculated $\delta^{18}O_{fluid}$ against $\delta^{13}C_{CO2}$ for hydrothermal calcites from main-stage vein generations containing electrum (vein stages II, III, and IV) and barren veins (stage V) at Brucejack. $\delta^{18}O$ and $\delta^{13}C$ values are temperature-corrected using equations from O'Neil et al. (1969) and Chacko et al. (1991) respectively. Error bars for one sample (BJ-A6-2) are shown to illustrate differences of ±10˚C in the temperature estimate used for fractionation calculations.

6.4.2 Oxygen isotopic compositions of hydrothermal vein quartz

The oxygen isotopic ratios of hydrothermal vein quartz samples are listed in Table 3 and shown in Figure 41. Stage II quartz samples have calculated $\delta^{18}O_{fluid}$ values ranging from -1.5 to -7.1‰ and a mean of -4.1‰ (n = 5). Stage III veins have $\delta^{18}O_{fluid}$ values ranging from -3.3 to -7.2‰, and a mean of -4.9‰ (n = 5). No quartz from stage IV veins

was collected because these veins are dominantly calcitic. Stage V quartz samples have $\delta^{18}O_{fluid}$ values ranging from -5.8 and -9.8‰, and a mean of -7.6‰ (n = 5).

Table 3: Calculated Oxygen Isotopic Values for Hydrothermal Vein Quartz

#	Sample	Vein Stage	Comments	δ^{18}Oqtz (VSMOW)	T (˚C)	δ^{18}O Water
1	HG-BJ-3	Iia	Au-within same vein	13.0	160	-1.5
2	HG-BJ-4	Iia	Au-within same vein	12.2	160	-2.3
3	VP003	Iia	Au-within same vein	7.7	160	-6.8
4	HG-BJ-1	Iib	Au-within same vein	11.6	160	-2.9
5	VP002	Iib	White quartz	7.4	160	-7.1
6	HG-BJ-2	III	Au-within same vein	11.2	160	-3.3
7	HG-BJ-2	III	Au-within same vein	11.2	160	-3.3
8	VP004	III	White quartz	8.9	160	-5.6
9	VP018	III	White quartz	7.3	160	-7.2
10	VP013	III	White quartz	9.6	160	-4.9
11	VP032	III	White quartz	9.5	160	-5.0
12	VP005	V	White quartz	8.7	160	-5.8
13	VP030	V	White quartz	7.3	160	-7.2
14	VP040	V	White quartz	6.4	160	-8.1
15	VP016	V	White quartz	4.7	160	-9.8
16	VP023	V	White quartz	7.2	160	-7.3

**Note: Vein generation Iia and Iib correspond to stringer and breccia veins respectively. Temperature correction for oxygen isotope values calculated using Matsuhisha et al., 1979.*

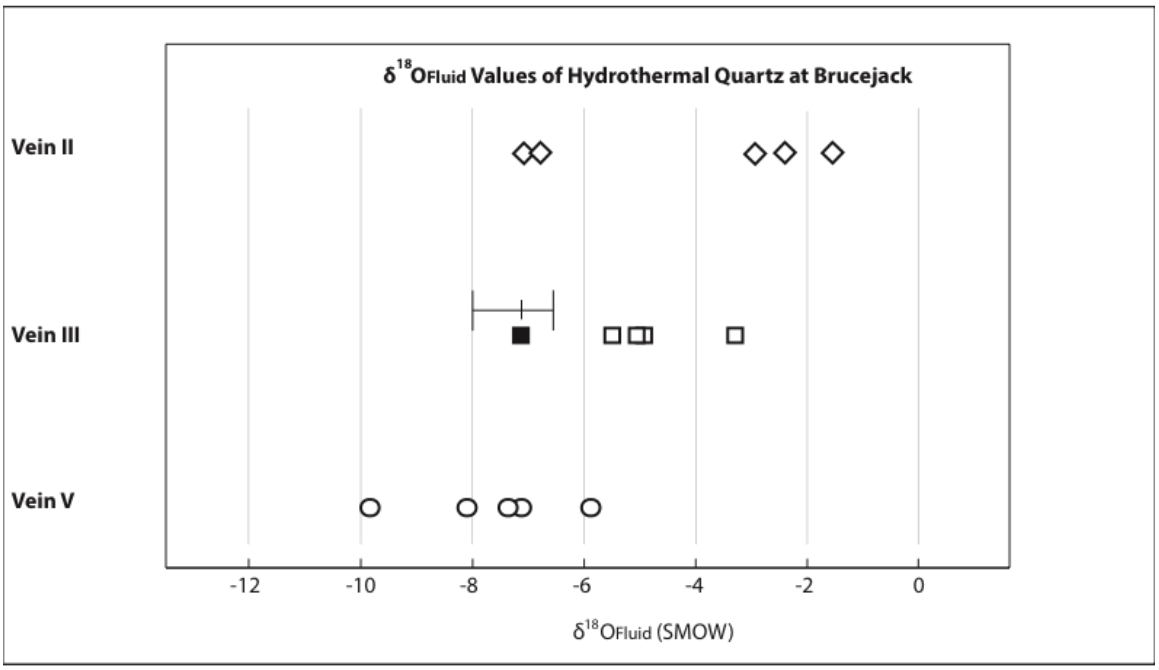

Figure 41: Graph showing calculated $\delta^{18}O_{fluid}$ values for hydrothermal quartz from vein stages II to V. $\delta^{18}O$ values are temperature-corrected using equations from Matsuhisha et al. (1979). Errors for one of these samples (VP018) are shown for differences in fractionation at 150˚C and 170˚C.

6.4.3 Sulfur isotopes of hydrothermal vein sulfides

Sulfur isotopic data for hydrothermal sulfides are listed in Table 4. Pyrite and sphalerite have $\delta^{34}S$ values ranging from -1.7 to 0.6‰ with a mean of -0.7 ± 0.7‰ (n = 15), which is independent of vein stage. A single galena sample from a stage III base metal sulfide vein has a lower $\delta^{34}S$ value of -4.2‰, consistent with the expected fractionation in this mineral.

Table 4: Sulfur Isotopic Values for Hydrothermal Vein Sulfides

#	Sample	Vein Stage	Mineral	$\delta^{32}S$
1	VP015	I	pyrite	0.0
2	VP021	I	pyrite	0.2
3	VP022	I	pyrite	-0.1
4	VP049	I	pyrite	-1.7
5	VP002	Iib	pyrite	0.1
6	VP024	Iib	pyrite	-0.5
7	VP057	Iib	pyrite	-0.2
8	VP004	III	sphalerite	-1.4
9	VP018	III	pyrite	-1.2
10	VP025	III	pyrite	-0.4
11	VP032-1	III	sphalerite	0.5
12	VP032-2	III	galena	-4.2
13	VP054	III	pyrite	-1.7
14	VP010	IV	pyrite	0.6
15	VP007	V	pyrite	-0.6
16	VP030	V	pyrite	0.1

**Note: Vein generation Iib corresponds to breccia veins.*

7.0 Discussion

7.1 Timing of magmatism and hydrothermal activity at Brucejack

The relatively broad range of U/Pb zircon measured for intermediate porphyritic latite flows at Brucejack dates (196.2 ± 0.2 Ma to 179.8 ± 1.1 Ma; Appendix I; pers. Comm. W. Board, June 2015) reveals a prolonged period of volcanism. The Early Jurassic (Sinemurian–Toarcian) age constraint for Brucejack volcanic rocks corresponds well to hornblende-plagioclase-porphyritic andesitic to dacitic flows and subordinate volcanic breccias (MacDonald et al., 1996) of the middle Hazelton Group Unuk River Formation. Dacitic pyroclastic and epiclastic rocks belonging to the Betty Creek Formation are also restricted to this age. Extrusive volcanic rocks similar to porphyritic latite flows at Brucejack are found elsewhere in the Iskut River area and have yielded

Early Jurassic U-Pb (zircon) dates ranging from 195–185 Ma (Anderson, 1993; Davies et al., 1994). One trachybasaltic dyke records a U/Pb age of 182.7 ± 1.0 Ma (pers. Comm. C. Greig, June 2015). Other trachybasaltic dykes are found to crosscut stage IV carbonate dominated veins, representing the last vein generation containing Au-mineralization. This date provides the minimum age of mineralization at Brucejack.

Two Re-Os ages of molybdenite from Bridge Zone (191.7 ± 0.8 and 191.5 ± 0.8 Ma) are distinctly older than molybednite from West Zone (188.9 ± 0.9 Ma), suggesting that these ore zones are not cogenetic and likely formed from a separate, but possibly related, period of hydrothermal activity. Textural and mineralogical discrepancies between Bridge Zone and West Zone also suggest this. West Zone features colloform and crustiform banding, open space filling with bladed calcite, and mineralization is hosted in quartz veinlets and stockworks with minor barite and adularia. In addition to physical features, West Zone has anomalously high Ag/Au when compared to other prospects at Brucejack (i.e. VOK and Bridge Zone). Bridge Zone mineralization is also hosted in quartz veinlets and stockworks, but has dissimilar textures and vein mineralogy contained within the West Zone.

Some hydrothermal systems may occur up to 1.5 m.y. after volcanism has ceased (Silberman, 1985; Heald et al., 1987; Hedenquist and Lowenstern, 1994; Conrad and McKee, 1996; Singer and Marchev, 2000), and a single large intrusive event may sustain hydrothermal convection for up to 0.8 m.y. (Cathles et al., 1997). However, most epithermal deposits record mineralization occurring <1 m.y. after initial volcanism (Heald et al., 1987; Arribas, 1995), and it is unlikely that hydrothermal mineralization occurred continuously at Brucejack over a period >1 m.y. period. The distinct Re-Os ages

suggest instead that multiple episodes of hydrothermal activity occurred, perhaps driven by multiple intrusions of porphyry stocks.

Apparent $^{40}Ar/^{39}Ar$ ages calculated for sericite at Brucejack (112–105 Ma; Appendix IV) do not reflect the timing of hydrothermal mineralization. These dates are similar to K-Ar dates provided by other studies (Margolis, 1993: 110.4 ± 2.6 Ma; Kirkham, 1989: 110.2 ± 2.3 Ma), and suggest thermal overprinting in the mid- to Late Cretaceous. Evenchick (1991b) suggested that this thermal peak was related to the formation of the Skeena Fold Belt (and associated structures) formed by deformation during the Cretaceous accretion of the Insular Belt.

7.2 Lithogeochemistry and Tectonic Setting

Ore-bodies at Brucejack are contained within, or proximal to, moderate phyllic alteration halos. This hydrothermal alteration has caused significant alkali element mobility, although REE and immobile elements show minimal effects.

Lithogeochemical data from this study indicate that porphyritic lava flows (termed latites in the field) belonging to the Hazelton Group and their derived volcaniclastic equivalents are of trachyandesite and trachydacite compositions, and trachybasaltic compositions are indicated for broadly coeval mafic post-mineralized dykes (Fig. 27). Relative enrichments of LILE in least-altered samples support a subduction-related tectonic environment (Gill, 1981; Wilson, 1989; McCulloch and Gamble, 1991) with a significant crustal component (Gribble et al., 1996). This is also indicated by enrichments of U and Pb, and depletions of Nb, Ta, and Ti (Fig. 31).

Enrichments in U and Pb result from crustal contamination during magma ascent from depth (Hildreth and Moorbath, 1988).

Negative Ti, Nb, and Ta anomalies result from retention in minerals such as rutile and magnetite under subduction conditions (Brenan et al., 1994; Audétat and Keppler, 2005; Richards, 2011). Weak Eu anomalies relative to adjacent REEs are also present (Fig. 30) and indicate minor plagioclase fractionation (Frey et al., 1978; Hanson, 1980) or oxidizing magmatic conditions, whereby Eu is mainly present as incompatible Eu^{3+}. Depletions of HREE relative to LREE with listric trends between MREE and HREE indicate a degree of hornblende and titanite fractionation (Green and Pearson, 1985; Sisson, 1994), typical of evolved hydrous arc magmas. From the Ta/Yb discrimination diagrams (Fig. 32; Pearce, 1984), intermediate porphyritic latite flows and both dyke series show calc-alkaline volcanic arc signatures. This is the tectonic environment interpreted for the Stikine terrane prior to Middle Jurassic accretion with exotic terranes already accreted to the North American craton.

Cenozoic basaltic trachyandesite dykes are postmetamorphic (<110 Ma; inferred from a general lack of alteration mineralogy) and have a syn-collisional geochemical character (Fig. 32b). Basaltic trachyandesite dykes at Brucejack are mantle-derived basaltic alkaline melts, where there is an absence in U, Pb, Eu, and Ti anomalies and only weak depletions in Nb and Ta, indicating a lesser degree of crustal assimilation (Fig. 31). The Canadian Cordillera was an active accretionary rogeny in the Early Cretaceous and these late dykes were likely formed in a collisional environment.

Typical calc-alkaline arc magmas are thought to be oxidized relative to MORB (ΔFMQ = +0.5 to +2; Gill, 1981; Ballhaus et al., 1991; Rowe et al., 2009; Zimmer et al.,

2010; Richards, 2011, 2015), suggesting that they are ideal transporting agents for chalcophile elements from the mantle (Botcharnikov et al., 2011). It is also documented that arc magmas have higher H_2O contents (~4 wt% H_2O; Plank et al., 2013) relative to OIB and MORB magmas (~1.7 wt% and 0.1-0.5 wt% H_2O respectively; Schmidt and Poli, 1998). The high H_2O contents of arc magmas are necessary for shallow crustal emplacement and generation of near-surface, potentially metal-forming hydrothermal systems (Richards et al., 2012).

7.3 Deposit Classification

One of the main objectives of this study was to evaluate and classify Brucejack in terms of deposit type. Many of the geological and geochemical features recognized at Brucejack are those that are typical for low- to intermediate-sulfidation epithermal, intermediate volcanic-hosted, Au-Ag deposits:

1) Host rocks are Early Jurassic, subaerial–subaqueous intermediate volcanic flows, volcaniclastic rocks, and associated volcanic sedimentary rocks, which were likely formed in a dynamic, tectonically active, subduction-related environment.
2) Hydrothermal breccias and stockworks are common and suggest episodic conditions with periodic pressure releases. Crustiform and cockade banded veins occur sporadically and indicate repetitive episodic veining and near surface conditions.

3) The hydrothermal alteration assemblages are dominantly represented by quartz, sericite, pyrite, calcite, and minor barite, which is consistent with phyllic alteration.
4) The absence of enargite, and presence of vein adularia and sericite reflect near neutral pH fluid conditions (Heald et al., 1987).
5) The large range of sulfosalt minerals, stability of chalcopyrite, tetrahedrite-tennantite, and FeS-poor sphalerite, scarcity of arsenopyrite, and absence of pyrrhotite at Brucejack is consistent with intermediate sulfidation states (Sillitoe and Hedenquist, 2003).
6) Enrichments in Au and Ag.
7) Stable isotope compositions suggest fluid mixing with modified magmatic fluids and meteoric fluids.
8) Fluid inclusions suggest bonanza Au was precipitated at low temperatures (~140–180˚C) and from low–moderate salinity (0.5–15.5wt % NaCl equiv.) fluids.

The Valley of the Kings is more typical of intermediate-sulfidation systems, because it contains base metal-poor veins, manganoan carbonates, and silver sulfides and sulfosalts (White et al., 1995), and does not contain colloform banding, open space filling, and only minor vuggy quartz, and no adularia or barite. West Zone contains features more suggestive of low-sulfidation epithermal deposits, where cockade textures, cryptocrystalline quartz, and replacement of bladed calcite by quartz is recognized (MacDonald et al., 1996); adularia and barite contained within vein mineralogy also suggest this. The younger age of 188.9 ± 0.9 Ma provides evidence for a younger LS-epithermal system cospatial

to other prospects more characteristic of IS-epithermal mineralization (i.e. VOK, Bridge Zone, Galena Hill Zone).

Mesothermal deposits, when compared to epithermal deposits, contain intermediate–high CO_2 content in fluid inclusions, have higher As, W, and Au/Ag values, and $\delta^{18}O_{H_2O}$ values ranging from +3 to +10‰, while epithermal deposits have $\delta^{18}O_{H_2O}$ values ranging between -14 to -7‰ (Nesbitt et al., 1986). Although Brucejack has anomalously high Au/Ag values when compared to typical low–intermediate epithermal deposits, the $\delta^{18}O_{H_2O}$ values are representative of epithermal systems with magmatic values; mesothermal systems typically involve metamorphic fluids (Nesbitt et al., 1986). Greenschist metamorphism is common to mesothermal deposits. Wallrocks at Brucejack show moderate–strong hydrothermal phyllic alteration proximal to fluid pathways, and lower-greenschist metamorphic conditions are not prevalent.

Table 5: Characteristics of the Valley of the Kings within the Brucejack deposit compared with mesothermal deposits from the Canadian Cordillera (from Nesbitt et al., 1985, and references therein)

	MESOTHERMAL	BRUCEJACK
AGE	Late Jurassic to Tertiary	Early Jurassic
PETROGRAPHY OF HOST ROCKS	Mafic to felsic volcanic rocks and plutons, clastic sedimentary rocks, carbonates, and serpentines: low to upper greenshcist facies metamorphism	Intermediate volcanic flows, volcaniclastic rocks, and associated volcanic sedimentary rocks
STRUCTURAL SETTING	Regional: major, transcurrent fault zones Deposit scale: vertical normal or reverse faults in highly deformed zones	Regional: basin marignal faults Deposit scale: vertical normal or reverse faults with evidence for brittle/ductile fault behavior
MINERALOGY	Quartz, Ca-Fe-Mg carbonates, albite, scheelite, mariposite, pryrite, pyrrhotite, arsenopyrite, graphite, galena, chalcopyrite, sphalerite, native Au, Au-Ag tellurides	Quartz, Ca-Mn carbonates, barite, adularia, pyrite, Fe-poor sphalerite, galena, chalcopyrite, rutile, molybdenite, arsenopyrite, electrum, Ag-sulfosalts
TEXTURES	Massive or ribboned veins 0.1 to 5 m width, ore shoots up to 100s m length and depth; replacement zones	Stockwork and breccia veins, crustiform and cockade banding
AU/AG	1:10	2:1 (exception of West Zone 1:28)
HYDROTHERMAL ALTERATION	Carbonatization, silicification, sericitization, development of pyrite, mariposite, albite, chlorite, talc, and graphite	Sericitization, silicification, pyritization, chloritization, minor barite and graphite
FLUID INCLUSION DATA	T_H = 200 to 350°C Low salinity; intermediate to high CO_2	T_H = 140 to 190°C Low to moderate salinity; low CO_2
STABLE ISOTOPE DATA	$\delta^{18}O_{Qtz}$ = +14 to +18‰; $\delta^{18}O_{Serp}$ = +7 to +9‰ δD_{Serp} = -110 to -180‰; $\delta D_{Fld\ Inc}$ = -80 to -160‰ $\delta^{18}O_{Fld}$ = +5 to +9‰ δD_{Fld} = -80 to -100‰ (south), -140 to -160‰ (north)	$\delta^{18}O_{Qtz}$ = +6 to +13‰; $\delta^{18}O_{Cal}$ = +6 to +13‰ $\delta^{18}O_{Fld}$ = -10 to +1‰

7.3.1 Depth of Emplacement

Although Brucejack is similar to low–intermediate-sulfidation epithermal deposits, it is believed that the depth of metal-emplacement is deeper than expected for typical near surface epithermal deposits. Brucejack has abundant stockwork veining and breccia-veins, and minor vuggy quartz, crustiform and cockade banded veins, along with adularia, acanthite, and bladed calcite suggesting these ore-forming conditions were at

shallow paleodepths within an epithermal environment. However, the absence of colloform banding and uncommon open-space filling suggest deeper levels of deposition, perhaps associated with a porphyry or mesothermal environment.

The presence of crystalline quartz rather than chalcedony and uncommon adularia led Sillitoe (1988) to postulate that deposits in the Philippines formed at deeper crustal levels than what is typical for epithermal deposits, which is consistent for Brucejack. The Porgera gold deposit, Papua New Guinea, is also classified as an epithermal deposit with deeper emplacement characteristics (Ronacher et al., 2000). Mineralizing fluids in the high-grade gold event (stage II) at Porgera contain small amounts of volatile gases including CO_2 (Richards et al., 1997). The presence of CO_2 and CH_4 has been shown to affect the total gas solubility, lowering the temperature and increasing the depth where boiling can occur in epithermal systems (Giggenbach, 1997; Richards et al., 1997; Lowenstern 2001, 2002; Baker, 2002). Hydrothermal fluids containing CO_2 and CH_4 may be a significant contributing factor in the anomalous vertical depths of ore emplacement in epithermal environments (Drummond and Ohmoto, 1985; Richards et al., 1997). Although no data are available for the gas content of the hydrothermal fluids at Brucejack, CO_2 clathrate was observed in some fluid inclusions. This may indicate that the fluids were relatively gassy (compared to typical low-sulfidation fluids), resulting in boiling (effervescence) at greater depths and lower temperatures than in gas-poor systems. This observation may explain the large vertical extent of mineralization at Brucejack (currently confirmed to exceed 1000 m).

7.4 Hydrothermal Mineralization

7.4.1 Source of ore fluid and metal

The bulk salinity for magmatic fluids is believed to be between 5 and 10 wt% NaCl equivalent (Burnham, 1979; Cline and Bodnar, 1991; Hedenquist and Lowenstern, 1994; Heinrich, 2005; Heinrich, 2007), and fluids <5 wt% NaCl equiv. salinity are believed to be of meteoric affinity. Fluid inclusion data indicate that vein stage II and IV are generally 3–7 wt% NaCl equivalent, and are likely condensed magmatic fluids. Vein stage III fluid inclusion salinities are not tightly clustered, and a large range of salinity is indicated for several fluid inclusion assemblages in this vein stage (i.e. sample A22 shows a range of 0.9–14.4 wt% NaCl equiv.). At the low temperatures of these fluids it is difficult to explain this large range in salinity by boiling (as suggested by Wilkinson, 2011), and it is considered more likely to reflect mixing between two end-member fluids. The moderate salinity end-member approximates the bulk salinity of magmatic fluids, whereas the more saline fluids are interpreted to be cooler brines of original meteoric origin (as indicated by oxygen isotopes; Fig. 42).

Mineralized calcite veins (stage IV) have $\delta^{18}O_{fluid}$ values as high as 1.4 ± 2.3‰, while vein stage II and III quartz veins are up to -1.5 and -3.3‰ respectively. These temperature corrected $\delta^{18}O_{fluid}$ values are lower than expected for exclusively magmatic fluids (typically ranging from 5.5–9.0‰; Taylor, 1979), and may be explained by early dilution of magmatic fluids with meteoric waters or isotopic exchange with surrounding sedimentary rocks as fluids ascended to higher levels in the crust.

Although it is more common for hydrothermal fluids in epithermal systems to fall between the magmatic water and the meteoric water line, magmatic fluids may be the

source of aqueous ore fluids in shallow epithermal gold deposits (*Creede, United States:* Wetlaufer, 1977; Bethke and Rye, 1979; *Eureka, United States*: Casadevall and Ohmoto, 1977; Heald et al., 1987; *Pueblo Viejo, Dominican Republic*: Muntean et al., 1990; *Metaliferi Mountains, Romania*: Alderton and Fallick, 2000; *Rosia Montana, Romania*: Wallier et al., 2006), and may be the source of metal, although this is debated.

Brucejack $\delta^{32}S$ values for sulfides all cluster close to zero per mil (n = 16) suggesting a magmatic source for sulfur. Calculated $\delta^{13}C_{CO_2}$ values for hydrothermal calcites range from -9.3 to -4.9‰ with mean values of -6.5 ± 1.3‰ (n = 25), suggesting a magmatic source with a minor sedimentary component. Furthermore, molybdenum is observed at Bridge Zone and West Zone, where the Re concentrations (within molybdenite) are anomalously high (>1000 ppm) and suggest mantle derived Re (Stein et al., 2001).

It is likely that Brucejack ore-forming fluids were low-salinity magmatic liquids exsolved and condensed from a calc-alkaline melt at shallow levels in the crust. These fluids underwent some isotopic exchange with the surrounding volcanic-sedimentary wallrocks and also mixed with more saline groundwater of meteoric origin.

7.4.2 Early Sulfidization and Phyllic Alteration of Wall Rocks

Wallrocks throughout the Brucejack deposit are strongly pyritized and sericitized, especially close to ore zones and lithological contacts (alteration persists for tens of meters away from these zones). This widespread sulfidization of surrounding rocks is suggested to have occurred during a pre-mineralization sulfidation hydrothermal event, possibly in an early porphyry-style event. Early pyritization is present as stage I stringer

veins, disseminated masses, and clots hosted throughout the wall rock, and has a magmatic isotopic signature ($\delta^{32}S$ = -1.7 to 0.5‰). Wallrocks in the VOK commonly contain 1–2 g/t Au (pers. Comm. W. Board, June 2015), where electrum is found associated with early pyritization. Formation of pyrite in wallrocks typically occurs by reactions between iron-bearing silicates and oxides with ascending H_2S-rich fluids (Gammons and William-Jones, 1997).

The formation of phyllosilicate alteration (illite) by reaction of feldspars with mildly acidic fluids occurred in two separate events: 1) during pre-mineralization sulfidization of surrounding rocks, and 2) with influx of fluids associated with gold mineralization. Low grade metamorphism associated with the accretion of the Insular Belt at 105–112 Ma, is thought to have caused recrystallization of illite to fine-grained sericite.

Heinrich et al. (2004) suggested fluid evolution paths from magmatic to epithermal conditions that act to maximize the efficiency of gold transport. High gold concentrations (>10 ppm) may be transported from high temperature (>450ºC) porphyry levels to lower temperature (i.e. 150ºC) epithermal depths without gold ever becoming saturated. This is possible where conditions permit fluids to contain high S/Fe ratios and feldspar and muscovite buffer acidity (Heinrich et al., 2004).

The pre-mineralization pyritization event at Brucejack led to abundant free ferrous Fe in surrounding wall rocks to be converted to pyrite. When later mineralizing fluids passed through these pyritic wall rocks they had no capacity to buffer H_2S (Gammons and Williams-Jones, 1997), and reduced S concentrations may have remained elevated and available for gold complexation (Heinrich et al., 2004). Precious metal

systems rich in CO_2 also may have high H_2S concentrations compared to systems depleted in gas (Hedenquist and Henley, 1985). With increased H_2S concentrations gold solubility will increase (Benning and Seward, 1996) and fluids will have a greater capacity to transport gold. Furthermore, feldspars and illite present in wallrocks during hydrothermal gold deposition buffers the acidity of the magmatic fluids through acid neutralization, again maximizing the free HS- ligand concentration (Heinrich et al., 2004). Zones of pervasive phyllic alteration (muscovite ± pyrite ± clay minerals ± sulfate ± carbonate) are the most favorable ascent paths for effective gold transport from the site of porphyry vapor separation to epithermal ore formation (Heinrich, 2005). This explains both the spatial relationship with gold mineralization to moderate–strong phyllic alteration zones at Brucejack, and the large capacity to transport gold.

7.4.3 Depositional Mechanism(s): Fluid Mixing and Boiling

In hydrothermal deposits two of the main processes responsible for ore mineral precipitation are boiling and fluid mixing. Stable isotopes at Brucejack provide evidence for fluid mixing, where veins show large ranges in $\delta^{18}O_{H_2O}$ in hydrothermal vein calcite and quartz. Hydrothermal calcite from vein stage IV shows the largest range in calculated $\delta^{18}O_{H_2O}$ from 1.4 to -5.8 ‰ (n = 15), and hydrothermal quartz from stage II and III also show large ranges in $\delta^{18}O_{H_2O}$ between -1.5 to -7.1 ‰ (n = 5) and -3.3 to -7.2 ‰ (n = 6) respectively. Fluid mixing is important in carbonate-rich late-stage veins in epithermal deposits (Simmons et al., 1988; Cooke and Bloom, 1990; Kwak, 1990; White and Hedenquist, 1990). At Brucejack vein stage IV manganoan calcites have $\delta^{18}O_{H_2O}$ values ranging from 1.4 to -5.8 ‰ (n = 15). This suggests mixing between modified juvenile

magmatic water and meteoric water. Hydrothermal circulation of meteoric waters mixing with ascending magmatic ore-bearing fluids and progressive dilution of magmatic fluids with meteoric fluids may account for these mixing trends.

Stage III fluid inclusions provide evidence for fluid mixing where a significant salinity range (0.5 to 15.5 wt % NaCl equiv.; $n = 89$) is observed over a restricted homogenization temperature interval (~140–180˚C). Variable salinities are also reflected in individual fluid inclusion assemblages, where stage III fluid inclusion assemblages have ranges in salinity of >10 wt. % NaCl equiv. Significant salinity variations would occur from the mixing two end-member fluids: a saline meteoric-derived groundwater and a relatively dilute magmatic fluid.

Boiling is by far the most important processes controlling the temperature of hydrothermal fluids leading to ore precipitation near the surface (White and Hedenquist, 1990). Brucejack fluid inclusions show evidence for boiling, where type 1 liquid-rich fluid inclusions are observed with type 2 vapor-rich fluid inclusions throughout electrum-bearing vein generations (mainly restricted to stages II and IV) in the paragenesis. Type 1 liquid-rich fluid inclusions are cospatial and cogenetic with type 2 vapor-rich fluid inclusions indicating fluids at the time of vein formation were on the H_2O liquid-boiling curve. Large-scale silica-flooded breccia veins (stage II) are another manifestation of boiling (Sillitoe, 1985). Hydraulically fractured quartz veins and hydrothermal breccias not only suggest boiling, but also indicate that hydrostatic pressure locally exceeded lithostatic pressure (DeRonde and Blattner, 1988), where pressure releases may have induced boiling events. Bladed calcite is found sporadically throughout West Zone and the VOK and again suggests boiling conditions (Browne, 1978).

7.4.4. Episodic Gold Mineralization

At Brucejack anomalously high gold grades are likely not the consequence of a single depositional event. Rather, it is more probable that multiple injections of gold-rich fluids occurred episodically, where gold was scavenged and reprecipitated repetitively through the duration of the hydrothermal system(s). An episodic ore-forming environment is recognized from the multiple overprinting vein relationships, where vein stages containing electrum (II–IV) are each found crosscutting one another locally. Stage II veins specifically have multiple episodes of veining characterized through the overprinting relationships of texturally dissimilar veins (i.e. stockwork, breccia, and stringer veins and veinlets). The presence of cockade and crustiform banded veins further provides evidence for repetitive fluid pulsing.

Temperature corrected oxygen isotope trends in stage II–V veins represent a shift from modified magmatic to meteoric water values, and a pulsing nature is revealed through the large ranges of $\delta^{18}O_{H_2O}$ in isolated vein generations. Bonanza gold mineralization at Brucejack may have resulted from an episodic process, such as fault fracturing, which led to instantaneous fluid migration. Seismic fault movement may have periodically released pressure (Sibson, 1992) and triggered localized boiling conditions, which may have been enhanced by small amounts of dissolved CO_2 (and possibly CH_4). Stage II and IV are likely to have formed under these conditions, where boiling is prevalent in fluid inclusion assemblages and the dilute (3–7 wt% NaCl equiv.) low-temperature (140–180˚C) fluids are derived from condensed magmatic solutions. A rapid pressure decrease produced through hydraulic fracturing would trigger the onset of

boiling, causing increases in pH by partitioning acidic volatiles into the vapor phase, promoting gold deposition (Williams-Jones et al., 2009). If this episodic fault-valve process occurred it would induce repeated gold saturation (Cox, 1995), and lead to the bonanza gold observed at Brucejack (up to 41582 g/t Au over 0.5m).

Evidence for local overpressure conditions are reflected in episodic hydraulic fractures within strongly silicified conglomerate rocks and vein breccias throughout the Valley of the Kings and West Zone prospects. Siliceous conglomerates (often cospatial with monomineralic metasomatized sericite) are found at the basal and upper contacts with volcanic sedimentary and tuffaceous rocks respectively. These rocks have been exposed to high water/rock ratios, likely from the rapid release of neutral pH hydrothermal fluids. Siliceous alteration may have formed through self-sealing silicification from convecting hydrothermal fluids, where preferential fluid migration was mainly restricted to permeable lithologies (i.e. porous volcanic conglomerate). As magmatic fluids cooled during ascent to the surface, local permeability may have been greatly reduced in response to precipitation of silica (Sillitoe, 1985). This would produce an effective aquitard in the shallow crust, below which magmatic fluids would stagnate and cool (Fig. 42).

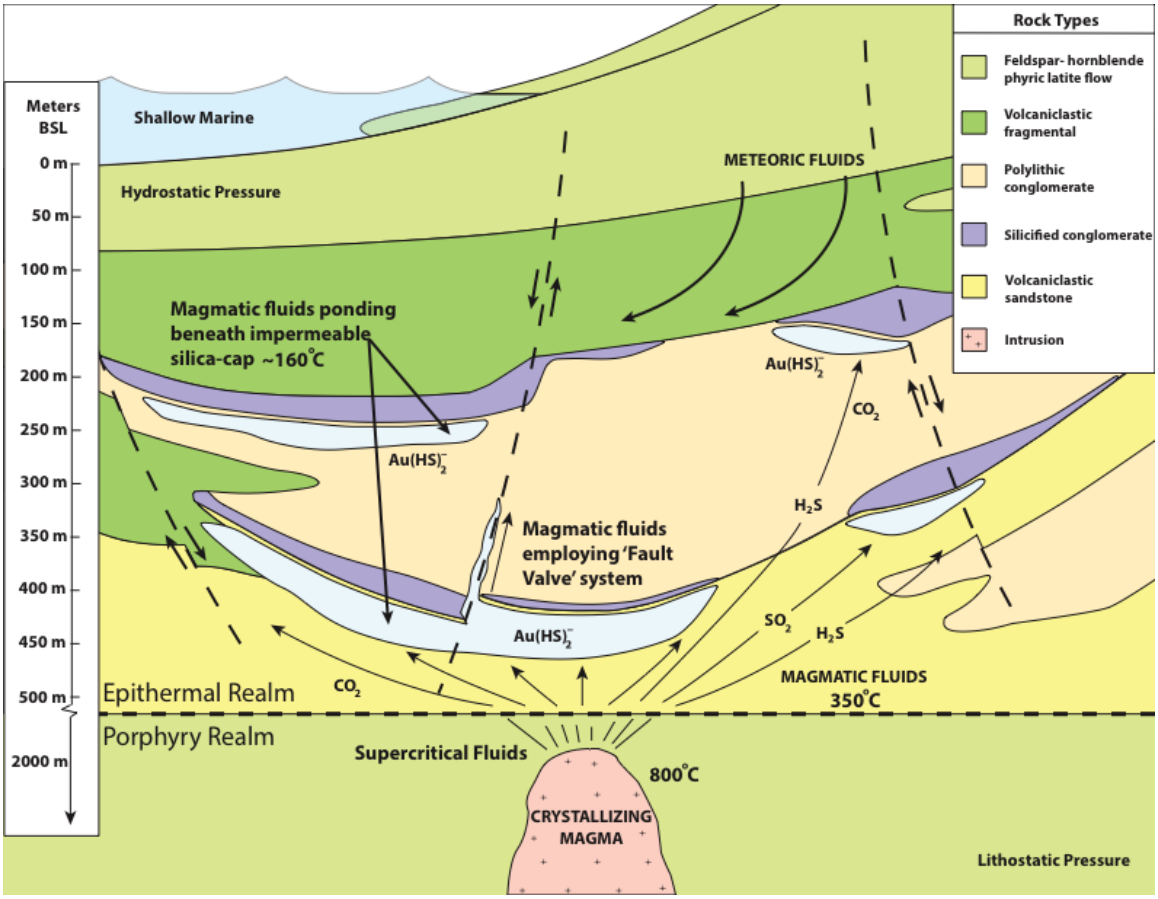

Figure 42: Ascending magmatic fluids circulate through interbedded, pre-folded rocks and collect at the basal and upper contacts of the porous conglomerate unit. Magmatic fluids (rich in CO_2, H_2S, and SO_2) form siliceous horizons and stagnate beneath, where temperatures are cooled to ~160˚C. Magmatic fluids also migrate along faults, where they are temporarily released in periods of seismic activity.

Hydrostatic pressures beneath this silicified barrier would increase in response to: (1) ascending magmatic fluids (Sillitoe, 1985); (2) transmission of deeper fluid pressure (Hedenquist and Henley, 1985); or (3) magmatic heating (Nelson and Giles, 1985). Hydraulic fracturing would result from fluid pressure exceeding the tensile strength of the silicified rock and lithostatic pressure. The pressure surge caused through the breach of fluid through the impermeable margin would initiate localized faulting and increase

permeability, where effervescing fluids would escape upward and outward (Fig. 43), forming extreme disequilibrium conditions and gold precipitation. The cycle was likely repetitive, where hydrothermal self-sealing would cause re-accumulation of the fluid pressure.

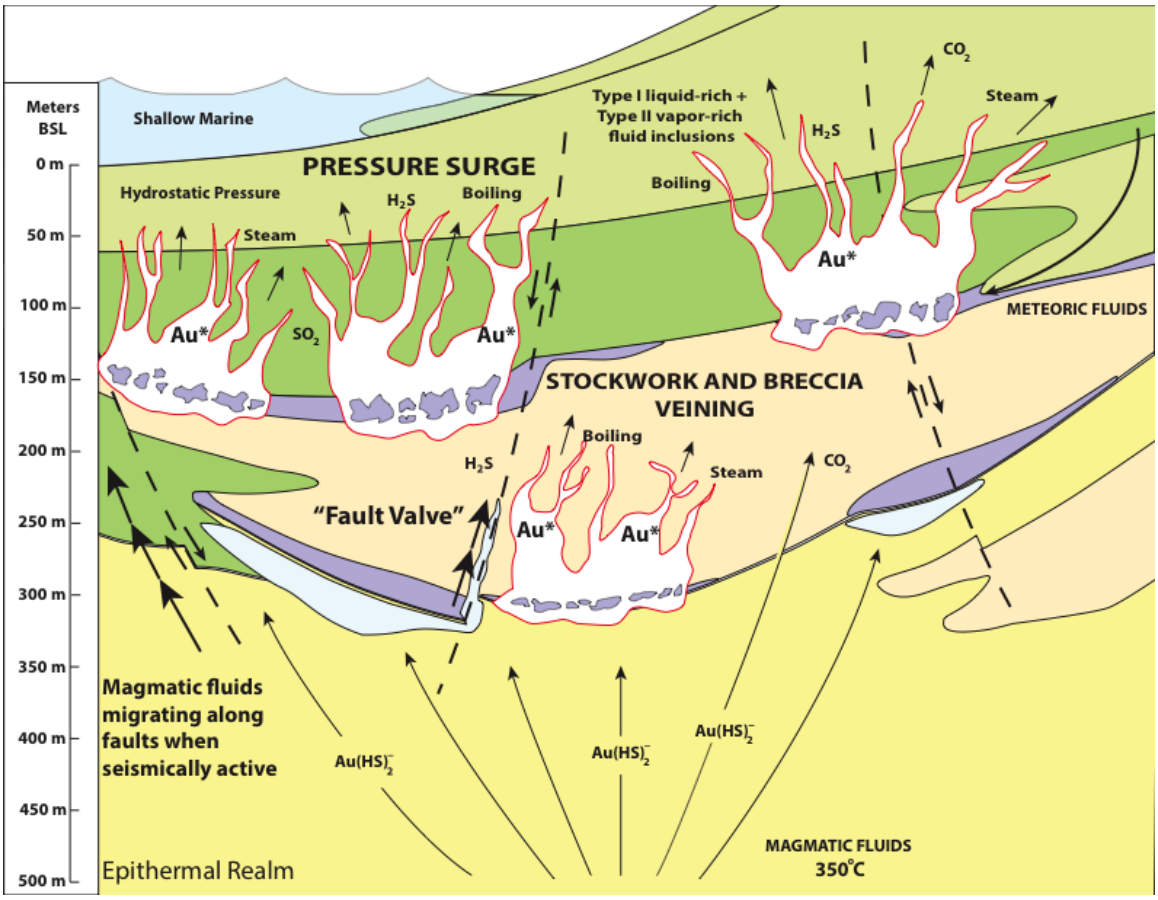

Figure 43: Magmatic fluid pressure increases below impermeable siliceous barrier and fluid pressure increases until it has breached the tensile strength of the rock and lithostatic pressure, where a pressure surge is created. The pressure surge forms stockwork and breccia veining and causes local fluids to effervesce, where boiling occurs and superheated, volatile-rich, steam is exsolved. Extreme disequilibrium conditions occur and gold-bisulfide complexes become unstable and precipitate gold.

Episodic veining is also implied through the large ranges in salinity throughout vein stage III (0.5 to 15.5 wt% NaCl equiv.; $n = 89$). It may be possible that ore minerals in stage III veins precipitated from moderate–high salinity fluids, or brines. These cooler saline fluids (having higher Pb-Zn-Ag solubility) may have mixed with warmer, more dilute magmatic fluids, resulting in deposition of Pb-Zn-Ag-Au. Sillitoe and Hedenquist (2003) suggest the fluid responsible for precipitating quartz and carbonate gangue in intermediate-sulfidation vein deposits have lower salinity than the episodic pulses of more saline fluids transporting ore and related sulfide minerals.

Simmons (1991) suggests that the fluids responsible for ore deposition at the glory hole at Cerro Proano and the Santo Nino vein in the Fresnillo mining district, Mexico, were precipitated by the injection of brines (>12 wt % NaCl equiv.) into otherwise dilute (<3 wt % NaCl equiv.) system. These dense brines may be present in a stably stratified, double-diffusive reservoir underlying a dilute, meteoric water-dominated system (Sillitoe and Hedenquist, 2003). The salinity composition of Brucejack stage III fluids is approximately 7.5 wt percent NaCl equiv., although salinities may be as high as 15.5 wt percent NaCl equiv., suggesting the reservoir composition shifted through time or the external saline fluid was unevenly distributed within the reservoir (Simmons, 1991).

These saline fluids may have ascended into meteoric water-dominated portions of the system through "fault-valve" processes, which creates an increase in pressure followed by significant pressure drop during eruptions, and is analogous to earthquake ruptures in active faults (Peterson and Mavrogenes, 2014). Episodic mineralizing conditions at the Porgera gold deposit based on fluctuating $\delta^{34}S$ values within individual pyrite crystals led Peterson and Mavrogenes (2014) to link high-grade gold

mineralization to earthquake-induced fault-valve processes (Richards, 1992; Richards and Kerrich, 1993). At Brucejack, intermittent, rapidly ascending, saline ore-forming fluids would inject into the meteoric water table and mixing would occur, providing the mixing trends in stage III fluid inclusion assemblages**.**

8.0 Conclusions

The Brucejack deposit is a high-grade Au-Ag deposit in northwestern British Columbia. Brucejack has characteristics similar to epithermal, porphyry, and mesothermal deposits. Fluid chemistry and deposit textures and mineralogy suggest the deposit is a transitional low to intermediate-sulfidation epithermal deposit. Mineralization is hosted in calc-alkaline, island-arc related, Early Jurassic plagioclase-hornblende porphyritic latite flows, and associated volcanic ash-tuff fragmental rocks, subordinate volcaniclastic rocks and volcanic sandstones and siltstones. The deposit formed in an episodic environment between 191.7 ± 0.8 Ma and 188.9 ± 0.8 Ma (Re-Os molybdenite model ages). Continued mineralization spanning nearly 3 m.y. is unlikely, and multiple stages of mineralization are implied, where a younger low-sulfidation epithermal system was responsible for forming the West Zone deposit ~189 Ma. The presence of crustiform and cockade banded veins, bladed calcite, and minor open space filling suggest boiling in a near surface ore-forming environment, but the presence minor amounts of dissolved CO_2 in fluid inclusions may have caused boiling (effervescence) and gold deposition to extend to greater depths than in typical epithermal-style deposits. Pre-gold mineralization pyritization and phyllosilicate alteration of volcanic wallrocks enabled continued re-

circulation of gold complexes without precipitation, contributing to large gold concentrations found throughout the deposit.

Five vein stages have been recognized for the Valley of the Kings, where stages II–IV contain high-grade gold mineralization. Fluid in stages II and IV are condensed magmatic fluids which precipitated gold when they boiled, or effervesced, in response to large pressure decreases. Stage III fluid inclusion data clearly indicate fluid mixing, where cooler saline fluids were injected into a warmer, more dilute end-member fluid resulting in deposition of Pb-Zn-Ag-Au. These two distinct mineralization styles, formed by distinct processes, give the deposit a transitional low to intermediate-sulfidation character.

Fluid mixing is recognized in hydrothermal quartz and calcite veining, where ranges in oxygen isotopes between meteoric and modified magmatic fluids are evident. Modified magmatic $\delta^{18}O_{Water}$ values are observed for gold-bearing veins and are the source of ore-forming fluids. Carbon and sulfur isotopes from carbonates and sulfides also show a magmatic inheritance. Boiling is commonly observed within fluid inclusion assemblages and is also suggested to produce silica-flooded breccia and stockwork veins and calcite-dominated veins, and is the main mechanism for gold precipitation. In contrast, fluid mixing led to the formation of stage III base metal veins.

Page left blank intentionally

References

Aberhan, M., 1999, Terrane history of the Canadian Cordillera: Estimating amounts of latitudinal displacement and rotation of Wrangellia and Stikinia: Geological Magazine, v. 136, p. 481–492.

Alldrick, D.J., 1987, Geology and mineral deposits of the Salmon River valley, Stewart area, NTS 104A and 104B: British Columbia Ministry of Energy, Open File Map 1987-22, Mines Pet. Resource

Alldrick, D.J., 1991, Geology and ore deposits of the Stewart Mining Camp, British Columbia: Unpublished MSc Thesis, Vancouver, University of British Columbia, p. 8.

Alldrick, D.J., 1993, Geology and metallogeny of the Stewart mining camp, Northwestern British Columbia: Geological Survey of British Columbia, Ministry of Energy, Mines and Petroleum Resources, Bulletin 85, p. 1–89.

Alldrick, D.J., and Britton, J.M., 1988, Geology and Mineral Deposits of the Sulphurets Area: British Columbia Ministry of Energy, Mines and Petroleum Resources, Open File Map 1988–4.

Alldrick, D.J., Nelson, J.L., and Barresi, T., 2005, Geology and mineral occurrences of the Upper Iskut River area: Tracking the Eskay Rift through northern British Columbia (Telegraph Creek NTS 104G/1,2; Iskut River NTS 104B/9, 10, 15, 16): Geological Fieldwork 2004, British Columbia Ministry of Energy, Mines and Petroleum resources, Paper 2005-1, 30 p.

Anderson, R.G., 1983, Geology of the Hotailuh batholith and surrounding volcanic and sedimentary rocks, north-central British Columbia: Unpublished Ph.D. Thesis, Ottawa, Carlton University.

Armstrong, R.L., 1988, Mesozoic and early Cenozoic magmatic evolution of the Canadian Cordillera: Geological Society of America, Special Paper 218, p. 55–92.

Arribas, A., 1995, Characteristics of high-sulfidation epithermal deposits, and their relation to magmatic fluid; *in* Magmas, Fluids, and Ore Deposits: Mineralogical Association of Canada Short Course, v. 23, p. 419–454.

Audétat, A., Keppler, H., 2005. Solubility of rutile in subduction zone fluids, as determined by experiments in the hydrothermal diamond anvil cell. Earth and Planetary Science Letters v. 232, p. 393–402

Ballhaus, C., Berry, R.F., and Green, D.H 1042., 1991, High pressure experimental calibration of the olivine-orthopyroxene-spinel oxygen geobarometer: implications for the oxidation state of the upper mantle: Contributions to Mineralogy and Petrology, v. 107, p. 27–40.

Barnes, H.L., 1979, Solubilities of ore minerals, *in* Barnes, H.L., ed., Geochemistry of hydrothermal ore deposits: New York, Wiley Intersci., p. 404–454.

Belasky, P., Stevens, C.H., and Hanger., R.A., 2002, Early Permian location of western North American terranes based on brachiopod, fusulinid and coral biogeography: Palaeogeography , Palaeoclimatology, Palaeoecology v. 179, p. 245-266.

Benning, L.G., and Seward, T.M., 1996, Hydrosulfide complexing of gold (I) in hydrothermal solutions from 150 to 500°C and 500 to 1500 bars: Geochimica et Cosmochimica Acta, v. 60, p. 1849–1872.

Berger, B.R., and Eimon, P.I., 1983, Comparitive models of epithermal silver-gold deposits, *in* Shanks, W.C., III, ed., Cameron volume on unconventional mineral resources: New York, Am. Inst. Mining Metall. Petroleum Engineers, p. 191-205.

Bethke, P.M., and Rye, R.O., 1979, Environment of ore deposition in the Creede mining district, San Juan Mountains, Colorado: Part IV. Source of fluids, from oxygen, hydrogen, and carbon isotope studies; Economic Geology, v. 74, p. 1832-1851.

Bitton, J.M., and Alldrick, D.J., 1988, Sulphurets Map Area: *in* Geological Fieldwork 1987, British Columiba Ministry of Energy, Mines and Petroleum Resources, Paper 1988-1.

Bodnar, R.J., Reynolds, T.J., and Kuehn, C.A., 1985, Fluid inclusion systematics in epithermal systems, *in* Berger, B.R., and Bethke, P.M., eds., Geology and geochemistry of epithermal systems: Soc. Econ. Geol., Reviews in Economic Geology, v. 2, p. 73–97.

Bodnar, R.J., 1991, Revised equation and table for determining the freezing point depression of H2O-NaCl solutions; Geochimica et Cosmochimica Acta, v.57, p. 683-684.

Bozzo, A., Chen, H.S., Kass, J.R., and Barduhn, A.J., 1975, The properties of the hydrates of chlorine and carbon dioxide; Desalination, v. 16, p. 303-320.

Brenan, J.M., Shaw, H.F., Phinney, D.L., Ryerson, F.J., 1994. Rutile–aqueous fluid partitioning of Nb, Ta, Hf, Zr, U and Th: implications for high field strength element depletions in island arc basalts. Earth and Planetary Science Letters v. 128, p. 327–339

Bridge, D.J., 1993, The deformed Early Jurassic Kerr copper-gold porphyry deposit, sulphurets gold camp, northwestern British Columbia: Unpublished MSc Thesis, Vancouver, University of British Columbia, p. 1-145

Bridge, D.J., and Godwin, C.I., 1991, Preliminary geology of the Kerr copper- (gold) deposit, northwestern British Columbia (104B/8): British Columbia Geological Survey, Geologic Fieldwork 1991, Paper 1992-1, p.1-4.

Bruha, D.I., and Noble, D.C., 1983, Hypogene quartz-alunite pyrite alteration formed by moderate saline, ascending hydrothermal solutions [asb.]: Geological Society of America, Rocky Mountain and Cordilleran Section, Abstracts with Program, v. 15, p. 325.

Brown, D.A., Logan, J.M., Gunning, M.H., Orchard, M.J., and Bamber, W.E., 1991, Stratigraphic evolution of the Paleozoic Stikine assemblage in the Stikine and Iskut rivers area, northwestern British Columbia: Canadian Journal of Earth Sciences, v. 28, p. 958-972.

Browne, K.E., 1978, Hydrothermal alteration in active geothermal fields: Ann. Rev. Earth Planet Sci., v. 6, p. 229-250

Burnham, C.W., 1979, Magmas and hydrothermal fluids. In: Barnes, H.L. (ed) Geochemistry of hydrothermal ore deposits, 2nd edn. Wiley, New York, p. 71–136.

Canet, C., Franco, S.I., Prol-Ledesma, R.A., Gonzalez-Partida, E., and Villanueva-Estrada, R.E., 2011, A model of boiling for fluid inclusion studies: Application to the Bolanos Ag-Au-Pb-Zn epithermal deposit, Western Mexico: Journal of Geochemical Exploration v. 110, p. 118-125

Casadevall, T., and Ohmoto, H., 1977, Sunnyside mine, Eureka mining district, San Juan County, Colorado: Geochemistry of gold and base-metal ore deposition in a volcanic environment; Economic Geology, v. 72, p. 1285-1320.

Cathles, L.M., Erendi, A.H., and Barrie, T., 1997, How long can a hydrothermal system be sustained by a single intrusive event?; Economic Geology, v. 92, p. 766-771.

Chacko, T., Mayeda, T.K., Clayton, R.N., and Goldsmith, J.R., 1991, Oxygen and carbon isotope fractionations between CO_2 and calcite, Geochim. Cosmochim. Acta, v. 55, p. 2867-2882.

Childe, F., 1996, U-Pb geochronology and Nd and Pb isotope characteristics of the Au-Ag-rich Eskay Creek volcanogenic massive sulfide deposit, British Columbia: Economic Geology, v. 91, p. 1209-1224.

Clayton, R., and Epstein, S., 1958, The relationships between $^{18}O/^{16}O$ ratios in coexisting quartz, carbonate and iron oxides from various geologic deposits. Journal of Geology, v.66, p.352-373.

Clayton, R.N., and Mayeda, T.K., 1963, The use of bromine pentafluoride in the extraction of oxygen from oxides and silicates for isotopic analysis; Geochimica et Cosmochimica Acta, v. 54, p. 1353-1357.

Cline, J.S., and Bodnar, R.J., 1991, Can economic porphyry copper mineralization be generated by a typical calc-alkaline melt? Journal of Geophysics Research, v. 96, p. 8113–8126.

Coney, P.J., 1972, Cordilleran tectonics and North American plate motion: American Journal of Science, v. 272, p. 603-628.

Coney, P.J., 1987, The regional tectonic setting and possible causes of Cenozoic extension in the North American Cordillera: Geological Society, London, Special Publications, v. 28, p. 177-186.

Coney, P.J., 1989, Structural aspects of suspect terranes and accretionary tectonics in western North America: Journal of Structural Geology, v. 11, p. 107-125.

Coney, P.J., and Evenchick, C.A., 1994, Consolidation of the American Cordilleras: Journal of South American Earth Sciences, v. 7, no. 3/4, p. 241-262.

Conrad, J.E., and McKee, E.H., 1996, High precision $^{40}Ar/^{39}Ar$ ages of rhyolitic host rocks and mineralized veins at the Sleeper deposit, Humbolt County, Nevada, *in* Coyner, A.R., and Fahey, P.L., eds., Geology and ore Deposits of the American Cordillera: Geological Society of Nevada Symposium Proceedings, Reno/Sparks, Nevada, April 1995, Proceedings, p.257-262.

Cowan, D.S., Brandon, M.T., and Garver, J.I., 1997, Geologic tests of hypothesis for large coastwise displacements- A critique illustrated by the Baja British Columbia controversy: American Journal of Science, v. 297, p. 117-173.

Cox, S.F., 1995, Faulting processes at high fluid pressures: An example of fault-behavior from the Wattle Gulley fault, Victoria, Australia: Journal of Geophysical Research, v. 100, p. 12841-12859.

Craig, H., 1957, Isotopic standards for carbon and oxygen an correction factors for mass-spectrometric analysis of carbon dioxide. Geochim. et Cosmochim. Acta, v.12, p.133-149.

Craig, H., 1961, Standard for reporting concentrations of adularia and oxygen-18 in natural waters: Science, v.133, p.1833-1834.

Crawford, M.L., Hollister, L.S., and Woodsworth, G.J., 1987, Crustal deformation and regional metamorphism across a terrane boundary, Coast Plutonic Complex, British Columbia: Tectonics, v. 6, no. 3, p. 343-361.

Davies, A.G.S., Lewis, P.D., and MacDonald, A.J., 1994, Stratigraphic and structural setting of the mineral deposits in the Brucejack Lake area, northwestern British Columbia: *in* Current Research 1994-A; Geological Survey of Canada, p. 37-43.

DeRonde, C.E.J., and Blattner, P., 1988, Hydrothermal alteration, stable isotopes, and fluid inclusions of the Golden Cross Epithermal gold-silver deposit, Waihi, New Zealand: Economic Geology, v. 83, p. 895-917.

Evenchick, C.A., 1991a, Geometry, evolution, and tectonic framework of the Skeena Fold Belt, north-central British Columbia: Tectonics, v. 10, no. 3, p. 527-546.

Evenchick, C.A., Mustard, P.S., Porter, J.S., and Greig, C.J., 1992, Regional Jurassic and Cretaceous facies assemblages, and structural geology in Bowser Lake map area (104A), B.C.: Geological Survey of Canada, Open File 2582, p. 1-17.

Foley, S.F., Barth, M.G., and Jenner, G.A., 2000, Rutile/melt partition coefficients for trace elements and an assessment of the influence of rutile on the trace element characteristics of subduction zone magmas: Geochimica at Cosmochimica Acta, v. 64, p. 933-938.

Frey, F.A., Chappell, B.W., and Roy, S.D., 1978, Fractionation of rare-earth elements in the Tuolumne Intrusive Series, Sierra Nevada batholith, California: Geology, v. 6, p. 239–242.

Friedman, R.M., Mahoney, J.B., and Cui, Y., 1995, Magmatic evolution of the southern Coast Belt: constraints from Nd-Sr isotopic systematics and geochronology of the southern Coast Plutonic Complex: Canadian Journal of Earth Science, v. 32, p. 1681-1698.

Gabrielse, H., 1991, Late Paleozoic and Mesozoic terrane interactions in north-central British Columbia: Canadian Journal of Earth Sciences, v. 28, p. 947-957.

Gagnon, J.F., and Waldron, J.W.F., 2011, Sedimentation styles and depositional processes in the Middle to Late Jurassic slope environment, Bowser Basin, northwestern British Columbia, Canada: Marine and Petroleum Geology, v. 28, p. 689-715.

Gagnon, J.F., Barresi, T., Waldron, J.W.F., Nelson, J.L., Poulton, T.P., and Cordey, F., 2012, Stratigraphy of the upper Hazelton Group and the Jurassic evolution of the Stikine terrane, British Columbia: Canadian Journal of Earth Sciences, v. 49, p. 1027-1052.

Gammons, C.H., and Williams-Jones, A.E., 1997, Chemical mobility of gold in the porphyry-epithermal environment: Economic Geology, v. 92, p. 45-59.

Gehrels, G.E., 2001, Geology of the Chatham Sound region, southeast Alaska and coastal British Columbia: Canadian Journal of Earth Science, v. 38, p. 1579-1599.

Ghaffari, H., Huang, J., Narciso, H., Cameron, M.M., Cowie, S., Sweeney, D.J., Hollett, G.R., Brown, F.H., Armstrong, T., Boyle, J.M., Wilchek, L., Newcomen, H.W., and Greisman, P., 2010, Technical report and preliminary assessment of the Snowfield-Brucjeack project; private report prepared for Silver Standard Resources Inc., p. 64.

Giesemann A., H.J. Jaeger., AL. Norman, AL. Krouse., HR. Krouse, WA. Brand, 1994, On-Line Sulfur Isotope Determination Using a Elemental Analyzer Coupled to a Mass Spectrometer: Anal. Chem., v. 66, p. 2816.

Gill, J.B., 1981, Orogenic Andesites and Plate Tectonics. Springer-Verlag, Berlin, p. 390.

Goldstein, R.H., and Reynolds, T.J., 1994, Systematics of fluid inclusions in diagenetic minerals: Society of Economic Paleontologists and Mineralogists: Short Course Handbook, v. 31, p. 199

Grant, M.A., Donaldson, I.A., and Bixley, P.F., 1982, Geothermal reservoir engineering: New York, Academic Press, p. 369.

Green, D.H., 1975, Genesis of Archean peridotitic magmas and constraints on Archean geothermal gradients and tectonics: Geology, v. 3, p. 15-18.

Green, D.H., and Pearson, N.J., 1985, Experimental determination of REE partition coefficients between amphibole and basaltic to andesitic liquids at high pressure: Geochimica et Cosmochimica Acta, v. 49, p. 1465–1468.

Gribble, R.F., Stern, R.J., Bloomer, S.H., Stuben, D., O'Hearn, T., and Newman, S., 1996, MORB mantle and subduction components interact to generate basalts in the southern Mariana Trough back-arc basin; Geochemica et Cosmochimica Acta, v. 60, p. 2153-2166.

Griffin, W.L., Powell, W.J., Pearson, N.J. and O'Reilly, S.Y., 2008, Glitter: Data reduction software for laser ablation ICP-MS; In Sylvester, P.J. (ed.), Laser Ablation ICP-MS in the Earth Sciences: Current Practices and Outstanding Issues, Mineralogical Association of Canada Short Course Series, Short Course 40, Vancouver, B.C., p. 308-311.

Gunning, M.H., 1990, Stratigraphy of the Stikine assemblage, Scud River area, Northwestern British Columbia: British Columbia Ministry of Energy, Mines and Petroleum Resources, Paper 1990-1, p. 153-161.

Gustafson, L.B., and Hunt, J.P., 1975, The porphyry copper deposit at El Salvador, Chile: Economic Geology, v. 70, p. 857-912.

Haas, J.L., 1976, Physical properties of the coexisting phases and thermochemical properties of the H2O component in boiling NaCl solutions: U.S. Geological Survey Bulletin 1421-A, p. 73.

Hanson, G.N., 1980, Rare earth elements in petrogenetic studies of igneous systems: Annual Review of Earth and Planetary Sciences, v. 8, p. 371–406.

Heald, P., Foley, N.K., and Hayba, D.O., 1987, Comparative anatomy of volcanic-hosted epithermal deposits-acid sulfate and adularia-sericite types: Economic Geology, v. 82, p. 1-26.

Hedenquist, J.W., and Henley, R.W., 1985, The importance of CO_2 on freezing point measurements of fluid inclusions: evidence from active geothermal systems and implications for epithermal ore deposition: Economic Geology, v. 80, p. 1379-1406

Hedenquist, J.W., and Lowenstern, J.B., 1994, The role of magmas in the formation of hydrothermal ore deposits: Nature, v. 370, p. 519-527.

Heinrich, C.A., Driesner, T., Stefansson, A., and Seward, T.M., 2004, Magmatic vapor contraction and the transport of gold from the porphyry environment to epithermal ore deposition: Geology, v. 32, no. 9, p. 761-764.

Heinrich, C.A., 2005, The physical and chemical evolution of low-salinity magmatic fluids at the porphyry to epithermal transition: a thermodynamic study: Mineralium Deposita, v.39, p. 864–889.

Heinrich, C.A., 2007, Fluid-fluid interactions in magmatic-hydrothermal ore formation: Reviews in Mineralogy and Geochemistry, v. 65, p. 363-387.

Hemley, J.J., Cygan, G.L., Robinson, G.R., and D'Angelo, W.M., 1991, Hydrothermal ore-forming processes in the light of studies in rock-buffered systems: I. Iron-copper-zinc-lead sulfide solubility relations: Economic Geology, v. 87, p. 1-22.

Hildreth, W., and Moorbath, S., 1988, Crustal contaminations to arc magmatism in the Andes of Central Chile: Contributions to Minerology and Petrology, v. 98, p. 455-489.

Hollister, L.S., and Andronicos, C.L., 1997, A candidate for the Baja British Columbia fault system in the Coast Plutonic Complex: GSA Today, v. 7, no. 11, p. 1-7.

Holser, W.T., and Kaplan, I.R., 1966, Isotope geochemistry of sedimentary sulfates: Chemical Geology, v.1, p. 93-135.

Ireland, D., Jones, I.W.O., Huang, J., Pelletier, P., Weatherly, H., Stoyko, H.W., Hafez, S.A., Keogh, C., Schmid, C., Cullen, V., McGuinness, M., McAfee, B., Chin, M., Gould, B., Wise, M., Greisman, P., Richards, C., Scott, W.E., Farah, A., Halisheff, K., Sriskandakumar, S.K., Molavi, M., 2013, Feasibility stuffy and technical report on the Brucejack project, Stewart, BC. Report to Pretium Resources Inc.

Ireland, D., Olssen, l., Huang, J., Pelletier, P., Weatherby, H., Stoyko, H.W., Hafez, S.A., Keoch, C., Schmid, C., McAfee, B., Chin, M., Gould, B., Wise, M.,, Greisman, P., Scott, W.E., Farah, A., Zazzi, G., Crozier, T., Blackmore, S., 2014, Feasibility study and technical report update on the Brucejack project, Stewart, BC. Report to Pretivm Resources Inc.

Irvine, T.N., and Baragar, W.R.A., 1971, A guide to the chemical classification of the commonplace volcanic rocks: Canadian Journal of Earth Science, v. 8, p. 523-548.

Jackson, J.L., Gehrels, G.E., Patchett, P.J., and Mihalynuk, M.G., 1991, Stratigraphic and isotopic link between the northern Stikine terrane and an ancient continental margin assemblage, Canadian Cordillera: Geology, v. 19, p. 1177-1180.

Jakobs, G.K., and Palfy, J., 1994, Upper Triassic to Middle Jurassic biostratigraphy and facies studies in the Iskut River map area, northwestern British Columbia; *in* Current Research 1994-E: Geological Survey of Canada, p. 17-28.

Jones, I.W.O, 2013, Mineral and resource update technical report; Brucejack Project; prepared for Pretium Resources Inc.

Kamilli, R.J., and Ohmoto, H., 1977, Paragenesis, zoing, fluid inclusion, and isotopic studies of the Finlandia vein, Colqui district, central Peru: Economic Geology, v. 72, p. 950-982.

Kirkham, R.V., 1963, The geology and mineral deposits in the vicinity of the Mitchell and Sulphurets glaciers, northwest British Columbia: Unpublished M.Ss. thesis, Vancouver, University of British Columbia, p. 1-116

Kirkham, R.V., 1992, Preliminary geological map of the Brucejack Creek area, British Columbia (part of 104B/8); Geological Survey of Canada, Open File 2550.

Kirkham, R.V. and Margolis, J., 1995, Overview of the Sulphurets area, northwestern British Columbia: Canadian Institute of Mining, Metallurgy and Petroleum Special Volume 46, p. 473-483.

Konkin, L., 2007, Diamond drilling & trenching assessment report on the Snowfield project [tenure#509216], Skeena mining division, British Columbia, Canada, NTS 104B/9E; Private report prepared for Silver Standard Resources Inc., p. 14.

Logan, J.M., and Koyanagi, V.M., 1994, Geology and mineral deposits of the Galore Creek area (104G/3, 4): British Columbia Ministry of Energy and Mines, Bulletin 92, p. 7

Ludwig, K., 2003, Isoplot/Ex, version 3: A geochronological toolkit for Microsoft Excel: Berkeley, California, Geochronology Center, Berkeley.

MacDonald, A.J., Lewis, P.D., Thompson, J.F.H., Nadaraju, G., Bartsch, R.D., Bridge, D.J., Rhys, D.A., Roth, T., Kaip, A., Godwin, C.I., and Sinclair, A.J., 1996, Metallogeny of an Early to Middle Jurassic Arc, Iskut River Area, Northwestern British Columbia: Economic Geology, v. 91, p. 1098-1114.

MacDonald, A.J., van der Heyden, P., Lefebure, D.V., and Alldrick, D.J., 1991, Geochronometry of the Iskut River area-an update (104A and B): British Columbia Ministry of Energy, Mines and Petroleum Resources, Paper 1992-1, p. 495-501.

Markey, R.J., Stein, H.J., Hannah. J.L., Selby, D., and Creaser, R.A., 2007, Standardizing Re-Os geochronology: A new molybdenite Reference Material (Henderson, USA) and the stoichiometry of Os salts: Chemical Geology, v. 244, p. 74-87.

Margolis, J., 1993, Geology and intrusion-related copper-gold mineralization, Sulphurets, British Columbia. Unpublished Ph.D. Dissertation; University of Oregon, Eugene, Oregon, p. 289.

Marsden, H. and Thorkelson, D.J., 1992, Geology of the Hazelton volcanic belt in British Columbia: Implications for the Early to the Middle Jurassic evolution of Stikinia: Tectonics, v. 11, p. 1266-1287.

Matsuhisha, Y., Goldsmith, J.R., Clayton, R.N., 1979, Oxygen isotopic fractionations in the system quartz-albite-anorthite-water; Geochimica et Cosmochimica Acta, v. 47, p. 1131-1140.

McCrea, J., 1950, On the isotopic chemistry of carbontes and a paleotemperature scale. Journal of Chemistry and Physics, v.18, p.849-857.

McCulloch, M.T., and Gamble, J.A., 1991, Geochemical and geodynamic constraints on subduction zone magmatism: Earth and Planetary Science Letters, v. 102, p. 358-374.

McMillan, W.J., 1992a, Overview of the tectonic evolution and setting of mineral deposits in the Canadian Cordillera: Ore deposits, tectonics and metallogeny in the Canadian Cordillera: British Columbia Ministry of Energy, Mines, and Petroleum Resources, Paper 1991:4, p. 5-24.

McMillan, W.J., 1992b, Porphyry deposits in the Canadian Cordillera: Ore deposits, tectonics and metallogeny in the Canadian Cordillera: British Columbia Ministry of Energy, Mines, and Petroleum Resources, Paper 1991:4, p. 253-276.

Meschede, M., 1986, A method of discrimination between different types of mid-ocean ridge basalts and continental tholeiites with the Nb-Zr-Y Diagram; Chemical Geology, v. 56, p. 206-218.

Mihalynuk, M.G., Erdmer, P., Ghent, E.D., Cordey, F., Archibald, D.A., Friedman, R.M., and Johannson, G.G., 2004, Coherent French Range blueschist: Subduction to exhumation in <2.5 m.y.?: Geological Society of America Bulletin, v. 116, no. 7/8, p. 910-922.

Mihalynuk, M.G., Nelson, J., and Diakow, L.J., 1994, Cache Creek terrane entrapment: Oroclinal paradox within the Canadian Cordillera: Tectonics, v. 13, p. 575-595.

Monger, J.W.H., 1977, Upper Paleozoic rocks of the western Canadian Cordillera and their bearing on cordilleran evolution: Canadian Journal of Earth Sciences, v.14, p. 1832-1859.

Monger, J.W.H., and Price, R., 2002, The Canadian Cordillera; geology and tectonic evolution: Canadian Society of Exploration Geophysicists Recorder, v. 27, February 2002, p. 17-36.

Monger, J.W.H., Richards, T.A., and Paterson, I.A., 1978, The hinterland belt of the Canadian Cordillera: New data from northern and central British Columbia: Canadian Journal of Earth Sciences, v.15, p. 823-830.

Monger, J.W.H., Souther J.G., and Gabrielse, H., 1972, Evolution of the Canadian Cordillera: A plate-tectonic model: American Journal of Science, v.272, p. 577-602.

Monger, J.W.H., Price, R.A., and Tempelman-Kluit, D.J., 1982, Tectonic accretion and the origin of the two major metamorphic and plutonic welts in the Canadian Cordillera: Geology, v. 10, p. 70-75.

Mortensen, J.K., Gordee, S.M., Mahoney, J.B., and Tosdal, R.M., 2003, Regional studies of Eskay Creek-type and other volcanogenic massive sulphide mineralization in the upper Hazelton Group in Stikinia: preliminary results: British Columbia Geological Survey, Bulletin 249, p. 249-262.

Mortimer, N., 1987, Lithologic map of Pavillion (92I/13) map area, British Columbia: British Columbia Ministry of Energy, Mines and Petroleum Resources, Open-file 1987-18.

Mullen, E.D., 1983, $MnO/TiO_2/P_2O_5$: a minor element discriminant for basaltic rocks of oceanic environments and its implications for petrogenesis: Earth and Planetary Science Letters, v.62, p. 53-62.

Nelson, C.E., and Giles, D.L., 1985, hydrothermal eruption mechanisms and hot spring gold deposits: Economic Geology, v. 80, p. 1633-1639.

Nelson, J.L., and Colpron, M., 2007, Tectonics and metallogeny of the British Columbia, Yukon, and Alaskan Cordillera, 1.8 Ga to present, *in* Goodfellow, W., ed., Mineral Deposits of Canada: A synthesis of major deposit types, distinct metallogeny, the evolution of geological provinces, and exploration methods: Geological Association of Canada, Mineral Deposits Division, Special Publication, p. 755-792.

Nelson, J.L., Colpron, M., Israel, S., 2013, The Cordillera of British Columbia, Yukon, and Alaska: Tectonics and metallogeny: Society of Economic Geologists, Special Publication Number 17, p. 53-110.

Norkleberg, W.J., Bundtzen, T.K., Eremin, R.A., Ratkin, V.V., Dawson, K.M., Shpikerman, V.I., Goryachev, N.A., Byalobzhesky, S.G., Frolov, Y.F., Khanchuk, A.I., Koch, R.D., Monger, J.W.H., Pozdeev, A.I., Rozenblum, I.S., Rodionov, S.M., Parfenov, L.M., Scotese, C.R., and Sidorov, A.A., 2005, Metallogenesis and tectonics of the Russian far east, Alaska, and the Canadian Cordillera: U.S. Geological Survey, Professional Paper 1697, p. 90-107.

Ohmoto, H., 1972, Schematics of sulfur and carbon isotopes in hydrothermal ore deposits: Economic Geology, v. 67, p. 551-578.

O'Niel, J.R., and Clayton, R.N., and Mayeda, T.K., 1969, Oxygen isotope fractionation in divalentmetal carbonates: Journal of Chemical Physics, v. 51, p. 5547-5558.

Osaki, S., 1973, Carbon and oxygen isotopic compositions of hydrothermal rhodochrosites from Oe, Inakuraishi and Jokoku mines, Hokkaido, Japan: Economic Geology, v.6, p. 151-162.

Pearce, J.A., Harris, N.B.W., and Tindle, A.G., 1984, Trace element discrimination diagrams for the tectonic interpretation of grantitic rocks: Journal of Petrology, v. 25, n. 4, p. 956-983.

Peterson, E.C., and Mavrogenes, J.A., 2014, Linking high-grade gold mineralization to earthquake-induced fault-valve processes in the Porgera gold deposit, Papua New Guinea; Geology, v. 42, p. 383-386.

Plank, T., Kelley, K.A., Zimmer, M.M., Hauri, E. H., and Wallace, P.J., 2013, Why do mafic arc magmas contain ~4 wt% water on average?: Earth and Planetary Science Letters, V. 364, p. 168-179.

Renne, P.R., Swisher, C.C, Deino, A.L., Karner, D.B., Owens, T.L., DePaolo, D.J., 1998, Intercalibration of standards, absolute ages and uncertainties in $^{40}Ar/^{39}Ar$ dating: Chemical Geology, v. 145, p. 117-152.

Rhys, D.A., 1993, Geology of the Snip mine, and its relationship to the magmatic and deformational history of the Johnny Mountain area, northwestern British Columbia: Unpublished M.Ss. thesis, Vancouver, University of British Columbia, p. 1-268.

Richards, J.P., Bray, C.J., Channer, D.M.Der., and Spooner, E.T.C., 1997, Fluid chemistry and processes at the Porgera gold deposit, Papua New Guinea: Mineralium Deposita, v. 32, p. 119-132.

Richards, J.P., 1992, Magmatic-epithermal transitions in alkalic systems: Porgera gold deposit, Papua New Guinea: Geology, v. 20, p. 547–550.

Richards, J.P., and Kerrich, R., 1993, The Porgera gold mine, Papua New Guinea: Magmatic-hydrothermal to epithermal evolution of an alkalic-type precious metal deposit: Economic Geology, v. 88, p. 1017–1052.

Richards, J.P., 2011, Magmatic to hydrothermal metal fluxes in convergent and collided margins: Ore Geology Reviews, v. 40, p. 1-26.

Richards, J.P., Spell, T., Rameh, E., Razique, A., and Fletcher, T., 2012, High Sr/Y magmas reflect arc maturity, high magmatic water content, and porphyry Cu ± Mo ± Au potential: examples from the Tethyan arcs of central and eastern Iran and western Pakistan: Economic Geology, v. 107, p. 295-332.

Richards, J.P., 2015, The oxidation state, and sulfur and Cu contents of arc magmas: Implications for metallogeny: Lithos, *in press*.

Ronacher, E., J.P., Richards, and Johnston, M.D., 2000, Evidence for fluid phase separation in high-grade ore zones at the Porgera gold deposit, Papua New Guinea: Mineralium Deposita, v. 35, p. 683-688.

Rowe, M.C., Kent, A.J.R., and Nielsen, R.L., 2009, Subduction influence on oxygen fugacity and trace and volatile elements in basalts across the Cascade Volcanic Arc: Journal of Petrology, v. 50, p. 61–91.

Rusmore, M.E., and Woodsworth, G.J., 1991, Coast Plutonic Complex: A mid-Cretaceous contractional orogen: Geology, v. 19, p. 941-944.

Samson, S.D., McClelland, W.C., Patchett, P.J., Gehrels, G.E., and Anderson, R.G., 1989, Evidence from neodymium isotopes from mantle contributions to Phanerozoic crustal genesis in the Canadian Cordillera: Nature, v. 337, p. 705-709.

Saunders, J.A., 2012, Textural evidence of episodic introduction of metallic nanoparticles into bonanza epithermal ores: Minerals; 2(3), p. 228-243.

Schmidt, M.W. and Poli, A., 1998, Experimentally based water budgets for dehydrating slabs and consequences for arc magmatism: Earth and Planetary Science Letters, V. 163, p. 361-379.

Selby, D., and Creaser, R.A., 2004, Macroscale NTIMS and microscale LA-MC-ICP-MS Re-Os isotopic analysis of molybdenite: Testing spatial restrictions for reliable Re-Os age determinations, and implications for the decoupling of Re and Os within molybdenite: Geochimicia et Cosmochimica Acta, v. 68, p. 3897-3908.

Sharma, T., and Clayton, R., 1965, Measurement of $^{18}O/^{16}O$ ratios of total oxygen of carbonates: Geochim. et Cosmochim. Acta, v.29, p.1347-1353.

Sharp, Z.D., 1990, A laser-based microanalytical method for the *in situ* determination of oxygen isotope ratios of silicates and oxides: Geochimica et Cosmochimica Acta, v. 54, p. 1353-1357.

Sherlock, R.L., Roth, T., Spooner, E.T.C, and Bray, C.J., 1999, Origin of the Eskay Creek precious metal-rich volcanogenic massive sulfide deposit: fluid inclusion and stable isotope evidence: Economic Geology, v. 94, p. 803-824.

Sibson, R.H., 1992, Implications of fault-valve behavior for ruture nucleation and recurrence: Tectonophysics, v. 211, p. 283-293.

Silberman, M.L., 1985, Geochronology of the hydrothermal alteration and mineralization: Tertiary epithermal precious-metal deposits in the Great Basin: U.S. Geological Survey Bulletin 1646, p. 55-70.

Sillitoe, R.H., 1973, The tops and bottoms of porphyry copper deposits: Economic Geology, v. 68, p. 799-815.

Sillitoe, R.H., 1977, Metallic mineralization affiliated to subaerial volcanism: a review; Geological Society, London, Special Publications, v. 7, p. 99-116.

Sillitoe, R.H., 1985, Ore-related breccias in volcanoplutonic arcs: Economic Geology, v. 80, p. 1467-1514.

Sillitoe, R.H., 2010, Porphyry copper systems: Economic Geology, v. 105, p. 3-41.

Simonetti, A., Heaman, L.M., Hartlaub, R.P., Creaser, R.A., MacHattie, T.G., and Bohm, C., 2005, U-Pb zircon dating by laser ablation-MC-ICP-MS using a new multi ion counting Faraday collector array; J. Anal. At. Spectrom, V. 20, P. 677-686.

Simmons, S.F., 1991, Hydrologic implications of alteration and fluid inclusion studies in the Fresnillo District, Mexico: Evidence for a brine reservoir and a descending water table during the formation of hydrothermal Ag-Pb-Zn orebodies: Economic Geology, v. 86, p. 1579-1601.

Singer, B., and Marchev, P., 2000, Temporal evolution of arc magmatism and hydrothermal activity, including epithermal gold veins, Borovista Caldera, southern Bulgaria: Economic Geology, v. 95, p. 1155-1164.

Singer, B., Jicha, B., Mandeville, C., and Nye, C.J., 2010, The role of water in generating the calc alkaline trend: New volatile data for Aleutian magmas and a new Tholeiitic Index: Journal of Petrology, v. 51, p. 2411–2444.

Sisson, T.W., 1994, Hornblende-melt trace-element partitioning measured by ion microprobe: Chemical Geology, v. 117, p. 331-344.

Sláma, J., Košler, J., Condon, D.J., Crowley, J.L., Gerdes, A., Hanchar, J.M., Horstwood, M.S.A., Morris, G.A., Nasdala, L., Norberg, N., Schaltegger, U., Xchoene, B., Tubrett, M.N. and Whitehouse, M.J., 2007, Plešovice zircon — A new natural reference material for U–Pb and Hf isotopic microanalysis: Chemical Geology, p. 249, 1-35.

Smith, G.T., and Mustard, P.S., 2005, The southern contact of the Bowser Lake and Skeena Groups: unconformity or transition?: *in* Summary of Activities 2005, British Columbia Ministry of Energy and Mines, p. 152-156.

Smoliar, M.I., Walker, R.J., and Morgan, J.W., 1996, Re-Os ages of Group IIA, IIIA, IVA, and IVB iron meteorites: Science, v. 271, p. 1099-1102.

Stach, F.J., 1980, Multistage vein ores of the Lake City district, western San Juan mountains, Colorado: Economic Geology, v. 75, p. 963-991.

Stein, H.J., Markey, R.J., Morgan, J.W., Hannah, J.L., and Schersten, A., 2001, The remarkable Re-Os chronometer in molybdenite: how and why it works: Terra Nova, v. 13, p. 479-486.

Sun, S.S., and McDonough, W.F., 1989, Chemical and isotopic systematics of oceanic basalts: Implications for mantle composition and processes, *in* Saunders, A.D., and Norry, M.J., eds., Magmatism in the oceanic basins: Geological Society of London, Special Publication 42, p. 313-345.

Tafti, R., Mortensen, J.K., Lang, J.R., Rebagliati, M. and Oliver, J.L., 2009, Jurassic U-Pb and Re-Os ages for newly discovered Xietongmen Cu-Au porphyry district, Tibet: Implications for metallogenic epochs in the southern Gangdese Belt: Economic Geology, v. 104, p. 127–136

Taylor, H.P., 1974, Stable isotope geochemistry of ore-forming fluids: Economic Geology, v. 69, p. 843-883.

Taylor, H.P., Jr., 1979, Oxygen and hydrogen isotope relationships in hydrothermal mineral deposits, in Barnes, H.L., ed., Geochemistry of hydrothermal ore deposits, 2nd edition: New York, John Wiley and Sons, p. 236–277

Thorkelson, D.J., Mortensen, J.K., and Taylor, R.P., 1995, Age and tectonic setting of early Jurassic episodic volcanism along the northeastern margin of Hazelton Trough, northern British Columbia: Geological Society of America, Special Paper 299, p. 83-94.

Tipper, H.W., and Richards, T.A., 1976, Jurassic stratigraphy and history of north-central British Columbia: Geological Survey of Canada, Bulletin 270, p. 73.

Van Achterbergh, E., Ryan, C.G., Jackson, S.E. and Griffin, W.L., 2001, Data reduction software for LA-ICP-MS: appendix; In Sylvester, P.J. (ed.), Laser Ablation –ICP-Mass Spectrometry in the Earth Sciences: Principles and Applications, Mineralogical

Association of Canada Short Course Series, Ottawa, Ontario, Canada, v. 29, p. 239-243.

Wernicke, B., and Klepacki, D., 1998, Escape hypothesis for the Stikine block: Geology, v. 16, p. 461-464.

Wetlaufer, P.H., 1977, Geochemistry and mineralogy of the carbonates of the Creede mining district, Colorado: U.S. Geological Survey Open-File Rept. 77-706, p. 134.

Woods, T.L., Bethke, P.M., and Roedder, E., 1982, Fluid inclusion data at Creede, Colorado, in relation to mineral paragenesis: U.S. Geological Survey Open-File Rept. 82-313, p. 61.

Wilson, M., 1989, Igneous Petrogenesis: A Global Tectonic Approach. Unwin Hyman, London, p. 466.

Wilkinson, J.J., 2001, Fluid inclusions in hydrothermal ore deposits: Lithos, v. 55, p. 229-272.

Williams-Jones, A.E., Bowell, R.J., and Migdisov, A.A., 2009, Gold in solution: Elements, v. 5, p. 281-287.

Winchester, J.A., and Floyd, P.A., 1977, Geochemical discrimination of different magma series and their differentiation products using immobile elements: Chemical Geology, v. 20, p. 325-343.

Zhu, Y., An, F., and Tan, J., 2011, Geochemistry of hydrothermal gold deposits: A review: Geoscience Frontiers, 2(3), p. 367-374

Zimmer, M.M., Plank, T., Hauri, E.H., Yogodzinski, G.M., Stelling, P., Larsen, J., 2010, The role of water in generating the calc-alkaline trend: New volatile data for Aleutian Magmas and a new tholeiitic index: Petrography, v. 51, n. 12, p. 2411-2444

APPENDIX A

U/Pb Geochronology

Sample Locations:

#	Sample	Area	Rock Type	Easting	Northing	Depth (m ASL)	(U/Pb) Age (Ma)	Error (Ma)
A	SU277	VOK	P1	426694	6257993	1295	196.2	0.1
B	RG-1206	Catear	P1	425216	6259996	1445	194.5	0.5
C	CG11-428B	Office Porphyry	P1	426312	6258229	1491	194.1	0.9
D	CG12-563	West Zone	P1	426335	6258984	1354	193.8	1.1
E	SU-262	Bridge Zone	P2	426673	6257685	1602	189.4	0.7
F	CG12-1866	Flow Dome	P2	428701	6258526	1473	186.8	0.9
G	CG11-1654	VOK	P1	426902	6257953	1529	186.5	0.7
H	RG2226	Shore Zone	P1	427099	6258911	1369	185.0	0.9
I	CG12-1888	Golden Marmot	P1	425030	6261786	1501	182.8	1.0
J	SU-539	VOK	V6	426491	6258172	1513	182.7	1.0
K	SU-580	VOK	P1	426850	6258180	1480	182.6	1.1
L	CG510	Gossan Hill	P1	426576	6259231	1445	182.5	2.3
M	ST2015-001	Flow Dome	P1	428503	6258466	1552	183.1	1.1
N	ST2015-002	Flow Dome	P1	428733	6257851	1701	179.8	1.1

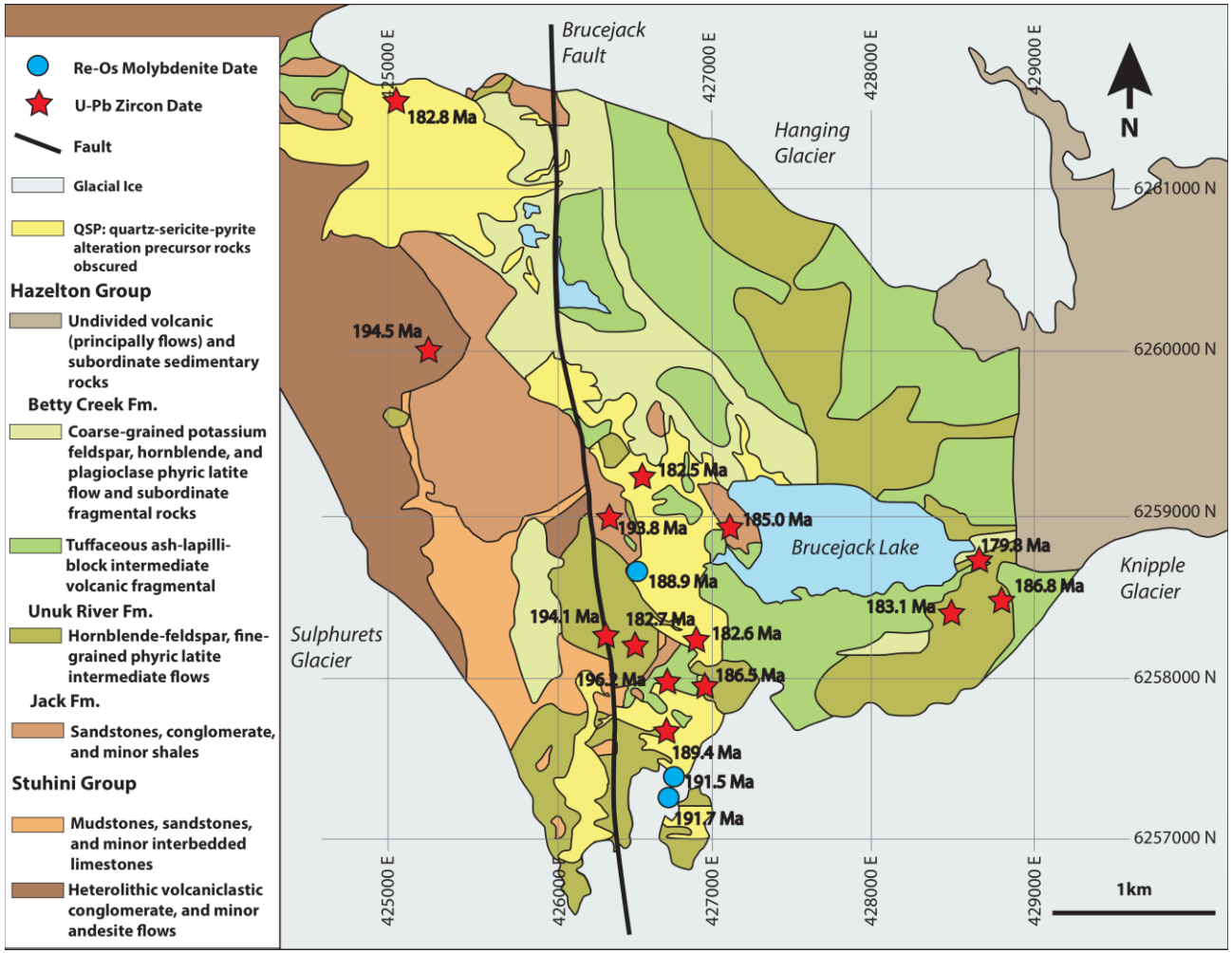

Figure 44: Geology of the Brucejack deposit and locations of main mineralized zones (modified from Ghaffari et al., 2010). UTM zone: NAD83-9V.

Laser Ablation Analysis Results:

Age estimates with 1 sigma uncertainty (Ma)							Isotopic Ratios with absolute errors								Counts /sec, background corrected							
Analysis No.	$^{207}Pb/^{235}U$ Ma	$^{207}Pb/^{235}U$ +/- 1s Error	$^{206}Pb/^{238}U$ Ma	$^{206}Pb/^{238}U$ +/- 1s Error	$^{207}Pb/^{206}Pb$ Ma	$^{207}Pb/^{206}Pb$ +/- 1s Error	$^{207}Pb/^{235}U$ Ratio	$^{207}Pb/^{235}U$ 1s Error	$^{206}Pb/^{238}U$ Ratio	$^{206}Pb/^{238}U$ 1s Error	Rho	$^{207}Pb/^{206}Pb$ Ratio	$^{207}Pb/^{206}Pb$ 1s Error	Th/U Ratio	202 Hg	204 Pb	206 Pb	207 Pb	208 Pb	232Th	235 U	238U
SU277-1	195.82	1.28	196.20	0.30	191.30	14.97	0.212707	0.716	0.030903	0.155	0.554	0.04992 1	0.644	0.328	N/A	N/A	N/A	N/A	N/A	N/A	N/A	N/A
2	194.44	4.95	196.44	0.44	170.26	61.05	0.211062	2.797	0.030942	0.229	0.808	0.04947 2	2.615	0.434	N/A	N/A	N/A	N/A	N/A	N/A	N/A	N/A
3	196.16	0.98	196.11	0.28	196.81	10.91	0.213112	0.551	0.030889	0.146	0.650	0.05003 9	0.469	0.282	N/A	N/A	N/A	N/A	N/A	N/A	N/A	N/A
3	194.88	4.92	196.04	0.46	180.84	60.71	0.211583	2.777	0.030878	0.238	0.740	0.04969 7	2.606	0.372	N/A	N/A	N/A	N/A	N/A	N/A	N/A	N/A
4	196.16	0.82	196.37	0.27	193.53	9.05	0.213106	0.460	0.030931	0.138	0.624	0.04996 9	0.389	0.342	N/A	N/A	N/A	N/A	N/A	N/A	N/A	N/A
RG1206-1	195.2	1.9	192.7	0.68	206.3	22.36	0.21193	0.00227	0.03034	0.00011	0.338 49	0.05024	0.00049	0.048 89	27	28	3875 5	1910	1006	2435 5	456 5	49362 1
2	198.2	1.64	194.7	0.59	206.1	19.08	0.21549	0.00197	0.03066	0.00009	0.321 09	0.05024	0.00042	0.153 00	0	20	4911 8	2419	3773	9558 7	568 7	61904 6
3	200.1	3.18	195.1	1.12	263	36.06	0.21788	0.00382	0.03073	0.00018	0.334 09	0.05149	0.00082	0.154 24	13	0	1333 0	672	1041	2609 8	156 4	16763 7
4	203.3	3.31	195.6	1.17	289.1	36.6	0.22166	0.00399	0.03081	0.00019	0.342 59	0.05209	0.00084	0.102 38	8	52	1681 0	858	929	2179 3	196 0	21090 0
5	203.2	1.65	194.5	0.59	249.1	18.54	0.22152	0.00199	0.03063	0.00009	0.327 08	0.05118	0.00041	0.154 74	0	0	7736 5	3879	5998	1524 41	886 8	97626 0
6	198.7	1.96	194.1	0.7	234.8	22.4	0.21615	0.00234	0.03057	0.00011	0.332 38	0.05087	0.00050	0.081 35	51	19	4665 1	2323	1892	4844 5	544 3	59003 6
7	197.1	1.45	193.7	0.52	209.1	16.83	0.21423	0.00173	0.03050	0.00008	0.324 81	0.05031	0.00037	0.150 36	0	0	9450 5	4653	7104	1818 07	109 98	11981 52
8	195.1	3.77	193.2	1.33	256.4	43.78	0.21180	0.00449	0.03042	0.00021	0.325 64	0.05135	0.00099	0.175 50	18	11	1029 6	517	1026	2318 5	123 6	13087 4
9	200.3	2.34	193.8	0.82	210.9	26.61	0.21802	0.00281	0.03052	0.00013	0.330 48	0.05034	0.00058	0.141 79	0	1	2974 0	1464	2211	5391 0	340 1	37680 3
10	197.5	2.43	195.9	0.87	194.6	28.11	0.21468	0.00291	0.03085	0.00014	0.334 79	0.04999	0.00061	0.156 84	47	0	3582 4	1751	2839	7108 4	413 0	44910 8
11	198.1	2.36	194.4	0.84	259.9	26.99	0.21546	0.00283	0.03061	0.00013	0.323 34	0.05142	0.00061	0.084 30	69	0	2539 8	1276	1154	2730 5	299 8	32090 9
12	196	2.44	194.7	0.88	228.2	28.19	0.21293	0.00291	0.03066	0.00014	0.334 12	0.05072	0.00062	0.143 48	38	0	3339 6	1654	2320	6102 3	393 3	42138 1
13	199.8	2.25	196	0.8	242.3	25.45	0.21748	0.00270	0.03087	0.00013	0.339 21	0.05103	0.00057	0.155 73	93	31	4015 1	2001	3266	7909 2	465 6	50323 9
14	201	2.59	195.4	0.92	255.9	29.02	0.21888	0.00311	0.03077	0.00015	0.343 09	0.05134	0.00065	0.139 45	13	0	2761 6	1384	1926	4886 3	319 9	34720 9
15	200.5	3.41	196	1.21	236.2	38.34	0.21829	0.00409	0.03088	0.00019	0.328 39	0.05090	0.00086	0.084 62	0	0	2428 1	1206	1014	2598 3	279 6	30424 5
16	195.2	2.36	196.8	0.86	156.5	27.64	0.21193	0.00282	0.03101	0.00014	0.339 29	0.04918	0.00059	0.134 08	0	6	5000 4	2399	3392	8444 3	572 7	62409 0
17	198.7	3.6	194.2	1.27	270.8	40.59	0.21615	0.00431	0.03058	0.00020	0.328 00	0.05167	0.00093	0.118 86	18	0	1378 2	694	822	2092 3	162 5	17440 8
18	199.7	2.85	195	1	219.6	32.26	0.21740	0.00341	0.03072	0.00016	0.332 05	0.05053	0.00071	0.084 74	33	0	2377 2	1171	1062	2561 2	272 5	29951 9

19	196.8	2.75	194.5	0.98	188.2	31.7	0.21390	0.00329	0.03063	0.00016	0.33962	0.04985	0.00069	0.16164	44	0	54581	2652	4675	11249	627 1	689721
20	203.4	3.36	193	1.17	339.1	36.54	0.22181	0.00405	0.03039	0.00019	0.34241	0.05324	0.00087	0.06524	16	0	20570	1067	782	17250	243 3	261990

CG428B-1	198	10.38	195.8	3.12	232.6	126.94	0.21530	0.01242	0.03085	0.00050	0.28096	0.05082	0.00284	0.11897	0	11	7651	393	931	23406	146 8	195271
2	173.1	14.98	195	4.58	0.1	13.64	0.18585	0.01750	0.03072	0.00074	0.25582	0.04414	0.00408	0.08230	0	0	6380	284	519	13569	123 3	163647
3	184.8	16.1	194.2	4.74	65.6	215.94	0.19960	0.01902	0.03058	0.00076	0.26081	0.04733	0.00442	0.06014	15	24	5118	244	249	7995	988	131956
4	183.9	9.34	190.3	3.12	131.5	124.12	0.19849	0.01102	0.02997	0.00050	0.30050	0.04866	0.00262	0.08745	39	2	10723	526	846	24872	214 1	282283
6	180.7	12.42	193.2	3.14	3.7	171.04	0.19484	0.01462	0.03042	0.00050	0.21905	0.04612	0.00340	0.07647	35	21	5912	274	437	11835	114 2	153625
7	226.1	23.86	214.6	6.02	349.7	249.26	0.24947	0.02938	0.03386	0.00096	0.24074	0.05349	0.00616	0.12039	0	0	3144	169	368	8910	550	734611
8	198.2	7.52	194.5	2.58	255.8	90.42	0.21554	0.00900	0.03063	0.00042	0.32839	0.05133	0.00204	0.09398	36	3	19827	1023	1846	48520	386 1	512397
10	194.4	12.44	191.1	3.8	275.3	152.86	0.21096	0.01484	0.03009	0.00060	0.28346	0.05177	0.00354	0.06766	0	0	6713	349	483	12058	134 9	176865
11	191.1	10.96	190.3	3.5	254.3	137.38	0.20708	0.01304	0.02996	0.00056	0.29683	0.05130	0.00314	0.06083	49	28	7756	399	500	12599	157 5	205528
12	187.6	15.1	186.1	4.36	172.5	194.8	0.20294	0.01788	0.02930	0.00070	0.27116	0.04952	0.00426	0.05324	0	33	5639	279	297	8201	112 9	152914
14	195.4	11.22	194.6	3.08	176	140.56	0.21219	0.01340	0.03064	0.00050	0.25841	0.04959	0.00306	0.08630	52	0	6804	337	652	15357	130 7	176650
15	193.1	16.36	191.8	5.16	165.8	204.24	0.20949	0.01950	0.03019	0.00082	0.29180	0.04938	0.00446	0.06975	7	26	6392	315	433	11841	123 9	168531
16	197	14.22	191.7	3.74	231.4	174.46	0.21416	0.01702	0.03019	0.00060	0.25007	0.05079	0.00394	0.09807	24	0	5125	259	532	13370	100 1	135326
17	196	13.12	194.6	3.5	229.1	162	0.21294	0.01568	0.03065	0.00056	0.24812	0.05074	0.00364	0.08563	0	19	5629	285	534	12641	110 5	146515
18	188.9	15.74	193.2	4.26	174.5	202.44	0.20450	0.01868	0.03043	0.00068	0.24464	0.04956	0.00444	0.07968	24	0	4381	216	340	9227	875	114922
19	193.3	6.76	194.4	2.2	153.3	84.16	0.20965	0.00806	0.03061	0.00036	0.30591	0.04911	0.00178	0.13747	0	0	18392	899	2646	66464	355 6	479911
20	216.9	17.72	213.4	4.7	247.9	197.32	0.23818	0.02160	0.03365	0.00076	0.24905	0.05116	0.00452	0.11664	0	4	4010	204	436	11193	711	952525
CG428B 1	197.2	5.68	196	2.12	223.5	70.3	0.21430	0.00680	0.03086	0.00034	0.34721	0.05062	0.00156	0.06284	35	0	13654	694	610	34466	327 7	545238
2	194.1	5.84	194.8	2.24	167.4	73.94	0.21066	0.00696	0.03068	0.00036	0.35516	0.04941	0.00158	0.14164	0	0	18208	903	2114	104275	434 4	731863
3	193.7	8.28	193	3.14	228.3	103.96	0.21018	0.00986	0.03039	0.00050	0.35071	0.05072	0.00232	0.10444	61	14	12792	651	1094	54584	314 3	519471
4	192.5	6.64	196.6	2.48	142.7	85.18	0.20876	0.00790	0.03096	0.00040	0.34141	0.04889	0.00180	0.08147	23	4	9824	482	620	32106	234 4	391759

CG-563-1	212.5	8.04	213.2	2.56	220.4	86.7	0.23281	0.00976	0.03363	0.00041	0.29081	0.05055	0.00195	0.10644	25	0	3434	170	212	4529	370	421809
2	194	10.73	190.7	3.93	401.1	118.87	0.21059	0.01279	0.03003	0.00063	0.34542	0.05473	0.00302	0.10983	28	0	7803	418	449	11902	100 7	107362
3	182.8	8.79	189.7	3.1	104.7	109.76	0.19725	0.01036	0.02986	0.00050	0.31881	0.04811	0.00231	0.12094	8	0	6914	325	432	11676	837	957085
4	189.5	9.85	193.6	3.5	113.4	117.59	0.20523	0.01170	0.03049	0.00056	0.32217	0.04829	0.00250	0.09767	0	27	6048	286	261	8080	706	820209
5	192	4.94	193.9	1.77	176.6	58.35	0.20814	0.00588	0.03053	0.00028	0.32465	0.04961	0.00126	0.13171	7	0	11988	582	814	21576	141 7	162395
6	198.1	3.59	199.5	1.27	211.5	41.03	0.21537	0.00429	0.03144	0.00020	0.31936	0.05036	0.00090	0.19748	44	11	14369	708	1433	37686	166 5	189169

7	198.3	9.23	190.7	3.18	295.1	102.63	0.21569	0.01105	0.03003	0.00051	0.33150	0.05222	0.00242	0.09767	0	4	5375	275	244	7301	645	74107
8	199.2	7.14	194.6	2.46	216.8	80.39	0.21672	0.00855	0.03064	0.00039	0.32263	0.05047	0.00180	0.11293	6	0	8761	433	505	13488	1011	11842
9	189.6	8.82	190.1	3.06	126.5	105.55	0.20526	0.01047	0.02992	0.00049	0.32106	0.04856	0.00225	0.11373	0	0	5727	272	345	9095	671	79302
10	205.5	6.7	194.8	2.27	384.9	71.2	0.22433	0.00807	0.03068	0.00036	0.32618	0.05434	0.00177	0.10388	71	0	5997	319	387	8501	718	81120
11	197.3	6.17	193.4	2.03	272.7	70.56	0.21453	0.00738	0.03045	0.00032	0.30549	0.05171	0.00163	0.10233	18	7	5172	262	348	7277	616	70497
12	181.1	5.86	192.5	2	24.1	75.01	0.19523	0.00689	0.03031	0.00032	0.29915	0.04651	0.00151	0.09487	4	16	5056	230	281	6627	595	69257
13	201.1	5.68	202.7	2.06	255	62.9	0.21908	0.00682	0.03195	0.00033	0.33179	0.05132	0.00143	0.21604	33	44	13803	693	1490	39114	1597	179453
14	194.1	5	192.3	1.72	258.6	58.02	0.21063	0.00596	0.03028	0.00028	0.32680	0.05140	0.00132	0.12277	0	5	6223	313	435	10575	750	85389
15	185.3	3.84	196.9	1.43	83.5	48.56	0.20015	0.00454	0.03101	0.00023	0.32698	0.04770	0.00097	0.21278	23	13	19230	898	2231	55320	2263	257718
16	199.1	4.44	196	1.59	318.8	49.21	0.21664	0.00531	0.03087	0.00025	0.33041	0.05277	0.00116	0.18338	0	1	11168	577	1033	27842	1342	150488
17	189.1	4.74	191.4	1.69	187.2	56.71	0.20467	0.00562	0.03013	0.00027	0.32635	0.04983	0.00124	0.12797	59	49	10888	531	713	19407	1307	150346
18	219.2	8.95	220.6	3.27	400.1	88.47	0.24099	0.01094	0.03482	0.00053	0.33530	0.05472	0.00222	0.17517	0	16	4878	261	514	10311	546	58317
19	199.8	8.86	215.4	3.26	203.5	99.85	0.21745	0.01063	0.03398	0.00052	0.31304	0.05018	0.00223	0.10778	133	0	4509	221	234	6010	513	55250
20	203.9	6.55	195.6	2.22	348.4	70.86	0.22244	0.00788	0.03080	0.00035	0.32078	0.05346	0.00171	0.11317	30	0	5713	299	374	8818	676	77244

SU262- 1	192.7	12.08	190.3	2.76	224.8	153.14	0.20903	0.01440	0.02997	0.00044	0.21311	0.05065	0.00344	0.09554	0	20	8379	423	773	18980	1465	197199
2	198.1	14.24	191.5	3.32	228.6	174.7	0.21546	0.01706	0.03016	0.00054	0.22613	0.05073	0.00394	0.09037	0	22	7685	388	621	16388	1308	180035
3	193.6	11.3	192.6	2.6	235	142.6	0.21006	0.01346	0.03033	0.00042	0.21611	0.05087	0.00322	0.05628	0	0	8672	439	478	11475	1521	202384
4	194.3	7.44	193.8	2.02	196	93.82	0.21095	0.00886	0.03051	0.00032	0.24972	0.05002	0.00204	0.08392	16	9	16007	798	1230	31445	2754	371931
5	182.3	12.1	189.6	2.84	70.1	167	0.19663	0.01426	0.02984	0.00046	0.21256	0.04743	0.00338	0.06083	0	0	8332	394	547	12151	1461	198300
6	192.3	12.32	190.9	2.64	156.9	158.6	0.20851	0.01468	0.03005	0.00042	0.19852	0.04919	0.00342	0.11837	9	13	8081	396	898	22855	1391	191692
7	201.2	14.04	190.8	3	324.4	168.08	0.21911	0.01686	0.03005	0.00048	0.20759	0.05290	0.00402	0.06515	20	32	6459	340	379	10076	1140	153512
8	186.4	13.18	190.5	2.82	187.5	173.42	0.20148	0.01558	0.02999	0.00046	0.19836	0.04984	0.00382	0.05913	0	0	7084	352	438	10069	1283	168993
9	191.9	6.64	191.8	1.86	152.2	85.52	0.20799	0.00790	0.03021	0.00030	0.26145	0.04909	0.00182	0.08207	44	0	16408	804	1266	32180	2842	389283
10	187.3	8.18	189	2.12	185.7	107.38	0.20254	0.00970	0.02975	0.00034	0.23863	0.04980	0.00234	0.08113	0	2	12894	641	995	25435	2331	311176
11	192.2	7.46	188.7	1.96	216	95.08	0.20835	0.00888	0.02970	0.00032	0.25280	0.05045	0.00210	0.07431	94	0	13808	695	956	25080	2468	335019
12	198.6	11.04	191.8	3	300.7	133.22	0.21601	0.01322	0.03020	0.00048	0.25970	0.05235	0.00312	0.08516	42	0	9663	505	784	19821	1731	231028
13	189.2	8.2	188.1	2.36	214.1	105.4	0.20482	0.00972	0.02961	0.00038	0.27043	0.05041	0.00234	0.06143	29	0	13003	654	775	19659	2371	317652
14	189.9	9.32	189.6	2.36	212.2	120.16	0.20562	0.01106	0.02985	0.00038	0.23667	0.05037	0.00266	0.06466	0	0	9777	491	657	15459	1778	237291
15	195.6	5.06	187.5	1.58	250.6	62.44	0.21241	0.00604	0.02951	0.00026	0.30984	0.05122	0.00140	0.08237	0	19	23950	1225	1858	48872	4295	589050
16	188.1	5.26	187.3	1.62	192	68.16	0.20356	0.00622	0.02948	0.00026	0.28863	0.04994	0.00148	0.08334	38	34	24269	1211	2057	50355	4445	599743

17	196.7	10.72	191.4	2.68	280.2	131.84	0.21382	0.01282	0.03013	0.00042	0.23249	0.05188	0.00306	0.05902	13	18	8605	446	560	12396	1562	208460
18	192.2	13.14	192	2.98	191.2	167.96	0.20834	0.01564	0.03023	0.00048	0.21151	0.04992	0.00370	0.06534	0	7	6541	326	413	10416	1174	158233
19	193.6	8.86	190.5	2.32	251.7	111.44	0.21004	0.01056	0.02999	0.00038	0.25203	0.05124	0.00252	0.06949	0	9	10271	526	699	17566	1882	250893
20	196.9	8.26	189.6	2.22	274.9	101.5	0.21399	0.00986	0.02984	0.00036	0.26183	0.05176	0.00234	0.06827	0	9	10925	565	725	18481	1988	268716
21	184.5	10.54	188.9	2.78	187.8	139.78	0.19924	0.01246	0.02974	0.00044	0.23658	0.04984	0.00306	0.06233	88	0	8922	444	547	13883	1686	221059
22	184.1	10.06	188.8	2.52	112.1	135.76	0.19883	0.01188	0.02972	0.00040	0.22526	0.04826	0.00284	0.05473	7	0	8576	414	438	11741	1575	214566
23	203.5	7.32	187.4	2.18	415.2	84.12	0.22191	0.00880	0.02950	0.00034	0.29064	0.05508	0.00212	0.07426	0	0	16685	919	1500	31292	3140	417247
24	187.8	7.3	188.8	2.06	172.2	95.46	0.20317	0.00864	0.02972	0.00032	0.25319	0.04951	0.00206	0.08458	24	0	12724	630	1085	27028	2356	317202
25	183.3	9.28	187.8	2.34	113.7	125.76	0.19786	0.01094	0.02957	0.00038	0.23242	0.04829	0.00262	0.06031	24	2	9762	471	574	14890	1814	245064

CG-1866-1	204.9	9.25	185.4	3.15	342.2	99.25	0.22363	0.01115	0.02918	0.00050	0.34367	0.05332	0.00242	0.10812	0	0	28078	1478	1652	44013	3686	403401
2	197.4	3.09	200.5	1.16	233.6	35.81	0.21457	0.00369	0.03160	0.00019	0.34963	0.05084	0.00080	0.09493	1	0	31129	1563	1537	39530	4055	412364
3	199.6	2.01	199.9	0.74	191.7	23.22	0.21724	0.00240	0.03149	0.00012	0.34493	0.04993	0.00050	0.07712	0	25	37792	1864	1458	36335	4768	501484
4	206.7	6.32	186.1	2.16	374.4	67.49	0.22578	0.00763	0.02929	0.00034	0.34350	0.05408	0.00166	0.03606	0	0	33370	1783	607	17299	4382	475298
5	193.3	2.94	197.6	1.09	160.6	35.32	0.20974	0.00351	0.03112	0.00017	0.32643	0.04927	0.00075	0.09051	11	0	24647	1200	1168	30147	3169	329899
6	193.7	6.71	185.3	2.37	257.5	78	0.21019	0.00800	0.02916	0.00038	0.34239	0.05137	0.00179	0.11818	0	4	17648	896	1174	30087	2353	251300
7	193.6	9.4	186.2	3.28	191.5	109.55	0.21002	0.01120	0.02931	0.00052	0.33268	0.04993	0.00243	0.08912	0	0	15504	765	687	19744	2008	219319
8	206.1	8.72	187.1	2.96	324.4	93.5	0.22503	0.01052	0.02944	0.00047	0.34150	0.05290	0.00225	0.08597	121	35	20217	1057	1207	24656	2585	284225
9	198.4	2.75	186.7	0.96	257.6	31.55	0.21579	0.00329	0.02938	0.00015	0.33487	0.05137	0.00071	0.18761	0	10	75426	3832	7831	20086	9755	1060905
10	187.4	4.65	187.1	1.7	193.6	56.85	0.20266	0.00551	0.02946	0.00027	0.33709	0.04997	0.00124	0.03012	69	11	36251	1791	628	15442	4848	507758
11	192.6	2.92	187.4	1.03	191.2	34.87	0.20885	0.00347	0.02949	0.00016	0.32655	0.04992	0.00076	0.12432	0	12	41447	2047	2605	72411	5357	577104
12	194.3	3.41	202.2	1.29	174.4	40.36	0.21090	0.00406	0.03186	0.00021	0.34239	0.04956	0.00087	0.10368	26	0	34118	1673	1836	45967	4323	439052
13	191.5	3.59	187.7	1.3	260.3	42.57	0.20759	0.00427	0.02955	0.00021	0.34549	0.05143	0.00097	0.15539	0	31	38178	1943	3417	82959	5095	528785
14	197.5	5.52	188.2	1.94	276.1	62.91	0.21466	0.00660	0.02962	0.00031	0.34005	0.05179	0.00145	0.06876	0	24	19166	982	827	18355	2486	264446
15	202.8	7.59	185.7	2.6	348.7	82.47	0.22108	0.00912	0.02922	0.00041	0.34014	0.05347	0.00201	0.08905	0	0	14833	785	689	18616	1926	207117
16	198.6	6.42	186.6	2.23	271	72.44	0.21606	0.00769	0.02937	0.00036	0.34439	0.05167	0.00167	0.07711	0	24	20595	1053	853	22228	2640	285637
17	198.4	4.23	193.3	1.49	201.9	48.72	0.21585	0.00506	0.03043	0.00024	0.33644	0.05015	0.00107	0.09233	51	31	17216	855	771	21408	2138	229731
18	202	3.59	200.8	1.3	189.5	40.73	0.22013	0.00431	0.03163	0.00021	0.33910	0.04988	0.00088	0.10715	85	28	31300	1546	1814	43394	3785	401202
19	195.5	6.37	185.9	2.19	151.5	74.42	0.21226	0.00760	0.02926	0.00035	0.33408	0.04908	0.00160	0.08523	20	44	31494	1531	1636	37467	3887	435713
20	207.8	6.51	184.4	2.22	454.4	68.36	0.22710	0.00787	0.02903	0.00035	0.34791	0.05606	0.00176	0.09980	0	3	26982	1498	1740	37852	3545	375747
21	197.2	3.24	206.6	1.24	181.8	37.69	0.21431	0.00387	0.03256	0.00020	0.34016	0.04972	0.00081	0.13169	0	0	48070	2368	3601	79236	5926	595780

1654-1	187.4	7.08	186.8	1.96	161.4	92.92	0.20273	0.00838	0.02941	0.00032	0.26323	0.04929	0.00198	0.11537	0	0	13718	677	1476	40621	2564	349515
2	188.8	10.22	189.1	2.54	160	133.6	0.20429	0.01212	0.02977	0.00040	0.22648	0.04926	0.00288	0.08785	9	16	8453	417	829	18866	1570	213176
3	189.5	10.42	185.2	2.54	233.1	133.9	0.20523	0.01236	0.02915	0.00040	0.22785	0.05083	0.00300	0.09844	45	6	8055	410	766	20613	1540	207847
4	176.8	10.56	185.2	2.6	76.2	150.54	0.19022	0.01238	0.02915	0.00042	0.22138	0.04755	0.00306	0.08020	0	6	7731	368	694	16146	1491	199831
5	188.7	9.24	186.2	2.42	200.9	119.92	0.20421	0.01096	0.02931	0.00038	0.24157	0.05013	0.00264	0.08015	26	22	9098	457	757	18924	1731	234377
6	180.9	9.9	188.3	2.66	128.5	135.04	0.19505	0.01164	0.02965	0.00042	0.23737	0.04860	0.00284	0.07752	0	26	8000	389	603	15974	1551	204502
7	191.3	7.36	189.8	2.04	193.5	94.12	0.20733	0.00874	0.02987	0.00032	0.25414	0.04997	0.00206	0.07578	20	0	13054	653	915	25330	2453	331807
8	186.8	4.42	186.5	1.44	191.2	57.28	0.20202	0.00524	0.02935	0.00022	0.28899	0.04992	0.00124	0.11029	0	0	27204	1361	2976	78344	5257	705076
9	182.8	10.3	186.9	2.54	119.3	139.7	0.19724	0.01214	0.02942	0.00040	0.22090	0.04841	0.00294	0.07803	18	0	8285	402	641	16876	1591	214679
10	185.5	10.24	185.8	2.54	182.6	135.66	0.20049	0.01212	0.02924	0.00040	0.22629	0.04974	0.00296	0.07758	36	7	8201	409	585	16742	1595	214209
11	181.4	7.12	185	1.96	113.1	97.26	0.19562	0.00838	0.02912	0.00032	0.25652	0.04828	0.00202	0.08413	0	0	13764	666	1061	30710	2673	362373
12	191.8	7.08	188	2.04	235.4	89.66	0.20786	0.00844	0.02960	0.00032	0.26625	0.05088	0.00200	0.08722	21	0	12946	660	1051	29523	2501	335996
13	184.5	6.28	184.3	1.88	199.1	82.82	0.19924	0.00742	0.02900	0.00030	0.27778	0.05009	0.00180	0.10745	0	3	15210	764	1608	43704	3024	403696
14	183.4	5.86	186.3	1.8	165.8	78.08	0.19798	0.00692	0.02932	0.00028	0.27322	0.04938	0.00166	0.14106	30	8	16615	823	2118	62100	3283	436956
15	190.9	10.92	184.6	2.82	298.5	137.42	0.20686	0.01298	0.02906	0.00046	0.25227	0.05230	0.00322	0.08923	0	34	7522	394	570	17984	1510	200032
16	185.2	9.74	186.8	2.56	177.3	129.04	0.20008	0.01152	0.02941	0.00040	0.23622	0.04962	0.00280	0.08846	0	0	8198	408	709	19274	1621	216275
17	187	7.58	183.1	2.14	244.4	98.24	0.20222	0.00898	0.02880	0.00034	0.26585	0.05108	0.00222	0.12220	0	0	11594	594	1302	38515	2339	312838
18	192.5	6.6	186.7	1.96	258	82.56	0.20876	0.00784	0.02938	0.00032	0.29002	0.05138	0.00186	0.10789	0	15	14323	739	1461	41260	2822	379615
19	180.8	9.78	186	2.62	125	133.86	0.19488	0.01152	0.02928	0.00042	0.24266	0.04853	0.00282	0.09209	7	0	8294	404	771	20510	1656	221050
20	192.6	10.12	189.2	2.7	248.7	127.54	0.20888	0.01206	0.02978	0.00042	0.24427	0.05117	0.00290	0.08650	0	0	7622	391	605	17438	1501	200104
21	183.9	9.88	182.9	2.74	223	130.44	0.19855	0.01168	0.02878	0.00044	0.25989	0.05061	0.00292	0.08128	32	24	8030	408	701	17933	1652	218984
22	184	9.78	187.5	2.74	150.1	130.26	0.19864	0.01154	0.02951	0.00044	0.25665	0.04905	0.00278	0.09125	76	0	9726	479	838	23877	1946	259730
23	186.5	6.02	187.7	1.92	183	78.06	0.20157	0.00712	0.02955	0.00030	0.28742	0.04974	0.00168	0.15368	0	16	17533	876	2749	72542	3514	468505
24	199.5	9.08	187.5	2.52	339.8	108.48	0.21708	0.01088	0.02951	0.00040	0.27045	0.05326	0.00260	0.09822	0	0	9803	525	926	26005	1957	262809

RG-2226-1	186.2	3.82	187.5	1.33	196.3	47.15	0.20122	0.00452	0.02952	0.00021	0.31669	0.05003	0.00103	0.12260	0	6	10542	516	624	18062	1315	146006
2	183.1	5.05	186.8	1.73	211.2	63.57	0.19757	0.00595	0.02941	0.00028	0.31613	0.05035	0.00141	0.13628	0	6	5722	282	392	10946	731	79586
3	180.2	6.79	185.7	2.37	121.7	87.11	0.19419	0.00799	0.02922	0.00038	0.31607	0.04846	0.00184	0.08674	45	13	4574	217	240	5606	572	64055
4	185.8	8.41	184.8	2.96	242.4	101.29	0.20075	0.00994	0.02908	0.00047	0.32642	0.05103	0.00232	0.10277	56	0	7486	374	389	10926	954	105359
5	190.6	6.87	185.8	2.43	280.4	80.26	0.20643	0.00816	0.02924	0.00039	0.33742	0.05189	0.00187	0.17432	24	13	9759	496	841	24032	1229	136634

6	187.4	8.2	184.5	2.84	263.4	97.65	0.20273	0.00971	0.02903	0.00045	0.32364	0.05150	0.00226	0.11865	0	0	5690	287	345	9614	724	80307
7	188.5	6.84	186.8	2.02	235.1	83.97	0.20404	0.00811	0.02939	0.00032	0.27393	0.05087	0.00190	0.08642	32	0	3634	181	163	4419	453	50679
8	185.3	6.78	186.7	2.34	83.8	85.36	0.20015	0.00801	0.02939	0.00037	0.31458	0.04770	0.00174	0.13849	29	0	7186	335	544	14003	857	100258
9	191.7	7.35	187	2.58	291.1	85.16	0.20783	0.00874	0.02943	0.00041	0.33128	0.05213	0.00200	0.11486	0	0	6657	340	350	10752	835	92772
10	193.5	5.31	183.5	1.75	215.5	62.56	0.20998	0.00633	0.02887	0.00028	0.32173	0.05044	0.00139	0.11789	0	12	7628	377	417	12885	916	108382
11	184.5	6.62	186.5	2.38	171.3	81.39	0.19922	0.00782	0.02936	0.00038	0.32973	0.04949	0.00177	0.19432	0	15	11365	551	1166	31175	1410	159025
12	186.1	4.85	184.3	1.6	152.7	60.59	0.20121	0.00574	0.02900	0.00025	0.30219	0.04910	0.00129	0.11506	27	0	5678	273	362	9338	691	80465
13	185.7	5.73	184.6	1.98	150.4	70.46	0.20073	0.00677	0.02905	0.00032	0.32661	0.04905	0.00151	0.13208	0	0	7813	375	596	14731	953	110575
14	188.2	8.49	186.8	2.95	171.1	101.86	0.20369	0.01007	0.02941	0.00047	0.32325	0.04949	0.00223	0.13511	0	39	6046	293	412	11524	733	84563
15	194.6	6.75	184.3	2.17	244.6	78.56	0.21129	0.00805	0.02900	0.00035	0.31678	0.05108	0.00179	0.11623	35	20	4572	228	259	7603	551	64863
16	188.7	3.36	192.2	1.19	174.6	40.85	0.20423	0.00398	0.03027	0.00019	0.32209	0.04956	0.00088	0.21487	0	0	14558	707	1595	42926	1761	198020
17	194.5	3.4	182.9	1.13	291.1	39.41	0.21113	0.00406	0.02878	0.00018	0.32524	0.05213	0.00091	0.10266	0	0	12544	640	723	18586	1543	179508
18	193	5.54	184.6	1.79	285.4	64.87	0.20933	0.00660	0.02905	0.00028	0.30570	0.05200	0.00151	0.11289	64	0	5077	258	325	8200	628	72008
19	186.5	5.19	183.2	1.75	125.8	64.28	0.20160	0.00614	0.02882	0.00028	0.31900	0.04854	0.00135	0.10830	0	32	6008	285	315	9383	720	85918
20	189.1	7.5	183.5	2.58	250.9	88.93	0.20467	0.00890	0.02887	0.00041	0.32659	0.05122	0.00204	0.12434	0	12	5535	277	357	9915	689	79054

CG1888-1	180.5	1.86	182.5	0.69	204.2	23.77	0.19453	0.00219	0.02871	0.00011	0.34033	0.05020	0.00052	0.42557	0	14	31506	1577	6589	22315	4210	520155
2	179.7	3.25	183.9	1.17	197.6	41.81	0.19356	0.00382	0.02894	0.00019	0.33267	0.05006	0.00091	0.09649	0	0	10428	520	532	16583	1395	170473
3	189.4	5.49	182.3	1.91	266.2	65.4	0.20509	0.00652	0.02868	0.00030	0.32903	0.05157	0.00150	0.12637	12	4	10127	520	657	21236	1315	166731
4	196.6	3.97	197.5	1.38	228.1	46.39	0.21363	0.00475	0.03111	0.00022	0.31805	0.05072	0.00103	0.12232	6	0	80138	404	535	14914	9793	120943
5	182	3.43	192.7	1.28	91.9	45.08	0.19630	0.00404	0.03034	0.00020	0.32030	0.04787	0.00090	0.19751	0	0	13831	658	1500	42541	1735	213650
6	187.7	3.73	189.4	1.34	176.5	45.71	0.20310	0.00442	0.02982	0.00021	0.32359	0.04960	0.00099	0.16682	0	7	14905	735	1331	39251	1869	233417
7	186.7	3.45	189.2	1.26	150.8	42.49	0.20181	0.00408	0.02979	0.00020	0.33208	0.04906	0.00090	0.22095	0	25	33906	1653	4263	11817	4228	530624
8	190.8	4.96	180.8	1.68	238	58.89	0.20678	0.00589	0.02844	0.00027	0.33329	0.05094	0.00132	0.19085	24	23	89006	450	817	28006	1123	145622
9	188.5	2.57	200.6	0.98	153.2	31.46	0.20400	0.00305	0.03160	0.00016	0.33866	0.04911	0.00067	0.17943	0	0	25861	1261	2248	68764	3186	380041
10	196.6	3.24	196.7	1.15	193.3	37.8	0.21360	0.00388	0.03098	0.00018	0.31986	0.04996	0.00082	0.26860	0	28	14165	702	1840	57396	1694	211988
11	195.2	2.83	199.5	1.03	196	33.19	0.21201	0.00337	0.03143	0.00016	0.32026	0.05002	0.00072	0.16571	0	0	15841	786	1291	38815	1904	232329
12	185.7	2.45	192.8	0.91	118.5	30.6	0.20063	0.00290	0.03035	0.00015	0.34192	0.04839	0.00063	0.08615	46	0	31994	1535	1356	42128	3929	485086
13	187	4.35	191.3	1.58	192.2	53.07	0.20221	0.00514	0.03012	0.00025	0.32653	0.04994	0.00116	0.16394	26	0	77875	385	658	19629	9786	118756
14	190	2.33	197.4	0.88	173.3	28.1	0.20579	0.00277	0.03109	0.00014	0.33454	0.04954	0.00060	0.15199	2	6	32593	1600	2603	73655	3986	480629
15	183.7	6.34	188.5	2.24	8.4	79.73	0.19828	0.00748	0.02967	0.00036	0.32163	0.04621	0.00159	0.15132	48	47	73142	334	563	17202	8658	112812

16	194	6.15	189.3	2.14	255.2	71.14	0.21051	0.00733	0.02981	0.00034	0.32756	0.05132	0.00162	0.19019	25	7	6518	331	585	19119	804	99724
17	193.6	4.51	187	1.51	244.9	53.06	0.21006	0.00538	0.02944	0.00024	0.31830	0.05109	0.00120	0.21796	0	16	7200	364	853	24461	886	111341
18	190.7	3.11	190.4	1.12	259.4	36.78	0.20666	0.00369	0.02998	0.00018	0.33626	0.05141	0.00083	0.12349	0	0	2232	1135	1504	42130	2806	338358
19	186.8	5.29	185.3	1.87	168.6	64.44	0.20198	0.00626	0.02916	0.00030	0.33195	0.04944	0.00139	0.14363	8	0	1006	492	738	22674	1244	156616
20	185	3.96	182.8	1.39	214.5	48.81	0.19985	0.00468	0.02876	0.00022	0.32666	0.05042	0.00108	0.17805	1	22	9232	460	880	26085	1174	145332

SU539-1	190.2	4.61	183.2	1.63	260.9	54.64	0.20601	0.00548	0.02883	0.00026	0.33903	0.05145	0.00125	0.08475	153	0	25496	1286	1142	34938	3251	408975
2	220.4	3.42	212.5	1.19	283.8	34.95	0.24240	0.00418	0.03351	0.00019	0.32880	0.05196	0.00080	0.06963	0	0	12990	661	497	12585	1421	179323
3	195.4	2.44	183.2	0.84	262.3	28.28	0.21220	0.00291	0.02883	0.00013	0.32881	0.05148	0.00064	0.09128	137	7	77644	3917	3851	114607	9617	124593
4	196.8	3.1	196.8	1.12	176.8	36.07	0.21392	0.00370	0.03099	0.00018	0.33582	0.04961	0.00078	0.09338	120	33	24614	1196	1091	34596	2914	367588
5	229.7	8.35	240.5	2.9	95.7	84.58	0.25380	0.01031	0.03801	0.00047	0.30439	0.04795	0.00173	0.24844	0	18	62747	294	722	19137	6056	764258
6	193.1	3.87	182	1.34	275.6	45.04	0.20951	0.00461	0.02864	0.00021	0.33323	0.05178	0.00103	0.12525	5	0	50129	2542	3193	102371	6325	811018
7	197.4	2.05	196.3	0.74	209.8	23.77	0.21460	0.00245	0.03092	0.00012	0.33994	0.05032	0.00052	0.04800	29	0	36560	1801	954	26514	4377	548000
8	194.1	2.57	182.6	0.89	282.6	29.81	0.21070	0.00306	0.02873	0.00014	0.33553	0.05194	0.00068	0.08821	103	53	79133	4023	3638	113560	9952	127746
9	202.4	2.07	194.5	0.74	262.4	23.16	0.22064	0.00249	0.03063	0.00012	0.34715	0.05148	0.00052	0.10293	56	4	40333	2036	2268	63477	4813	611895
10	199.1	2.16	195.7	0.78	235.9	24.71	0.21668	0.00259	0.03083	0.00012	0.32563	0.05089	0.00055	0.08968	34	10	30290	1508	1336	41234	3637	456148
11	193.6	4.69	182.1	1.61	245	54.58	0.21006	0.00559	0.02866	0.00026	0.34090	0.05109	0.00123	0.08164	149	0	47343	2366	1988	63128	5877	767337
12	231.5	5.18	225.1	1.82	293.9	49.75	0.25607	0.00641	0.03554	0.00029	0.32597	0.05219	0.00116	0.20950	53	0	12395	632	1351	34222	1290	162064
13	207.3	2.3	207.9	0.85	254.6	25.13	0.22644	0.00278	0.03277	0.00014	0.34798	0.05131	0.00056	0.08979	13	1	42893	2152	2062	55062	4962	608270
14	201.6	2.45	197.4	0.88	241.3	27.57	0.21968	0.00295	0.03110	0.00014	0.33522	0.05101	0.00062	0.07186	43	16	37619	1876	1497	40732	4460	562325
15	199	3.15	210.1	1.2	204.9	36.04	0.21650	0.00378	0.03312	0.00019	0.32857	0.05021	0.00079	0.10489	99	0	32566	1598	1837	48374	3856	457338
16	190.3	4.03	195.4	1.46	161.3	48.59	0.20617	0.00478	0.03078	0.00023	0.32230	0.04928	0.00104	0.18751	42	10	15324	738	1446	43795	1870	231687
17	206	2.2	199.7	0.78	235.5	24.13	0.22493	0.00265	0.03146	0.00012	0.32376	0.05088	0.00054	0.06887	13	2	64981	3230	2312	66718	7505	961288
18	217.7	6.25	234.8	2.33	185.5	65.4	0.23914	0.00763	0.03709	0.00037	0.31266	0.04980	0.00143	0.31427	14	0	70947	345	1051	28225	7547	890585
19	199.1	4.44	200.1	1.6	218.7	50.54	0.21662	0.00532	0.03153	0.00026	0.33577	0.05051	0.00112	0.15023	0	4	13298	656	916	29753	1583	196473

SU580-1	197.5	2.3	192.8	0.82	240.2	26.82	0.21476	0.00275	0.03037	0.00013	0.33429	0.05099	0.00060	0.19961	0	0	21932	1109	2505	58782	2796	291687
2	177.7	4.46	182.2	1.63	102.5	58.63	0.19131	0.00523	0.02867	0.00026	0.33173	0.04807	0.00121	0.18080	58	0	15005	715	1450	38583	2023	211379
3	192	3.33	192.1	1.17	153.2	40.48	0.20815	0.00396	0.03024	0.00019	0.33026	0.04911	0.00086	0.12678	40	33	10242	498	776	17505	1296	136776
4	190.5	6.3	181.8	2.22	270.2	74.4	0.20635	0.00748	0.02861	0.00035	0.33748	0.05166	0.00172	0.12937	26	2	13360	684	1047	24636	1794	188636
5	182.3	5.2	181.3	1.88	200.2	65.24	0.19667	0.00612	0.02853	0.00030	0.33791	0.05011	0.00144	0.19375	0	0	18589	923	1791	51486	2540	263197

6	212.2	7.52	182.2	2.45	424.5	77.04	0.23247	0.00912	0.02867	0.00039	0.34674	0.05531	0.00196	0.15632	21	14	13564	743	1215	30152	1730	191162
7	192.8	5.94	182.9	2.04	142.3	70.74	0.20910	0.00707	0.02878	0.00032	0.32885	0.04888	0.00151	0.15240	85	0	26828	1299	2145	57912	3361	376628
8	191.1	6.18	183.3	2.17	231.4	73.27	0.20709	0.00735	0.02884	0.00035	0.34194	0.05079	0.00165	0.15084	0	35	14825	745	1145	31622	1948	207694
9	191.9	5.87	183	2.02	138.8	70.23	0.20804	0.00698	0.02880	0.00032	0.33117	0.04881	0.00149	0.14922	54	30	19871	960	1573	41979	2497	278835
10	192.7	6.27	181.9	2.15	207.4	73.96	0.20903	0.00747	0.02862	0.00034	0.33243	0.05027	0.00164	0.13437	50	0	12253	610	922	23461	1577	173024
11	194.8	3.4	190.4	1.23	253	39.79	0.21150	0.00406	0.02998	0.00020	0.34752	0.05127	0.00090	0.18008	100	20	19341	981	1897	47404	2508	260725
12	186.9	3.05	183.1	1.07	199.4	37.71	0.20214	0.00361	0.02882	0.00017	0.33029	0.05009	0.00082	0.13616	100	3	12361	612	936	23830	1638	173375
13	183.5	2.57	198.4	0.97	105	32.91	0.19813	0.00303	0.03126	0.00016	0.33469	0.04812	0.00068	0.15711	44	0	17131	815	1458	35152	2224	221520
14	192.3	2.37	194.3	0.86	175.2	28.51	0.20852	0.00282	0.03060	0.00014	0.33830	0.04958	0.00061	0.19878	1	0	24529	1203	2609	65034	3117	324043
15	189.1	2.84	198	1.08	193.6	34.64	0.20471	0.00337	0.03119	0.00017	0.33109	0.04997	0.00075	0.21123	3	0	16227	802	1816	44874	2117	210344
16	190.7	4.05	182.8	1.43	255.4	48.3	0.20655	0.00482	0.02876	0.00023	0.34270	0.05132	0.00109	0.18697	33	24	15860	804	1774	42081	2105	222966
17	190.2	2.84	193.8	1.05	176.4	34.54	0.20596	0.00338	0.03052	0.00017	0.33941	0.04960	0.00074	0.17221	0	0	17149	841	1696	39507	2205	227213
18	189.8	4.3	197.5	1.58	181.7	52.3	0.20555	0.00511	0.03111	0.00025	0.32325	0.04972	0.00113	0.14609	0	9	11693	574	929	22419	1509	151955
19	190.2	4.02	189.6	1.4	154.2	49.14	0.20596	0.00478	0.02985	0.00022	0.31757	0.04913	0.00105	0.12885	0	33	97543	473	718	17186	1241	132142
20	192.4	2.56	199.3	0.96	168.5	30.62	0.20861	0.00305	0.03140	0.00015	0.32674	0.04944	0.00065	0.19525	7	9	25083	1225	2748	63688	3171	323008

CG510-1	193.2	13.28	210.1	4.7	75.3	165.98	0.20956	0.01582	0.03313	0.00075	0.29988	0.04753	0.00348	0.10748	31	0	1079	50	86	8151	219	75620
2	194.3	15.41	181.6	5.67	406.3	178.67	0.21084	0.01838	0.02857	0.00090	0.36136	0.05485	0.00463	0.63217	23	5	3564	194	1763	62	832	28969 4
3	210.1	9.46	219.3	3.67	235	106.43	0.22989	0.01146	0.03460	0.00059	0.34207	0.05087	0.00243	0.21660	0	0	1934	97	318	2819 7	384	12979 6
4	193.3	12.74	179.9	4.3	162.6	155.56	0.20969	0.01518	0.02831	0.00069	0.33668	0.04931	0.00344	0.38794	45	29	1601	78	416	5112 2	337	13144 1
5	178.5	17.07	181.6	6.25	121.3	222.89	0.19214	0.02004	0.02857	0.00100	0.33559	0.04845	0.00491	0.06571	4	14	1357	65	62	7276	306	11042 2
6	217.8	21.25	183.7	7.05	481.8	215.75	0.23929	0.02594	0.02890	0.00113	0.36069	0.05677	0.00592	0.55243	0	0	2464	139	1162	1098 35	523	19829 9
7	193.9	6.76	214.4	2.83	154.8	83.04	0.21039	0.00806	0.03382	0.00045	0.34732	0.04915	0.00179	0.71197	0	0	4251	207	2027	2088 34	888	29243 0
8	225.7	20.11	183.1	6.64	618.4	193.82	0.24889	0.02474	0.02882	0.00106	0.37002	0.06041	0.00577	0.60099	10	0	2532	152	1329	1232 29	550	20449 4
9	192.2	13.12	180.2	4.31	119.6	162.2	0.20842	0.01562	0.02835	0.00069	0.32475	0.04841	0.00350	0.56647	0	0	1595	76	571	7439 1	331	13099 3
10	206.5	16.69	182.1	5.71	380.9	182.61	0.22551	0.02014	0.02865	0.00091	0.35565	0.05424	0.00466	0.84137	42	3	2538	137	1262	1739 65	545	20621 8
11	193.9	11.46	181.7	4.09	268.3	137.27	0.21042	0.01366	0.02858	0.00065	0.35034	0.05161	0.00322	1.00624	0	0	3050	156	2053	2508 98	667	24867 6
12	199	11.35	183.7	4.03	372.9	130.29	0.21653	0.01360	0.02890	0.00064	0.35258	0.05405	0.00327	0.61481	0	0	2807	151	1090	1395 84	625	22641 2
13	207.9	13.16	184.8	4.47	312.1	145.49	0.22720	0.01590	0.02908	0.00071	0.34888	0.05261	0.00353	0.69275	38	0	2306	120	1060	1284 38	476	18492 8
14	182.4	11.98	181.1	4.38	140.5	155.02	0.19681	0.01412	0.02849	0.00070	0.34247	0.04885	0.00338	0.59510	0	0	1981	96	784	9678 1	438	16219 2
15	196.6	13.76	183.6	4.65	283.4	161.42	0.21364	0.01644	0.02890	0.00074	0.33275	0.05196	0.00386	0.65430	32	0	1413	73	592	7482 4	306	11405 1

16	194.8	21.51	182	7	180.7	252.95	0.21152	0.02567	0.02863	0.00112	0.32235	0.04969	0.00584	0.49684	4	1	708	35	241	28785	148	57788
17	188.5	10.97	183.6	4.04	255.7	135.32	0.20402	0.01301	0.02889	0.00064	0.34740	0.05133	0.00315	0.48591	12	12	2659	136	1037	104704	595	214884
18	178.9	13.74	183.3	5.07	156.6	179.72	0.19265	0.01614	0.02884	0.00081	0.33524	0.04918	0.00399	0.71592	45	0	1693	83	742	98390	384	137048
19	192.3	9.8	182.6	3.58	279.4	118.32	0.20856	0.01167	0.02873	0.00057	0.35457	0.05186	0.00278	0.72378	50	12	4005	207	2270	23639	885	325649
20	164.9	12.61	183.9	4.92	0.1	157.37	0.17630	0.01460	0.02895	0.00078	0.32535	0.04554	0.00367	0.48446	0	0	1732	78	591	67915	397	139791

*ST20150 01-1	187.2	6.13	185.4	6.51	209.7	10.34	0.20247	0.00728	0.02918	0.00104	0.992	0.050	0.000	N/A	N/A	N/A	N/A	N/A	N/A	N/A	N/A	N/A
2	189.0	5.41	184.1	5.55	250.1	16.51	0.20454	0.00643	0.02897	0.00089	0.973	0.051	0.000	N/A	N/A	N/A	N/A	N/A	N/A	N/A	N/A	N/A
3	186.6	5.58	181.7	5.75	248.9	15.16	0.20171	0.00662	0.02858	0.00092	0.979	0.051	0.000	N/A	N/A	N/A	N/A	N/A	N/A	N/A	N/A	N/A
4	185.5	5.81	183.5	6.13	210.5	13.55	0.20039	0.00689	0.02887	0.00098	0.985	0.050	0.000	N/A	N/A	N/A	N/A	N/A	N/A	N/A	N/A	N/A
5	183.0	7.41	179.5	7.73	228.2	18.46	0.19746	0.00877	0.02823	0.00123	0.984	0.051	0.000	N/A	N/A	N/A	N/A	N/A	N/A	N/A	N/A	N/A
6	185.4	5.61	182.8	5.90	218.8	12.64	0.20030	0.00665	0.02876	0.00094	0.986	0.051	0.000	N/A	N/A	N/A	N/A	N/A	N/A	N/A	N/A	N/A
7	182.2	5.68	179.7	6.00	214.1	10.37	0.19652	0.00671	0.02827	0.00096	0.991	0.050	0.000	N/A	N/A	N/A	N/A	N/A	N/A	N/A	N/A	N/A
8	180.7	6.34	176.1	6.45	241.7	22.39	0.19483	0.00748	0.02770	0.00103	0.967	0.051	0.000	N/A	N/A	N/A	N/A	N/A	N/A	N/A	N/A	N/A
9	192.8	5.94	184.4	5.97	297.2	19.04	0.20915	0.00710	0.02902	0.00095	0.969	0.052	0.000	N/A	N/A	N/A	N/A	N/A	N/A	N/A	N/A	N/A
10	179.8	5.36	177.1	5.64	215.8	10.37	0.19374	0.00632	0.02785	0.00090	0.990	0.050	0.000	N/A	N/A	N/A	N/A	N/A	N/A	N/A	N/A	N/A
11	193.7	7.94	184.5	6.14	307.7	67.06	0.21019	0.00950	0.02903	0.00098	0.747	0.053	0.002	N/A	N/A	N/A	N/A	N/A	N/A	N/A	N/A	N/A
12	183.1	5.51	180.3	5.73	219.4	16.23	0.19758	0.00652	0.02836	0.00091	0.977	0.051	0.000	N/A	N/A	N/A	N/A	N/A	N/A	N/A	N/A	N/A
13	190.1	5.52	185.3	5.68	250.9	16.30	0.20594	0.00658	0.02916	0.00091	0.975	0.051	0.000	N/A	N/A	N/A	N/A	N/A	N/A	N/A	N/A	N/A
14	186.1	5.97	183.0	6.28	226.2	12.46	0.20118	0.00709	0.02879	0.00100	0.988	0.051	0.000	N/A	N/A	N/A	N/A	N/A	N/A	N/A	N/A	N/A
15	185.5	5.52	179.3	5.52	264.8	21.65	0.20039	0.00654	0.02820	0.00088	0.957	0.052	0.000	N/A	N/A	N/A	N/A	N/A	N/A	N/A	N/A	N/A
16	184.8	5.46	182.0	5.74	219.7	12.03	0.19956	0.00647	0.02864	0.00092	0.987	0.051	0.000	N/A	N/A	N/A	N/A	N/A	N/A	N/A	N/A	N/A
17	184.3	5.09	180.8	5.25	228.4	15.74	0.19897	0.00602	0.02845	0.00084	0.974	0.051	0.000	N/A	N/A	N/A	N/A	N/A	N/A	N/A	N/A	N/A
18	183.1	5.23	180.3	5.32	218.7	21.06	0.19756	0.00618	0.02837	0.00085	0.956	0.051	0.000	N/A	N/A	N/A	N/A	N/A	N/A	N/A	N/A	N/A
19	181.2	4.73	180.4	5.01	191.5	11.05	0.19537	0.00559	0.02838	0.00080	0.986	0.050	0.000	N/A	N/A	N/A	N/A	N/A	N/A	N/A	N/A	N/A
20	178.1	5.15	177.3	5.31	189.2	20.05	0.19172	0.00606	0.02788	0.00085	0.962	0.050	0.000	N/A	N/A	N/A	N/A	N/A	N/A	N/A	N/A	N/A
21	191.0	4.90	188.4	5.03	222.8	18.03	0.20694	0.00583	0.02966	0.00080	0.961	0.051	0.000	N/A	N/A	N/A	N/A	N/A	N/A	N/A	N/A	N/A
22	186.2	6.02	183.2	6.21	224.4	19.83	0.20122	0.00714	0.02882	0.00099	0.970	0.051	0.000	N/A	N/A	N/A	N/A	N/A	N/A	N/A	N/A	N/A
23	177.6	4.91	176.2	5.19	196.2	10.25	0.19109	0.00577	0.02770	0.00083	0.989	0.050	0.000	N/A	N/A	N/A	N/A	N/A	N/A	N/A	N/A	N/A
24	185.0	7.12	183.3	7.47	205.9	20.57	0.19980	0.00845	0.02885	0.00119	0.977	0.050	0.000	N/A	N/A	N/A	N/A	N/A	N/A	N/A	N/A	N/A
25	185.2	7.12	185.0	7.64	187.3	12.12	0.20008	0.00845	0.02912	0.00122	0.992	0.050	0.000	N/A	N/A	N/A	N/A	N/A	N/A	N/A	N/A	N/A
26	185.8	6.68	184.5	7.10	202.1	13.59	0.20081	0.00793	0.02904	0.00113	0.989	0.050	0.000	N/A	N/A	N/A	N/A	N/A	N/A	N/A	N/A	N/A

27	188.1	7.93	185.3	8.30	223.1	21.01	0.20353	0.00944	0.02917	0.00133	0.980	0.051	0.000	N/A	N/A	N/A	N/A	N/A	N/A	N/A	N/A	N/A
28	176.1	5.21	175.8	5.42	181.2	18.70	0.18942	0.00612	0.02764	0.00086	0.968	0.050	0.000	N/A	N/A	N/A	N/A	N/A	N/A	N/A	N/A	N/A
29	183.3	5.94	180.7	6.26	217.1	12.18	0.19780	0.00703	0.02842	0.00100	0.989	0.050	0.000	N/A	N/A	N/A	N/A	N/A	N/A	N/A	N/A	N/A
30	178.0	6.15	176.8	6.52	194.0	12.52	0.19156	0.00724	0.02780	0.00104	0.990	0.050	0.000	N/A	N/A	N/A	N/A	N/A	N/A	N/A	N/A	N/A
*ST20150 02-1	187.8	6.56	184.5	6.38	229.9	35.21	0.20318	0.00779	0.02903	0.00102	0.916	0.05076	0.00078	N/A	N/A	N/A	N/A	N/A	N/A	N/A	N/A	N/A
2	188.7	8.13	186.6	8.25	215.1	34.72	0.20424	0.00968	0.02937	0.00132	0.948	0.05043	0.00076	N/A	N/A	N/A	N/A	N/A	N/A	N/A	N/A	N/A
3	187.4	7.08	183.2	6.89	240.5	37.04	0.20267	0.00841	0.02883	0.00110	0.920	0.05099	0.00083	N/A	N/A	N/A	N/A	N/A	N/A	N/A	N/A	N/A
4	182.2	7.22	179.8	7.20	214.3	35.27	0.19660	0.00854	0.02828	0.00115	0.935	0.05042	0.00078	N/A	N/A	N/A	N/A	N/A	N/A	N/A	N/A	N/A
5	185.7	6.42	183.9	6.28	208.9	35.56	0.20070	0.00762	0.02894	0.00100	0.913	0.05030	0.00078	N/A	N/A	N/A	N/A	N/A	N/A	N/A	N/A	N/A
6	187.1	6.34	182.3	5.91	248.0	39.63	0.20234	0.00753	0.02868	0.00094	0.884	0.05116	0.00089	N/A	N/A	N/A	N/A	N/A	N/A	N/A	N/A	N/A
7	185.3	7.28	182.4	7.20	221.5	36.83	0.20016	0.00864	0.02870	0.00115	0.928	0.05058	0.00081	N/A	N/A	N/A	N/A	N/A	N/A	N/A	N/A	N/A
8	186.5	8.22	183.6	8.29	223.7	35.90	0.20166	0.00977	0.02889	0.00132	0.946	0.05062	0.00079	N/A	N/A	N/A	N/A	N/A	N/A	N/A	N/A	N/A
9	183.4	4.98	180.4	4.38	221.1	38.35	0.19791	0.00589	0.02839	0.00070	0.826	0.05057	0.00085	N/A	N/A	N/A	N/A	N/A	N/A	N/A	N/A	N/A
10	178.1	5.38	176.8	5.05	195.6	36.38	0.19176	0.00633	0.02781	0.00081	0.877	0.05001	0.00079	N/A	N/A	N/A	N/A	N/A	N/A	N/A	N/A	N/A
11	184.6	6.20	181.2	5.87	228.5	37.98	0.19937	0.00735	0.02850	0.00094	0.892	0.05073	0.00084	N/A	N/A	N/A	N/A	N/A	N/A	N/A	N/A	N/A
12	194.9	7.60	180.4	6.53	374.9	49.53	0.21166	0.00910	0.02838	0.00104	0.854	0.05409	0.00121	N/A	N/A	N/A	N/A	N/A	N/A	N/A	N/A	N/A
13	178.5	5.50	175.2	5.14	222.6	36.12	0.19222	0.00647	0.02755	0.00082	0.883	0.05060	0.00080	N/A	N/A	N/A	N/A	N/A	N/A	N/A	N/A	N/A
14	180.5	7.24	177.9	7.21	214.4	35.51	0.19454	0.00855	0.02798	0.00115	0.936	0.05042	0.00078	N/A	N/A	N/A	N/A	N/A	N/A	N/A	N/A	N/A
15	183.9	6.04	180.5	5.75	227.7	36.19	0.19856	0.00715	0.02840	0.00092	0.898	0.05071	0.00080	N/A	N/A	N/A	N/A	N/A	N/A	N/A	N/A	N/A
16	185.9	7.92	183.5	7.95	215.8	36.69	0.20090	0.00941	0.02888	0.00127	0.940	0.05045	0.00081	N/A	N/A	N/A	N/A	N/A	N/A	N/A	N/A	N/A
17	185.5	5.48	182.4	4.94	224.8	39.19	0.20043	0.00650	0.02870	0.00079	0.848	0.05065	0.00087	N/A	N/A	N/A	N/A	N/A	N/A	N/A	N/A	N/A
18	182.9	5.29	178.4	4.59	241.4	41.00	0.19732	0.00625	0.02805	0.00073	0.823	0.05101	0.00092	N/A	N/A	N/A	N/A	N/A	N/A	N/A	N/A	N/A
19	180.2	6.28	177.8	6.08	210.9	36.42	0.19415	0.00741	0.02797	0.00097	0.909	0.05034	0.00080	N/A	N/A	N/A	N/A	N/A	N/A	N/A	N/A	N/A
20	182.4	5.33	181.1	5.02	199.7	35.18	0.19678	0.00630	0.02849	0.00080	0.878	0.05010	0.00077	N/A	N/A	N/A	N/A	N/A	N/A	N/A	N/A	N/A
21	182.6	6.19	180.9	6.05	204.7	34.69	0.19704	0.00731	0.02846	0.00096	0.913	0.05021	0.00076	N/A	N/A	N/A	N/A	N/A	N/A	N/A	N/A	N/A
22	182.1	7.32	179.8	7.29	211.3	36.20	0.19638	0.00865	0.02829	0.00116	0.934	0.05035	0.00080	N/A	N/A	N/A	N/A	N/A	N/A	N/A	N/A	N/A
23	185.0	6.19	181.5	5.85	230.3	38.22	0.19990	0.00734	0.02856	0.00093	0.890	0.05077	0.00085	N/A	N/A	N/A	N/A	N/A	N/A	N/A	N/A	N/A
24	185.1	6.60	180.2	6.29	247.8	37.96	0.19995	0.00782	0.02835	0.00100	0.905	0.05115	0.00085	N/A	N/A	N/A	N/A	N/A	N/A	N/A	N/A	N/A
25	179.4	5.95	175.7	5.69	229.3	35.12	0.19330	0.00701	0.02763	0.00091	0.906	0.05075	0.00078	N/A	N/A	N/A	N/A	N/A	N/A	N/A	N/A	N/A
26	181.4	7.26	179.5	7.10	206.1	40.63	0.19561	0.00858	0.02824	0.00113	0.915	0.05024	0.00089	N/A	N/A	N/A	N/A	N/A	N/A	N/A	N/A	N/A
27	181.5	9.16	179.4	9.40	208.7	35.21	0.19567	0.01083	0.02822	0.00150	0.961	0.05030	0.00077	N/A	N/A	N/A	N/A	N/A	N/A	N/A	N/A	N/A

28	181.2	7.99	176.8	7.69	238.9	45.04	0.19539	0.00944	0.02781	0.00123	0.912	0.05096	0.00101	N/A	N/A	N/A	N/A	N/A	N/A	N/A	N/A	N/A
29	178.0	6.33	175.7	6.19	209.5	35.38	0.19166	0.00745	0.02763	0.00099	0.918	0.05031	0.00078	N/A	N/A	N/A	N/A	N/A	N/A	N/A	N/A	N/A
30	178.4	4.69	176.6	4.21	201.6	35.78	0.19203	0.00552	0.02778	0.00067	0.840	0.05014	0.00078	N/A	N/A	N/A	N/A	N/A	N/A	N/A	N/A	N/A

Notes: * Indicates asmples with errors reported to 2 sigma. Abbreviations are as follows: P1= fine-grained porphyry flow, P2= coarse-grained porphyry flow, V6= Mesozoic basaltic andesite dyke

Concordia Diagrams:

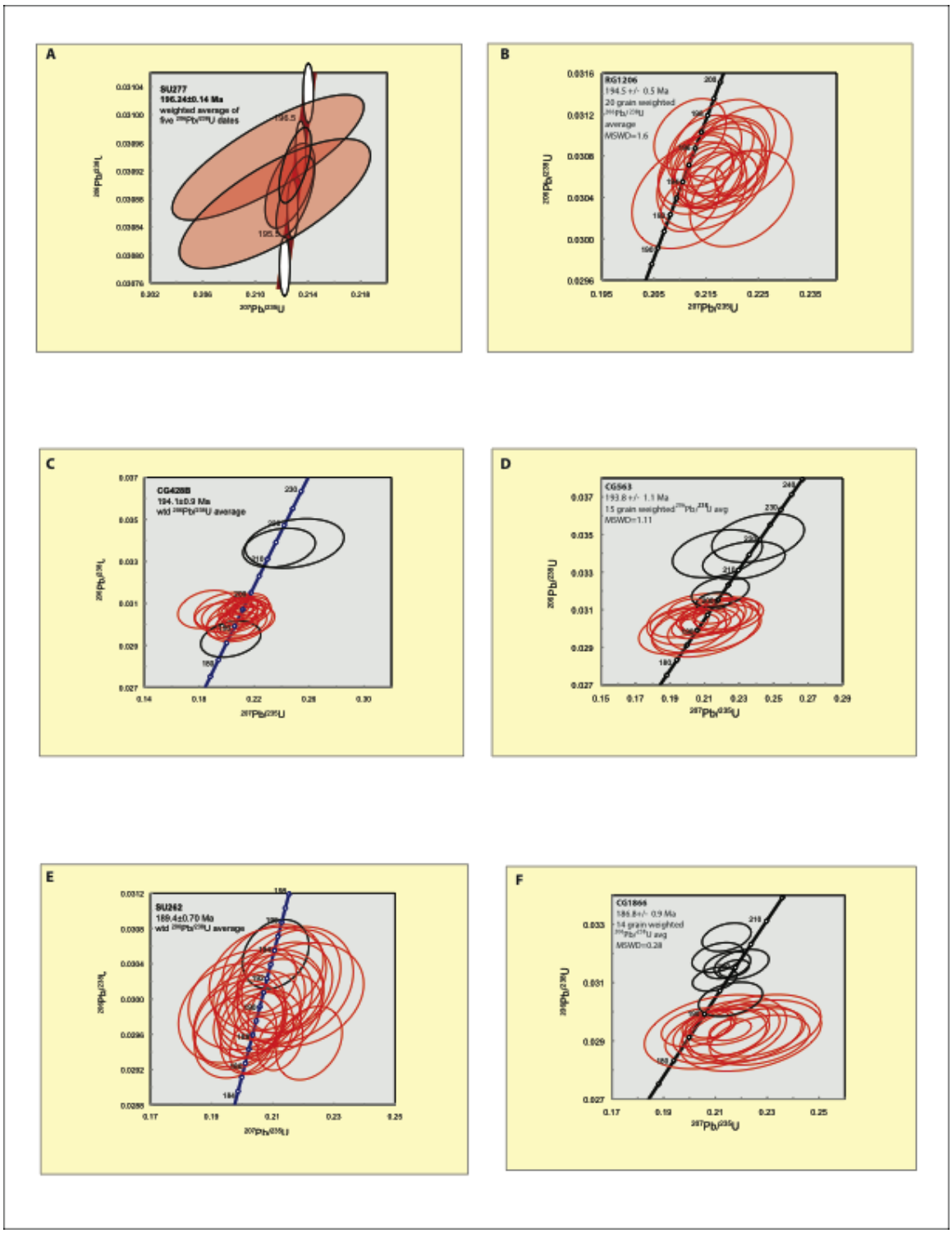

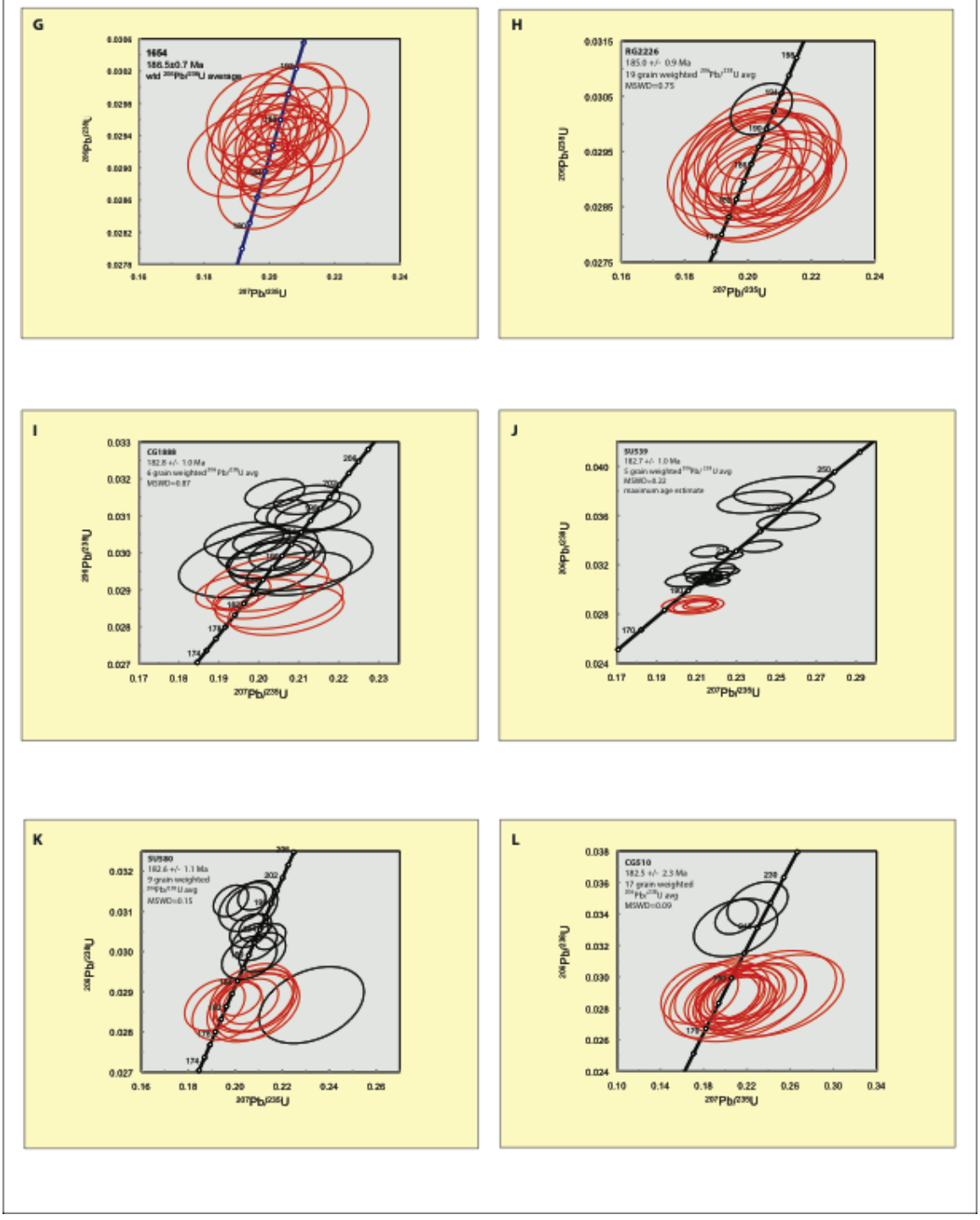
G
1654
186.5±0.7 Ma
wtd 206Pb/238U average
H
RG2226
185.0 +/- 0.9 Ma
19 grain weighted 206Pb/238U avg
MSWD=0.75
I
CG1888
182.8 +/- 1.0 Ma
6 grain weighted 206Pb/238U avg
MSWD=0.87
J
SU539
182.7 +/- 1.0 Ma
5 grain weighted 206Pb/238U avg
MSWD=0.22
maximum age estimate
K
SU580
182.6 +/- 1.1 Ma
9 grain weighted
206Pb/238U avg
MSWD=0.15
L
CGS10
182.5 +/- 2.3 Ma
17 grain weighted
206Pb/238U avg
MSWD=0.09
207Pb/235U
206Pb/238U

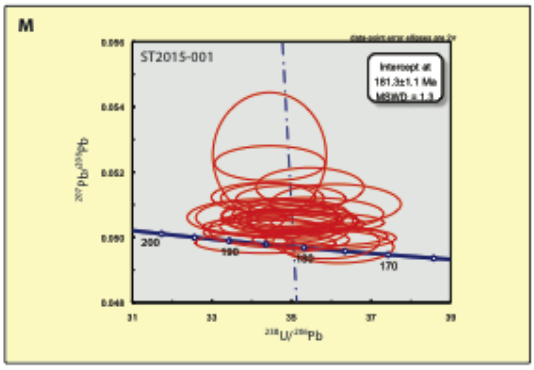
M
ST2015-001
Intercept at
161.3±1.1 Ma
MSWD = 1.3
200
190
180
170
31
33
35
37
39
$^{238}U/^{206}Pb$
$^{207}Pb/^{206}Pb$

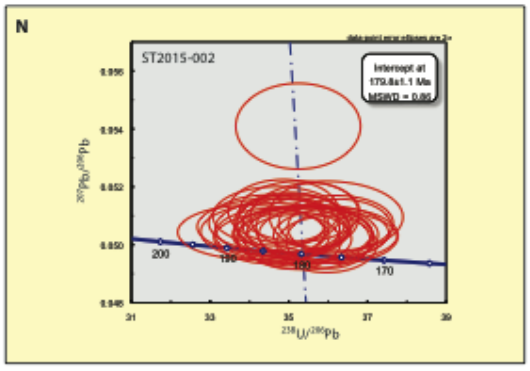
N
ST2015-002
Intercept at
179.8±1.1 Ma
200
190
180
170
31
33
35
37
39
$^{238}U/^{206}Pb$
$^{207}Pb/^{206}Pb$

APPENDIX B

Samples and Locations

#	Sample ID	Location	Easting	Northing	Depth (ASL-m)	Vein Stage	Orientation
1	A1	SU-447 (71.66-71.79m)	426452	6257949	1509	IV	-
2	A2	SU-450 (57.90-58.10m)	426601	6258857	1323	-	-
3	A3	SU-455 (13.26-13.41m)	426526	6258122	1535	III	-
4	A4	SU-455 (32.2m)	426527	6258113	1519	III	-
5	A5	SU-453 (52.05m)	426376	6258079	1481	-	-
6	A6	SU-455 (102.2m)	426527	6258076	1460	IIb	-
7	A7	SU-455 (381.55m)	426527	6257929	1222	III	-
8	A8	SU-463 (43.5)	426452	6257936	1511	-	-
9	A9	SU-463 (43.85m)	426453	6257936	1511	-	-
10	A10	SU-465 (91.1m)	426799	6257957	1467	-	-
11	A11	SU-465 (104.3m)	426799	6257965	1456	-	-
12	A12	SU-492 (23.1m)	426425	6258148	1502	-	-
13	A13	SU-491 (142.15m)	426638	6257881	1402	-	-
14	A14	SU-490 (132.75m)	426351	6258043	1406	-	-
15	A15	SU-487 (260.4m)	426288	6257622	1452	-	-
16	A16	SU-489 (44.3m)	426675	6258114	1513	III	-
17	A17	SU-492 (120m)	426425	6258054	1477	-	-
18	A18	SU-488 (35.8)	426464	6258360	1479	-	-
19	A19	SU-490 (300.25m)	426351	6257954	1263	-	-
20	A20	SU-491 (318.1m)	426638	6257884	1227	-	-
21	A21	SU-491 (338.3m)	426638	6257870	1206	-	-
22	A22	SU-497 (112m)	426677	6258183	1428	III	-
23	A23	SU-498 (283m)	426224	6258234	1462	-	-
24	A24	SU-504 (176.35m)	426501	6257995	1531	-	-
25	A25	SU-505 (283.2m)	426424	6257955	1422	-	-
26	A26	SU-515 (10m)	427003	6258086	1496	-	-
27	A27	SU-511 (305.6)	426176	6258293	1456	-	-
28	A28	SU-516 (59.1m)	426452	6258157	1457	-	-
29	A29	SU-525 (114.8m)	426478	6257943	1545	IV	-
30	A30	SU-528 (34.9m)	426441	6257946	1503	-	-
31	A31	SU-528 (70m)	426441	6257928	1473	IV	-
32	A32	SU-526 (400.75m)	427002	6257736	1324	IIc	-
33	HG-01	SU-526 (401.9m)	427002	6257736	1324	IIc	-
34	HG-02	SU-452 (51m)	426626	6257869	1493	III	-
35	HG-03	SU-176 (305.5m)	426505	6257948	1486	IIa	-
36	HG-04	SU-490 (78.75m)	426351	6258071	1451	IIa	-
37	HG-05	SU-459 (283m)	426627	6258141	1457	IIa	-
38	VP-BJ-001	615-15W	426615	6257969	1350	IV	203/88

39	VP-BJ-002	660-7W	426660	6258035	1350	IIb	302/62
40	VP-BJ-003	660-7	426660	6258035	1350	IIa	289/80
41	VP-BJ-004	660-4E	426660	6258028	1350	III	302/62
42	VP-BJ-005	660S (DB)	426658	6258016	1350	V	109/48
43	VP-BJ-006	615-10W	426615	6257982	1350	V	113/33
44	VP-BJ-007	615-13E	426615	6257974	1350	V	198/87
45	VP-BJ-008	615-13W	426615	6257974	1350	IV	225/71
46	VP-BJ-009	615-16W	426615	6257966	1350	IV	133/70
47	VP-BJ-010	615-17W	426615	6257963	1350	IV	227/85
48	VP-BJ-011	615-15	426615	6257969	1350	IV	195/81
49	VP-BJ-012	615-15E	426615	6257968	1350	IIa	252/68
50	VP-BJ-013	615-26W	426615	6257939	1350	III	302/62
51	VP-BJ-014	615- (SW of DB)	426615	6257932	1350	III	304/85
52	VP-BJ-015	615-18W	426615	6257960	1350	I	190/61
53	VP-BJ-016	645-20W	426645	6258975	1350	V	265/29
54	VP-BJ-017	7948-1N [645]	426645	6257952	1350	IIa	125/82
55	VP-BJ-018	645-19W	426645	6257962	1350	III	121/70
56	VP-BJ-019	645-15E	426645	6257972	1350	V	103/41
57	VP-BJ-020	645-14W	426645	6257975	1350	V	080/09
58	VP-BJ-021	660-1N	426660	6258011	1350	I	139/80
59	VP-BJ-022	660-2W	426660	6258008	1350	I	150/85
60	VP-BJ-023	555-3W	426555	6258003	1350	V	002/21
61	VP-BJ-024	555-8E	426555	6257990	1350	IIb	106/68
62	VP-BJ-025	555-9W	426555	6257987	1350	III	299/56
63	VP-BJ-026	555-12E	426555	6257979	1350	IIb	332/68
64	VP-BJ-027	555-13W	426555	6257976	1350	IIb	149/70
65	VP-BJ-028	555-15E	426555	6257971	1350	IIb	139/71
66	VP-BJ-029	7960-4E [555]	426555	6257961	1350	IIb	296/69
67	VP-BJ-030	585-6W	426585	6257993	1350	V	089/37
68	VP-BJ-031	585-9W	426585	6257985	1350	IIa	297/86
69	VP-BJ-032	585-20E	426585	6257956	1350	III	300/61
70	VP-BJ-033	585-11W	426585	6257980	1350	IV	142/67
71	VP-BJ-034	600-5E	426600	6258005	1350	V	358/68
72	VP-BJ-035	600-16E	426600	6257966	1350	IIc	162/69
73	VP-BJ-036	600-18E	426600	6257961	1350	IIc	141/71
74	VP-BJ-037	600-19E	426600	6257958	1350	III	129/82
75	VP-BJ-038	600-W (DB)	426600	6257929	1350	IIb	301/81
76	VP-BJ-039	600-12W	426600	6257977	1350	IIa	254/76
77	VP-BJ-040	600-8E	426600	6257989	1350	V	095/24
78	VP-BJ-041	VAR-154	426600	6258085	1350	IIc	135/79
79	VP-BJ-042	645N-4E	426645	6258028	1350	IIc	125/68
80	VP-BJ-043	645N-6E	426645	6258032	1350	IIb	224/88
81	VP-BJ-044	VU-239- 62.18m	426564	6257962	1301	IV	-
82	VP-BJ-045	VU-239-53.56m	426565	6257968	1301	IV	-
83	VP-BJ-046	VU-184-62.7-62.9	426622	6257985	1386	IV	-
84	VP-BJ-047	615-16 [VGHS049]	426617	6257966	1350	IV	-
85	VP-BJ-	VU-125-54.25m	426659	6257973	1308	IIa	-

	048						
86	VP-BJ-049	VU-113-28.74	426659	6257988	1364	I	-
87	VP-BJ-050	VU-125-26.24-26.74	426659	6257993	1328	IIb	-
88	VP-BJ-051	615-13E [VGHS023]	426617	6257974	1350	V	-
89	VP-BJ-052	VU-215-53.80-54.05m	426547	6258010	1376	IIa	-
90	VP-BJ-053	VU-138-69.35m	426591	6258015	1305	IIb	-
91	VP-BJ-054	555-16W [VGHS047]	426617	6257966	1350	III	-
92	VP-BJ-055	VU-059-50.62m	426554	6258004	1350	IIa	-
93	VP-BJ-056	VU-044-36.17m	426667	6257979	1323	IV	-
94	VP-BJ-057	VU-068-26.3-26.5m	426644	6258003	1350	IIb	-
95	VP-BJ-058	615-13W [VGHS030]	426617	6257974	1350	IV	-
96	VP-BJ-059	VU-141-1.44m	426569	6258003	1350	I	-
97	VP-BJ-060	8015-8E [VGHS002]	426573	6258014	1350	V	-
98	BJ-D001	615-21E	426615	62587953	1350	-	251/79
99	BJ-D002	645-20W	426645	6257959	1350	-	246/87
100	BJ-D003	600-19E	426600	6257958	1350	-	129/82
101	BJ-D004	VAR-	426600	6258190	1350	-	114/69
102	P-BJ-001	585-15W	426585	6257970	1350	-	245/80
103	P-BJ-002	660-4W	426658	6258030	1350	-	124/64
104	P-BJ-003	VOK Access	426600	6258515	1327	-	-
105	P-BJ-004	VU-138-116.70m	426627	6258015	1277	-	-
106	P-BJ-005	VU-138-114.5m	426627	6258015	1277	-	-
107	P-BJ-006	600- Access	426602	6257974	1345	-	-
108	2BJ-001	VOK Access	426600	6258385	1350	IIc	-
109	2BJ-002	VOK Access	426600	6258365	1350	IIb	-
110	2BJ-005	600-11E	426600	6257970	1350	-	-
111	2BJ-006	6000-15face	426600	6257945	1350	IIc	-
112	2BJ-007	600-9W	426600	6257985	1350	IIc	-
113	2BJ-008	8015-08E	426630	6258015	1350	IV	-
114	HG-BJ-B1	8015E-3 (face)	426615	6258015	1350	IIa	-
115	HG-BJ-B2	600-11S (face)	426600	6257975	1350	IIa	-
116	HG-BJ-B3	600-9W	426600	6257980	1350	IIa	-
117	HG-BJ-B4	600-9W	426600	6257985	1350	IIa	-
118	HG-BJ-B5	600-15 (face)	426600	6257970	1350	IIa	-

APPENDIX C

Whole-rock lithogeochemistry

Actlabs:

Sample:			A2	A15	A18	A19	A26	A27	BJ-D001	BJ-D002	BJ-D003	BJ-D004
Lithology:			Coarse Latite Phyric Flow	Coarse Latite Phyric Flow	Latite Phyric Flow	Alkali-Basalt Dyke	Coarse Latite Phyric Flow	Latite Phyric Flow	Basaltic-Andesite Dyke	Basaltic-Andesite Dyke	Basaltic-Andesite Dyke	Basaltic-Andesite Dyke
Easting:			426601.34	426287.68	426464.39	426452.63	427002.51	426176.10	426615.00	426645.00	426600.00	426600.00
Northing:			6258856.71	6257622.39	6258360.47	6257936.47	6258086.23	6258293.01	62587952.62	6257959.34	6257958.19	6258190.00
Elevation (m):			1322.76	1451.86	1478.60	1263.25	1495.83	1456.49	1347.00	1347.00	1347.00	1347.00
Element	**Det. Lim.**	**Analytical Meth.**										
Weight Percent												
SiO2	0.01	FUS-ICP	55.59	59.04	55.25	52	59.64	56.27	65.51	43.32	41.93	42.01
Al2O3	0.01	FUS-ICP	16.52	16.29	16.72	15.84	16.33	15.84	16.36	16.89	24.57	27.33
Fe2O3	0.01	FUS-ICP	3.86	1.73	1.54	9.84	0.5	1.5	2.93	8.50	11.06	8.07
MgO	0.01	FUS-ICP	2.07	2.12	2.34	3.42	1.57	1.86	1.05	3.09	2.94	2.43
MnO	0.001	FUS-ICP	0.258	0.118	0.265	0.127	0.121	0.203	0.05	0.39	0.26	0.10
CaO	0.01	FUS-ICP	5.61	3.44	5.37	6.25	4.21	5.73	2.56	10.71	1.97	1.35
Na2O	0.01	FUS-ICP	0.36	3.97	2.4	4.27	2.79	1.48	0.14	0.76	0.17	0.10
K2O	0.01	FUS-ICP	3.59	4.11	3.59	1.83	2.51	4.52	5.16	3.69	5.81	7.95
TiO2	0.001	FUS-ICP	0.601	0.534	0.521	2.103	0.562	0.507	1.86	1.56	2.39	2.85
P2O5	0.01	FUS-ICP	0.28	0.19	0.22	0.77	0.27	0.19	0.67	0.56	0.89	0.95
LOI	0.01	FUS-ICP	8.58	5.6	6.6	2.65	5.34	7.09	4.49	11.34	6.13	6.11
TOTAL			97.32	97.14	94.82	99.10	93.84	95.19	100.78	100.81	98.12	99.25

Parts per million (except where indicated)*												
Au*	1	INAA MULT INAA /	<det lim	<det lim	<det lim	19	<det lim	<det lim	81	96	337	388
Ag	0.5	TD-ICP	<det lim	<det lim	<det lim	<det lim	<det lim	1.3	3.20	<det lim	3.60	9.60
As	1	INAA	23	23	73	18	8	460	196.00	38.00	256.00	1300.00
Ba	1	FUS-ICP	<det lim	<det lim	<det lim	954	<det lim	<det lim	3164.00	2153.00	2867.00	3427.00
Bi	0.1	FUS-MS	<det lim	<det lim	<det lim	<det lim	<det lim	<det lim	<det lim	<det lim	<det lim	<det lim
Cd	0.5	TD-ICP	0.8	<det lim	<det lim	<det lim	<det lim	2.3	1.00	<det lim	1.00	0.60
Co	0.1	INAA	9.7	5.7	11.8	28.2	8	10.6	36.10	24.20	25.50	67.60
Cr	0.5	INAA	9.6	0	10.8	41.5	8.4	12.4	12.00	0.00	15.20	98.60
Cs	0.1	FUS-MS	9.3	5.4	8.9	0.5	5.3	5.3	7.30	5.00	15.70	24.10
Cu	1	TD-ICP	17	24	11	20	28	22	45.00	29.00	44.00	57.00
Ga	1	FUS-MS	17	16	16	22	16	16	13.00	17.00	28.00	28.00
Hf	0.1	FUS-MS	2.4	2.5	2.4	4.7	2.4	2.5	2.30	2.10	3.10	3.90
Hg	1	INAA	<det lim	<det lim	<det lim	<det lim	<det lim	<det lim	<det lim	<det lim	<det lim	<det lim
Li	0.1	INAA	<det lim	<det lim	<det lim	<det lim		<det lim	<det lim	<det lim	<det lim	<det lim
Mo	2	FUS-MS	<det lim	<det lim	<det lim	<det lim	<det lim	<det lim	<det lim	<det lim	<det lim	<det lim
Nb	0.2	FUS-MS	7.5	4.9	4.9	24.8	6.8	6	10.30	1.00	12.40	13.50
Ni	1	TD-ICP	2	5	7	22	3	5	12.00	10.00	12.00	87.00
Pb	5	TD-ICP	<det lim	<det lim	<det lim	<det lim	<det lim	<det lim	<det lim	<det lim	<det lim	<det lim
Rb	1	FUS-MS	132	109	129	31	83	160	204.00	131.00	248.00	313.00
Sb	0.1	INAA	3.7	3.5	4.1	2	3.2	16.2	9.20	1.80	7.70	47.40
Sc	0.01	INAA	<det lim	<det lim	<det lim	<det lim	<det lim	<det lim	<det lim	<det lim	<det lim	<det lim
Se	0.5	INAA	<det lim	<det lim	<det lim	<det lim	<det lim	<det lim	<det lim	<det lim	<det lim	<det lim
Sn	1	FUS-MS	<det lim	<det lim	<det lim	2	<det lim	<det lim	<det lim	<det lim	2.00	2.00
Sr	2	FUS-ICP	266	376	258	945	218	190	145.00	441.00	187.00	130.00
Ta	0.01	FUS-MS	0.43	0.2	0.29	1.45	0.43	0.39	0.51	0.36	0.62	0.77

Te	0.01	FUS-MS	<det lim	<det lim	<det lim	<det lim	<det lim	<det lim	<det lim	<det lim	<det lim	<det lim
Th	0.05	FUS-MS	4.6	3.96	3.24	5.28	5.02	4.31	1.61	1.26	1.93	1.58
U	0.01	FUS-MS	2.56	2.66	2.26	1.69	3.88	2.73	1.86	0.53	1.38	1.28
V	5	FUS-ICP	115	107	134	122	128	101	301.00	320.00	559.00	512.00
W	1	INAA	<det lim	<det lim	<det lim	<det lim	<det lim	<det lim	18.00	5.00	70.00	51.00
Y	1	FUS-ICP	18	17	15	15	18	17	28.00	24.00	36.00	41.00
Zn	1	MULT INAA / TD-ICP	70	29	112	137	75	521	72.00	98.00	221.00	90.00
Zr	1	FUS-ICP	91	96	87	255	83	106	108.00	98.00	135.00	171.00
La	0.05	FUS-MS	19.1	14.6	14.5	46.4	17.9	15.6	21.40	23.00	26.50	19.80
Ce	0.05	FUS-MS	35.4	28.3	27.6	90.5	32.7	28.5	44.40	47.40	55.50	44.60
Pr	0.01	FUS-MS	4.14	3.4	3.21	11	3.75	3.29	5.90	6.11	7.35	6.34
Nd	0.05	FUS-MS	16.5	13.6	13	41.8	14.6	13	25.40	25.70	32.20	29.60
Sm	0.01	FUS-MS	3.56	3.16	2.89	8.04	3.47	2.95	6.10	5.79	7.10	8.02
Eu	0.005	FUS-MS	1.2	1.02	0.902	2.27	1.02	0.799	1.61	1.50	1.98	1.63
Gd	0.01	FUS-MS	3.43	3.08	2.68	5.55	3.28	2.8	5.82	5.36	6.89	8.44
Tb	0.01	FUS-MS	0.53	0.5	0.43	0.79	0.5	0.47	0.93	0.85	1.13	1.40
Dy	0.01	FUS-MS	3.1	2.99	2.61	3.68	2.99	2.84	5.55	4.81	6.85	8.35
Ho	0.01	FUS-MS	0.63	0.62	0.52	0.58	0.6	0.58	1.06	0.92	1.29	1.62
Er	0.01	FUS-MS	1.89	1.86	1.57	1.38	1.78	1.8	3.11	2.67	3.76	4.54
Tl	0.05	FUS-MS	1.83	1.08	1.89	0.82	0.79	2.38	4.31	1.75	4.68	9.70
Tm	0.005	FUS-MS	0.286	0.281	0.248	0.17	0.276	0.277	0.50	0.42	0.57	0.69
Yb	0.01	FUS-MS	1.9	1.87	1.83	0.99	2	1.9	3.41	2.70	3.57	4.35
Lu	0.002	FUS-MS	0.299	0.307	0.294	0.146	0.322	0.3	0.51	0.40	0.52	0.65

Notes Listed elements below analytical detection denoted as <det lim. Abbreviations for analytical methods: FUS-ICP: fusion inductively couple plasma analysis; FUS-MS: fusion mass spectrometry; INAA: instrumental neutron activation analysis; TD-ICP: inductively coupled plasma total dissolution; MULT: multiple analysis; TD-ICP: inductively coupled plasma total dissolution; MULT: multiple.

ALS:

Sample:			RG-298	RG-316A	RG-533	RG-539	RG-565	CG12-84	CG11-310	SU 193	RG-036B	RG-429	RG-466	RG-491
Lithology:			Alkali-Basalt Dyke	Basaltic-Andesite Dyke	Basaltic-Andesite Dyke	Basaltic-Andesite Dyke	Basaltic-Andesite Dyke	Basaltic-Andesite Dyke	Alkali-Basalt Dyke	Alkali-Basalt Dyke	Latite Phyric Flow	Latite Phyric Flow	Latite Phyric Flow	Latite Phyric Flow
Easting:			426388.00	426411.00	425842.00	425899.00	424912.00	426041.00	425460.00	426256.91	425785.00	425688.00	424991.00	426056.00
Northing:			6257222.00	6256423.00	6259607.00	6259501.00	6259877.00	6259165.00	6261442.00	6257711.00	6258782.00	6259121.00	6259579.00	6259163.00
Elevation (m):			1548.00	1592.00	1402.00	1415.00	1309.00	1373.00	1578.00	1512.19	1376.00	1350.00	1233.00	1379.00
Element	**Det. Lim.**	**Analytical Meth.**												
Weight Percent														
SiO2	0.01	ME-ICP06	51.30	47.80	45.90	46.80	63.30	39.20	51.60	50.10	59.50	61.00	56.80	52.20
Al2O3	0.01	ME-ICP06	15.65	13.25	14.40	13.65	12.85	16.05	15.80	16.10	16.05	17.80	16.95	15.65
Fe2O3	0.01	ME-ICP06	9.37	11.35	9.71	9.94	9.82	10.90	9.91	9.72	4.56	4.79	4.95	8.11
MgO	0.01	ME-ICP06	3.33	6.15	6.88	8.09	2.06	8.01	3.28	2.98	1.39	1.94	1.60	3.51
MnO	0.01	ME-ICP06	0.14	0.16	0.16	0.19	0.14	0.26	0.13	0.13	0.14	0.12	0.15	0.19
CaO	0.01	ME-ICP06	4.20	9.41	7.95	9.36	2.23	9.37	4.86	5.56	5.37	3.17	4.92	5.40
Na2O	0.01	ME-ICP06	4.69	3.10	4.68	3.70	0.51	0.22	5.05	5.53	0.28	0.66	2.97	2.56
K2O	0.01	ME-ICP06	2.46	2.34	0.24	0.41	2.65	2.31	2.35	1.69	3.99	4.49	4.15	3.36
TiO2	0.01	ME-ICP06	2.04	1.92	1.02	1.03	1.18	1.43	2.09	2.02	0.44	0.48	0.71	0.82
P2O5	0.01	ME-ICP06	0.77	0.77	0.39	0.37	0.47	0.22	0.75	0.78	0.21	0.23	0.33	0.41
LOI	0.01	OA-GRA05	4.81	4.13	7.68	4.97	4.77	12.45	2.79	3.10	6.90	5.96	7.76	7.27
TOTAL			98.76	100.38	99.01	98.51	99.98	100.42	98.61	97.71	98.83	100.64	101.29	99.48
Parts per million (except where indicated)*														
Au*	1	ME-4ACD81	<det lim	<det lim	<det lim	<det lim	<det lim	<det lim	<det lim	<det lim	<det lim	<det lim	<det lim	<det lim
Ag	0.5	ME-4ACD81	<det lim	<det lim	<det lim	<det lim	0.50	<det lim	0.25	0.25	<det lim	<det lim	<det lim	<det lim
As	0.'1	ME-MS42	17.10	3.60	6.50	5.90	42.10	97.40	5.00	10.30	38.90	10.50	24.90	15.80
Ba	0.5	ME-MS81	2360.00	2830.00	605.00	769.00	1215.00	919.00	1880.00	2360.00	2750.00	2940.00	1990.00	2700.00
Bi	0.1	ME-MS42	0.03	0.07	0.05	0.05	0.05	0.01	0.01	0.02	0.01	0.01	0.05	0.04

Cd	0.5	ME-4ACD81	<det lim	<det lim	<det lim	<det lim	<det lim	<det lim	0.25	0.25	<det lim	<det lim	<det lim	<det lim
Co	1	ME-4ACD81	23.00	32.00	35.00	39.00	11.00	34.00	24.00	21.00	7.00	6.00	12.00	18.00
Cr	10	ME-MS81	40.00	210.00	340.00	390.00	10.00	190.00	30.00	30.00	10.00	10.00	10.00	40.00
Cs	0.01	ME-MS81	1.29	0.91	3.49	1.10	3.99	4.01	0.97	0.79	7.81	11.75	4.43	6.26
Cu	1	ME-4ACD81	4.00	29.00	99.00	71.00	53.00	71.00	12.00	16.00	19.00	17.00	12.00	87.00
Ga	0.'1	ME-MS81	23.50	20.90	17.90	17.90	19.70	17.30	25.10	23.00	19.70	20.80	20.60	19.30
Hf	0.2	ME-MS81	6.10	6.40	2.80	2.70	6.90	1.70	6.00	6.80	2.80	3.30	3.50	2.70
Hg	0.0051	ME-MS42	0.01	0.01	0.03	0.01	0.01	0.01	0.02	0.00	0.07	0.07	0.01	0.01
Li	10	ME-4ACD81	60.00	20.00	30.00	20.00	30.00	90.00	<det lim	<det lim	30.00	20.00	10.00	30.00
Mo	1	ME-4ACD81	<det lim	<det lim	<det lim	<det lim	2.00	<det lim	3.00	1.00	<det lim	<det lim	<det lim	<det lim
Nb	0.2	ME-MS81	25.50	13.80	6.70	6.20	12.90	2.30	26.30	24.70	7.90	8.60	7.80	8.20
Ni	1	ME-4ACD81	15.00	64.00	82.00	96.00	0.50	92.00	21.00	13.00	0.50	0.50	1.00	8.00
Pb	2	ME-4ACD81	3.00	15.00	4.00	5.00	5.00	<det lim	3.00	7.00	6.00	4.00	0.00	0.00
Rb	0.2	ME-MS81	55.50	44.50	6.60	5.00	98.00	106.50	52.30	26.90	144.50	150.50	151.00	119.00
Sb	0.05	ME-MS42	2.62	2.09	1.93	0.62	1.32	1.77	4.58	1.30	1.19	0.96	1.12	1.09
Sc	1	ME-4ACD81	9.00	22.00	24.00	26.00	18.00	32.00	<det lim	<det lim	9.00	10.00	10.00	22.00
Se	0.2	ME-MS42	0.40	1.10	0.60	0.50	0.60	0.30	0.50	0.40	<det lim	<det lim	0.40	0.30
Sn	1	ME-MS81	2.00	2.00	1.00	1.00	2.00	1.00	2.00	2.00	1.00	1.00	1.00	1.00
Sr	0.1	ME-MS81	636.00	1070.00	569.00	864.00	44.00	244.00	817.00	1050.00	175.00	271.00	383.00	357.00
Ta	0.1	ME-MS81	1.50	0.80	0.40	0.40	0.80	0.10	1.60	1.50	0.50	0.50	0.50	0.50
Te	0.01	ME-MS42	0.01	0.02	0.01	0.01	0.01	0.02	0.05	0.01	<det lim	<det lim	<det lim	<det lim
Th	0.05	ME-MS81	6.13	8.33	2.68	2.39	4.48	0.28	5.92	6.23	6.09	6.30	4.25	4.91
U	0.05	ME-MS81	2.00	2.42	1.79	1.58	2.35	0.14	1.51	1.86	3.70	4.27	2.42	2.79
V	5	ME-MS81	126.00	221.00	243.00	253.00	55.00	293.00	125.00	112.00	122.00	129.00	168.00	267.00
W	1	ME-MS81	1.00	2.00	1.00	1.00	7.00	12.00	2.00	2.00	1.00	3.00	1.00	9.00
Y	0.5	ME-MS81	18.70	31.10	23.80	23.20	48.70	24.90	19.20	17.70	17.30	19.10	23.20	24.00
Zn	2	ME-4ACD81	179.00	158.00	92.00	89.00	80.00	94.00	138.00	130.00	55.00	64.00	17.00	92.00

Zr	2	ME-MS81	274.00	235.00	102.00	101.00	304.00	59.00	293.00	275.00	106.00	116.00	133.00	107.00
La	0.5	ME-MS81	48.60	71.70	15.30	14.20	17.80	5.30	49.00	48.50	18.00	19.20	19.80	23.10
Ce	0.5	ME-MS81	95.40	140.50	31.80	29.60	39.80	12.60	96.60	97.70	31.10	33.10	37.60	42.00
Pr	0.03	ME-MS81	11.85	17.85	4.31	4.10	5.56	2.26	12.25	11.90	3.65	3.85	4.78	5.36
Nd	0.1	ME-MS81	44.40	67.10	18.00	17.10	24.10	11.80	47.60	46.50	13.50	14.70	18.80	20.90
Sm	0.03	ME-MS81	8.81	12.60	4.54	4.40	6.83	3.55	8.73	8.64	2.97	3.17	4.40	4.56
Eu	0.03	ME-MS81	2.44	3.38	1.53	1.40	1.75	1.46	2.54	2.41	0.80	0.68	1.36	1.55
Gd	0.05	ME-MS81	6.75	9.22	4.70	4.46	7.58	4.73	7.09	6.46	2.75	3.10	3.98	4.15
Tb	0.01	ME-MS81	0.84	1.20	0.69	0.67	1.21	0.77	0.85	0.81	0.43	0.48	0.62	0.63
Dy	0.05	ME-MS81	4.14	6.27	4.22	4.07	7.84	4.53	4.16	4.08	2.67	3.13	3.91	3.94
Ho	0.01	ME-MS81	0.69	1.13	0.86	0.80	1.69	0.89	0.69	0.63	0.56	0.67	0.82	0.81
Er	0.03	ME-MS81	1.57	2.90	2.41	2.28	5.09	2.64	1.54	1.62	1.75	2.08	2.48	2.39
Tl	0.5	ME-MS81	0.90	<det lim	<det lim	<det lim	1.40	8.20	0.50	0.25	1.10	1.50	2.90	2.90
Tm	0.01	ME-MS81	0.20	0.43	0.37	0.36	0.79	0.37	0.20	0.19	0.29	0.34	0.42	0.37
Yb	0.03	ME-MS81	1.11	2.49	2.29	2.09	4.92	2.27	1.10	1.10	1.81	2.17	2.64	2.41
Lu	0.01	ME-MS81	0.16	0.38	0.36	0.32	0.78	0.33	0.15	0.15	0.30	0.36	0.45	0.38

Sample:			RG-491B	RG-575	RG-698	RG-1063	RG-1098	RG-1107	RG-1118	RG-1151	RG-1172	RG-1206	RG-1232
Lithology:			Latite Phyric Flow	Latite Phyric Flow	Latite Phyric Flow	Latite Phyric Flow	Latite Phyric Flow	Latite Phyric Flow	Latite Phyric Flow	Latite Phyric Flow	Latite Phyric Flow	Latite Phyric Flow	Latite Phyric Flow
Easting:			426054.00	425155.00	426285.00	425490.00	425928.00	425723.00	425537.00	425964.00	425807.00	425216.00	426195.00
Northing:			6259159.00	6260000.00	6258571.00	6260814.00	6260784.00	6260887.00	6260738.00	6260552.00	6260583.00	6259996.00	6260757.00
Elevation (m):			1377.00	1392.00	1427.00	1505.00	1547.00	1557.00	1509.00	1509.00	1531.00	1445.00	1605.00
Element	**Det. Lim.**	**Analytical Meth.**											
Weight Percent													
SiO2	0.01	ME-ICP06	62.20	59.90	57.10	58.60	56.90	58.10	58.70	57.80	57.10	59.70	60.20
Al2O3	0.01	ME-ICP06	15.85	16.35	16.20	17.75	15.80	14.75	16.85	17.35	15.80	16.95	15.25
Fe2O3	0.01	ME-ICP06	4.57	5.97	5.58	7.84	6.07	5.69	5.96	6.90	6.60	5.56	5.81
MgO	0.01	ME-ICP06	1.52	1.87	2.19	2.58	1.68	1.10	1.39	1.84	1.98	2.05	1.24
MnO	0.01	ME-ICP06	0.10	0.22	0.17	0.19	0.12	0.21	0.18	0.16	0.21	0.19	0.23
CaO	0.01	ME-ICP06	3.01	3.35	4.88	0.92	6.61	6.88	5.01	4.38	4.83	3.29	5.32
Na2O	0.01	ME-ICP06	3.89	5.68	3.07	4.51	2.25	1.25	2.12	2.88	1.19	5.30	3.32
K2O	0.01	ME-ICP06	2.92	2.43	3.27	3.33	2.01	2.85	3.21	2.30	2.71	2.86	2.14
TiO2	0.01	ME-ICP06	0.45	0.60	0.52	0.89	0.68	0.54	0.73	0.68	0.60	0.57	0.52
P2O5	0.01	ME-ICP06	0.21	0.26	0.22	0.36	0.35	0.24	0.33	0.24	0.24	0.22	0.23
LOI	0.01	OA-GRA05	4.43	2.03	5.79	3.16	8.03	7.98	6.18	6.21	7.06	2.55	5.84
TOTAL			99.15	98.66	98.99	100.13	100.50	99.59	100.66	100.74	98.32	99.24	100.10
Parts per million (except where indicated)*													
Au*	1	ME-4ACD81	<det lim	<det lim	<det lim	<det lim	<det lim	<det lim	<det lim	<det lim	<det lim	<det lim	<det lim
Ag	0.5	ME-4ACD81	0.60	<det lim	<det lim	<det lim	<det lim	<det lim	<det lim	<det lim	<det lim	<det lim	<det lim
As	0.'1	ME-MS42	5.50	7.10	79.20	16.80	27.60	38.80	25.80	0.60	31.00	2.40	2.30
Ba	0.5	ME-MS81	1560.00	2430.00	1960.00	2980.00	1705.00	821.00	1225.00	1910.00	1375.00	2290.00	2050.00
Bi	0.1	ME-MS42	0.07	0.03	0.02	0.11	<det lim	0.01	0.20	<det lim	<det lim	0.01	<det lim
Cd	0.5	ME-4ACD81	<det lim	<det lim	<det lim	<det lim	<det lim	<det lim	<det lim	<det lim	<det lim	0.90	<det lim
Co	1	ME-4ACD81	6.00	9.00	10.00	12.00	8.00	13.00	11.00	12.00	13.00	9.00	12.00

Cr	10	ME-MS81	10.00	10.00	10.00	20.00	<det lim	10.00	10.00	10.00	10.00	10.00	<det lim
Cs	0.01	ME-MS81	5.92	1.39	6.29	5.17	9.98	9.66	11.85	7.86	11.70	2.33	8.67
Cu	1	ME-4ACD81	783.00	22.00	19.00	47.00	0.50	28.00	40.00	16.00	23.00	14.00	0.50
Ga	0.'1	ME-MS81	18.40	19.40	17.50	22.30	18.80	16.90	20.10	19.20	18.00	19.10	17.00
Hf	0.2	ME-MS81	2.80	3.40	2.80	3.90	2.90	2.60	3.50	3.00	2.50	3.20	2.40
Hg	0.0051	ME-MS42	0.01	0.02	0.01	0.03	0.01	0.03	0.05	0.01	0.03	0.01	0.01
Li	10	ME-4ACD81	20.00	20.00	20.00	30.00	40.00	30.00	30.00	40.00	40.00	20.00	30.00
Mo	1	ME-4ACD81	<det lim	<det lim	<det lim	<det lim	<det lim	<det lim	<det lim	<det lim	<det lim	<det lim	<det lim
Nb	0.2	ME-MS81	7.90	6.00	5.40	8.50	7.80	8.70	7.50	6.00	8.70	5.90	6.50
Ni	1	ME-4ACD81	0.50	1.00	0.50	3.00	0.50	0.50	1.00	0.50	0.50	0.50	0.50
Pb	2	ME-4ACD81	3.00	13.00	6.00	7.00	0.00	0.00	3.00	<det lim	<det lim	15.00	<det lim
Rb	0.2	ME-MS81	97.20	56.10	138.00	92.90	67.50	112.00	107.50	86.20	98.40	65.90	81.30
Sb	0.05	ME-MS42	0.97	0.87	0.97	3.45	0.93	3.91	2.52	0.52	1.41	0.83	1.11
Sc	1	ME-4ACD81	10.00	10.00	11.00	16.00	11.00	13.00	12.00	14.00	16.00	9.00	10.00
Se	0.2	ME-MS42	1.00	0.30	0.30	0.60	0.20	0.20	0.40	0.20	0.20	0.30	0.20
Sn	1	ME-MS81	1.00	1.00	1.00	1.00	1.00	1.00	1.00	1.00	1.00	1.00	1.00
Sr	0.1	ME-MS81	284.00	586.00	295.00	515.00	214.00	340.00	247.00	197.00	144.50	752.00	241.00
Ta	0.1	ME-MS81	0.50	0.40	0.40	0.60	0.50	0.70	0.50	0.50	0.60	0.40	0.40
Te	0.01	ME-MS42	0.01	0.01	0.00	0.22	0.00	0.01	0.03	<det lim	<det lim	<det lim	<det lim
Th	0.05	ME-MS81	6.21	3.07	3.42	4.57	5.26	7.82	4.14	3.78	6.28	3.09	4.54
U	0.05	ME-MS81	3.36	2.11	2.48	2.75	2.64	3.57	2.43	2.60	2.49	2.05	2.56
V	5	ME-MS81	135.00	125.00	143.00	236.00	167.00	156.00	182.00	191.00	144.00	102.00	109.00
W	1	ME-MS81	2.00	1.00	1.00	1.00	1.00	2.00	1.00	2.00	2.00	<det lim	1.00
Y	0.5	ME-MS81	12.00	24.90	17.80	27.60	23.20	17.80	27.40	19.50	19.30	23.40	17.70
Zn	2	ME-4ACD81	40.00	93.00	68.00	115.00	27.00	59.00	70.00	74.00	88.00	203.00	62.00
Zr	2	ME-MS81	92.00	128.00	97.00	139.00	101.00	89.00	129.00	101.00	102.00	135.00	93.00
La	0.5	ME-MS81	16.60	15.70	12.90	19.60	19.90	19.80	20.10	13.60	16.40	13.90	15.50

Ce	0.5	ME-MS81	28.20	30.10	24.10	37.60	37.10	34.60	38.30	26.40	27.60	24.90	26.10
Pr	0.03	ME-MS81	3.29	3.94	3.07	4.92	4.58	4.06	4.88	3.34	3.60	3.37	3.35
Nd	0.1	ME-MS81	12.10	15.80	12.00	19.50	17.70	14.80	19.60	13.60	14.10	14.30	13.40
Sm	0.03	ME-MS81	2.52	3.95	2.85	4.81	4.01	3.23	4.72	3.16	3.05	3.31	2.92
Eu	0.03	ME-MS81	0.83	1.25	0.94	1.36	1.33	1.02	1.39	1.19	1.02	1.19	0.99
Gd	0.05	ME-MS81	2.30	4.03	2.97	5.03	4.01	3.18	4.68	3.41	3.49	3.90	3.29
Tb	0.01	ME-MS81	0.35	0.64	0.47	0.78	0.62	0.48	0.74	0.55	0.55	0.64	0.52
Dy	0.05	ME-MS81	2.14	4.01	2.95	4.91	3.97	3.05	4.60	3.43	3.21	3.80	3.05
Ho	0.01	ME-MS81	0.44	0.86	0.63	1.01	0.83	0.61	0.98	0.72	0.63	0.79	0.61
Er	0.03	ME-MS81	1.38	2.59	1.90	3.03	2.40	1.83	2.91	2.19	1.97	2.53	1.92
Tl	0.5	ME-MS81	2.20	0.60	1.80	1.00	0.50	0.90	1.20	0.70	0.70	0.50	0.60
Tm	0.01	ME-MS81	0.21	0.41	0.31	0.50	0.39	0.31	0.46	0.37	0.30	0.38	0.29
Yb	0.03	ME-MS81	1.48	2.67	2.02	3.17	2.43	1.95	2.94	2.21	2.06	2.69	1.85
Lu	0.01	ME-MS81	0.26	0.46	0.32	0.52	0.39	0.33	0.49	0.34	0.32	0.41	0.30

Sample:			RG-1415	RG-1498	RG-2059	RG-2062	RG-2068	RG-2088	RG-2226	CG12-982A	CG12-1155	CG12-1159B	CG12-1164D	CG12-1168
Lithology:			Latite Phyric Flow	Latite Phyric Flow	Latite Phyric Flow	Latite Phyric Flow	Latite Phyric Flow	Latite Phyric Flow	Latite Phyric Flow	Latite Phyric Flow	Latite Phyric Flow	Latite Phyric Flow	Latite Phyric Flow	Latite Phyric Flow
Easting:			426457.00	426797.00	426139.00	425879.00	425966.00	425818.00	427099.00	426303.00	426502.00	426336.00	426408.00	426412.00
Northing:			6260315.00	6259783.00	6258380.00	6258372.00	6258473.00	6258750.00	6258911.00	6259573.00	6258538.00	6258436.00	6258353.00	6258395.00
Elevation (m):			1489.00	1439.00	1494.00	1512.00	1481.00	1396.00	1369.00	1445.00	1446.00	1467.00	1500.00	1502.00
Element	**Det. Lim.**	**Analytical Meth.**												
Weight Percent														
SiO2	0.01	ME-ICP06	59.90	60.60	59.70	58.40	56.20	59.90	54.40	52.50	58.90	57.00	56.80	58.90
Al2O3	0.01	ME-ICP06	17.00	16.35	17.00	16.00	16.45	17.15	15.25	16.70	17.40	15.85	16.25	16.70
Fe2O3	0.01	ME-ICP06	5.74	5.60	5.50	3.93	6.07	4.57	5.20	9.28	6.14	5.78	5.54	5.90
MgO	0.01	ME-ICP06	1.79	0.94	2.21	1.48	2.10	1.26	1.68	3.07	2.12	2.03	2.17	2.15
MnO	0.01	ME-ICP06	0.12	0.23	0.18	0.20	0.16	0.12	0.21	0.25	0.18	0.15	0.19	0.18
CaO	0.01	ME-ICP06	3.25	1.82	3.78	5.50	7.00	4.36	8.63	3.62	3.31	5.29	5.93	5.04
Na2O	0.01	ME-ICP06	1.61	3.68	5.02	0.16	0.54	2.17	0.89	4.33	1.36	2.94	2.08	5.05
K2O	0.01	ME-ICP06	2.22	3.77	2.21	4.66	4.04	3.39	3.14	2.17	4.80	3.30	3.45	1.71
TiO2	0.01	ME-ICP06	0.58	0.63	0.58	0.46	0.53	0.46	0.54	0.92	0.55	0.52	0.52	0.54
P2O5	0.01	ME-ICP06	0.20	0.28	0.27	0.24	0.20	0.24	0.21	0.43	0.24	0.22	0.22	0.22
LOI	0.01	OA-GRA05	5.63	3.18	4.89	7.44	8.40	5.96	8.86	4.75	5.54	5.93	7.38	4.03
TOTAL			98.04	97.08	101.34	98.47	101.69	99.58	99.01	98.02	100.54	99.01	100.53	100.42
Parts per million (except where indicated)*														
Au*	1	ME-4ACD81	<det lim	<det lim	<det lim	<det lim	<det lim	<det lim	<det lim	<det lim	<det lim	<det lim	<det lim	<det lim
Ag	0.5	ME-4ACD81	<det lim	<det lim	<det lim	<det lim	<det lim	<det lim	0.70	<det lim	1.00	0.50	<det lim	<det lim
As	0.'1	ME-MS42	1.30	16.30	6.90	81.60	7.90	1.30	30.90	9.80	68.80	38.00	7.90	3.30
Ba	0.5	ME-MS81	2310.00	2330.00	1625.00	2240.00	1795.00	3240.00	1750.00	1520.00	2250.00	1760.00	2390.00	2120.00
Bi	0.1	ME-MS42	0.05	0.01	0.02	0.01	0.02	<det lim	0.02	0.00	0.28	0.02	0.03	0.01
Cd	0.5	ME-4ACD81	<det lim	<det lim	<det lim	<det lim	<det lim	<det lim	<det lim	<det lim	<det lim	<det lim	<det lim	<det lim
Co	1	ME-4ACD81	8.00	10.00	10.00	5.00	10.00	6.00	9.00	20.00	11.00	10.00	10.00	11.00

Cr	10	ME-MS81	10.00	<det lim	10.00	10.00	10.00	10.00	10.00	30.00	20.00	10.00	10.00	10.00
Cs	0.01	ME-MS81	9.02	8.42	5.63	9.67	5.14	5.41	6.27	7.11	12.60	6.80	7.62	2.90
Cu	1	ME-4ACD81	57.00	0.50	42.00	2.00	28.00	13.00	20.00	61.00	5.00	1.00	20.00	11.00
Ga	0.'1	ME-MS81	20.40	19.40	17.70	19.90	17.80	19.40	15.40	19.20	17.90	17.50	17.60	17.60
Hf	0.2	ME-MS81	3.00	3.00	2.70	2.90	2.70	3.00	2.70	2.90	2.50	2.60	2.60	2.70
Hg	0.0051	ME-MS42	0.02	0.01	0.02	0.05	0.01	0.01	0.03	<det lim	0.01	<det lim	<det lim	<det lim
Li	10	ME-4ACD81	50.00	10.00	20.00	30.00	20.00	30.00	30.00	30.00	30.00	20.00	20.00	20.00
Mo	1	ME-4ACD81	<det lim	<det lim	<det lim	<det lim	<det lim	<det lim	<det lim	<det lim	<det lim	<det lim	<det lim	<det lim
Nb	0.2	ME-MS81	6.10	8.10	6.30	8.00	5.50	8.30	4.80	7.80	5.80	5.40	5.60	5.70
Ni	1	ME-4ACD81	1.00	1.00	2.00	0.50	0.50	2.00	6.00	6.00	1.00	1.00	0.50	0.50
Pb	2	ME-4ACD81	3.00	7.00	6.00	7.00	4.00	2.00	16.00	4.00	20.00	13.00	2.00	8.00
Rb	0.2	ME-MS81	73.40	137.50	88.30	189.00	167.50	122.00	127.50	78.40	216.00	126.50	137.50	56.80
Sb	0.05	ME-MS42	0.47	1.64	0.75	0.93	0.52	0.27	0.81	1.06	2.13	1.45	0.67	1.28
Sc	1	ME-4ACD81	11.00	9.00	12.00	8.00	11.00	9.00	10.00	24.00	13.00	11.00	12.00	12.00
Se	0.2	ME-MS42	0.00	0.20	<det lim	<det lim	<det lim	<det lim	0.40	0.30	1.30	0.30	0.30	0.20
Sn	1	ME-MS81	1.00	1.00	1.00	1.00	1.00	<det lim	<det lim	<det lim	<det lim	1.00	1.00	1.00
Sr	0.1	ME-MS81	330.00	338.00	270.00	172.50	210.00	284.00	164.50	487.00	116.00	250.00	238.00	919.00
Ta	0.1	ME-MS81	0.30	0.50	0.40	0.40	0.30	0.50	0.30	0.50	0.40	0.40	0.40	0.40
Te	0.01	ME-MS42	<det lim	<det lim	<det lim	0.01	0.01	<det lim	0.01	<det lim	0.01	<det lim	0.01	<det lim
Th	0.05	ME-MS81	3.19	5.72	3.43	6.29	3.29	6.33	2.80	4.87	3.60	3.18	3.32	3.51
U	0.05	ME-MS81	2.19	2.61	1.90	3.49	2.25	3.24	1.74	2.41	2.20	2.31	2.31	2.44
V	5	ME-MS81	114.00	76.00	121.00	97.00	122.00	123.00	98.00	276.00	153.00	135.00	139.00	145.00
W	1	ME-MS81	1.00	1.00	11.00	1.00	1.00	1.00	1.00	1.00	5.00	3.00	2.00	1.00
Y	0.5	ME-MS81	22.00	17.10	16.60	18.70	17.30	17.50	18.80	24.00	15.80	17.60	17.50	18.20
Zn	2	ME-4ACD81	90.00	74.00	79.00	56.00	87.00	63.00	81.00	96.00	114.00	70.00	76.00	78.00
Zr	2	ME-MS81	132.00	114.00	113.00	113.00	104.00	110.00	94.00	103.00	92.00	95.00	95.00	97.00
La	0.5	ME-MS81	11.10	15.80	11.60	16.60	11.80	17.80	10.90	21.00	12.90	12.90	13.30	13.90

Ce	0.5	ME-MS81	20.60	25.90	20.50	26.80	21.00	31.70	21.70	40.70	25.30	24.70	25.50	25.90
Pr	0.03	ME-MS81	2.79	3.31	2.78	3.35	2.78	3.69	2.80	5.18	3.17	3.09	3.19	3.25
Nd	0.1	ME-MS81	12.00	13.20	11.40	13.00	11.40	14.60	12.10	21.70	12.90	12.00	12.70	12.90
Sm	0.03	ME-MS81	2.73	2.79	2.59	2.60	2.52	2.96	2.80	4.67	2.85	2.66	2.93	2.96
Eu	0.03	ME-MS81	0.86	1.02	1.01	0.85	0.93	0.90	1.14	1.50	0.96	0.85	1.00	1.00
Gd	0.05	ME-MS81	3.24	3.16	2.99	3.08	2.98	3.09	3.42	5.03	3.03	2.69	2.93	3.11
Tb	0.01	ME-MS81	0.55	0.49	0.48	0.51	0.48	0.48	0.55	0.79	0.48	0.43	0.45	0.47
Dy	0.05	ME-MS81	3.41	2.84	2.84	3.00	2.92	2.92	3.25	4.34	2.77	2.76	2.85	3.02
Ho	0.01	ME-MS81	0.70	0.58	0.56	0.61	0.62	0.61	0.69	0.91	0.60	0.60	0.59	0.64
Er	0.03	ME-MS81	2.28	1.88	1.74	2.02	1.94	1.90	2.08	2.69	1.78	1.76	1.78	1.94
Tl	0.5	ME-MS81	0.50	0.80	1.00	1.90	1.80	0.90	1.50	0.60	2.60	1.20	1.60	0.70
Tm	0.01	ME-MS81	0.34	0.28	0.27	0.30	0.31	0.31	0.34	0.42	0.29	0.29	0.31	0.31
Yb	0.03	ME-MS81	2.38	1.95	1.85	2.15	2.03	2.15	2.29	2.74	2.03	1.90	1.92	2.04
Lu	0.01	ME-MS81	0.38	0.30	0.29	0.32	0.32	0.35	0.37	0.42	0.32	0.31	0.33	0.33

Sample:			CG12-1183	CG12-1601	CG12-1928	CG12-1980	CG12-1991	SU580	CG11-051	CG11-052	CG11-061	CG11-068	CG11-137	CG11-214C
Lithology:			Latite Phyric Flow	Latite Phyric Flow	Latite Phyric Flow	Latite Phyric Flow	Latite Phyric Flow	Latite Phyric Flow	Latite Phyric Flow	Latite Phyric Flow	Latite Phyric Flow	Latite Phyric Flow	Latite Phyric Flow	Latite Phyric Flow
Easting:			426309.00	426301.00	426171.00	426254.00	426248.00	426852.97	426964.00	426462.00	426606.00	426338.00	426493.00	425965.00
Northing:			6258261.00	6258566.00	6258759.00	6258605.00	6258648.00	6258151.03	6257994.00	6258365.00	6259265.00	6259574.00	6258963.00	6261723.00
Elevation (m):			1485.00	1436.00	1404.00	1426.00	1420.00	1511.18	1529.00	1515.00	1436.00	1463.00	1627.00	1784.00
Element	**Det. Lim.**	**Analytical Meth.**												
Weight Percent														
SiO2	0.01	ME-ICP06	57.20	58.10	56.40	57.10	58.30	66.00	57.10	56.20	46.60	48.90	53.80	58.30
Al2O3	0.01	ME-ICP06	16.25	16.50	16.10	16.40	16.65	14.25	16.65	17.40	15.95	16.25	17.30	16.40
Fe2O3	0.01	ME-ICP06	5.64	5.97	5.51	5.86	5.85	5.79	5.14	5.67	8.08	7.89	9.16	5.22
MgO	0.01	ME-ICP06	2.44	2.23	2.25	2.15	2.41	0.88	1.47	2.17	2.58	2.27	2.87	1.14
MnO	0.01	ME-ICP06	0.19	0.16	0.15	0.18	0.20	0.11	0.15	0.21	0.24	0.19	0.25	0.18
CaO	0.01	ME-ICP06	5.44	4.60	4.52	4.82	3.54	3.68	6.22	4.66	9.17	6.82	2.35	4.36
Na2O	0.01	ME-ICP06	1.68	3.20	3.71	1.98	3.05	0.06	0.34	4.02	2.14	3.87	2.57	2.81
K2O	0.01	ME-ICP06	3.80	3.97	2.83	4.95	4.98	4.24	3.21	2.53	3.45	1.73	4.82	3.15
TiO2	0.01	ME-ICP06	0.53	0.54	0.52	0.53	0.54	0.55	0.55	0.54	0.75	0.86	0.86	0.60
P2O5	0.01	ME-ICP06	0.21	0.20	0.23	0.23	0.23	0.23	0.24	0.23	0.43	0.39	0.49	0.25
LOI	0.01	OA-GRA05	6.95	4.70	6.02	5.75	4.60	5.26	7.80	5.40	9.37	8.22	4.50	5.49
TOTAL			100.33	100.17	98.24	99.95	100.35	101.05	98.87	99.03	98.76	97.39	98.97	97.90
Parts per million (except where indicated)*														
Au*	1	ME-4ACD81	<det lim	<det lim	<det lim	<det lim	<det lim	<det lim	<det lim	<det lim	<det lim	<det lim	<det lim	<det lim
Ag	0.5	ME-4ACD81	<det lim	<det lim	<det lim	<det lim	0.70	1.50	0.25	0.25	0.25	0.50	1.50	0.25
As	0.'1	ME-MS42	53.50	22.50	8.00	2.10	19.00	0.00	2.40	2.20	2.20	4.00	30.80	9.70
Ba	0.5	ME-MS81	1925.00	3610.00	2080.00	3190.00	3010.00	1340.00	2250.00	2140.00	1845.00	1190.00	2820.00	2490.00
Bi	0.1	ME-MS42	0.02	0.01	0.01	0.02	0.01	0.00	0.05	0.01	0.05	0.01	0.31	0.01
Cd	0.5	ME-4ACD81	<det lim	<det lim	<det lim	<det lim	<det lim	<det lim	0.25	0.25	0.25	0.25	0.80	0.25
Co	1	ME-4ACD81	10.00	11.00	10.00	10.00	10.00	9.00	6.00	9.00	15.00	11.00	18.00	9.00

Cr	10	ME-MS81	10.00	10.00	10.00	10.00	10.00	10.00	5.00	10.00	20.00	20.00	20.00	5.00
Cs	0.01	ME-MS81	6.11	5.19	6.14	7.62	4.68	10.80	8.66	6.79	9.49	7.26	7.02	7.27
Cu	1	ME-4ACD81	8.00	24.00	6.00	25.00	25.00	18.00	0.50	5.00	73.00	326.00	82.00	6.00
Ga	0.'1	ME-MS81	18.10	18.50	18.10	18.40	17.60	15.60	18.00	18.20	17.40	17.00	20.70	19.50
Hf	0.2	ME-MS81	2.60	2.70	2.60	2.60	2.80	2.40	2.60	2.70	2.50	2.70	2.90	3.20
Hg	0.0051	ME-MS42	<det lim	<det lim	<det lim	<det lim	0.01	0.04	0.00	0.00	0.00	0.02	0.01	0.00
Li	10	ME-4ACD81	20.00	20.00	20.00	20.00	20.00	10.00	<det lim	<det lim	<det lim	<det lim	<det lim	<det lim
Mo	1	ME-4ACD81	<det lim	<det lim	<det lim	<det lim	<det lim	<det lim	0.50	1.00	0.50	1.00	2.00	2.00
Nb	0.2	ME-MS81	5.60	5.80	5.60	5.70	5.80	7.90	8.70	6.30	8.50	8.20	8.20	8.90
Ni	1	ME-4ACD81	0.50	0.50	1.00	0.50	1.00	0.50	0.50	0.50	6.00	7.00	9.00	2.00
Pb	2	ME-4ACD81	4.00	7.00	5.00	10.00	8.00	8.00	7.00	6.00	4.00	19.00	27.00	6.00
Rb	0.2	ME-MS81	165.00	159.50	133.00	204.00	172.00	188.00	122.00	104.50	145.50	71.60	209.00	110.50
Sb	0.05	ME-MS42	1.05	1.86	0.67	1.00	0.78	3.46	0.30	0.57	0.26	0.86	1.85	3.26
Sc	1	ME-4ACD81	12.00	12.00	11.00	11.00	12.00	13.00	<det lim	<det lim	<det lim	<det lim	<det lim	<det lim
Se	0.2	ME-MS42	0.20	0.20	0.20	0.30	0.20	0.70	0.20	0.30	0.50	0.40	4.30	0.40
Sn	1	ME-MS81	1.00	1.00	1.00	1.00	1.00	1.00	1.00	1.00	1.00	1.00	1.00	1.00
Sr	0.1	ME-MS81	208.00	760.00	336.00	355.00	274.00	87.50	218.00	440.00	630.00	360.00	335.00	266.00
Ta	0.1	ME-MS81	0.30	0.40	0.40	0.40	0.40	0.60	0.50	0.40	0.50	0.50	0.40	0.60
Te	0.01	ME-MS42	<det lim	<det lim	<det lim	<det lim	<det lim	0.01	0.05	0.05	0.05	0.05	0.02	0.05
Th	0.05	ME-MS81	3.38	3.50	3.38	3.36	4.02	6.44	5.14	3.54	5.44	4.55	6.28	6.08
U	0.05	ME-MS81	2.44	2.41	2.38	2.39	2.40	3.12	2.49	2.30	2.46	2.43	2.27	2.39
V	5	ME-MS81	141.00	149.00	142.00	146.00	143.00	140.00	103.00	140.00	237.00	238.00	284.00	123.00
W	1	ME-MS81	2.00	1.00	2.00	3.00	3.00	2.00	1.00	1.00	1.00	2.00	5.00	2.00
Y	0.5	ME-MS81	18.30	18.90	17.50	17.60	17.70	15.80	19.30	20.80	25.40	22.70	24.90	21.80
Zn	2	ME-4ACD81	75.00	76.00	76.00	75.00	75.00	73.00	71.00	98.00	79.00	180.00	144.00	81.00
Zr	2	ME-MS81	96.00	98.00	93.00	97.00	93.00	86.00	103.00	120.00	111.00	108.00	115.00	121.00
La	0.5	ME-MS81	13.60	14.20	13.20	13.90	14.70	17.60	17.00	14.40	26.70	22.00	29.30	20.80

Ce	0.5	ME-MS81	25.40	26.70	25.00	26.00	27.70	31.50	31.90	28.20	50.80	41.80	54.70	37.20
Pr	0.03	ME-MS81	3.22	3.36	3.17	3.30	3.48	3.80	3.56	3.23	5.66	4.75	6.92	4.63
Nd	0.1	ME-MS81	12.50	13.20	12.50	12.70	13.70	13.90	14.90	13.40	24.00	20.10	27.50	18.40
Sm	0.03	ME-MS81	2.98	3.07	2.91	2.98	3.20	3.03	3.23	3.00	4.99	4.53	5.67	3.98
Eu	0.03	ME-MS81	0.86	0.95	0.90	0.97	1.00	0.83	1.10	0.90	1.53	1.35	1.46	1.14
Gd	0.05	ME-MS81	2.85	3.01	2.83	2.88	3.13	2.79	3.04	3.11	4.35	3.96	5.18	4.16
Tb	0.01	ME-MS81	0.46	0.49	0.46	0.45	0.48	0.41	0.49	0.48	0.66	0.62	0.72	0.61
Dy	0.05	ME-MS81	2.91	3.04	2.91	2.86	3.00	2.62	3.03	3.12	4.05	3.81	4.37	3.65
Ho	0.01	ME-MS81	0.60	0.64	0.61	0.61	0.62	0.54	0.65	0.68	0.82	0.77	0.90	0.77
Er	0.03	ME-MS81	1.84	2.02	1.85	1.78	1.88	1.59	2.04	2.13	2.58	2.46	2.53	2.26
Tl	0.5	ME-MS81	2.20	2.20	1.40	2.20	2.60	1.70	0.80	1.20	1.20	0.60	2.30	0.60
Tm	0.01	ME-MS81	0.30	0.31	0.31	0.30	0.31	0.26	0.31	0.32	0.37	0.37	0.39	0.34
Yb	0.03	ME-MS81	1.88	2.09	1.96	1.93	2.04	1.71	2.01	2.17	2.52	2.37	2.52	2.18
Lu	0.01	ME-MS81	0.33	0.34	0.32	0.32	0.33	0.29	0.31	0.33	0.36	0.37	0.39	0.35

Sample:			CG11-267	CG11-290	SU 188	SU 189A	SU 189B	SU 198B	SU 199C	SU 199D	SU 199E	SU 199F	SU 199G	SU 199H	CG11-366
Lithology:			Latite Phyric Flow	Latite Phyric Flow	Latite Phyric Flow	Latite Phyric Flow	Latite Phyric Flow	Latite Phyric Flow	Latite Phyric Flow	Latite Phyric Flow	Latite Phyric Flow	Latite Phyric Flow	Latite Phyric Flow	Latite Phyric Flow	Latite Phyric Flow
Easting:			426314.00	426106.00	426344.53	426033.09	426033.09	426534.28	425959.19	425959.19	425959.19	425959.19	425959.19	425959.19	426205.00
Northing:			6260047.00	6260400.00	6258045.50	6258069.00	6258069.00	6259131.00	6258131.00	6258131.00	6258131.00	6258131.00	6258131.00	6258131.00	6258719.00
Elevation (m):			1510.00	1515.00	1526.08	1538.13	1538.13	1452.95	1532.67	1532.67	1532.67	1532.67	1532.67	1532.67	1394.00
Element	**Det. Lim.**	**Analytical Meth.**													
Weight Percent															
SiO2	0.01	ME-ICP06	53.40	53.60	55.20	57.70	59.10	47.80	56.70	56.20	57.50	53.00	53.70	57.10	57.70
Al2O3	0.01	ME-ICP06	18.35	17.45	17.10	17.05	17.55	16.45	17.95	16.45	17.00	19.55	16.25	17.80	18.20
Fe2O3	0.01	ME-ICP06	6.68	6.83	6.34	6.06	5.78	8.81	5.58	5.37	5.52	7.28	5.51	6.39	6.52
MgO	0.01	ME-ICP06	1.05	1.87	2.23	1.92	1.86	3.19	1.52	1.64	1.82	2.58	2.08	2.36	2.36
MnO	0.01	ME-ICP06	0.13	0.23	0.18	0.27	0.18	0.35	0.17	0.15	0.12	0.13	0.19	0.20	0.16
CaO	0.01	ME-ICP06	4.94	5.91	5.77	4.91	4.61	8.74	3.40	5.50	3.47	3.07	5.89	4.05	2.80
Na2O	0.01	ME-ICP06	2.71	4.28	2.11	4.83	4.44	1.95	0.66	1.92	1.49	0.46	2.02	3.65	5.57
K2O	0.01	ME-ICP06	3.17	1.56	3.94	3.07	3.57	4.79	6.66	3.94	4.97	5.65	3.91	3.06	2.61
TiO2	0.01	ME-ICP06	0.73	0.75	0.58	0.54	0.60	0.80	0.60	0.55	0.58	0.65	0.54	0.59	0.60
P2O5	0.01	ME-ICP06	0.29	0.30	0.23	0.32	0.21	0.43	0.19	0.19	0.19	0.26	0.21	0.20	0.23
LOI	0.01	OA-GRA05	6.07	7.35	7.59	3.48	3.48	7.69	6.47	5.49	5.46	5.60	10.15	5.39	2.28
TOTAL			97.52	100.13	101.27	100.15	101.38	101.00	99.90	97.40	98.12	98.23	100.45	100.79	99.03
Parts per million (except where indicated)*															
Au*	1	ME-4ACD81	<det lim	<det lim	<det lim	<det lim	<det lim	<det lim	<det lim	<det lim	<det lim	<det lim	<det lim	<det lim	<det lim
Ag	0.5	ME-4ACD81	0.25	0.25	0.25	0.25	0.25	0.90	1.50	1.00	0.50	0.50	0.25	0.25	0.25
As	0.'1	ME-MS42	1.30	0.70	96.20	6.90	18.80	29.40	199.00	93.60	100.00	24.60	61.30	14.10	5.30
Ba	0.5	ME-MS81	2750.00	1510.00	2440.00	2800.00	2400.00	2850.00	3920.00	2170.00	2980.00	4190.00	2180.00	2650.00	2900.00
Bi	0.1	ME-MS42	0.02	0.06	0.05	0.09	0.04	0.01	0.01	0.01	0.04	0.04	0.04	0.04	0.04
Cd	0.5	ME-4ACD81	0.25	0.25	0.25	0.25	0.25	0.25	0.25	0.25	0.25	0.25	0.25	0.25	0.25
Co	1	ME-4ACD81	7.00	11.00	11.00	9.00	8.00	16.00	9.00	9.00	9.00	12.00	10.00	11.00	11.00

Cr	10	ME-MS81	5.00	5.00	10.00	20.00	10.00	20.00	10.00	10.00	10.00	10.00	10.00	10.00	10.00
Cs	0.01	ME-MS81	8.06	5.56	6.84	3.35	5.45	7.87	8.10	6.07	6.03	8.03	5.89	6.82	4.29
Cu	1	ME-4ACD81	46.00	35.00	12.00	17.00	22.00	63.00	14.00	13.00	18.00	25.00	21.00	19.00	24.00
Ga	0.'1	ME-MS81	22.00	21.60	17.20	18.20	18.10	18.00	20.30	18.40	18.40	20.70	17.60	18.60	19.30
Hf	0.2	ME-MS81	2.80	3.10	2.50	2.90	2.90	2.70	3.20	2.90	3.00	3.00	2.40	2.70	2.80
Hg	0.0051	ME-MS42	0.02	0.02	0.01	0.01	0.00	0.01	0.01	0.01	0.02	0.02	0.01	0.02	0.00
Li	10	ME-4ACD81	<det lim	<det lim	<det lim	<det lim	<det lim	<det lim	<det lim	<det lim	<det lim	<det lim	<det lim	<det lim	<det lim
Mo	1	ME-4ACD81	2.00	2.00	1.00	3.00	2.00	0.50	1.00	1.00	2.00	0.50	0.50	0.50	0.50
Nb	0.2	ME-MS81	6.60	7.80	6.00	7.60	7.60	7.90	7.70	7.00	7.30	6.50	5.80	6.20	6.30
Ni	1	ME-4ACD81	2.00	3.00	2.00	2.00	1.00	6.00	3.00	0.50	3.00	2.00	2.00	4.00	4.00
Pb	2	ME-4ACD81	6.00	9.00	6.00	10.00	13.00	5.00	6.00	4.00	10.00	11.00	5.00	19.00	8.00
Rb	0.2	ME-MS81	121.00	54.70	132.00	78.20	123.00	197.50	254.00	154.50	206.00	261.00	141.50	126.00	77.80
Sb	0.05	ME-MS42	0.77	0.78	0.96	1.79	1.16	1.74	2.04	1.21	2.13	1.91	0.80	1.08	1.33
Sc	1	ME-4ACD81	<det lim	<det lim	<det lim	<det lim	<det lim	<det lim	<det lim	<det lim	<det lim	<det lim	<det lim	<det lim	<det lim
Se	0.2	ME-MS42	0.30	0.40	0.20	0.50	0.40	0.50	0.60	0.40	0.50	0.50	0.50	0.30	0.30
Sn	1	ME-MS81	1.00	1.00	1.00	1.00	1.00	1.00	1.00	1.00	1.00	1.00	1.00	1.00	1.00
Sr	0.1	ME-MS81	243.00	393.00	247.00	481.00	293.00	652.00	126.50	191.50	158.50	108.50	262.00	371.00	756.00
Ta	0.1	ME-MS81	0.40	0.50	0.40	0.50	0.50	0.50	0.60	0.50	0.50	0.40	0.40	0.40	0.40
Te	0.01	ME-MS42	0.05	0.06	0.01	0.03	0.04	0.05	0.51	0.52	0.14	0.06	0.01	0.01	0.05
Th	0.05	ME-MS81	4.00	4.11	3.34	4.56	4.66	5.82	4.97	4.54	4.70	3.97	3.33	3.65	3.72
U	0.05	ME-MS81	2.27	2.07	2.81	2.84	2.85	2.58	2.86	2.75	2.85	2.72	2.26	2.38	2.38
V	5	ME-MS81	163.00	145.00	160.00	129.00	128.00	238.00	117.00	106.00	110.00	163.00	136.00	148.00	152.00
W	1	ME-MS81	2.00	2.00	1.00	1.00	1.00	5.00	5.00	4.00	4.00	5.00	4.00	7.00	2.00
Y	0.5	ME-MS81	24.60	26.90	18.30	19.60	19.60	26.60	19.90	19.00	17.60	18.00	18.40	17.30	19.90
Zn	2	ME-4ACD81	62.00	105.00	69.00	40.00	48.00	92.00	52.00	36.00	88.00	89.00	57.00	129.00	84.00
Zr	2	ME-MS81	110.00	124.00	102.00	118.00	121.00	105.00	127.00	113.00	117.00	120.00	98.00	108.00	110.00
La	0.5	ME-MS81	13.60	16.50	12.90	16.20	16.30	27.90	17.30	16.80	17.10	11.60	13.70	15.10	15.40

Ce	0.5	ME-MS81	26.30	32.40	24.80	30.50	30.60	50.70	31.70	30.50	31.40	23.00	25.30	27.60	28.80
Pr	0.03	ME-MS81	3.42	4.21	3.13	3.78	3.82	6.16	3.76	3.60	3.66	2.88	3.12	3.35	3.50
Nd	0.1	ME-MS81	14.30	17.50	12.40	14.70	15.10	25.00	14.90	14.20	14.30	11.80	12.60	13.80	14.20
Sm	0.03	ME-MS81	3.50	3.89	2.78	3.18	3.23	5.40	3.27	3.16	3.05	2.71	2.77	3.09	3.25
Eu	0.03	ME-MS81	1.05	1.15	0.97	1.04	1.09	2.23	0.86	0.94	0.81	0.83	0.79	0.99	1.03
Gd	0.05	ME-MS81	3.87	4.48	2.94	3.11	3.17	5.34	3.50	3.22	3.00	2.92	2.86	3.01	3.32
Tb	0.01	ME-MS81	0.64	0.70	0.44	0.47	0.50	0.75	0.52	0.48	0.45	0.42	0.43	0.45	0.50
Dy	0.05	ME-MS81	3.85	4.34	2.79	2.99	3.12	4.49	3.22	3.09	2.96	2.78	2.89	2.87	3.25
Ho	0.01	ME-MS81	0.88	0.99	0.61	0.66	0.68	0.95	0.73	0.68	0.66	0.64	0.65	0.63	0.73
Er	0.03	ME-MS81	2.52	2.79	1.82	1.92	1.99	2.73	2.14	2.06	1.93	2.01	1.96	1.88	2.19
Tl	0.5	ME-MS81	0.60	0.25	1.40	0.80	1.30	2.20	2.50	1.30	1.90	2.10	1.30	1.20	0.70
Tm	0.01	ME-MS81	0.39	0.45	0.28	0.29	0.30	0.38	0.31	0.30	0.29	0.29	0.28	0.29	0.30
Yb	0.03	ME-MS81	2.50	2.84	1.87	1.94	1.98	2.57	2.21	2.06	2.01	2.18	2.01	2.02	2.20
Lu	0.01	ME-MS81	0.41	0.45	0.31	0.32	0.33	0.37	0.33	0.32	0.31	0.34	0.32	0.31	0.34

Sample:			CG11-596	SU 224B	CG12-1866	CG11-008	CG11-009	CG11-025A	CG11-097	CG11-103	CG11-113	CG11-115	CG11-121	SU 197A
Lithology:			Latite Phyric Flow	Latite Phyric Flow	Coarse Latite Phyric Flow	Coarse Latite Phyric Flow	Coarse Latite Phyric Flow	Coarse Latite Phyric Flow	Coarse Latite Phyric Flow	Coarse Latite Phyric Flow	Coarse Latite Phyric Flow	Coarse Latite Phyric Flow	Coarse Latite Phyric Flow	Coarse Latite Phyric Flow
Easting:			426960.00	426558.06	425365.00	425668.00	425268.00	425539.00	426973.00	427001.00	427663.00	427589.00	426819.00	425368.03
Northing:			6258000.00	6257642.00	6261378.00	6261647.00	6261327.00	6261882.00	6260189.00	6260518.00	6260997.00	6261193.00	6258894.00	6261339.00
Elevation (m):			1528.00	1563.76	1507.00	1733.00	1452.00	1712.00	1588.00	1766.00	2252.00	2357.00	1647.00	1494.58
Element	**Det. Lim.**	**Analytical Meth.**												
Weight Percent														
SiO2	0.01	ME-ICP06	54.60	65.50	58.50	54.60	57.30	59.20	55.20	56.80	57.80	59.50	60.70	56.40
Al2O3	0.01	ME-ICP06	16.80	16.10	17.05	18.20	17.95	16.05	18.70	15.60	17.55	16.50	17.30	17.60
Fe2O3	0.01	ME-ICP06	5.19	5.28	4.73	6.07	6.00	5.00	6.50	5.29	6.45	6.45	5.86	6.13
MgO	0.01	ME-ICP06	1.61	0.97	1.90	1.83	2.78	1.48	2.02	1.36	2.26	2.12	1.98	1.27
MnO	0.01	ME-ICP06	0.18	0.04	0.18	0.15	0.19	0.16	0.20	0.14	0.10	0.12	0.15	0.17
CaO	0.01	ME-ICP06	6.97	0.41	4.10	3.27	2.29	3.14	3.82	5.37	3.89	3.95	3.06	3.57
Na2O	0.01	ME-ICP06	0.34	0.06	1.96	2.04	4.93	2.56	3.31	2.78	5.32	3.88	6.38	4.60
K2O	0.01	ME-ICP06	3.41	5.34	6.52	5.84	3.79	4.98	3.06	3.77	1.85	4.53	0.61	5.83
TiO2	0.01	ME-ICP06	0.60	0.54	0.57	0.67	0.58	0.50	0.67	0.59	0.65	0.61	0.64	0.61
P2O5	0.01	ME-ICP06	0.25	0.18	0.27	0.32	0.26	0.20	0.26	0.28	0.20	0.19	0.26	0.32
LOI	0.01	OA-GRA05	8.40	5.00	4.64	4.88	2.70	4.49	5.29	5.29	3.59	2.50	2.39	3.98
TOTAL			98.35	99.42	100.42	97.87	98.77	97.76	99.03	97.27	99.66	100.35	99.33	100.48
Parts per million (except where indicated)*														
Au*	1	ME-4ACD81	<det lim	<det lim	<det lim	<det lim	<det lim	<det lim	<det lim	<det lim	<det lim	<det lim	<det lim	<det lim
Ag	0.5	ME-4ACD81	0.25	1.10	<det lim	0.25	0.25	0.25	0.25	0.25	0.25	0.25	0.25	0.25
As	0.'1	ME-MS42	0.50	166.50	169.00	14.60	22.50	9.70	2.40	2.80	10.50	8.00	3.30	10.80
Ba	0.5	ME-MS81	3010.00	2270.00	3900.00	3350.00	3290.00	2850.00	1670.00	1850.00	1625.00	2350.00	564.00	3910.00
Bi	0.1	ME-MS42	0.05	0.49	0.10	0.74	0.03	0.02	0.02	0.05	0.08	0.03	0.01	0.03
Cd	0.5	ME-4ACD81	0.25	0.25	0.00	0.25	0.25	0.25	0.25	0.25	0.25	0.25	0.25	0.25
Co	1	ME-4ACD81	7.00	9.00	10.00	8.00	10.00	6.00	11.00	7.00	13.00	12.00	8.00	10.00

Cr	10	ME-MS81	5.00	10.00	10.00	10.00	10.00	5.00	5.00	70.00	10.00	10.00	5.00	10.00
Cs	0.01	ME-MS81	7.00	12.50	9.57	14.50	4.78	8.16	7.00	9.70	1.65	1.98	1.90	9.32
Cu	1	ME-4ACD81	1.00	10.00	28.00	10.00	23.00	11.00	3.00	1.00	34.00	38.00	8.00	33.00
Ga	0.'1	ME-MS81	18.50	18.00	20.30	19.60	20.50	18.70	19.30	15.80	20.20	17.90	20.90	17.90
Hf	0.2	ME-MS81	2.80	2.80	2.70	2.90	2.60	2.50	3.20	2.90	4.80	4.60	2.90	2.50
Hg	0.0051	ME-MS42	0.01	0.03	0.01	0.02	0.00	0.00	0.00	0.00	0.04	0.02	0.00	0.01
Li	10	ME-4ACD81	<det lim	<det lim	20.00	<det lim	<det lim	<det lim	<det lim	<det lim	<det lim	<det lim	<det lim	<det lim
Mo	1	ME-4ACD81	0.50	1.00	<det lim	1.00	3.00	2.00	2.00	2.00	2.00	4.00	2.00	1.00
Nb	0.2	ME-MS81	8.30	7.60	8.10	9.10	8.90	8.90	9.30	9.20	9.70	8.90	8.40	8.10
Ni	1	ME-4ACD81	1.00	2.00	0.50	1.00	8.00	3.00	2.00	9.00	6.00	5.00	3.00	4.00
Pb	2	ME-4ACD81	4.00	24.00	5.00	9.00	10.00	8.00	8.00	10.00	10.00	11.00	3.00	7.00
Rb	0.2	ME-MS81	125.00	246.00	222.00	227.00	92.50	184.50	100.50	111.00	42.50	125.50	22.60	141.50
Sb	0.05	ME-MS42	0.34	2.57	4.37	0.63	1.12	0.49	0.43	0.44	1.27	1.58	0.64	6.12
Sc	1	ME-4ACD81	<det lim		14.00	<det lim	<det lim	<det lim	<det lim	<det lim	<det lim	<det lim	<det lim	<det lim
Se	0.2	ME-MS42	0.30	3.20	0.20	1.80	0.20	0.30	0.30	0.40	0.40	0.40	0.30	0.30
Sn	1	ME-MS81	1.00	1.00	1.00	2.00	1.00	1.00	1.00	1.00	1.00	1.00	1.00	1.00
Sr	0.1	ME-MS81	197.00	74.10	271.00	281.00	454.00	365.00	311.00	383.00	817.00	675.00	1010.00	470.00
Ta	0.1	ME-MS81	0.60	0.50	0.50	0.60	0.50	0.60	0.60	0.60	0.70	0.60	0.50	0.50
Te	0.01	ME-MS42	0.05	0.16	0.21	0.34	0.32	0.02	0.05	0.05	0.05	0.05	0.05	0.03
Th	0.05	ME-MS81	5.33	4.56	5.42	4.55	5.61	5.83	6.41	5.66	11.25	10.15	5.26	5.08
U	0.05	ME-MS81	2.76	2.75	3.40	2.36	3.09	2.93	2.48	3.41	4.43	3.96	2.37	2.92
V	5	ME-MS81	113.00	103.00	185.00	126.00	181.00	108.00	136.00	99.00	189.00	167.00	126.00	195.00
W	1	ME-MS81	2.00	4.00	4.00	1.00	2.00	1.00	1.00	1.00	3.00	3.00	2.00	3.00
Y	0.5	ME-MS81	20.70	6.10	19.10	26.20	22.40	20.50	22.00	19.80	23.20	22.50	21.40	19.30
Zn	2	ME-4ACD81	78.00	100.00	114.00	89.00	61.00	68.00	91.00	60.00	62.00	66.00	90.00	50.00
Zr	2	ME-MS81	102.00	109.00	96.00	114.00	108.00	99.00	125.00	118.00	193.00	180.00	109.00	95.00
La	0.5	ME-MS81	20.40	13.00	16.70	18.20	18.80	19.10	20.10	17.90	26.00	22.90	18.70	16.20

Ce	0.5	ME-MS81	36.80	23.10	29.10	36.30	34.00	34.70	37.10	35.40	47.10	43.70	34.50	29.20
Pr	0.03	ME-MS81	4.39	2.58	3.52	4.28	3.74	3.93	4.32	4.06	5.82	5.42	4.27	3.53
Nd	0.1	ME-MS81	17.70	11.30	13.60	17.90	15.10	15.60	17.40	16.60	22.40	20.90	17.70	14.00
Sm	0.03	ME-MS81	3.87	1.89	3.13	4.20	3.28	3.40	3.99	3.56	4.69	4.36	3.82	3.14
Eu	0.03	ME-MS81	1.32	0.24	0.82	1.20	1.04	0.95	1.22	1.03	1.50	1.11	1.27	0.88
Gd	0.05	ME-MS81	3.88	1.31	3.18	4.26	3.39	3.14	3.82	3.41	4.63	4.17	4.09	3.08
Tb	0.01	ME-MS81	0.55	0.17	0.52	0.69	0.55	0.51	0.56	0.51	0.65	0.62	0.63	0.49
Dy	0.05	ME-MS81	3.40	1.25	3.20	4.31	3.39	3.12	3.45	3.11	3.74	3.59	3.66	3.12
Ho	0.01	ME-MS81	0.72	0.22	0.66	0.90	0.73	0.66	0.75	0.65	0.83	0.79	0.76	0.66
Er	0.03	ME-MS81	2.10	0.67	1.96	2.77	2.32	2.17	2.47	2.18	2.36	2.21	2.10	1.94
Tl	0.5	ME-MS81	0.80	2.70	3.30	2.90	0.90	1.70	0.60	0.25	0.25	0.60	0.25	3.40
Tm	0.01	ME-MS81	0.30	0.12	0.34	0.42	0.36	0.32	0.35	0.32	0.37	0.35	0.33	0.30
Yb	0.03	ME-MS81	2.03	0.82	2.13	2.62	2.30	2.06	2.28	2.18	2.48	2.31	2.10	1.96
Lu	0.01	ME-MS81	0.31	0.17	0.35	0.38	0.35	0.30	0.37	0.32	0.39	0.37	0.33	0.32

Sample:			SU 197B	SU 198	CG11-382	CG11-391
Lithology:			Coarse Latite Phyric Flow	Coarse Latite Phyric Flow	Coarse Latite Phyric Flow	Coarse Latite Phyric Flow
Easting:			425368.03	426534.28	426098.00	425915.00
Northing:			6261339.00	6259131.00	6258709.00	6258578.00
Elevation (m):			1494.58	1452.95	1435.00	1448.00
Element	**Det. Lim.**	**Analytical Meth.**				
Weight Percent						
SiO2	0.01	ME-ICP06	55.40	50.40	55.00	57.40
Al2O3	0.01	ME-ICP06	17.70	18.50	17.10	17.30
Fe2O3	0.01	ME-ICP06	5.21	6.38	6.03	4.56
MgO	0.01	ME-ICP06	1.23	0.65	2.11	1.41
MnO	0.01	ME-ICP06	0.21	0.89	0.15	0.14
CaO	0.01	ME-ICP06	6.38	5.31	5.35	4.19
Na2O	0.01	ME-ICP06	0.20	0.30	1.82	3.31
K2O	0.01	ME-ICP06	6.86	9.69	3.92	3.19
TiO2	0.01	ME-ICP06	0.62	0.54	0.56	0.48
P2O5	0.01	ME-ICP06	0.32	0.39	0.22	0.19
LOI	0.01	OA-GRA05	6.39	6.39	6.79	5.39
TOTAL			100.52	99.44	99.05	97.56
Parts per million (except where indicated)*						
Au*	1	ME-4ACD81	<det lim	<det lim	<det lim	<det lim
Ag	0.5	ME-4ACD81	0.50	3.60	0.25	0.25
As	0.'1	ME-MS42	79.80	0.00	0.90	43.90
Ba	0.5	ME-MS81	2660.00	4720.00	3150.00	2880.00
Bi	0.1	ME-MS42	0.10	0.03	0.03	0.04
Cd	0.5	ME-4ACD81	0.25	0.25	0.25	0.25
Co	1	ME-4ACD81	10.00	6.00	11.00	7.00
Cr	10	ME-MS81	10.00	10.00	10.00	10.00
Cs	0.01	ME-MS81	14.90	12.25	6.82	4.99
Cu	1	ME-4ACD81	31.00	19.00	28.00	13.00
Ga	0.'1	ME-MS81	18.40	21.40	17.90	20.00
Hf	0.2	ME-MS81	2.60	3.10	2.60	3.00
Hg	0.0051	ME-MS42	0.04	0.23	0.00	0.01
Li	10	ME-4ACD81	<det lim	<det lim	<det lim	<det lim
Mo	1	ME-4ACD81	0.50	0.50	0.50	0.50
Nb	0.2	ME-MS81	8.30	9.40	5.90	8.50
Ni	1	ME-4ACD81	2.00	1.00	8.00	4.00
Pb	2	ME-4ACD81	18.00	27.00	1.00	18.00
Rb	0.2	ME-MS81	205.00	285.00	172.00	118.00
Sb	0.05	ME-MS42	6.47	22.80	0.38	0.79
Sc	1	ME-4ACD81	<det lim	<det lim	<det lim	<det lim

Se	0.2	ME-MS42	0.40	0.70	0.30	0.30
Sn	1	ME-MS81	1.00	1.00	1.00	1.00
Sr	0.1	ME-MS81	218.00	271.00	257.00	343.00
Ta	0.1	ME-MS81	0.50	0.60	0.40	0.50
Te	0.01	ME-MS42	0.06	0.08	0.05	0.05
Th	0.05	ME-MS81	5.17	7.16	3.47	6.52
U	0.05	ME-MS81	3.10	3.27	2.33	3.90
V	5	ME-MS81	198.00	139.00	142.00	120.00
W	1	ME-MS81	7.00	37.00	4.00	3.00
Y	0.5	ME-MS81	17.90	15.30	17.60	18.10
Zn	2	ME-4ACD81	106.00	132.00	76.00	64.00
Zr	2	ME-MS81	100.00	118.00	102.00	117.00
La	0.5	ME-MS81	16.10	18.90	13.70	17.90
Ce	0.5	ME-MS81	29.10	35.20	25.60	31.40
Pr	0.03	ME-MS81	3.53	4.04	3.10	3.60
Nd	0.1	ME-MS81	13.70	16.10	12.80	13.90
Sm	0.03	ME-MS81	2.90	3.44	2.83	2.91
Eu	0.03	ME-MS81	0.82	1.11	0.92	0.79
Gd	0.05	ME-MS81	2.97	3.24	3.03	2.84
Tb	0.01	ME-MS81	0.49	0.48	0.46	0.43
Dy	0.05	ME-MS81	2.91	2.84	2.92	2.91
Ho	0.01	ME-MS81	0.64	0.61	0.65	0.66
Er	0.03	ME-MS81	1.88	1.78	1.98	1.96
Tl	0.5	ME-MS81	2.90	6.00	1.30	0.90
Tm	0.01	ME-MS81	0.28	0.26	0.29	0.29
Yb	0.03	ME-MS81	1.91	1.88	2.04	2.16
Lu	0.01	ME-MS81	0.32	0.30	0.32	0.32

Notes: Listed elements below analytical detection denoted as <det lim. Analytical methods: ME-ICP06: fused bead, acid digestion and inductively coupled plasma-atomic emission spectroscopy: OA-GRA05: thermal decomposition furnace (1000C for 1hr); ME-4ACD81: multi-element four acid digestion and inductively coupled plasma-atomic emission spectroscopy; ME-MS42: multi element inductively coupled plasma-atomic emission spectroscopy; ME-MS42: multi element multi-element by lithium borate fusion and inductively coupled plasma-mass spectroscopy. * Indicates ppb (parts per billion).

APPENDIX D

$^{40}Ar/^{39}Ar$ Geochronology

Sample A8

step	T (C)	t (min.)	36Ar	37Ar	38Ar	39Ar	40Ar	%40Ar*	% 39Ar rlsd	Ca/K	40Ar*/39ArK	Age (Ma)	2s.d.
1	750	12	0.222	0.023	0.194	10.179	257.282	78.0	1.7	0.027019209	19.379666	59.12	1.76
2	810	12	2.817	0.028	0.700	11.495	1091.61	27.6	2.0	0.029127233	26.314207	79.81	6.14
3	870	12	1.426	0.033	0.487	15.050	804.057	50.5	2.6	0.026219671	27.070997	82.06	3.50
4	910	12	0.223	0.045	0.451	30.749	898.640	93.7	5.3	0.017499684	27.472708	83.25	2.16
5	940	12	0.219	0.074	1.051	75.445	2338.77	97.5	12.9	0.011728682	30.490263	92.16	2.32
6	970	12	0.247	0.119	1.813	130.126	4313.57	98.4	22.3	0.010935301	32.945661	99.38	2.48
7	1000	12	0.203	0.100	1.400	98.842	3418.36	98.4	16.9	0.012097802	34.355116	103.52	2.59
8	1050	12	0.233	0.147	1.210	86.094	2998.40	97.9	14.7	0.020417074	34.416588	103.70	2.60
9	1110	12	0.253	0.227	1.026	70.127	2527.91	97.4	12.0	0.038707221	36.032442	108.42	2.72
10	1170	12	0.165	0.202	0.619	42.020	1525.35	97.4	7.2	0.057484283	35.561099	107.04	2.69
11	1250	12	0.117	0.119	0.159	9.479	358.643	92.9	1.6	0.150123982	34.755140	104.69	2.74
12	1400	12	0.231	0.252	0.121	4.666	243.135	76.9	0.8	0.645929051	38.897653	116.77	3.46
								Cumulative %39Ar rlsd =	100.0		Total gas age =	99.26	1.44
											Plateau age =	105.41	2.41
											(steps 7-11)		
											No isochron		

Sample A20

step	T (C)	t (min.)	36Ar	37Ar	38Ar	39Ar	40Ar	%40Ar*	% 39Ar rlsd	Ca/K	40Ar*/39ArK	Age (Ma)	2s.d.
1	620	12	1.050	0.016	0.216	2.192	296.958	0.6	0.3	0.08682594	0.870443	2.69	8.08
2	690	12	0.175	0.017	0.076	2.697	89.620	49.6	0.4	0.074978461	15.344870	46.81	2.48
3	760	12	0.321	0.025	0.230	12.820	390.503	78.3	1.8	0.023196043	23.693126	71.77	2.13
4	820	12	1.788	0.074	0.904	42.179	1771.52	71.8	5.8	0.02086878	30.385277	91.54	2.83
5	870	12	1.048	0.051	0.603	32.189	1351.22	78.5	4.4	0.018846212	33.168426	99.70	2.88
6	920	12	0.480	0.088	0.922	62.984	2225.65	94.1	8.6	0.01661933	33.536838	100.77	2.61
7	960	12	0.649	0.220	2.174	158.691	5840.33	96.9	21.7	0.01649041	36.017092	108.01	2.76
8	1000	12	0.461	0.196	1.586	116.354	4395.76	97.1	15.9	0.020037165	37.042746	110.99	2.81
9	1050	12	0.306	0.135	0.832	59.605	2321.02	96.5	8.1	0.026940986	37.890885	113.45	2.86
10	1130	12	0.761	0.380	2.270	163.171	6338.50	96.6	22.3	0.02770149	37.917074	113.53	2.84
11	1220	12	0.349	0.500	0.773	53.177	2064.08	95.5	7.3	0.111845736	37.354594	111.90	2.84
12	1400	12	0.284	1.200	0.436	26.408	1051.810	93.3	3.6	0.540597207	37.252004	111.60	2.88
								Cumulative %39Ar rlsd =	100.0		Total gas age =	107.46	1.56
											Plateau age =	112.29	2.57
											(steps 8-12)		

Sample BJ-B6

step	T (C)	t (min.)	36Ar	37Ar	38Ar	39Ar	40Ar	%40Ar*	% 39Ar rlsd	Ca/K	40Ar*/39ArK	Age (Ma)	2s.d.
1	800	12	0.527	0.011	0.261	10.897	430.760	68.2	6.3	0.067113979	26.201076	79.61	1.06
2	850	12	4.486	0.017	1.211	26.725	2100.48	40.1	15.4	0.042291714	31.623292	95.66	1.92
3	890	12	0.355	0.022	0.487	32.197	1122.14	92.4	18.6	0.045428851	32.058585	96.94	1.12
4	930	12	0.204	0.010	0.361	24.925	873.870	95.2	14.4	0.026673924	33.083526	99.96	1.13
5	960	12	0.167	0.018	0.220	14.290	503.159	94.4	8.3	0.083747077	32.202619	97.37	1.17
6	990	12	0.185	0.013	0.180	10.812	405.499	91.7	6.2	0.07994038	32.974321	99.64	1.35
7	1020	12	0.171	0.008	0.146	8.794	339.275	91.3	5.1	0.060482527	33.393895	100.87	1.23
8	1050	12	0.156	0.012	0.122	7.290	280.840	91.0	4.2	0.109442595	32.779775	99.06	1.29
9	1080	12	0.136	0.012	0.122	7.032	265.040	92.7	4.1	0.113458114	32.523081	98.31	2.15
10	1120	12	0.136	0.018	0.152	9.840	356.800	94.7	5.7	0.121621856	32.653624	98.69	1.17
11	1160	12	0.123	0.018	0.204	13.102	460.917	98.4	7.6	0.091340894	32.885203	99.37	1.13
12	1220	12	0.124	0.026	0.097	5.446	206.197	96.1	3.1	0.317435111	31.869082	96.38	1.20
13	1400	12	0.114	0.075	0.055	1.831	93.973	100.0	1.1	2.72546029	31.990317	96.74	1.56
								Cumulative %39Ar rlsd =	100.0		Total gas age =	96.90	0.54
											No plateau		
											No isochron		

Sample BJ-005

step	T (C)	t (min.)	36Ar	37Ar	38Ar	39Ar	40Ar	%40Ar*	% 39Ar rlsd	Ca/K	40Ar*/39ArK	Age (Ma)	2s.d.
1	800	12	4.030	0.020	1.398	47.101	2459.72	54.1	7.4	0.028694551	28.385456	84.68	1.30
2	850	12	0.181	0.013	0.690	50.099	1649.84	97.8	7.9	0.017535269	32.218147	95.81	1.10
3	890	12	0.172	0.010	1.170	88.019	2979.34	98.8	13.9	0.007677511	33.725325	100.17	1.14
4	930	12	0.151	0.004	1.503	114.620	3958.78	99.2	18.0	0.002358282	34.486172	102.37	1.16
5	960	12	0.141	0.011	0.973	72.739	2501.60	99.1	11.5	0.010219333	34.137667	101.37	1.15
6	990	12	0.149	0.007	0.625	46.154	1583.68	98.4	7.3	0.010249104	33.681026	100.05	1.14
7	1020	12	0.162	0.008	0.477	34.286	1167.08	97.6	5.4	0.015767799	32.969552	97.99	1.14
8	1060	12	0.149	0.012	0.406	29.326	1017.56	97.6	4.6	0.027652083	33.487253	99.49	1.14
9	1100	12	0.109	0.013	0.418	30.211	1034.41	98.8	4.8	0.029078893	33.485523	99.48	1.13
10	1140	12	0.113	0.010	0.551	40.646	1378.79	99.6	6.4	0.016625711	33.457500	99.40	1.13
11	1210	12	0.150	0.013	0.928	69.027	2340.61	99.3	10.9	0.012726878	33.609738	99.84	1.13
12	1400	12	0.387	0.035	0.246	12.825	534.475	85.4	2.0	0.184429399	33.526695	99.60	1.25
								Cumulative %39Ar rlsd =	100.0		Total gas age =	98.92	0.48
											No plateau		
											No isochron		

Note: isotope beams in mV, rlsd = released, error in age includes J error, all errors 2 sigma (36Ar through 40Ar are measured beam intensities, corrected for decay for the age calculations) 4 amu discrimination = 1.0487 ± 0.32%, 40/39K = 0.04795 ± 48.28%, 36/37Ca = 0.000260 ± 6.87%, 39/37Ca = 0.000677 ± 5.05%

APPENDIX E

Fluid Inclusions

Vein Stage II:

#	Sample #	Vein Generation	Inclusion Host Min	Primar	Designation	Fr	Tm(ice)	FPD	NaCl (wt%)	Tm (Clath)	Th	Ti
1	VP017-1-1	2	Qtz	P	Q2	0.9	-2.5	2.5	4.18	-	174.1	174.1
2	VP017-1-2	2	Qtz	P	Q2	0.9	-2.3	2.3	3.87	-	174.3	174.3
3	VP017-1-3	2	Qtz	P	Q2	0.95	-2.6	2.6	4.34	-	165.5	165.5
4	VP017-1-4	2	Qtz	P	Q2	0.95	-2.6	2.6	4.34	-	173.4	173.4
5	VP017-1'-1	2	Qtz	P	Q2	0.95	-4.7	4.7	7.45	-	171.2	171.2
6	VP017-1'-2	2	Qtz	P	Q2	0.9	-4.3	4.3	6.88	-	171.2	171.2
7	VP017-1'-3	2	Qtz	P	Q2	0.85	-3.5	3.5	5.71	-	169.5	169.5
8	VP017-1'-4	2	Qtz	P	Q2	0.95	-4.2	4.2	6.74	-	165	165
9	VP017-1'-5	2	Qtz	P	Q2	0.95	-3.9	3.9	6.30	-	160.1	160.1
10	VP017-3-1	2	Qtz	P	Q2	0.95	-3.8	3.8	6.16	-	172.1	-
11	VP017-3-2	2	Qtz	P	Q2	0.95	-2.2	2.2	3.71	-	172.5	-
12	VP017-3-3	2	Qtz	P	Q2	0.95	-2.7	2.7	4.49	-	172.6	-
13	VP017-3-4	2	Qtz	P	Q2	0.95	-3.8	3.8	6.16	-	172.8	-
14	VP017-3-5	2	Qtz	P	Q2	0.95	-3.8	3.8	6.16	-	177.4	-
15	VP017-3-6	2	Qtz	P	Q2	0.9	-4.5	4.5	7.17	-	165.5	-
16	VP017-3-7	2	Qtz	P	Q2	0.95	-4.1	4.1	6.59	-	165.6	-
17	VP017-3-8	2	Qtz	P	Q2	0.9	-3.2	3.2	5.26	-	165.5	-
18	A32-1-1	2	Qtz	P	Q2	0.95	-3.2	3.2	5.26	-	136.3	136.3
19	A32-1-2	2	Qtz	P	Q2	0.95	-3.1	3.1	5.11	-	145.8	145.8
20	A32-2-1	2	Qtz	P	Q2	0.95	-3.3	3.3	5.41	-	141.9	142.9

Vein Stage III:

#	Sample #	Vein Generation	Inclusion Host Min	Primary	Designation	Fr	Tm(ice)	FPD	NaCl (wt%)	Tm (Clath)	Th	Ti
1	A22-5-1	3	Sph	P	S3	0.95	-	-	14.32	1.1	125.2	-
2	A22-5-2	3	Sph	P	S3	0.9	-	-	8.95	5	146.2	-
3	A22-5-3	3	Sph	P	S3	0.9	-0.5	0.5	0.88	-	176.2	-
4	A22-5-4	3	Sph	P	S3	0.9	-	-	14.44	1	130.4	-
5	A22-5-5	3	Sph	P	S3	0.7	-1.3	1.3	2.24	-	181.1	-
6	A22-5-6	3	Sph	P	S3	0.85	-	-	10.16	4.2	126.9	-
7	A22-5-7	3	Sph	P	S3	0.95	-	-	12.27	2.7	119.5	-
8	A7-1-1	3	Sph	P	S3	0.8	-6.7	6.7	10.11	-	149.5	-
9	A7-1-3	3	Sph	P	S3	0.95	-5.9	5.9	9.08	-	150.4	-
10	A7-1-4	3	Sph	P	S3	0.9	-6.3	6.3	9.60	-	147.9	-
11	VP032-10-1	3	Sph	P	S3	0.8	-2.4	2.4	4.03	-	150.1	-
12	VP032-10-3	3	Sph	P	S3	0.8	-2.7	2.7	4.49	-	178.6	-

13	VP032-8-2	3	Sph	P	S3	0.9	-2.1	2.1	3.55	-	196.4	-
14	VP032-8-3	3	Sph	P	S3	0.9	-2.6	2.6	4.34	-	186.9	-
15	VP032-7-1	3	Sph	P	S3	0.8	-1.7	1.7	2.90	-	189.2	-
16	VP032-7-2	3	Sph	P	S3	0.7	-2.1	2.1	3.55	-	185.4	189.2
17	VP032-7-4	3	Sph	P	S3	0.9	-	-	10.16	4.2	115.1	115.1
18	VP032-7-5	3	Sph	P	S3	0.75	-0.9	0.9	1.57	-	183.8	185.4
19	VP032-7-6	3	Sph	P	S3	0.95	-	-	12.40	2.6	125.7	125.7
20	VP032-7-7	3	Sph	P	S3	0.9	-	-	9.11	4.9	124.1	124.1
21	VP032-7-8	3	Sph	P	S3	0.75	-0.6	0.6	1.05	-	176	201.1
22	VP032-7-10	3	Sph	P	S3	0.90	-	-	6	6.60	117.30	117.3
23	VP032-15-1	3	Sph	P	S3	0.85	-4.8	4.8	7.59	-	151	183.8
24	VP032-15-2	3	Sph	P	S3	0.85	-4.7	4.7	7.45	-	148.9	176
25	VP032-15-3	3	Sph	P	S3	0.85	-4.5	4.5	7.17	-	152.6	-
26	VP032-15-4	3	Sph	P	S3	0.9	-4.5	4.5	7.17	-	141.5	-
27	VP032-15-5	3	Sph	P	S3	0.9	-4.5	4.5	7.17	-	154.2	-
28	VP032-15-6	3	Sph	P	S3	0.9	-4.5	4.5	7.17	-	146.5	-
29	VP032-15-7	3	Sph	P	S3	0.9	-4.5	4.5	7.17	-	166.2	-
30	VP032-15-8	3	Sph	P	S3	0.9	-4.5	4.5	7.17	-	137.7	-
31	VP032-15-9	3	Sph	P	S3	0.8	-4.8	4.8	7.59	-	134.4	-
32	VP032-15-10	3	Sph	P	S3	0.85	-4.4	4.4	7.02	-	141.3	-
33	VP032-15-12	3	Sph	P	S3	0.8	-4.8	4.8	7.59	-	155.6	-
34	VP032-1-1	3	Qtz	P	Q3	0.8	-5.8	5.8	8.95	-	168.3	-
35	VP032-1-2	3	Qtz	P	Q3	0.85	-5.4	5.4	8.41	-	175.1	-
36	VP032-1-3	3	Qtz	P	Q3	0.9	-5.6	5.6	8.68	-	165.1	-
37	VP032-1-4	3	Qtz	P	Q3	0.95	-5.6	5.6	8.68	-	152.5	-
38	VP032-1-9	3	Qtz	P	Q3	0.95	-5.3	5.3	8.28	-	134.6	-
39	VP032-1-10	3	Qtz	P	Q3	0.75	-6.4	6.4	9.73	-	146.2	-
40	VP032-2-1	3	Qtz	P	Q3	0.75	-5	5	7.86	-	175.3	-
41	VP032-2-2	3	Qtz	P	Q3	0.9	-2.9	2.9	4.80	-	157.5	-
42	VP032-2-3	3	Qtz	P	Q3	0.85	-2.9	2.9	4.80	-	173.5	-
43	VP032-2-4	3	Qtz	P	Q3	0.7	-2.7	2.7	4.49	-	172.1	-
44	VP032-2-5	3	Qtz	P	Q3	0.9	-2.7	2.7	4.49	-	175.1	-
45	VP032-2-6	3	Qtz	P	Q3	0.9	-2.8	2.8	4.65	-	157	-
46	VP032-2-7	3	Qtz	P	Q3	0.9	-2.9	2.9	4.80	-	147.2	-
47	VP032-2-8	3	Qtz	P	Q3	0.6	-2.9	2.9	4.80	-	158.2	-
48	VP032-2-9	3	Qtz	P	Q3	0.9	-4.3	4.3	6.88	-	157	-
49	VP032-2-11	3	Qtz	P	Q3	0.85	-1.9	1.9	3.23	-	162.5	-
50	VP032-2-12	3	Qtz	P	Q3	0.9	-4.6	4.6	7.31	-	154.7	-
51	VP032-2-13	3	Qtz	P	Q3	0.9	-3.5	3.5	5.71	-	148.6	-
52	VP032-2-14	3	Qtz	P	Q3	0.95	-5.5	5.5	8.55	-	159.5	-
53	VP032-2-17	3	Qtz	P	Q3	0.9	-4.8	4.8	7.59	-	144.2	-
54	VP032-2-18	3	Qtz	P	Q3	0.9	-2.7	2.7	4.49	-	169.2	-
55	VP032-3-1	3	Qtz	P	Q3	0.9	-3	3	4.96	-	165.5	-
56	VP032-3-2	3	Qtz	P	Q3	0.8	-3.5	3.5	5.71	-	170.9	-
57	VP032-3-5	3	Qtz	P	Q3	0.8	-3.4	3.4	5.56	-	176.4	-
58	VP032-3-8	3	Qtz	P	Q3	0.75	-5	5	7.86	-	172.6	165.5

59	VP032-3-9	3	Qtz	P	Q3	0.95	-5.1	5.1	8.00	-	157.6	170.9
60	VP032-3-10	3	Qtz	P	Q3	0.8	-6	6	9.21	-	163.3	176.4
61	VP032-3-11	3	Qtz	P	Q3	0.9	-3.5	3.5	5.71	-	144.2	172.6
62	VP032-3-13	3	Qtz	P	Q3	0.95	-5.4	5.4	8.41	-	170.4	157.6
63	VP032-3-16	3	Qtz	P	Q3	0.9	-3.3	3.3	5.41	-	175.2	163.3
64	VP032-3-17	3	Qtz	P	Q3	0.95	-3.1	3.1	5.11	-	150	144.2
65	VP032-3-18	3	Qtz	P	Q3	0.95	-3.2	3.2	5.26	-	140.5	170.4
66	VP032-3-19	3	Qtz	P	Q3	0.85	-3.8	3.8	6.16	-	176.5	174.9
67	VP032-3-20	3	Qtz	P	Q3	0.95	-3.6	3.6	5.86	-	141.8	182.5
68	VP032-9-1	3	Qtz	P	Q3	0.75	-5.1	5.1	8.00	-	133.7	175.2
69	VP032-9-3	3	Qtz	P	Q3	0.9	-4.9	4.9	7.73	-	138.2	150
70	VP032-9-4	3	Qtz	P	Q3	0.9	-3.8	3.8	6.16	-	150	140.5
71	VP032-9-5	3	Qtz	P	Q3	0.9	-5	5	7.86	-	168.4	176.5
72	VP032-9-6	3	Qtz	P	Q3	0.95	-5.5	5.5	8.55	-	138.5	141.8
73	VP032-9-7	3	Qtz	P	Q3	0.85	-4.7	4.7	7.45	-	150.70	-
74	VP032-9-8	3	Qtz	P	Q3	0.80	-5.1	5.1	8.00	-	166.50	-
75	VP032-9-9	3	Qtz	P	Q3	0.90	-5.1	5.1	8.00	-	169.50	-
76	VP032-9-10	3	Qtz	P	Q3	0.90	-3.1	3.1	5.11	-	167.20	-
77	VP032-9-11	3	Qtz	P	Q3	0.95	-5	5	7.86	-	135.60	-
78	VP032-9-12	3	Qtz	P	Q3	0.90	-5	5	7.86	-	147.70	-
79	VP032-9-13	3	Qtz	P	Q3	0.85	-5	5	7.86	-	135.6	-
80	HG02-4-1	3	Qtz	P	Q3	0.90	-9.70	9.7	12	2.80	120.10	-
81	HG02-4-2	3	Qtz	P	Q3	0.85	-6.8	6.8	10.24	-	161.1	-
82	HG02-4-3	3	Qtz	P	Q3	0.95	-6.6	6.6	9.98	-	155.3	-
83	HG02-4-4	3	Qtz	P	Q3	0.9	-11.2	11.2	15.17	-	157.7	-
84	HG02-4-5	3	Qtz	P	Q3	0.9	-11.5	11.5	15.47	-	134.2	-
85	HG02-4-6	3	Qtz	P	Q3	0.9	-9.5	9.5	13.40	-	157.6	-
86	HG02-4-7	3	Qtz	P	Q3	0.9	-9.7	9.7	13.62	-	146.2	-
87	HG02-4-8	3	Qtz	P	Q3	0.9	-8.2	8.2	11.93	-	143.6	-
88	HG02-4-9	3	Qtz	P	Q3	0.9	-8.5	8.5	12.28	-	154.1	-
89	HG02-4-10	3	Qtz	P	Q3	0.9	-8.1	8.1	11.81	-	141.5	-

Vein Stage IV:

#	Sample #	Vein Generation	Inclusion Host Min	Primary	Designation	Fr	Tm(ice)	FPD	NaCl (wt%)	Tm (Clath)	Th
1	A29-3-1	4	Qtz	P	Q4	0.95	-1.6	1.6	2.74	-	169.4
2	A29-3-2	4	Qtz	P	Q4	0.95	-1.5	1.5	2.57	-	155.2
3	A29-3-3	4	Qtz	P	Q4	0.8	-1.8	1.8	3.06	-	182.4
4	A29-3-4	4	Qtz	P	Q4	0.95	-1.7	1.7	2.90	-	180
5	A29-1-1	4	Qtz	P	Q4	0.85	-1.7	1.7	2.90	-	157.8
6	A29-1-2	4	Qtz	P	Q4	0.9	-2.3	2.3	3.87	-	171.2
7	A29-1-4	4	Qtz	P	Q4	0.9	-1.7	1.7	2.90	-	151.6
8	VP033-5-1	4	Qtz	P	Q4	0.85	-3.4	3.4	5.56	-	159.4
9	VP033-5-2	4	Qtz	P	Q4	0.95	-3.1	3.1	5.11	-	154.1
10	VP033-5-3	4	Qtz	P	Q4	0.9	-3.1	3.1	5.11	-	145.2
11	VP033-5-4	4	Qtz	P	Q4	0.95	-1.8	1.8	3.06	-	152.7

12	VP033-5-5	4	Qtz	P	Q4	0.95	-1.8	1.8	3.06	-	153.5
13	VP033-5-6	4	Qtz	P	Q4	0.8	-2.9	2.9	4.80	-	154.7
14	VP033-5-7	4	Qtz	P	Q4	0.95	-2.1	2.1	3.55	-	158.4
15	VP033-5-8	4	Qtz	P	Q4	0.9	-2.5	2.5	4.18	-	143.3
16	VP033-2-1	4	Qtz	P	Q4	0.95	-0.3	0.3	0.53	-	155.5
17	VP033-2-2	4	Qtz	P	Q4	0.8	-0.9	0.9	1.57	-	163.5
18	VP009-7-1	4	Qtz	P	Q4	0.85	-2.3	2.3	3.87	-	148
19	VP009-7-2	4	Qtz	P	Q4	0.95	-2	2	3.39	-	144.1
20	VP009-7-3	4	Qtz	P	Q4	0.9	-1.4	1.4	2.41	-	154.2
21	VP009-7-4	4	Qtz	P	Q4	0.9	-2.5	2.5	4.18	-	151.5
22	VP009-7-5	4	Qtz	P	Q4	0.95	-3.1	3.1	5.11	-	165.8
23	VP009-7-6	4	Qtz	P	Q4	0.95	-1.9	1.9	3.23	-	169.5
24	VP009-7-7	4	Qtz	P	Q4	0.85	-2.4	2.4	4.03	-	150.9
25	VP009-7-8	4	Qtz	P	Q4	0.9	-2.5	2.5	4.18	-	165.5
26	VP009-7-9	4	Qtz	P	Q4	0.9	-1.9	1.9	3.23	-	158
27	VP009-6-1	4	Qtz	P	Q4	0.85	-1.9	1.9	3.23	-	161.2
28	VP009-6-2	4	Qtz	P	Q4	0.9	-1.8	1.8	3.06	-	165.5
29	VP009-1-1	4	Qtz	P	Q4	0.9	-2.5	2.5	4.18	-	155.6
30	VP009-1-2	4	Qtz	P	Q4	0.9	-2.6	2.6	4.34	-	149.4
31	VP009-1-3	4	Qtz	P	Q4	0.9	-2.7	2.7	4.49	-	160
32	VP009-1-4	4	Qtz	P	Q4	0.95	-2.3	2.3	3.87	-	149.2
33	VP009-1-5	4	Qtz	P	Q4	0.9	-2.5	2.5	4.18	-	159.5
34	VP009-1-6	4	Qtz	P	Q4	0.9	-2.6	2.6	4.34	-	154.2

APPENDIX F

Stable Isotopes

Hydrothermal Vein Calcite:

#	Sample	Easting	Northing	Depth ASL (m)	Vein Gen	Comments	$\delta^{18}O$ (VSMOW)	$\delta^{13}C$ (VPDB)	T (K)	$\delta^{18}O$ Water	$\delta^{13}C$ CO_2
1	HG-BJ-B2	426600	6257975	1350	IIa	white calcite	8.4	-6.6	433	-3.6	-5.7
2	HG-BJ-B3	426600	6257980	1350	IIa	white calcite	7.9	-7.6	433	-4.1	-6.7
3	HG-BJ-B4	426600	6257985	1350	IIa	white calcite	7.6	-7.3	433	-4.3	-6.3
4	BJ-A6-1	426527	6258076	1460	IIb	white calcite	10.0	-4.8	433	-1.9	-3.9
5	BJ-A6-2	426527	6258076	1460	IIb	white calcite	10.5	-5.8	433	-1.4	-4.9
6	BJ-A9	426453	6257936	1511	IIb	white calcite	10.4	-7.1	433	-1.5	-6.2
7	VP004	426660	6258028	1350	III	white calcite	7.7	-6.8	433	-4.2	-5.9
8	VP008	426615	6257974	1350	IV	white calcite	7.2	-7.3	433	-4.7	-6.4
9	VP010-1	426615	6257963	1350	IV	white calcite	6.7	-8.7	433	-5.3	-7.8
10	VP047-2	426617	6257966	1350	IV	white calcite	7.6	-7.6	433	-4.4	-6.7
11	VP058-2	426617	6257974	1350	IV	white calcite	6.8	-9.6	433	-5.2	-8.7
12	VP010	426615	6257963	1350	IV	grey calcite	7.8	-7.9	433	-4.2	-7.0
13	VP047	426617	6257966	1350	IV	grey calcite	8.1	-7.7	433	-3.8	-6.8
14	VP058	426617	6257974	1350	IV	grey calcite	8.1	-8.9	433	-3.8	-8.0
15	BJ-HG05	426627	6258141	1457	IV	grey calcite	8.1	-4.6	433	-3.8	-3.6
16	VP047-1	426617	6257966	1350	IV	orange calcite	7.5	-9.0	433	-4.4	-8.1
17	VP058-1	426617	6257974	1350	IV	orange calcite	6.6	-10.2	433	-5.3	-9.3
18	BJ-B8	426630	6258015	1350	IV	orange calcite	6.1	-8.7	433	-5.8	-7.7
19	A1	426452	6257949	1509	IV	orange calcite	13.1	-7.1	433	1.2	-6.2
20	A1-1	426452	6257949	1509	IV	orange calcite	13.4	-7.3	433	1.4	-6.4
21	BJ-A29	426453	6257936	1511	IV	orange calcite	12.2	-6.7	433	0.2	-5.8
22	BJ-A31	426478	6257943	1545	IV	orange calcite	10.1	-7.4	433	-1.9	-6.4
23	VP005	426658	6258016	1350	V	white calcite	7.9	-7.4	433	-4.0	-6.5
24	VP040	426600	6257989	1350	V	white calcite	8.0	-7.3	433	-3.9	-6.4
25	VP040-1	426600	6257989	1350	V	white calcite	8.0	-7.2	433	-3.9	-6.3

**Note: Vein generation IIa and IIb correspond to stringer and breccia veins respectively. Temperature correction for oxygen isotope values calculated using O'Niel et al., 1969. Temperature correction for carbon isotope values calculated using Chacko et al., 1991.*

Hydrothermal Vein Quartz:

#	Sample	Easting	Northing	Depth ASL (m)	Vein Stage	Comments	$\delta^{18}O$qtz (VSMOW)	T (K)	$\delta^{18}O$ Water
1	HG-BJ-3	426505	6257948	1486	IIa	Au-within same vein	13.0	433	-1.5
2	HG-BJ-4	426351	6258071	1451	IIa	Au-within same vein	12.2	433	-2.3
3	VP003	426660	6258035	1347	IIa	Au-within same vein	7.7	433	-6.8
4	HG-BJ-1	427002	6257736	1324	IIb	Au-within same vein	11.6	433	-2.9
5	VP002	426660	6258035	1347	IIb	White quartz	7.4	433	-7.1

6	HG-BJ-2	426626	6257869	1493	III	Au-within same vein	11.2	433	-3.3
7	HG-BJ-2	426626	6257869	1493	III	Au-within same vein	11.2	433	-3.3
8	VP004	426660	6258028	1347	III	White quartz	8.9	433	-5.6
9	VP018	426615	6257974	1347	III	White quartz	7.3	433	-7.2
10	VP013	426615	6257939	1347	III	White quartz	9.6	433	-4.9
11	VP032	426585	6257956	1347	III	White quartz	9.5	433	-5.0
12	VP005	426658	6258016	1347	V	White quartz	8.7	433	-5.8
13	VP030	426585	6257993	1347	V	White quartz	7.3	433	-7.2
14	VP040	426600	6257989	1347	V	White quartz	6.4	433	-8.1
15	VP016	426645	6258975	1347	V	White quartz	4.7	433	-9.8
16	VP023	426555	6258003	1347	V	White quartz	7.2	433	-7.3

**Note: Vein generation IIa and IIb correspond to stringer and breccia veins respectively. Temperature correction for oxygen isotope values calculated using Matsuhisha et al., 1979.*

Hydrothermal Vein Sulfides:

#	Sample	Easting	Northing	Depth ASL (m)	Vein Stage	Mineral	$\delta^{32}S$
1	VP015	426615	6257960	1347	I	pyrite	0.0
2	VP021	426660	6258011	1347	I	pyrite	0.2
3	VP022	426660	6258008	1347	I	pyrite	-0.1
4	VP049	426659	6257988	1364	I	pyrite	-1.7
5	VP002	426660	6258035	1347	IIb	pyrite	0.1
6	VP024	426555	6257990	1347	IIb	pyrite	-0.5
7	VP057	426644	6258003	1347	IIb	pyrite	-0.2
8	VP004	426660	6258028	1347	III	sphalerite	-1.4
9	VP018	426645	6257962	1347	III	pyrite	-1.2
10	VP025	426555	6257987	1347	III	pyrite	-0.4
11	VP032-1	426585	6257956	1347	III	sphalerite	0.5
12	VP032-2	426585	6257956	1347	III	galena	-4.2
13	VP054	426617	6257966	1347	III	pyrite	-1.7
14	VP010	426615	6257963	1347	IV	pyrite	0.6
15	VP007	426615	6257974	1347	V	pyrite	-0.6
16	VP030	426585	6257993	1347	V	pyrite	0.1

**Note: Vein generation IIb corresponds to breccia veins.*